



3 4456 0313705 9

ORNL/TM-11216

omni

**OAK RIDGE
NATIONAL
LABORATORY**

MARTIN MARIETTA

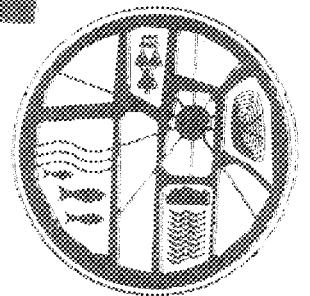
Hydrogeology of Melton Valley Determined from Hydraulic Head Measuring Station Data

R. B. Dreier
L. E. Toran

Environmental Sciences Division
Publication No. 3338

ESD - 3338

OAK RIDGE NATIONAL LABORATORY
CENTRAL RESEARCH LIBRARY
CIRCULATION SECTION
E-200N ROOM 122
LIBRARY LOAN COPY
DO NOT TRANSFER TO ANOTHER PERSON
If you wish someone else to see this
report, send its name with report and
the library will arrange a loan.



OPERATED BY
MARTIN MARIETTA ENERGY SYSTEMS, INC.
FOR THE UNITED STATES
DEPARTMENT OF ENERGY

This report has been reproduced directly from the best available copy.

Available to DOE and DOE contractors from the Office of Scientific and Technical Information, P.O. Box 62, Oak Ridge, TN 37831; prices available from (615) 576-8401, FTS 626-8401

Available to the public from the National Technical Information Service, U.S. Department of Commerce, 5285 Port Royal Rd., Springfield, VA 22161
NTIS price codes—Printed Copy: A11 Microfiche A01

This report was prepared as an account of work sponsored by an agency of the United States Government. Neither the United States Government nor any agency thereof, nor any of their employees, makes any warranty, express or implied, or assumes any legal liability or responsibility for the accuracy, completeness, or usefulness of any information, apparatus, product, or process disclosed, or represents that its use would not infringe privately owned rights. Reference herein to any specific commercial product, process, or service by trade name, trademark, manufacturer, or otherwise, does not necessarily constitute or imply its endorsement, recommendation, or favoring by the United States Government or any agency thereof. The views and opinions of authors expressed herein do not necessarily state or reflect those of the United States Government or any agency thereof.

ENVIRONMENTAL SCIENCES DIVISION

**HYDROGEOLOGY OF MELTON VALLEY DETERMINED
FROM HYDRAULIC HEAD MEASURING STATION DATA**

R. B. Dreier
L. E. Toran

Environmental Sciences Division
Publication No. 3338

ENVIRONMENTAL COMPLIANCE PROGRAM

Date Published -- June 1989

Prepared for the
Office of Energy Research
(Activity No. KG 02 00 00 0)

Prepared by the
OAK RIDGE NATIONAL LABORATORY
Oak Ridge, Tennessee 37831-6285
operated by
MARTIN MARIETTA ENERGY SYSTEMS, INC.
for the
U.S. Department of Energy
under contract DE-AC05-84OR21400

MARTIN MARIETTA ENERGY SYSTEMS LIBRARIES



3 4456 0313705 9

CONTENTS

	<u>Page</u>
LIST OF FIGURES.....	vii
LIST OF TABLES	ix
LIST OF ACRONYMS.....	xi
EXECUTIVE SUMMARY.....	xiii
1. INTRODUCTION	1
1.1 PURPOSE	1
1.2 WELL DESIGN.....	2
1.3 GEOLOGIC SETTING	7
2. GEOLOGIC DATA COLLECTION.....	10
3. GEOLOGIC DATA INTERPRETATION.....	12
3.1 INTRODUCTION	12
3.2 STRATIGRAPHY	12
3.3 STRUCTURE.....	18
3.3.1 Criteria for Identifying Fault Zones, Faults, or Fractures	28
3.3.2 Cross Section Discussion	32
3.3.3 Fault Zone Characterization	35
3.3.3.1 Thrust Fault -- HHMS 8A	35
3.3.3.2 Tear Fault -- HHMS 10A	36
4. HYDROGEOLOGY AND GROUNDWATER GEOCHEMISTRY.....	38
4.1 INTRODUCTION.....	38
4.2 POTENTIOMETRIC HEAD.....	38
4.2.1 Methods	38
4.2.2 Hydrographs.....	39
4.2.3 Hydraulic Gradients.....	40

4.3	HYDRAULIC CONDUCTIVITY MEASUREMENTS	43
4.3.1	Methods.....	43
4.3.2	Results.....	46
4.4	GEOCHEMISTRY.....	52
4.4.1	Methods	52
4.4.2	Results.....	53
5.	DISCUSSION	63
5.1	INFLUENCE OF FAULTS ON LOCAL FLOW PATHS.....	63
5.2	TRANSITION BETWEEN FLOW SYSTEMS	64
5.3	POTENTIAL FLOW PATHS FOR TRITIUM TO HHMS 3A.....	73
5.4	FUTURE WORK.....	77
6.	SUMMARY	80
	REFERENCES CITED.....	82
APPENDIX 1.	GENERAL WELL SITE INFORMATION, DRILLERS LOGS AND GEOPHYSICAL LOGS FOR HHMS SITE 1.....	85
APPENDIX 2.	GENERAL WELL SITE INFORMATION, DRILLERS LOGS AND GEOPHYSICAL LOGS FOR HHMS SITE 2.....	93
APPENDIX 3.	GENERAL WELL SITE INFORMATION, DRILLERS LOGS AND GEOPHYSICAL LOGS FOR HHMS SITE 3.....	101
APPENDIX 4.	GENERAL WELL SITE INFORMATION, DRILLERS LOGS AND GEOPHYSICAL LOGS FOR HHMS SITE 4.....	109
APPENDIX 5.	GENERAL WELL SITE INFORMATION, DRILLERS LOGS AND GEOPHYSICAL LOGS FOR HHMS SITE 5.....	117
APPENDIX 6.	GENERAL WELL SITE INFORMATION, DRILLERS LOGS AND GEOPHYSICAL LOGS FOR HHMS SITE 6.....	125
APPENDIX 7.	GENERAL WELL SITE INFORMATION, DRILLERS LOGS AND GEOPHYSICAL LOGS FOR HHMS SITE 7.....	133
APPENDIX 8.	GENERAL WELL SITE INFORMATION, DRILLERS LOGS AND GEOPHYSICAL LOGS FOR HHMS SITE 8.....	141
APPENDIX 9.	GENERAL WELL SITE INFORMATION, DRILLERS LOGS AND GEOPHYSICAL LOGS FOR HHMS SITE 9.....	151

APPENDIX 10.	GENERAL WELL SITE INFORMATION, DRILLERS LOGS AND GEOPHYSICAL LOGS FOR HHMS SITE 10.....	161
APPENDIX 11.	GENERAL WELL SITE INFORMATION, DRILLERS LOGS AND GEOPHYSICAL LOGS FOR HHMS SITE 11.....	171
APPENDIX 12.	CONASAUGA GROUP STRATIGRAPHY.....	183
APPENDIX 13.	HYDROGRAPHS.....	189

LIST OF FIGURES

<u>Figure</u>		<u>Page</u>
1	HHMS well construction diagram.....	3
2	Location map of the HHMS sites.....	6
3	Generalized geologic map of the Oak Ridge Reservation.....	8
4	Stratigraphic correlations observed in the Nolichucky Shale determined from natural gamma-ray and epithermal neutron geophysical logs	14
5	Stratigraphic correlations observed in the Maryville Limestone determined from natural gamma-ray and epithermal neutron geophysical logs	15
6	Stratigraphic correlations observed in the Rogersville Shale, Rutledge Limestone, and Pumpkin Valley Shale determined from natural gamma-ray and epithermal neutron geophysical logs	16
7	Location map of the geologic cross sections	19
8	Strike-perpendicular geologic cross section through SWSA 6 and White Oak Lake.....	20
9	Strike-perpendicular geologic cross section through the central portion of the Pits and Trenches area.....	21
10	Strike-perpendicular geologic cross section through the eastern portion of the Pits and Trenches area	22
11	Strike-parallel geologic cross section through the southern portion of the Pits and Trenches area	23
12	Strike-parallel geologic cross section along a portion of the White Oak Creek floodplain south of the Pits and Trenches area.....	24
13	Porosity crossplot determined from epithermal neutron and interval transit time data from borehole HHMS 8A.....	31
14	Generalized potentiometric surface for HHMS B wells	41
15	Generalized potentiometric surface for HHMS C wells	42
16	Cross section models through White Oak Lake showing two different interpretations of vertical potentiometric head data	44
17	Diagram of field set up for a packer test to measure K.....	47

18	Histogram of geometric mean of hydraulic conductivity data by well type (HHMS A, B, and C depths).....	49
19	Hydraulic conductivity versus depth showing scatter in the trend of lower K with depth	50
20	Trilinear diagram of chemical analyses from GY 1986 HHMS wells	57
21	Histogram of arithmetic mean conductivity for different well depths	59
22	Deuterium vs ^{18}O for three clusters	62
23	Flow system characteristics for the intermediate-depth wells	66
24	Area Containing HHMS B Wells with Shallow Flow System Characteristics	67
25	Variability of hydraulic conductivity values measured from intermediate-depth wells that also sample the same stratigraphic horizons	69

LIST OF TABLES

<u>Table</u>		<u>Page</u>
1	Well coordinate, elevation, and open interval data	4
2	Conasauga Group stratigraphic contacts	13
3	Fault identification criteria	25
4	Summary of hydraulic conductivity data by different techniques.....	48
5	Samples collected in summer 1987 for FY 1986 HHMS wells.....	54
6	Abbreviated summary of screening data and field data from HHMS wells ...	55
7	Deuterium and ¹⁸ O isotope ratios (per mil) for three HHMS clusters	61
8	Structural characteristics of the open intervals	70

LIST OF ACRONYMS

BHTV	Borehole televiewer
CCTS	Copper Creek Thrust Sheet
DOE	United States Department of Energy
GPP	General plant project
HHMS	Hydraulic head measuring station
ITT	Interval transit time
NHF	New Hydrofracture Facility
OHF	Old Hydrofracture Facility
ORNL	Oak Ridge National Laboratory
ORR	Oak Ridge Reservation
RAP	Remedial Action Program
RCRA	Resource Conservation and Recovery Act of 1976
SP	Spontaneous potential
SPR	Single point resistance
SWSA	Solid waste storage area
USGS	United States Geological Survey
VDL	Variable density log
WOCF	White Oak Creek Fault

EXECUTIVE SUMMARY

DREIER, R. B., and L. E. TORAN. 1989. Hydrogeology of Melton Valley determined from Hydraulic Head Measuring Station data. ORNL/TM-11216. Oak Ridge National Laboratory, Oak Ridge, Tennessee. 205 pp.

The hydraulic head measuring stations (HHMSs) are well clusters that provide data required for evaluating both the transition between shallow and deep groundwater system(s) and the nature of the deep system(s). This information can be used to aid the characterization of the local hydrologic framework as dictated by state and federal regulatory agencies. Specifically this project provides a means for defining the lower boundary of the uppermost aquifer and for identifying potential pathways for off-site contaminant migration for shallow, intermediate, and deep groundwater flow. In addition, this project provides some of the geologic and hydrologic background information required to perform a risk assessment for individual waste sites.

The objectives of the HHMS general plant projects are threefold: (1) to characterize potentiometric head levels in and near waste management areas in Melton Valley, (2) to characterize the geology in Melton Valley, and (3) to determine groundwater quality at their respective locations. This report presents results of data collected from wells constructed in FY 1986 and FY 1988. To meet these objectives, each HHMS was designed to consist of three telescoping wells, approximately 25 ft apart. The deepest well was drilled to approximately 400 ft, and the intermediate and shallow wells are approximately 200 and 80 ft deep, respectively. The open interval extends at least 20 ft below the bottom of the cased section of each well.

Data from the 11 existing cluster sites, which are concentrated in the Pits and Trenches area and in solid waste storage area 6, show that the lower boundary of the uppermost aquifer is gradational and may extend to depths of up to 200 ft. This depth clearly extends the uppermost aquifer into bedrock and beyond the regolith zone, which has at times in the past been considered a lower boundary. Comparison of hydraulic conductivities from along-strike wells suggests that this boundary is not totally stratigraphically controlled because conductivity values from the intermediate wells that sample the same stratigraphy show a wide range in values (10^{-8} to 10^{-5} cm/s), whereas values from the shallow wells show a tight clustering. Hydrologic evidence (response to rainfall, hydraulic conductivities, and electrical conductances) suggests the depth of the uppermost aquifer increases in the

vicinity of White Oak Lake and White Oak Creek, where thrust faults identified in the geophysical logs and the White Oak Creek Fault may enhance the permeability of the rock.

Average hydraulic conductivity decreases with depth in the HHMS wells. The geometric mean hydraulic conductivity of the deep wells is 8×10^{-9} cm/s. The mean hydraulic conductivity of the intermediate-depth wells is 9×10^{-7} cm/s. The highest hydraulic conductivities were observed in the shallow wells, which average 2×10^{-5} cm/s. Three wells shows anomalously low hydraulic conductivity values for their sampling depth. Two of the anomalies may be related to fault-induced permeability changes. The third well is the only shallow well that samples the Rogersville Shale, and its low conductivity may be lithologically controlled.

The water level records of the intermediate and shallow wells typically show a response to rainfall events, indicating connectivity with shallow flow systems. The water level records of the deep wells show long-term recovery from dewatering during drilling, which was used as a "slug test" to estimate hydraulic conductivity. Only a few of the deep wells have recovered sufficiently from dewatering for the head measurement to be an equilibrium value.

Anomalous levels of tritium (2000 bq/L) were measured in the deep well of HHMS cluster 3. The present data cannot unequivocally explain the presence of tritium in a 400-ft-deep well. Three possible sources of tritium are considered: the Pits and Trenches area, SWSA 4, and deep groundwater contaminated by hydrofracture. If the source of contamination is in the vicinity of the drill site, a 300- to 400-ft continuous crack along the well casing or fracture in the bedrock is required to enhance vertical transport. However, well construction records do not indicate any problems during the grouting procedure, and the presence of extensive vertical fractures is unlikely near HHMS 3. Deep groundwater from hydrofracture could have risen along a thrust fault identified in the geophysical logs, and evidence of upward migration of deep groundwater is presented. If the source of tritium is distant (i.e. SWSA 4, other parts of the Pits and Trenches area, or the hydrofracture facility), the travel times would require an extremely low porosity, on the order of 0.00001.

Geologic cross sections are used to determine the occurrence and two - or three-dimensional shape of potential flowpaths concentrated near faults and fault zones. Several

generalizations can be made about the occurrence of faults in Melton Valley. (1) Thrust faults with minor amounts of displacement (20 to 250 ft) are common within the Copper Creek Thrust Sheet, particularly within the Nolichucky Shale and the Maryville Limestone. (2) These faults form to accommodate shape changes of the CCTS. Hence other areas that show an uneven thrust sheet shape should also contain minor thrust faults. (3) Thrust faults commonly diverge to form imbricate splays. (4) Horizons with a preexisting structural fabric may partly control the location or initiation of these minor thrust faults. (5) Correlating thrust faults along a strike-parallel direction is difficult because the faults can cut either up or down the stratigraphic section or may die out along strike. (6) Although these faults show minor displacement, associated fracture zones can develop before and during fault displacement. In addition, although a fracture zone may enhance fracture porosity and permeability, the associated fault plane may act as a barrier to fluid flow.

Without this specific data from the HHMS sites, it would have been impossible to perform these characterization studies, and similar data are necessary for other waste disposal sites.

Geophysical and hydrologic data acquired as part of this project are included as appendixes.

1. INTRODUCTION

1.1 PURPOSE

The hydraulic head measuring stations (HHMSs) consist of 11 well clusters that provide data for evaluating both the transition between shallow and deep groundwater system(s) and the nature of the deep system(s). This information can be used to aid characterization of the local hydrologic framework near several waste disposal facilities, as requested by state and federal regulatory agencies. Specifically this project provides a means for defining the lower boundary of the uppermost aquifer and identifies potential pathways for on-site or off-site contaminant migration for shallow, intermediate, and deep groundwater. In addition, this project provides necessary background information required to perform a risk assessment for individual waste sites.

The objectives of the HHMS general plant projects (GPPs) are threefold: (1) to characterize potentiometric levels in and near waste management areas in Melton Valley, (2) to characterize the geology in Melton Valley, and (3) to determine groundwater geochemistry at the well site. This report presents results of data collected from wells that were constructed in FY 1986 and FY 1988 to acquire the necessary information.

The report is divided into three main parts: (1) geology--Sections 2 and 3, (2) hydrology--Section 4, and (3) discussion--Section 5. The purpose of the geology section is to present background regional (km^3) structural and stratigraphic data so that interpretations of geologic influences on local hydrologic systems can be evaluated in this report and in future studies. Interpretations of the relationship between local geology and hydrologic systems are presented in the discussion section. The geology sections do not discuss detailed hydrogeologic information (i.e. porosity and permeability data). Porosity values determined from geophysical logs have not been calibrated to the local thin-bedded interlayered shale and limestone lithologies. Hence only relative porosity changes, and estimated porosity values can be determined. In addition, it is not possible to determine permeabilities from the available geologic data, and the best permeability estimates come from well investigations (Sect. 4.3.2).

In Melton Valley, the geologic structure appears to be a major influence on the hydrology (this report; Dreier and Leat 1988). Fracture zones can increase or decrease local permeabilities and create preferred flow paths. In contrast, there are not enough lithologic

differences between the formations of the Conasauga Group for stratigraphic divisions to be equivalent to hydrologic boundaries. Nevertheless, subtle lithologic or stratigraphic changes may either directly influence the groundwater hydrology or constrain the magnitude of geologic deformation (Dreier and others 1988a, Dreier and others 1988b), thereby indirectly influencing the hydrologic transport mechanisms. In addition, an understanding of the stratigraphic column allows one to correlate both the stratigraphy and structure between well sites. Hence, in order to evaluate potential local flow paths, it is vital that both the regional stratigraphy and structure be understood.

1.2 WELL DESIGN

Each HHMS consists of three wells, approximately 25 ft apart (Fig. 1). The deepest well of the cluster is approximately 400 ft deep. The depth of the intermediate well is determined from geophysical logs of the deep well and is selected to investigate potential fracture zones at a depth of approximately 200 ft. The final depth of the shallow well is approximately 80 to 100 ft, placed 20 to 25 ft below the top of bedrock, as determined by air-rotary drilling.

Each well includes a conductor casing that extends approximately 5 ft into bedrock. In addition, the intermediate and deep wells have a well casing that extends from ground surface to the top of the open interval (Fig. 1). The open interval of the intermediate and deep well has no screen or casing and extends at least 20 ft below the bottom of well casing. The open interval of the shallow well has no screen or casing and extends for at least 20 ft below the conductor casing. The downhole depth of the open interval for each well is given in Table 1.

HHMS well cluster locations are shown in Fig. 2 and given in Table 1. Cluster locations were chosen to allow at least 50 ft of stratigraphic overlap between the deep wells of each cluster and to provide information on lateral changes in both the geology and hydrology throughout Melton Valley. The clusters are numbered chronologically by the sequence of drilling for the clusters. At each cluster, the deep, intermediate, and shallow wells are designated A, B, and C, respectively.

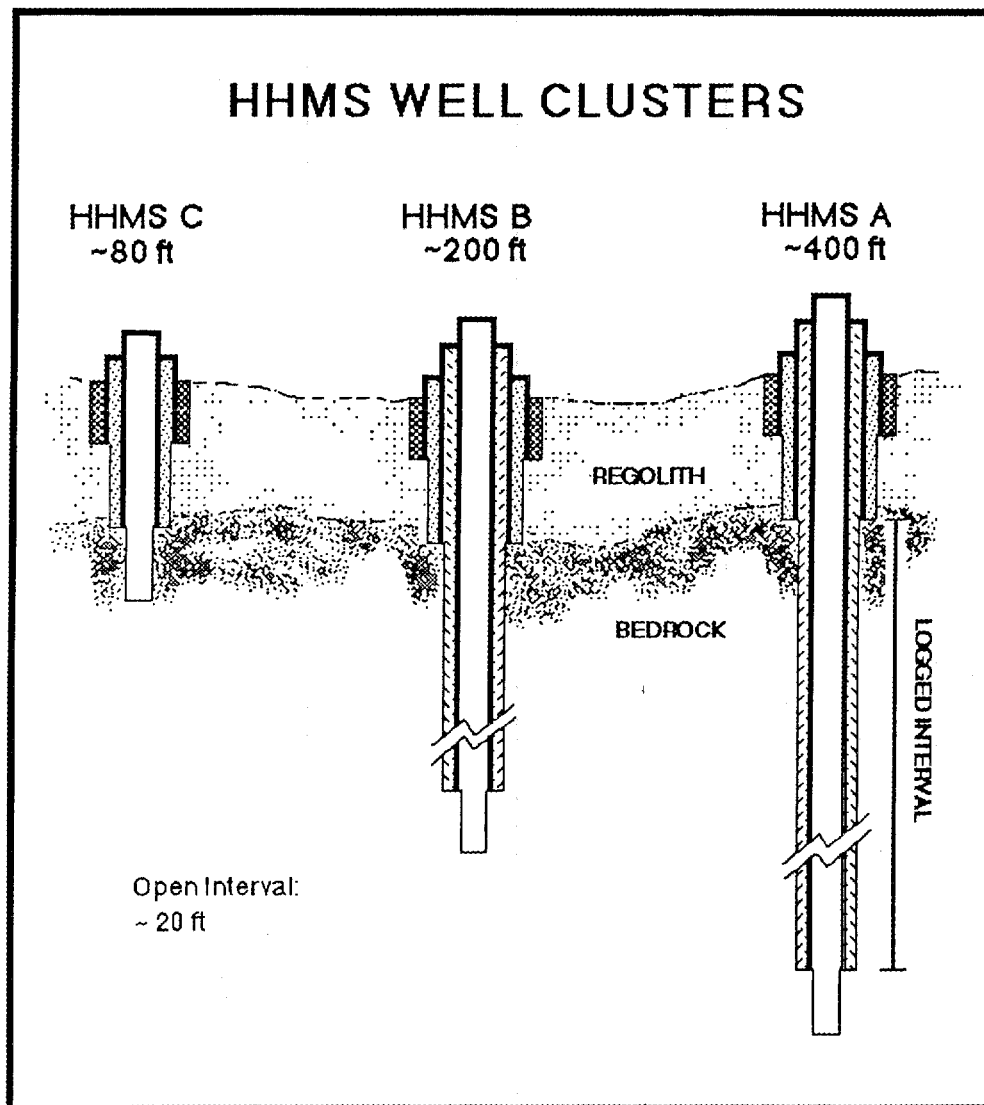


Fig. 1. HHMS well construction diagram.

Table 1. Well coordinate, elevation, and open interval data

Well name	ORNL N (ft)	ORNL E (ft)	Ground elevation (ft)	Top of casing (ft)	Total depth (ft)	Open interval depth (ft)
HHMS 1 A	18014.84	27964.36	870.11	873.1	400	380-400
HHMS 1 B	17989.34	27966.49	870.08	873.01	201.2	182.3-201.2
HHMS 1 C	17963.94	27976.47	869.84	872.94	101	63.7-101
HHMS 2 A	17225.06	27562.33	806.5	809.52	400.5	380-400
HHMS 2 B	17214.92	27535.95	807.68	810.89	200.5	180.6-200.6
HHMS 2 C	17208.13	27510.61	807.36	810.28	81.1	62.3-81.1
HHMS 3 A	17213.8	26724.48	818.79	821.19	399.1	380-400
HHMS 3 B	17195.99	26705.25	818.81	821.29	211.5	189.7-211.6
HHMS 3 C	17175.96	26689.95	817.98	820.98	80.5	62-80.6
HHMS 4 A	16144.55	24609.77	790.37	793.89	400.4	380-400
HHMS 4 B	16148.2	24688.37	787.78	791.05	215.3	174.28-215.28
HHMS 4 C	16170.59	24676.08	787.86	790.71	61.5	40.8-61.5
HHMS 5 A	15814.83	24525.34	767.48	770.3	400.4	380-400
HHMS 5 B	15827.63	24595.29	766.43	769.26	219.5	196.08-219.48
HHMS 5 C	15833.46	24561.12	766.79	769.95	63	42.1 -63
HHMS 6 A	15305.95	24764.04	762.09	763.88	402.5	38-400
HHMS 6 B	15289.25	24745.16	762.27	764.85	165.4	145-165.4
HHMS 6 C	15268.72	24732.51	762.47	764.91	60.8	40.8-60.8
HHMS 7 A	17540.65	24512.09	808.54	811.35	402.5	380-400
HHMS 7 B	17518.9	24509.4	808.64	810.53	295	275-295
HHMS 7 C	17498.37	24506.56	808.76	810.69	178	158-178
HHMS 8 A	16862.02	24694.84	786.06	787.95	400	380-400
HHMS 8 B	16810.7	24697.05	783.53	785.59	197	177-197
HHMS 8 C	16782.51	24668.21	786.09	788.62	79	59-79

Table 1. (continued)

Well Name	ORNL N (ft)	ORNL E (ft)	Ground Elevation (ft)	Top of Casing (ft)	Total Depth (ft)	Open Interval Depth (ft)
HHMS 9 A	18805.38	27929.18	860.43	861.7	400	380-400
HHMS 9 B	18809.57	27904.42	859.25	862.61	238	218-238
HHMS 9 C	18815.87	27875.83	860.87	862.93	80	60-80
HHMS 10 A	17450.15	28666.09	777.75	779.71	400	380-400
HHMS 11 A	13802.36	22749.62	779.95	782.12	400	380-400
HHMS 11 B	13827.33	22754.05	779.83	782.58	253	233-253
HHMS 11 C	13853.02	22751.24	778.58	781.13	114	94-114

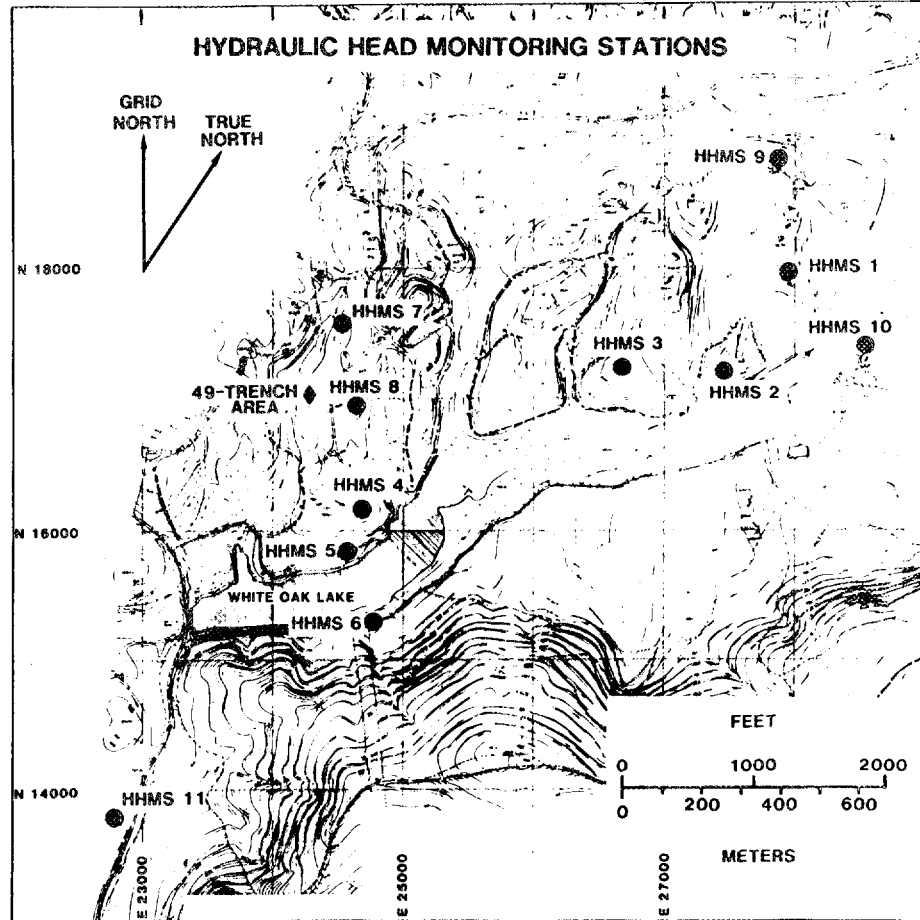


Fig. 2. Location map of the HHMS sites. The 49-trench area rain gage station is also shown.

The wells were constructed under three GPPs. HHMS sites 1 through 3 and HHMS sites 4 through 6 plus HHMS 7A were constructed as consecutive GPP 84 and GPP 85 packages during FY 1986. HHMS 7B and 7C and HHMS sites 8 through 11 were constructed as a GPP 86 during FY 1988. HHMS site 10 consists of only one deep well (HHMS 10A) because nearby United States Geological Survey (USGS) wells 466 and 467 could be used as intermediate and shallow wells to complete the cluster (Webster and Bradley 1988). Water level recovery of the deep wells drilled in FY 1986 was very slow (Sect. 4.2.2), and the large volume of water required to fill the borehole was a contributing factor. Hence, it was decided to reduce the diameter of the well casing from 6 in. to 4 in. for the GPP 86 construction package.

1.3 GEOLOGIC SETTING

The United States Department of Energy (DOE) Oak Ridge Reservation (ORR) is located in the Tennessee section of the Valley and Ridge Province, which is part of the Southern Appalachian Fold and Thrust Belt. The area is characterized by a succession of northeast-trending thrust faults that structurally stack and duplicate Paleozoic rocks of this area (Fig. 3). As a result of thrusting and subsequent differential erosion, a series of valleys and ridges has formed that parallels the thrust faults. In general, the more-resistant siltstone, sandstone and dolostone units are ridge-formers, and the less-resistant shales and shale-rich limestones underlie the valleys of the region.

The geology of the ORR is strongly influenced by structural features at all scales, including regional thrust faults, local thrust faults and tear faults, local folding of relatively weak units, and widespread fracture development. The large-scale structures formed during the Permian-Pennsylvanian Alleghanian Orogeny and historically have not been active. Fractures may have developed at any time from the Ordovician (because of burial processes) to the present (because of unloading processes). However, the Alleghanian Orogeny was probably the strongest control on fracture formation.

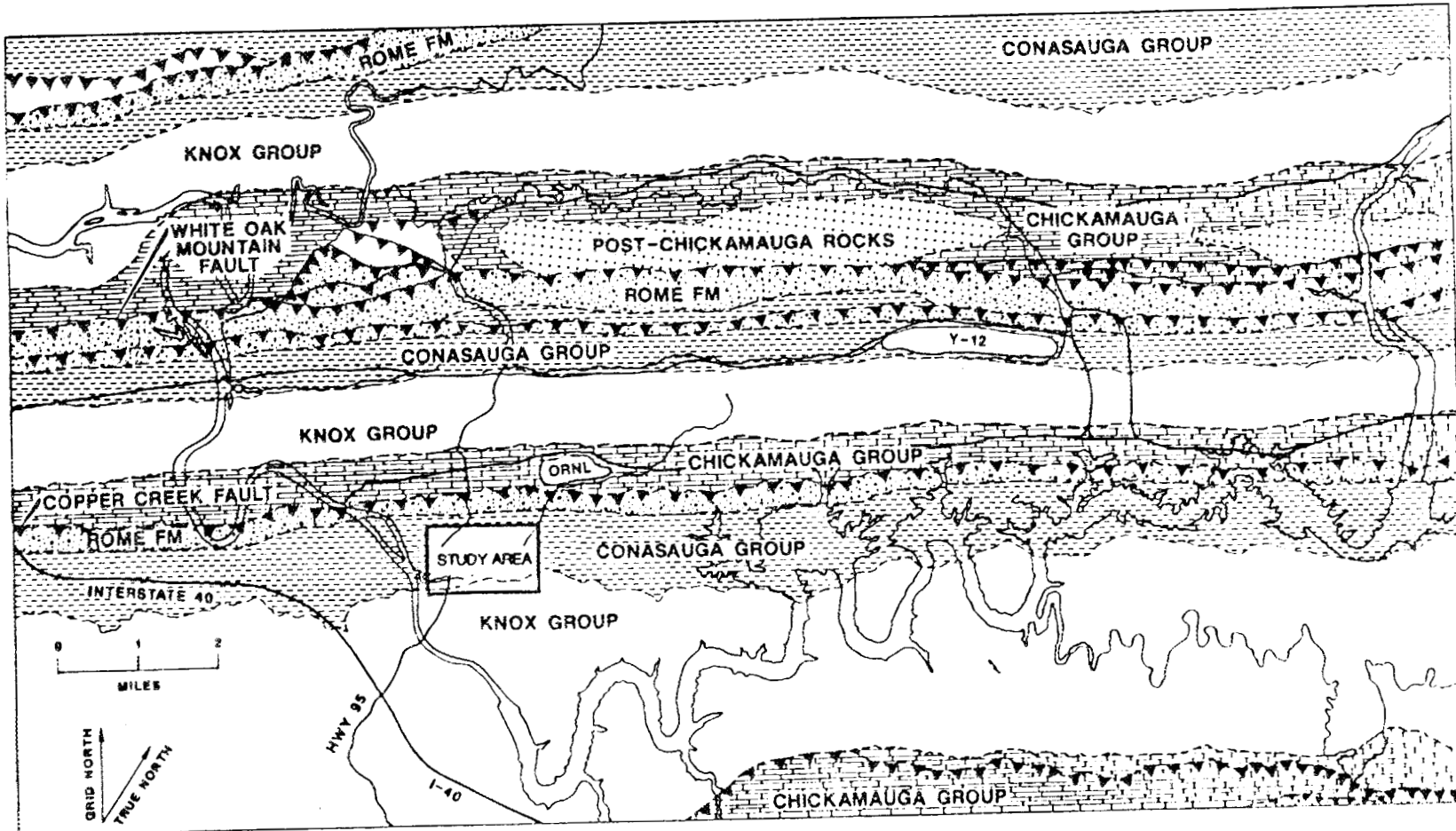


Fig. 3. Generalized geologic map of the Oak Ridge Reservation (after McMaster, 1963). Major stratigraphic units and thrust faults are illustrated. The HHMS sites are located within the study area outlined in black.

The area contains a wide spectrum of sedimentary rocks but is dominated by a Cambrian and Ordovician package of carbonate and marine clastic rocks. The oldest unit at the site is the Cambrian Rome Formation, consisting of interlayered siltstone, shale, and sandstone. The Rome Formation is overlaid by the Middle and Upper Cambrian Conasauga Group, a sequence of interlayered shales and limestones. The Conasauga Group, in turn, is succeeded by the Cambro-Ordovician Knox Group, a massive dolostone and limestone package, and the Middle Ordovician Chickamauga Group, which at the ORR consists mostly of limestone with some interbedded shale.

Melton Valley, the site of all HHMS construction, is located on the Copper Creek Thrust Sheet (CCTS) above the Copper Creek Fault (Fig. 3) and is underlain by the Cambrian Conasauga Group.

2. GEOLOGIC DATA COLLECTION

Geologic data collected from the HHMS drill sites include geophysical logs and relevant construction information and drillers' logs. All data are presented in Appendixes 1 through 11 and a general description of the geophysical logging is given below.

Geophysical logs were run in the deep well of each cluster. The logs were obtained after the main portion of the well was drilled and before installation of well casing. The logs were collected for strata between the bottom of conductor casing and the top of the open interval (Fig. 1). Hence, the logs provide data on the main portion of the well but not on the open interval of the deep well, which was drilled after the logs were run. All geophysical field records were taken with English units. Therefore, to facilitate correlation with the original records, this report maintains the use of English units.*

Each GPP was logged as a separate group. The 84 GPP (HHMS sites 1 to 3) and the 85 GPP (HHMS sites 4 to 7) were logged by Seaburn and Robertson, Inc., Geophysical Services between April and August 1986. The logs include temperature, deviation, caliper, electric [long-short normal, single-point resistance (SPR), and spontaneous potential (SP)], nuclear (natural gamma ray, side-walled epithermal neutron, gamma-gamma density) and acoustic logs [velocity and borehole televiewer (BHTV)]. The SPR sonde was not functioning correctly when HHMS 1A was being logged and is not included in the log package for that well. For each well, the temperature log was acquired first and, except for HHMS 5A, the measurements were taken as the sonde was lowered down the borehole. For HHMS 5A, the temperature log signature was recorded as the sonde was pulled up the hole. All of these logs were acquired in analog form, except for the BHTV log, which was exposed onto 70-mm film. The analog data, except for the SPR log for HHMS 2A, were later hand-digitized by Oak Ridge National Laboratory (ORNL) staff. The digital data are archived in the Remedial Action Program (RAP) database (Voorhees and others 1989).

During FY 1987, between construction of the 85 GPP and the 86 GPP, modifications were made to the logging specifications and procedures. Specification changes required that the data be collected in a digital format. This was done to facilitate geologic interpretation, data transfer, and record keeping. Procedural changes (J. Greene, ORNL, Oak Ridge, Tenn.,

* Conversion from English to metric units is as follows: (1) Feet X 0.0348 = meters; (2) (degrees Fahrenheit - 32)/1.8 = degrees Celsius.

personal communication to R. B. Dreier, ORNL, Oak Ridge, Tenn., 1987) were created to avoid potential problems from logging with a radioactive source tool. Currently, the procedures require that the geophysical logger, site engineer, and site geologist have as much information as possible about the condition of the borehole before a decision is made to log a borehole with a source tool.

The 86 GPP (HHMS sites 8 through 11) was logged by Gearhart Co. in January 1988, and the logging was continuously supervised by R. B. Dreier. The logs include temperature, deviation, and caliper, as well as electric (dual induction and SP), nuclear (natural gamma ray, side-walled epithermal neutron, gamma-gamma density) and acoustic logs [velocity and variable density (VDL)]. At each site, the temperature log was the first log to be run (from the surface to total depth), and the borehole fluids were undisturbed for approximately 6 weeks before temperature logs were taken. At HHMS site 9, the temperature tool was not running properly when it was initially lowered into the borehole. Because of this, the borehole was allowed to stand overnight (16 h) before the tool was reintroduced into the hole. Thus, interpretation of the temperature log for HHMS 9A is not as straightforward as for the other boreholes that equilibrated over a longer period. In addition to minor problems with the temperature log, the spacing for the Gearhart VDL was too large to detect fractures in the thin-bedded interlayered shale and carbonate sequence common at ORNL. No other technical problems were encountered during the geophysical logging by Gearhart. Geophysical logging by ORNL staff was conducted to obtain logs that Gearhart Co. were unable to provide (BHTV, SPR) or to recheck Gearhart logs (caliper, VDL). The Gearhart Co. digital data is part of the RAP database (Voorhees and others 1989). The BHTV data was taken on Polaroid film and is presented in Appendixes 8 through 11. The remainder of the data collected by ORNL staff resides on floppy disks under the custody of R. O. Kennard. The original data were acquired on a system that is no longer used at ORNL, and currently software is not available to translate those data onto the electronic RAP database. Hard copies of these data are available and are in the custody of R. B. Dreier.

3. GEOLOGIC DATA INTERPRETATION

3.1 INTRODUCTION

This section presents a summary of the geology in the eastern region of Melton Valley, which includes the area between and including solid waste storage area (SWSA) 6 and the Pits and Trenches area. The summary is an interpretation of geologic data, primarily geophysical logs, acquired from the HHMS wells. Where necessary to complete the interpretation, data from other deep (>200-ft) wells in this portion of Melton Valley have been included.

3.2 STRATIGRAPHY

This section summarizes the geophysical characteristics of stratigraphic contacts between the members of the Conasauga Group strata, which are sampled by HHMS wells. Additional descriptions of Conasauga Group stratigraphy are included in Appendix 12. Much of this data has been described by C. S. Haase (C. S. Haase, ORNL, Oak Ridge, Tenn., personal communication to R. B. Dreier, ORNL, Oak Ridge Tenn., June, 1986). Other detailed discussions of stratigraphic, lithologic and geophysical data for this portion of Melton Valley are presented in deLaguna and others (1968), Haase and others (1985), and Haase (1987). Stratigraphic contacts and correlations are determined from natural gamma, epithermal neutron, and long-short normal or dual-induction resistivity logs. The contact positions are downhole values referenced to ground surface at the borehole and are summarized in Table 2.

The Conasauga Group in the Oak Ridge vicinity consists of six formations of alternating shale and carbonate-rich lithologies, which are, in descending stratigraphic order, the Maynardville Limestone (Cmn), the Nolichucky Shale (Cn), the Maryville Limestone (Cm), the Rogersville Shale (Crg), the Rutledge Limestone (Crt), and the Pumpkin Valley Shale (Cpv). Most boreholes sample either the Maryville Limestone or the Nolichucky Shale. However, HHMS 11A samples the lower 50 ft of the Maynardville Limestone, and HHMS 9A samples the Rogersville Shale, the Rutledge Limestone, and the upper Pumpkin Valley Shale. Natural gamma-ray and epithermal neutron logs that illustrate the stratigraphy of the Conasauga Group are presented in Fig. 4 (Nolichucky Shale), Fig. 5 (Maryville Limestone and Rogersville Shale), and Fig. 6 (Rogersville Shale, Rutledge Limestone, and Pumpkin Valley Shale).

Table 2. Conasauga Group stratigraphic contacts^a

WELL NAME	Cpv/Crt	Crt/Crg	Crg/Cm	Cm/Cn
HHMS 1A	-	-	329	-
HHMS 2A	-	-	363	-
HHMS 3A	-	-	355	-
HHMS 4A	-	-	-	280
HHMS 5A	-	-	-	336
HHMS 6A	-	-	-	-
HHMS 7A	-	-	297	-
HHMS 8A	-	-	352	-
HHMS 9A	239	110	-	-
HHMS 10A	-	-	339	-
HHMS 11A	-	-	-	-

^aCpv = Pumpkin Valley Shale, Crt = Rutledge Limestone, Crg = Rogersville shale, Cm = Maryville Limestone, and Cn = Nolichucky shale.

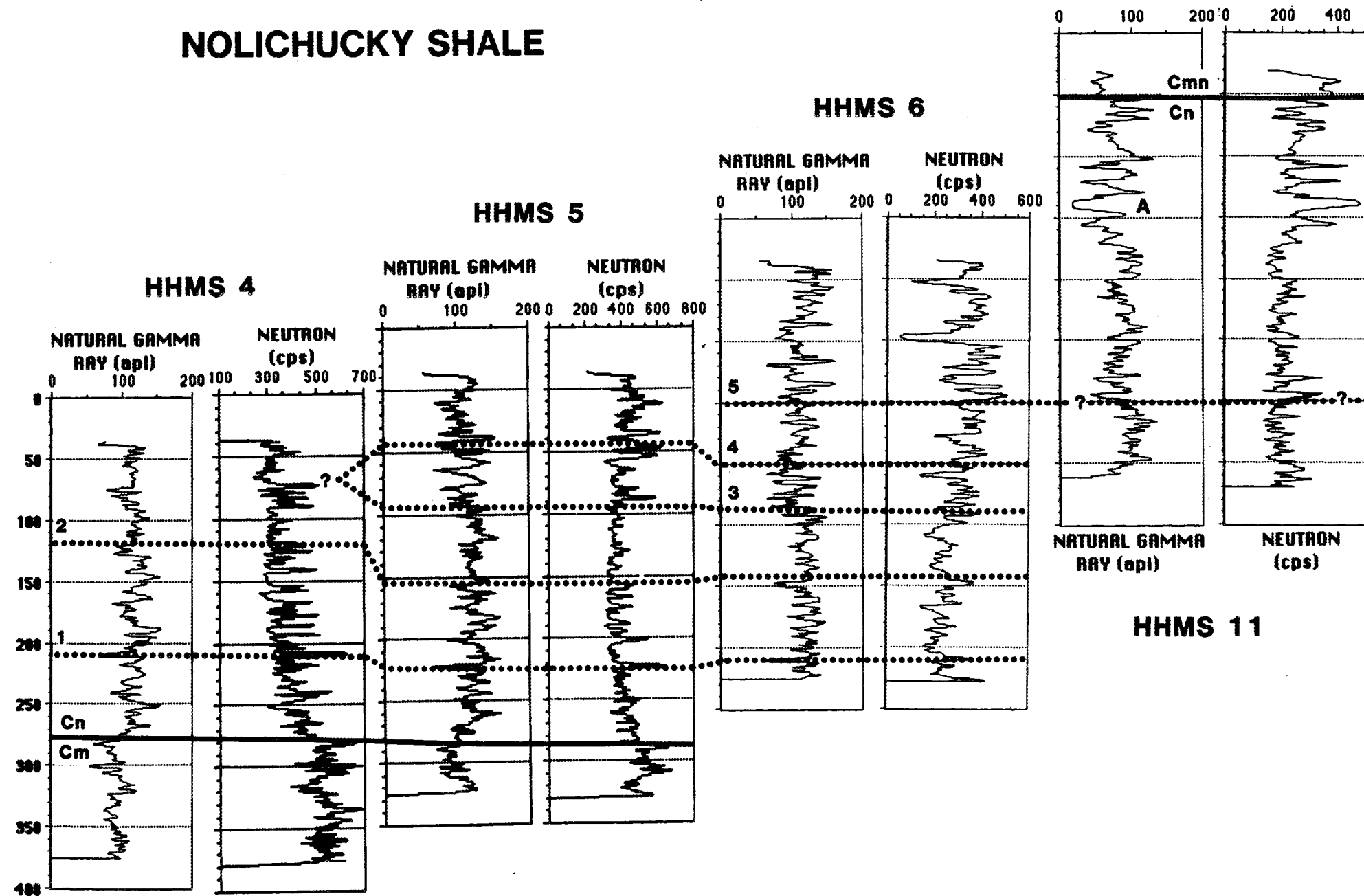


Fig. 4. Stratigraphic correlations observed in the Nolichucky Shale determined from natural gamma-ray and epithermal neutron geophysical logs. Solid lines represent formational contacts. Numbered dotted lines represent informal stratigraphic markers within the Nolichucky Shale. Detailed discussions of the geophysical log signature are given in Appendix 13.

MARYVILLE LIMESTONE

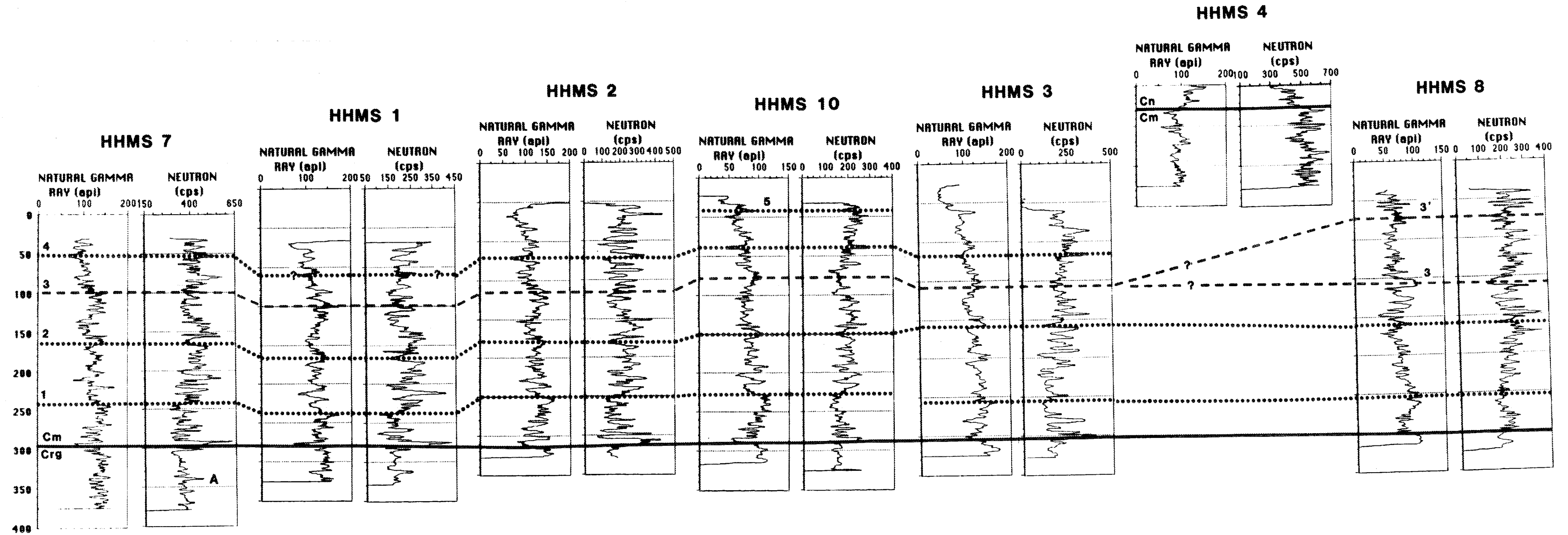


Fig. 5. Stratigraphic correlations observed in the Maryville Limestone determined from natural gamma-ray and epithermal neutron geophysical logs. Solid lines represent formal contacts. The numbered dashed line represents the informal contact between the upper and lower members of Maryville Limestone. Numbered dotted lines represent informal stratigraphic markers within the Maryville Limestone. Detailed discussions of the geophysical log signature are given in Appendix 13.

ORNL-DWG 89-13319

ROGERSVILLE SHALE
RUTLEDGE LIMESTONE
PUMPKIN VALLEY SHALE
HHMS 9

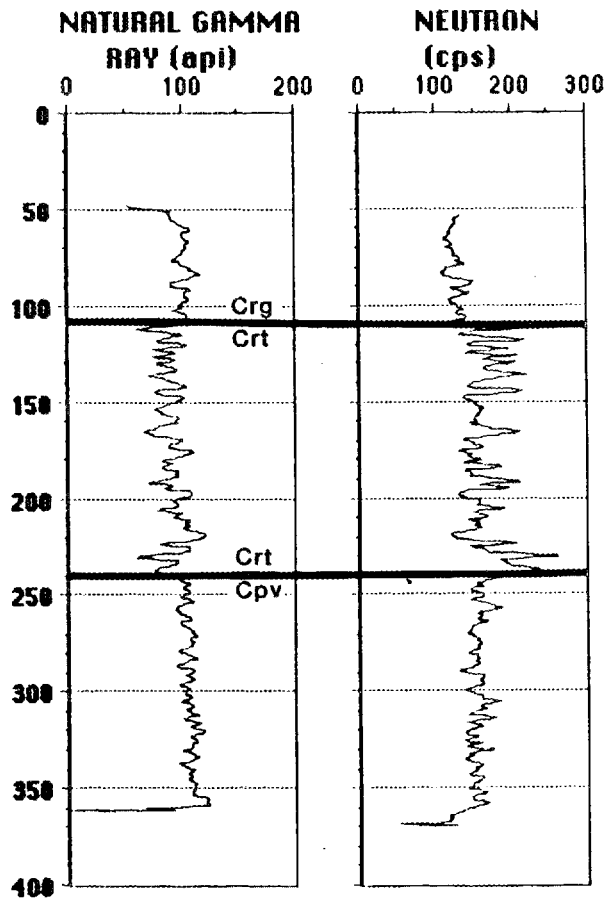


Fig. 6. Stratigraphic correlations observed in the Rogersville Shale, Rutledge Limestone, and Pumpkin Valley Shale determined from natural gamma-ray and epithermal neutron geophysical logs. Solid lines represent formational contacts. Detailed discussions of the geophysical log signature are given in Appendix 13.

The Maynardville Limestone - Nolichucky Shale contact is gradational (Fig. 4). The geophysical log signature of this interval consists of increasing gamma-ray and decreasing neutron values and is characterized by significant changes in baselines for both logs from those typical of most of the Maynardville Limestone. The upper contact of the Nolichucky Shale is placed at the first substantial shale bed within the transition zone at the bottom of the Maynardville Limestone and corresponds to a point where the baselines of the gamma-ray and neutron logs have stabilized at values typical of the Nolichucky Shale (HHMS 11A, Fig. 4).

The Nolichucky Shale - Maryville Limestone contact is marked by a baseline shift to increasing gamma-ray log values and decreasing neutron log values (HHMS 4A and HHMS 5A, Fig. 4). Both the Nolichucky Shale and the Maryville Limestone contain interbedded shales and limestones, and the baseline shifts in the geophysical logs occur because the top of the Maryville Limestone is significantly more limestone-rich than the basal Nolichucky Shale (Haase and others 1985).

The Maryville Limestone - Rogersville Shale contact is not characterized by pronounced baseline shifts on either the gamma or neutron logs but is characterized by a sharp anomaly on the gamma-ray and neutron logs (Fig. 5) that is associated with a prominent limestone bed. The lower Maryville Limestone is significantly more shale-rich than the upper portion (Haase and others 1985) and resembles the underlying Rogersville Shale; thus no significant baseline shift would be expected in these logs.

The Rogersville Shale - Rutledge Limestone contact is characterized by pronounced baseline shifts in both the gamma-ray and neutron logs (Fig. 6). This baseline shift is associated with an increase in the limestone content of the Rutledge Limestone with respect to the Rogersville Shale.

The Rutledge Limestone - Pumpkin Valley Shale contact is characterized by a prominent anomaly on the gamma and neutron logs (Fig. 6). This anomaly has been termed the "three limestone beds" (deLaguna and others 1968) and corresponds to three limestone rich beds within a predominantly shale-rich portion of the lower Rutledge Limestone (Haase and others 1985). There is little baseline shift in the gamma and neutron logs at this contact since lower Rutledge Limestone is shale-rich and is similar to the Pumpkin Valley Shale.

3.3 STRUCTURE

This section summarizes the general structural framework of the upper 400 to 500 ft of strata intersected by HHMS boreholes. In this report, the terms *fracture*, *fault*, *fracture zone* and *fault zone* are used as follows. A *fracture* consists of a crack or rupture. Examination of fractures in outcrop (Dreier and others, 1987) and core (C. T. Lutz, ORNL, Oak Ridge, Tenn., personal communication to R. B. Dreier, ORNL, Oak Ridge, Tenn., 1988) show that fractures in the study area are commonly short, less than 10 cm, and (where it can be determined) show minimal displacements of 0 to 5 cm. A *fault* is an abrupt structural discontinuity that shows relative displacement on either side of the discontinuity and commonly extends tens of meters to kilometers. The term *fault* is more precise than *fracture* and is preferred because it provides more information on the geologic setting. A *fracture zone* is a densely fractured volume of rock. A *fault zone* is a fracture zone that is associated with a major fault.

The structural interpretations are presented in a series of geologic cross sections and are derived from borehole geophysical logs. In order to present as complete an interpretation as possible, other wells have been included in the cross sections. These include WOL-1, DM2, DM3A, DM3RT, and HF4-NW400; their locations are shown on Fig. 7.

Five low-angle thrust faults and a thick (up to 150 ft) deformation zone are identified in this portion of Melton Valley and are shown on interpretive geologic cross sections (Figs. 8 through 12). In addition, new evidence from this report supports the existence of a regional tear fault, the White Oak Creek Fault (WOCF), proposed to underlie White Oak Creek [R. B. Dreier June 1986, Campbell and others (1989)] at the eastern boundary of the Pits and Trenches area (Fig. 7). Table 3 lists the faults that are shown on the cross sections and the borehole data that were used to identify each fault. The criteria for fault identification are described below (Sect. 3.3.1). In general, the strongest evidence for fault identification includes stratigraphic thickness changes, stratigraphic discontinuities, and abrupt dip changes with associated deviation log anomalies. The other criteria listed in Sect. 3.3.1 apply equally to an open fracture or to a single fault. A fault interpretation is used where fault characteristics can be correlated between wells, because it is unlikely that a single fracture will extend several hundred feet, whereas it is very reasonable that a fault or fault zone would show these dimensions.

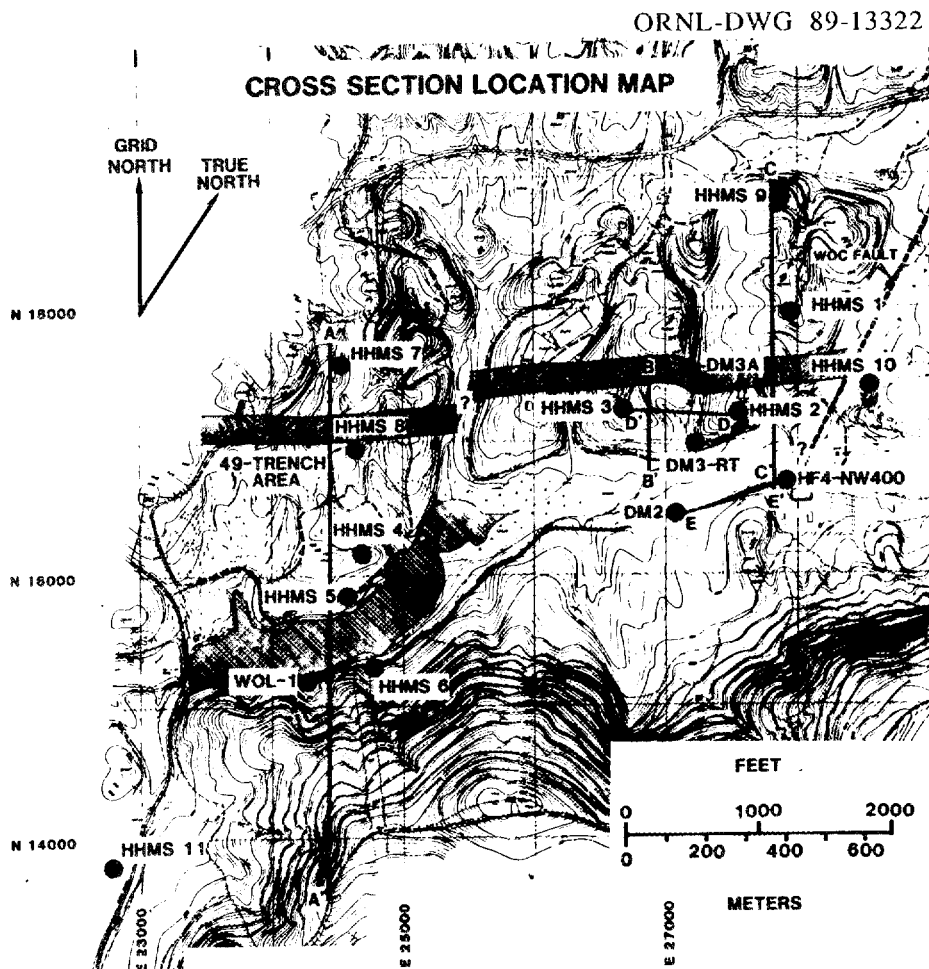


Fig. 7. Location map of the geologic cross sections. Section A - A" is shown in Fig. 8. Section B - B" is shown in Fig. 9. Section C - C" is shown in Fig. 10. Section D - D" is shown in Fig. 11. Section E - E" is shown in Fig. 12. The surface trace of the proposed White Oak Creek Fault is shown between HHMS 1 and HHMS 10 in the floodplain of White Oak Creek. The projected surface trace of the fault zones identified within the Maryville Limestone is shown. These projections are preliminary and need to be confirmed by additional studies.

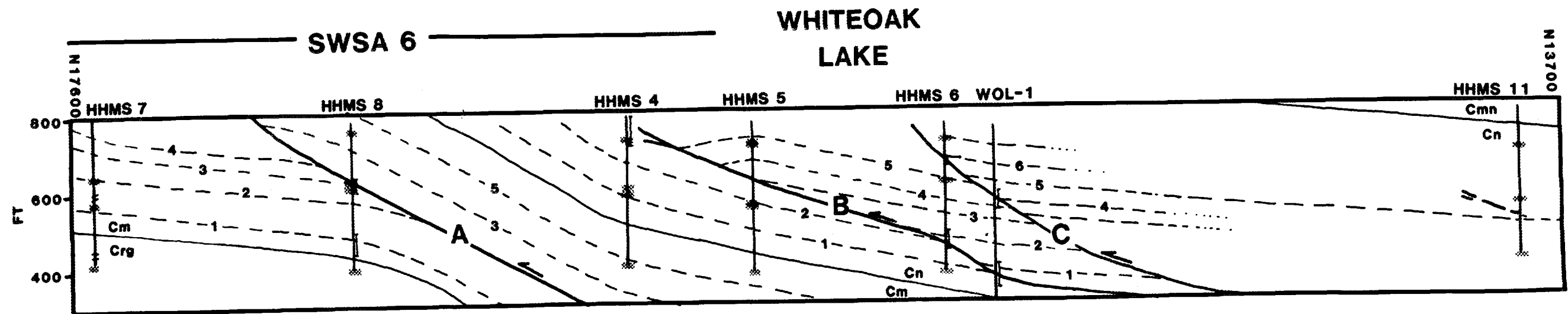


Fig. 8. Strike-perpendicular geologic cross section through SWSA 6 and White Oak Lake. Stratigraphic and structural data from HHMS A boreholes from site 4 through 8, WOL - 1, and HHMS 11A are projected along a grid-east direction to the line of section. Stippled pattern on boreholes shows the open interval of the HHMS A, B, and C wells. The depths of the open intervals for the B and C wells are projected onto the A well by assuming a grid-east strike and by using local dips that are shown in the cross section.

ORNL-DWG 89-12125

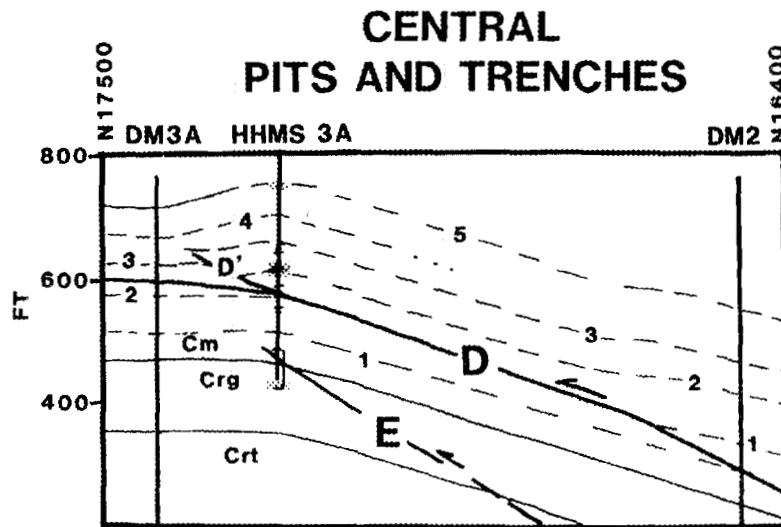


Fig. 9. Strike-perpendicular geologic cross section through the central portion of the Pits and Trenches area. Stratigraphic and structural data from boreholes DM 3A and HHMS 3A are projected along a grid-east direction to the line of section. Data from DM2 are projected along a grid-N74E direction because of local strike changes along the length of the section. Stipled pattern on boreholes shows the open interval of the HHMS A, B and C wells. The depths of the open intervals for the B and C wells are projected onto the A well by assuming a grid-east strike and by using local dips that are shown in the cross section.

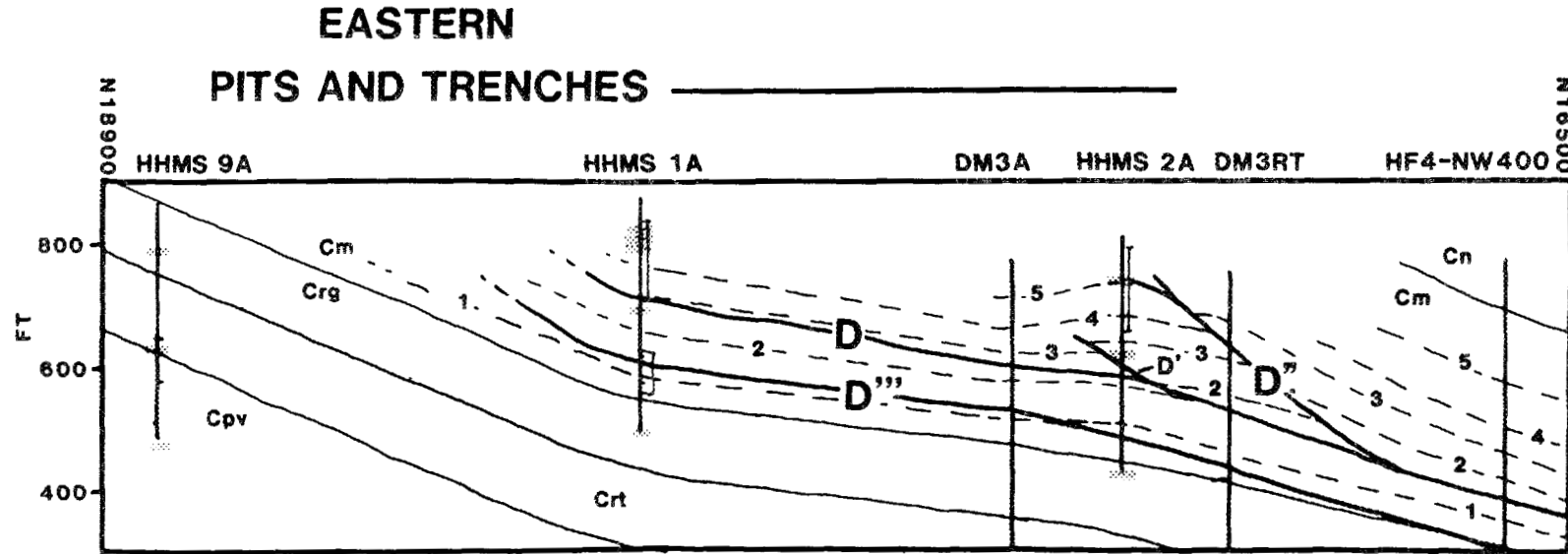


Fig. 10. Strike-perpendicular geologic cross section through the eastern portion of the Pits and Trenches area. Stratigraphic and structural data from boreholes HHMS 9A, HHMS 1A, HHMS 2A, DM3A, and DM3RT are projected along a grid-east direction to the line of section. Data from HF4-NW400 are projected along a grid-N74E direction because of local strike changes along the length of the section. Stipled pattern on boreholes shows the open interval of the HHMS A, B, and C wells. The depths of the open intervals for the HHMS B and C wells are projected onto the A well by assuming a grid-east strike and by using local dips that are shown in the cross section.

ORNL-DWG 89-12386

SOUTHERN PITS AND TRENCHES

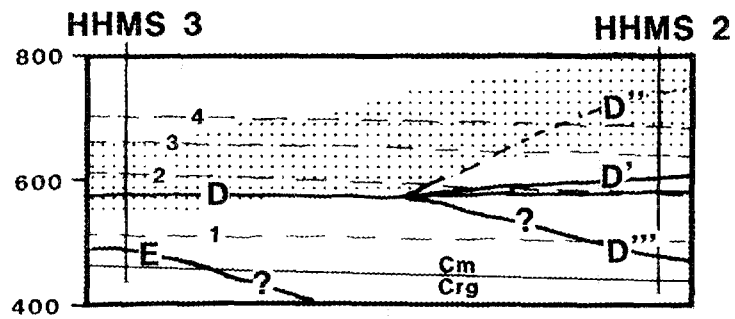


Fig. 11. Strike-parallel geologic cross section through the southern portion of the Pits and Trenches area. Stipled pattern shows a thick deformation zone, which does not correlate directly with identified faults.

ORNL-DWG 89-12388

WHITE OAK CREEK AREA

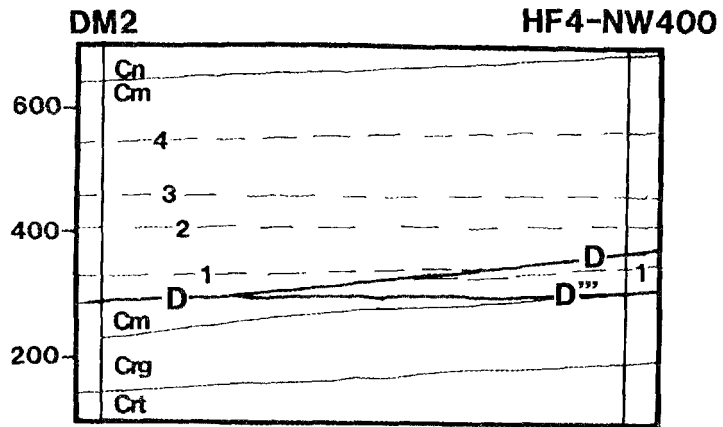


Fig. 12. Strike-parallel geologic cross section along a portion of the White Oak Creek floodplain south of the Pits and Trenches area.

Table 3. Fault Identification Criteria

Fault zone (Well)	Stratigraphic duplication (Gamma-ray Neutron)	Dip changes (BHTV) (dipmeter log)	Borehole televiwer anomalies	Temperature anomalies	Spontaneous potential anomalies	Caliper anomalies	Cycle skips (acoustic velocity log)	Deviation anomalies	Porosity crossplot anomalies	Neutron anomalies
A (HHMS 8A)	X	X	X	X	X ^a	X	NA	X	X	-
B (HHMS 4A)	-	X ^b	-	-	-	-	-	-	NA	-
B (HHMS 5A)	-	X	X	-	-	-	X	X ^a	NA	-
B (HHMS 6A)	-	-	X	-	X	-	-	-	NA	-
B (WOL-1)	-	X	NA	-	X ^a	-	-	-	NA	-
C (HHMS 6A)	X ^c	X	X	-	-	X	-	-	NA	X
C (WOL-1)	-	X	NA	-	-	-	-	-	NA	-
D (DM3A)	-	NA	NA	-	X ^d	X ^d	NA	-	NA	-
D=D' (HHMS 3A)	-	X ^e	X	-	X	X ^a	-	X ^a	NA	-
D (DM2)	X	NA	NA	-	X	X ^a	NA	X ^a	NA	-

Table 3. (continued)

Fault zone (Well)	Stratigraphic duplication (Gamma-ray Neutron)	Dip changes (BHTV) (dipmeter log)	Borehole televiwer anomalies	Temperature anomalies	Spontaneous potential anomalies	Caliper anomalies	Cycle skips (acoustic velocity log)	Deviation anomalies	Porosity crossplot anomalies	Neutron anomalies
D (HHMS 1A)	-	X	-	X ^a	X ^a	-	X ^a	-	NA	-
D (HHMS 2A)	-	-	X	X	-	-	-	-	NA	-
D (DM3RT)	X ^c	NA	NA	NA	-	-	X	NA	NA	-
D (HF4-NW400)	-	NA	NA	-	X	X	-	NA	NA	-
D' (HHMS 2A)	X ^c	X ^e	X	X	-	X ^a	-	-	NA	-
D'' (DM3RT)	X	NA	NA	NA	-	X	-	NA	NA	-
D''' (HHMS 1A)	-	-	X	X ^a	X	-	-	-	NA	-
D''' (DM3A)	-	NA	NA	-	X ^d	X ^d	NA	-	NA	-
D''' (HHMS 2A)	-	-	X	-	-	-	-	X ^a	NA	-
D''' (DM3RT)	-	NA	NA	NA	X	-	-	NA	NA	-

Table 3. (continued)

Fault zone (Well)	Stratigraphic duplication (Gamma-ray Neutron)	Dip changes (BHTV) (dipmeter log)	Borehole viewer anomalies	Temperature anomalies	Spontaneous potential anomalies	Caliper anomalies	Cycle skips (acoustic velocity log)	Deviation anomalies	Porosity crossplot anomalies	Neutron anomalies
D ^{'''} (HF4-NW400)	-	NA	NA	-	X	X	-	NA	NA	-
E (HHMS 3A)	-	-	X	X	-	X	-	-	NA	-
TDZ ^f (DM3A)	-	-	-	-	X ^d	X ^d	-	-	NA	-
TDZ ^f (HHMS 3A)	-	-	X	X	-	X	-	-	NA	-
TDZ ^f (HHMS 1A)	-	X	-	-	-	-	X	-	NA	-
TDZ ^f (HHMS 2A)	-	X	-	-	-	X	X	-	NA	-

^a Supporting, not independent, evidence.

^b Steeply dipping beds in front of leading edge of fault.

^c Apparent thickening of strata, no duplication of stratigraphic markers.

^d Entire borehole shows anomalies.

^e Dip change is interpreted from stratigraphic correlation, not borehole viewer or dipmeter log.

^f Thick deformation zone.

HHMS A wells for sites 9 through 11 are not listed in Table 3. Both HHMS 9A and HHMS 11A are at the ends of the cross sections, and fault zones observed in these wells could not be correlated with zones in neighboring wells. HHMS 9 does not show enough stratigraphic overlap with HHMS 1A (Fig. 10), and probable fault zones identified in HHMS 11A are not observed in HHMS 6A (Fig. 8). HHMS 10A is not included on the cross sections because it is located on the other side of the proposed WOCF. However, it is discussed later (Sect. 3.3.3.2).

3.2.1 Criteria for Identifying Fault Zones, Faults or Fractures

Stratigraphic duplication. Measured downhole thicknesses of geologic units commonly increase, sometimes substantially, between boreholes, or a marker horizon appears to be repeated in a borehole. Such apparent thickness changes may result from structural duplication of the strata caused by low-angle thrust faulting. Where thickness changes could be reasonably accommodated by the presence of a local fault, this interpretation is used instead of local stratigraphic thickening.

Regional dip changes. Abrupt changes in dip are commonly associated with fault zones, and they represent a rotation of the strata before or during fault displacement. These changes can be determined from a BHTV log or a dipmeter log. These logs are available only from the HHMS wells and from WOL-1.

Deviation anomalies. During drilling, a borehole will commonly change orientation from vertical so that it is normal to bedding. Hence, if the deviation log shows a significant trend or dip change, this suggests that the bedding has changed orientation. It is preferable that fault evidence from deviation data be backed up by other geophysical logs such as the BHTV and dipmeter logs, which have a better resolution on the depth of dip change. Deviation data are not available from DM3RT and HF4-NW400.

BHTV anomalies. The BHTV log presents a three-dimensional picture of the borehole by measuring acoustic impedance of the entire borehole wall. Fractures commonly have contrasting acoustic properties with the surrounding rock and are represented on the logs as dark sinusoidal curves. This log is extremely sensitive to borehole rugosity, and the signal is difficult to interpret in rough portions of a borehole. Unfortunately, it can be difficult to drill through a thick deformed zone, and the resultant borehole, especially if it is drilled by air-rotary methods, is generally rough in these zones. Nevertheless, faults or fractures

have been independently interpreted by C. M. Beaudoin (a student intern at ORNL) and R. B. Dreier in these zones, and they usually correlate with other geophysical anomalies (Table 3).

Temperature anomalies. The temperature log records a temperature profile of the standing column of water in a borehole. If the tool has a fine resolution and the standing column of water has not been disturbed, much information can be derived from these logs. In particular, temperature deflections represent horizons where water of contrasting temperature has entered the borehole, presumably from a fracture or fault. In some cases, the deflections show an increase of 2 - 5° F (HHMS 8A and HHMS 3A), and these deflections are interpreted as water that has been transported from a deeper source along a fault zone. For example, analysis of HHMS temperature logs shows an average gradient of 1°F/100 ft. Hence, a 5° F increase suggests that the source of the water is at least 500 ft below the logging interval. The quality of the temperature log can vary considerably, depending on the logging procedure. It should be the first tool that enters the borehole so the water is undisturbed, and the signal should be recorded as the tool is slowly lowered into the borehole. A temperature log is not available from DM3RT.

SP anomalies. In Melton Valley, deflections in the SP logs from the Conasauga Group rarely correspond to stratigraphic changes, as is commonly the case in other geologic environments, and the logs generally show a smooth signature with minor deflections. Haase and King (1986) suggest that at the ORR, SP log deflections are related to streaming potential; that is, they are marking fluid transport, in this case along fractures. This interpretation is supported by data from the HHMS wells because SP anomalies commonly correspond to BHTV, temperature, or caliper anomalies (Table 3).

Caliper anomalies. If bedding is disrupted or steeply dipping, as is common in fault zones, it can be difficult to drill, and the resultant borehole, especially if it is drilled by air-rotary methods, is generally rough in these zones. In addition, open fractures or faults can be detected by a caliper log and recorded as thin (dependent on the resolution of the tool) horizons with increased borehole diameter.

Cycle skips. The acoustic velocity log [or interval transit time log (ITT) or sonic log] measures the velocity of an acoustic signal as it is transmitted through the borehole wall. If the signal is substantially attenuated because of an open water-filled fracture, it is not

detected by the receiver and the arrival of a subsequent pulse is treated as a first arrival (cycle skip). This signal shows up as a sharp spike on the acoustic log and is useful for detecting fractures. Newer recording systems automatically recognize cycle skips and delete them from the record because they interfere with the velocity analysis. This was the case for the HHMS A wells from sites 8 through 11 and WOL-1. However the velocity logs for the HHMS A wells from sites 1 through 7, DM3RT, and HF4-NW400 could show cycle skips. Sonic logs are not available for DM3A and DM2.

Porosity crossplot log. Porosity crossplots can be used to identify horizons with enhanced fracture (secondary) porosity. They are compiled with digital data from the neutron porosity log and the ITT log. The neutron porosity was calculated by Gearhardt Industries, Inc., from epithermal neutron data that were also acquired by Gearhardt Industries, Inc. Neutron porosity is sensitive to total porosity (primary and secondary) because it is strongly influenced by the presence of hydrogen. On the other hand, porosity measurements derived from the ITT log are indicative only of matrix porosity, not of fracture porosity. The sonic signal that gives the first arrival time travels preferentially through the rock matrix as opposed to vugs or fractures (Keys and MacCary 1971). Hence, high values of neutron porosity relative to ITT values show regions of increased secondary porosity (Fig. 13).

The crossplot for HHMS 8A shows a fracture porosity over a wide range of ITT values representative of the varying shales and carbonates common to the Maryville Limestone (Fig. 13). Thus, development of a fracture porosity is not constrained to a particular rock type.

To illustrate graphically the depth relationships of the porosity crossplot, a value has been assigned to each data point equivalent to the zero ITT-intercept of a line that intersects the data point and is parallel to the overall trend of the data. On such porosity crossplot logs, higher zero-intercept values correspond to relatively higher fracture porosity values (see porosity crossplot logs in Appendixes 8 through 11). Porosity crossplots are available only for HHMS A boreholes from sites 8 through 11 because digital geophysical data from these boreholes were of a sufficiently high caliber to form a linear trend on the crossplot. Geophysical logs from other boreholes were not used. Because they were recorded with analog techniques, data resolution was lost in their subsequent manual digitization, and crossplots constructed from the data did not show a linear trend.

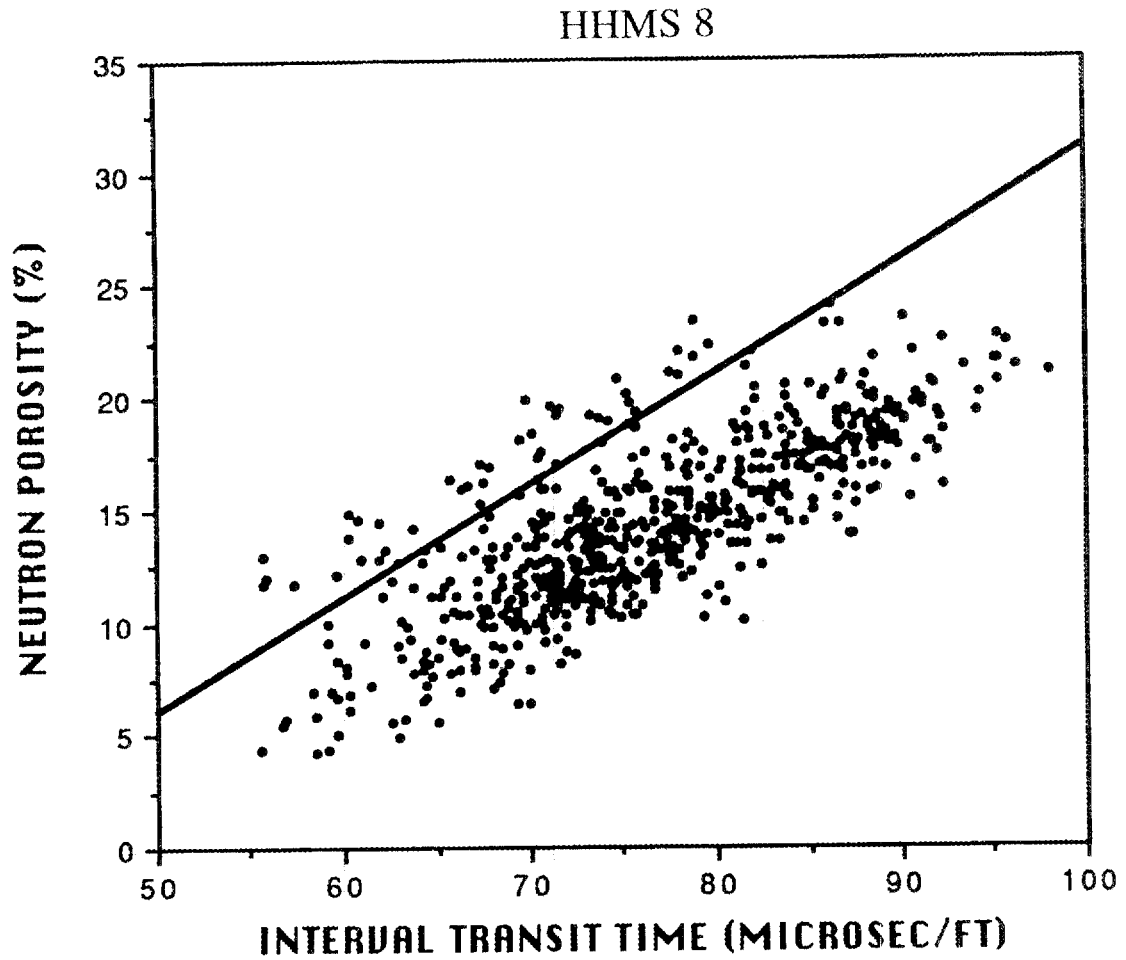


Fig. 13. Porosity crossplot determined from epithermal neutron and interval transit time data from borehole HHMS 8A. Data points above the solid line represent horizons with elevated fracture, or secondary, porosity.

Neutron anomalies. Neutron anomalies are rarely observed in the HHMS geophysical data. However, because the neutron log is sensitive to hydrogen, this log is potentially important for detecting open, as opposed to healed, fractures. Neutron and natural gamma-ray logs generally appear as mirror images of each other (see Figs. 4 and 5) because the signal reflects local lithologic changes that are detected by both log types. Neutron anomalies occur when a neutron signal decrease is not matched by a corresponding gamma-ray signal increase. In this case, the increase in hydrogen content (as shown by a decrease in the count-per-second reading) is not related to an increase in clay minerals (with chemically bound hydrogen) but is interpreted to result from an increase in water in an open fracture. The gamma-ray log is not as sensitive to porosity changes as the neutron log.

3.3.2 Cross Section Discussion

Five minor thrust faults (A-E) are identified in the vicinity of White Oak Lake (Fig. 8), in the central and southern portions of SWSA 6 (Fig. 8) and the Pits and Trenches area (Figs. 9 through 12). The faults appear to be related to minor changes in the shape of the CCTS. Interpretation of seismic reflection data by R. B. Dreier suggests that this portion of the CCTS is very shallowly dipping at approximately 5° to the grid-south. These dip values are also observed between WOL-1 and HHMS 11 (Fig. 8). North of WOL-1, however, dip values increase to $10\text{-}25^\circ$ (Figs. 8 and 9), and this change most likely reflects a change in the geometry of the Copper Creek Fault. The thrust faults form as a mechanism to accommodate the resultant shape and local volume changes of the strata.

The presence of thrust faults is supported in part by surface data. There are slight changes in contaminant movement trends (deLaguna and others 1958) near the projected surface trace of fault system D in the western portion of the Pits and Trenches area. This area also shows an increase in fold intensity observed from historical photographs taken of trench walls in the projected fault zone. In addition, surface investigations in SWSA 6 show significant folding and faulting south of fault B, and a change in strike that coincides with the projected surface trace of this fault (Dreier and others, 1987). The projected surface trace of the fault zones identified within the Maryville Limestone are shown in Fig. 7. These projections are preliminary and need to be confirmed by additional studies directed toward constructing a detailed geologic map of Melton Valley.

The amount of displacement along these faults is relatively minor in comparison to the regional thrust faults of the area, which show displacements on the order of miles. Note

however, that development of a fracture zone associated with a fault is not dependent on the amount of displacement (see Sect. 3.3.3.1). Fault displacement is interpreted to be greatest for fault A, which shows approximately 250 ft of movement (Fig. 8). Other faults have displacement (faults B, C, and D; Figs. 7, 8, and 9) on the order of 20 to 75 ft because these thrusts are low-angle imbricates that transect the stratigraphy. If the stratigraphy is not thickened or duplicated, displacement is considered to be minimal. Comparison of stratigraphic thicknesses (Figs. 4 through 6; Haase and others 1985) shows that formation thicknesses remain fairly constant, and no consistent stratigraphic duplication occurs across the study area. Thus, the thrusts are laterally discontinuous structures (Figs. 8 through 12).

Several regional-scale folds (wavelengths of several hundred feet) have formed as a result of local faulting. The most prominent of these are centered about HHMS 5A (Fig. 7), HHMS 3A (Fig. 8) and HHMS 2A (Fig. 9). In each case, the northern fold limb with north-trending dip direction is substantiated by BHTV data. In addition, stratigraphic correlations of HHMS 2A and HHMS 3A with DM3A also support a northerly dip between these wells.

Strike-parallel fault-pattern interpretations in the Pits and Trenches area show a complex transition from a single fault in the central part of the area to a system of related faults in the eastern portion (Figs. 11 and 12). In general, Fault D appears to climb up stratigraphic section to the east. However, this feature is masked by the initiation of faults D', D'', and D'''. In the northern part of the area, this transition is placed at a grid-north-trending topographic depression (Figs. 7 and 11), which may represent a local small tear fault or transfer zone in the CCTS. South of the Pits and Trenches area (Fig. 11), the continuation of the tear fault is not clear-cut, and the transition from single to multiple faults has been placed farther to the west.

Faults D' and D'' are imbricate splays off D. However, the relationship between faults D and D''' is not as straightforward. In the cross sections presented here, D''' is considered to be another imbricate splay off D, and the imbrications occur south of HF4-NW400 (Fig. 9). Alternate interpretations are possible. For example D''' may not merge with D along strike but may die out east of HHMS 3A and DM2. Similarly, D may not continue from HHMS 2A to HHMS 1A but may end as D' (Fig. 9).

Fault E, which occurs at the base of HHMS 3A, has not been correlated with any other faults in the Pits and Trenches area (Fig. 11), primarily because the temperature log anomaly (Appendix 3) suggests that it is in hydrologic communication with deeper-seated strata. Although no other Pits and Trenches boreholes show such a strong temperature deflection (Appendixes 1 and 2), fault A, observed in HHMS 8A in SWSA 6, shows a similar temperature deflection. If fault A is correlated with fault E on the basis of temperature data, this suggests that the fault has cut down section to the east (along strike), from the middle of the Maryville Limestone to the Rogersville Shale. Alternatively, a correlation based on common stratigraphy would favor linking fault A with fault D since both occur in the middle part of the Maryville Limestone. Another interpretation includes merging all the faults within the upper Rogersville Shale - lower Maryville Limestone (faults A, D, D', D'', D''', and E) into one fault system, similar to the D fault system. Currently, it is not possible to differentiate between the interpretations although the A-E correlation is favored because of the temperature data

A deformation zone, approximately 150 ft thick, is identified in the HHMS A wells in sites 1 through 3 and is listed in Table 3. This interval corresponds to the upper 150 ft in HHMS 1A and HHMS 2A and corresponds to downhole depths between 160 and 275 ft in HHMS 3A. Although fractures or faults can be identified throughout the interval, they do not correspond to the larger, more regionally extensive faults (faults D and E; Fig. 11). A deformed interval near the contact of the the upper and lower Maryville Limestone had previously been noted in ORNL Joy No. 2 (Haase and others 1985) and may be equivalent to this zone. Because ORNL Joy No. 2 is located to the south on Copper Ridge in an area with shallow dips and no local faulting, this zone may be an interval of inherited deformation. Some or all of the structural fabric may have formed during an earlier deformation phase in the tectonic transport history when the CCTS moved over a different portion of the White Oak Mountain Thrust Sheet. The deformed zone associated with the middle Maryville Limestone may have localized later faulting, so that preexisting zones of weakness are simply reactivated during displacement of faults A and D.

In summary, geologic cross sections can be used to determine the occurrence and the two- or three-dimensional shape of potential flow paths concentrated near faults and fault zones. Several generalizations can be made about the occurrence of faults in Melton Valley. (1) Thrust faults with minor amount of displacement (20 to 250 ft) are common within the CCTS, particularly within the Nolichucky Shale and the Maryville Limestone. (2) These

faults form to accommodate shape changes of the CCTS. Hence other areas that show an uneven thrust sheet shape should also contain minor thrust faults. (3) Thrust faults commonly diverge to form imbricate splays (e.g. fault system D). (4) Horizons with a preexisting structural fabric may partly control the location or initiation of these minor thrust faults. (5) Correlating thrust faults along a strike-parallel direction is difficult because the faults can cut either up or down the stratigraphic section or may die out along strike. (6) Although these faults show minor displacement, associated fracture zones can develop before and during fault displacement. This is described further in Sect. 3.3.3 and other hydrologic aspects of faulting are discussed in Sect. 5.1.

3.3.3 Fault Zone Characterization

The geophysical log data suggest that well-developed fault zones, such as those in Melton Valley, have complex geologic characteristics. Implicitly, the corresponding hydrology should also be complex. However, before hydrologic data can be correctly interpreted within the context of a fault zone, it is important to characterize the zone as completely as possible. Geophysical logs from HHMS 8A best show an example of a fracture zone associated with a local thrust fault. Similarly, geophysical logs from HHMS 10A best represent the geology near a fracture zone associated with a local high-angle tear fault. Logs from both wells will be used to illustrate representative fault zones.

3.3.3.1 Thrust Fault--HHMS 8A

Comparisons of the BHTV and porosity crossplot logs show that the total thickness of the fracture zone is approximately 25 ft. The BHTV log (Appendix 8) shows a marked change in the structural orientation of the strata at 150 ft. The lower boundary of the fracture zone, placed at 173 ft, is gradational and is marked by a continuous decrease in structural dip. The porosity crossplot log for HHMS 8A shows elevated fracture porosity in the interval from 147 to 163 ft and from 168 to 170 ft (Appendix 8).

The fault plane, as identified from the BHTV log with supporting evidence from the caliper log, divides this larger zone into two smaller fracture zones--a hanging-wall and a footwall fracture zone. Identification of the fault plane within the fracture zone has been placed at 159 ft because of an abrupt change from steeply dipping to shallowly dipping beds observed on the BHTV log (Appendix 8). An additional fault splay is also identified from the BHTV log at 153 ft by an abrupt change in dip direction (Appendix 8). The caliper log

shows a fairly rough hole for the entire depth of the well; however, there is one deflection at 159.5 ft that may correspond to the fault plane (Appendix 8).

The temperature and dual-induction logs suggest that there is very limited hydrologic communication between the footwall and hanging-wall fracture zones, and the fault plane may be a relatively impermeable boundary that separates the two fracture zones. Both logs show distinctly contrasting signatures for the hanging-wall and footwall fracture zones, although both zones sample the same lithology. The strongest temperature deflection at 159 to 178 ft is completely contained within the footwall of the fault zone. In addition, the 6° F temperature deflection in the footwall fracture zone suggests that the fluid may have been transported up along this zone a minimum of 600 ft, assuming an approximate thermal gradient of 1°F/100 ft. The average temperature gradient for the 11 HHMS sites is 0.91°F/100 ft, and the average gradient for wells logged by Gearhart Co. under better logging conditions (see Sect. 2.1), is 1.09°F/100 ft. A deep source of fluids is also supported by water sample electrical conductivity measurements, where the conductivity of HHMS 8B, which samples the fracture zone, is greater than that of HHMS 8A (3.0 vs. 1.9 mS/cm). The dual-induction log shows a relatively sharp transition between 153 and 163 ft in the relative resistance of the medium- and deep-induction signal, which corresponds to the location of the fault plane.

3.3.3.2 Tear Fault--HHMS 10A

Another fracture zone common to this area is associated with high-angle tear faults. The most prominent of these faults in Melton Valley is the WOCF underneath White Oak Creek. HHMS 10A is collared between 150 and 450 ft from the surface trace of the fault plane. Although it is unlikely that the borehole is drilled through the fault plane, the borehole is close enough to the fault so that effects of the fracture zone may be observed.

A borehole located near a tear fault is expected to show a characteristic fracture behavior over large intervals because the associated fracture zone is near-vertical and subparallel to the borehole. In contrast, thrust-related fracture zones intersect vertical boreholes over a short interval. The logs for HHMS 10A (Appendix 10) appear to show a response to fracturing over large downhole depth intervals, which is presumably related to the WOCF. The temperature log is quite ragged over almost the entire borehole and does not show a linear base line, although linear temperature gradients are observed for other HHMS A wells. This nonlinear trend may result from water of varying temperature entering the

borehole over a large fractured interval, so that the temperature profile is caused by convective as well as conductive heat transfer.

The porosity crossplot log reveals several zones of enhanced fracture porosity beginning at depths of 119 ft and continuing to 296 ft. Comparison of the dual-induction log with the porosity crossplot log suggests that most secondary porosity is confined to carbonate-rich horizons. Porosity crossplot correlations with the temperature log are not as clear as with HHMS 8A. Most crossplot anomalies show up in the central portion of the borehole, whereas temperature deflections become more pronounced at the bottom of the borehole. There is overlap, however, of fracture porosity and temperature deflections between 220 and 300 ft.

The dual-induction log for HHMS 10A differs significantly from other dual-induction or resistivity logs run in Melton Valley. There is a persistent separation between the medium- and deep-induction logs, which can be an indication of borehole fluid infiltration through fractures into the rock immediately surrounding the borehole. In addition, the deep-induction log, which penetrates the farthest into the strata, shows a response that is consistently more electrically conductive than the medium-induction log, even at shallow borehole depths. This has not been observed in dual-induction logs from other HHMS A wells, where the deep-induction log normally shows a transition from a less conductive to a more conductive signal with respect to the medium-induction log.

4. HYDROGEOLOGY AND GROUNDWATER GEOCHEMISTRY

4.1 INTRODUCTION

The regional groundwater flow system at depth on the ORR could provide a path for contaminants to move off-site if contaminated groundwater enters this system and if the discharge areas are off-site. The potential for flow from a (contaminated) shallow flow system to a deep system is a function of the hydraulic gradient (difference in potentiometric head) and the hydraulic conductivity. Flow is from higher potential to lower potential, and has greater magnitude with higher hydraulic conductivity. An additional factor in determining the groundwater travel time (average linear velocity) is the effective porosity; for example, a tight formation in some cases can transport a particle of water faster by a narrow pathway. As a final step in understanding connectivity between different flow systems, groundwater geochemistry can sometimes be distinct for different systems, which may help confirm hypotheses about travel paths.

Thus, our understanding about the flow system and the potential for vertical connectivity is divided into three sections: potentiometric head data, hydraulic conductivity measurements, and some preliminary groundwater geochemistry data. The final factor in studying this problem is to determine the location of the deep, regional flow system. This question is introduced in this section and discussed in Sect. 5.2 in conjunction with geologic data.

4.2 POTENTIOMETRIC HEAD

4.2.1 Methods

HHMS clusters 1 through 3 were drilled in spring 1986, and continuous digital punch recorders were installed in August of that year. HHMS clusters 4 through 6, plus HHMS 7A were drilled in summer and fall 1986, and recorders were installed in late May 1987. The recorders use a float-and-pulley system with tape punches to record the hourly water level. The USGS maintained the recorders, processed the data, and provided a computer data base of daily average water levels (Zehner 1989) until October 1988, when funding for this project was stopped.

In addition, weekly to biweekly water level measurements were made with an echo sounding device from January 1987 until the recorders were installed. Echo sounding measurements taken the day before the recorders were installed were not consistent with

subsequent recorder measurements. Therefore, the echo data presented here were corrected by subtracting the difference between the two values, the echo sounder typically measuring 4 ft less than the recorder. Gaps in the data records for the hydrographs are caused by recorder down time (minimal), water sampling, and hydraulic conductivity tests.

The hydrographs of the new wells are for the most part taken from weekly measurements with an echo sounder. A few pressure transducers and data loggers were available to collect continuous data in two clusters (HHMS 7B and HHMS 7C and in HHMS 8B and HHMS C) until the equipment had to be removed for installation of a cap in the SWSA 6 area. At that time the transducers were moved to HHMS 9B and HHMS 9C and to HHMS 11B and HHMS 11C.

4.2.2 Hydrographs

Water level hydrographs show (1) how responsive a well is to precipitation events and (2) whether different wells have similar response patterns. If the wells are in the same flow system, their response pattern tends to be similar. Deeper wells might lag in their response or have no response to precipitation events, depending on distance from the recharge area and storativity.

The hydrographs of the intermediate and shallow wells drilled in FY 1986 with the exception of HHMS 3B show significant response to rainfall (Appendix 13). The daily rainfall data for comparison with the hydrographs were available from the 49-trench area of SWSA 6. The wells show responses to events such as the mid-January 1987 precipitation and the reduced rainfall in late spring and summer of 1987 and 1988. Shallow wells HHMS 2C and HHMS 3C fluctuate rapidly. The peaks of wells HHMS 1C, HHMS 1B and HHMS 2B show some lag time from the rainfall events. HHMS 3B recovered slowly and shows only a subdued response to precipitation. The water levels in the HHMS B and C wells fluctuate approximately 2 to 10 ft over wet and dry seasons. A similar magnitude of fluctuation is seen in shallower (10 to 50 ft deep) wells located in Melton Valley.

The HHMS B and C wells at clusters 1, 4, 5, and 6 have quite similar hydrographs, and the shallow and intermediate wells are probably hydraulically connected. HHMS 2B has a subdued match to HHMS 2C. HHMS 3B does not seem to be locally connected to HHMS 3C, which may be related to the fault zone indicated in the geophysical logs (Fig. 9; also see Sect. 5.1).

Because the hydrographs of the wells drilled in FY 1988 are for the most part taken from weekly measurements, rainfall response is not as clear (Appendix 13). HHMS 8C and the USGS wells near HHMS 10A have variable water levels that appear to be responsive to rainfall. The B and C wells in HHMS cluster 7 had recorders that monitor daily average water level, but these wells do not show immediate rainfall response. HHMS 8B and HHMS 9B responded more slowly to dewatering from drilling than the HHMS C wells and other HHMS B wells, which may indicate they are in a zone that is less responsive to recharge events.

The hydrographs of the deep (HHMS A) wells are distinctly different from the shallow and intermediate wells and probably represent a separate flow system. The depth rather than the geologic unit seems to be the key factor since these deep wells have open intervals in three different formations: the Nolichucky Shale, the Maryville Limestone, and the Rogersville Shale. Most of the HHMS A wells have not yet recovered from drilling (i.e. water from the surrounding rock is flowing slowly into the bore hole and equilibrium has not yet been established). The heads in wells HHMS 2A and HHMS 3A leveled off and reached a hydraulic potential within 5 ft of water levels in the shallow and intermediate wells after about a year. HHMS 7A approached recovery after about a year and a half, and HHMS 1A recovered over 2 years after drilling. The heads in the other deep wells are still rising. The estimation of hydraulic conductivity from the slow recovery is discussed in Sect. 4.3.2.

4.2.3 Hydraulic Gradients

Generalized maps of potentiometric head for the HHMS B and C wells (Figs. 14 and 15) show gradients of about 0.005 toward White Oak Lake and White Oak Creek at both depths. Only data from the HHMS wells were used to construct these maps.

Vertical gradients between the HHMS B and C wells range from 0.2 to 0.006. The gradients do not imply anything about the connectivity between the different depths. The steepest gradient observed was between HHMS 9B and HHMS 9C. It has already been noted that HHMS 9B recovered more slowly from drilling than other HHMS B wells, so it may be finished in a separate flow system. For wells located on hilltops (Fig. 2), the vertical gradients were generally downward, with the exception of HHMS 2. The wells

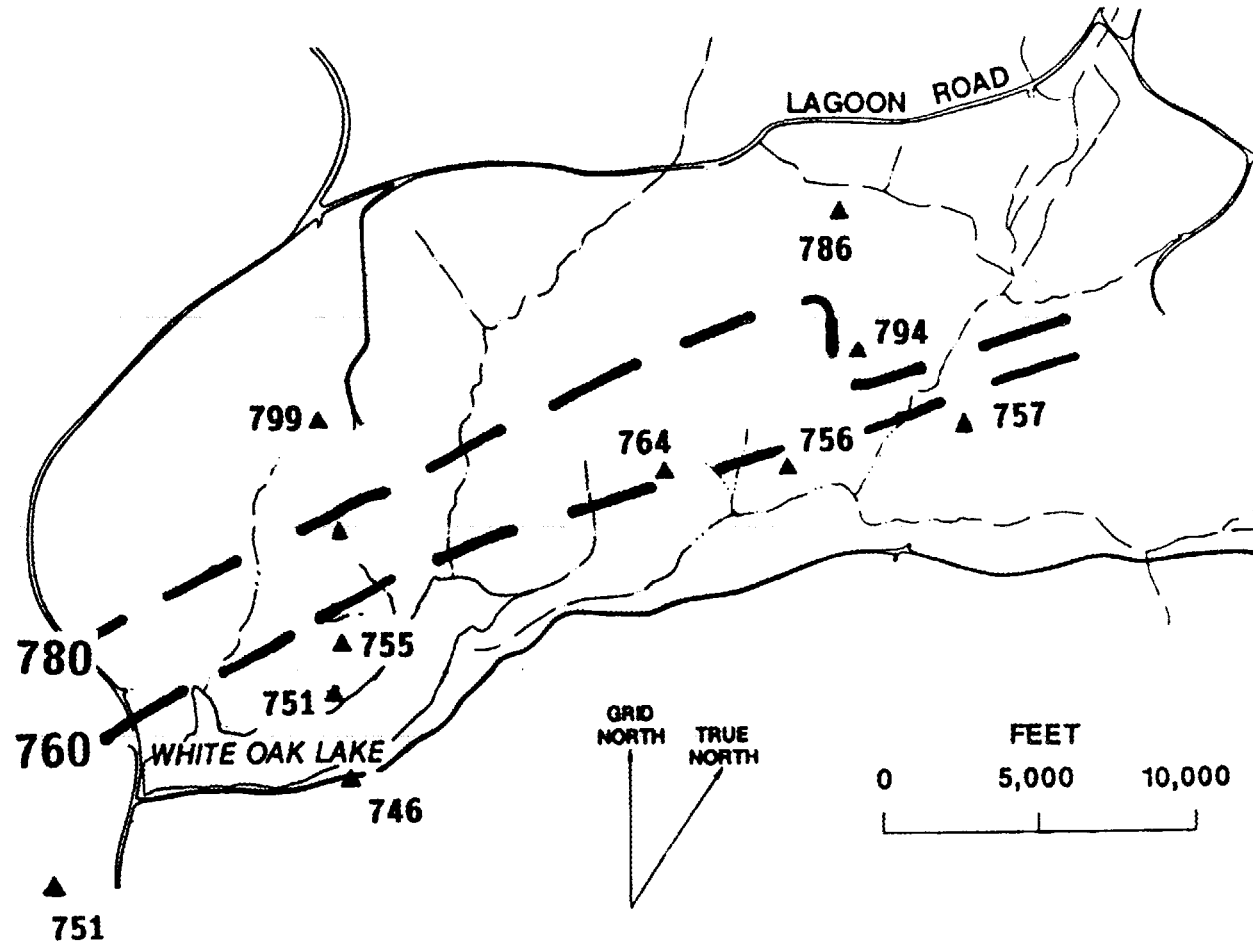


Fig. 14. Generalized potentiometric surface for HHMS B wells. These are intermediate depth wells, 165 to 250 ft deep, and water level measurements were made in summer 1988. Data points and contours are in feet above mean sea level. Contours are approximate.

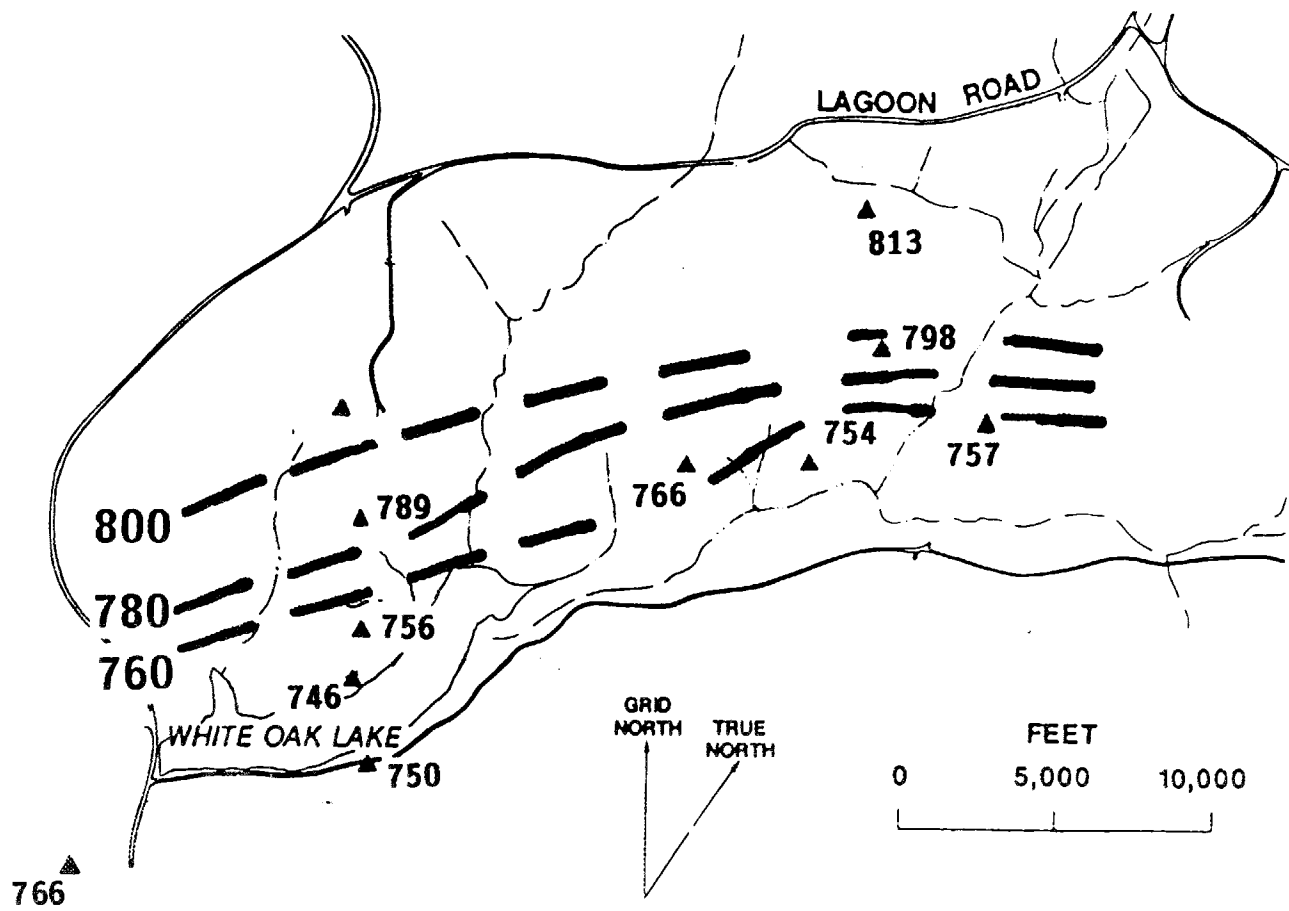


Fig. 15. Generalized potentiometric surface for HHMS C wells. These are shallow wells, 60 to 115 ft deep, and water level measurements were made in summer 1988. Data points and contours are in feet above mean sea level. Contours are approximate.

located on valley slopes showed both upward (HHMS 5 and HHMS 11) and downward (HHMS sites 6, 7, 8, and 10) gradients.

The groundwater flow patterns in cross section can be difficult to interpret. For example, a cross section across White Oak Lake can be interpreted to indicate the lake is a discharge area with the contours showing anisotropy caused by preferential flow along tilted bedding planes (Fig. 16a). However, there could be underflow below the lake since there is a significant gradient from HHMS 5B to HHMS 6B (Fig. 16b). These two interpretations cannot be distinguished until more data are available, in particular more detailed vertical sampling of heads. Webster and Bradley (1988) found discharge to a depth of about 150 ft into White Oak Creek south of SWSA 5, but deeper data are lacking.

The difficulty in interpreting vertical cross sections with only two vertically distributed data points has led to the suggestion of a new construction design, using a single piezometer with multilevel monitoring at more depths. The new piezometer design is discussed later (Sect. 5.4).

4.3 HYDRAULIC CONDUCTIVITY MEASUREMENTS

4.3.1 Methods

Three methods were used to estimate hydraulic conductivity (K) in the HHMS wells: short-term slug tests, slug tests using the slow water level recovery after drilling, and packer tests (Toran 1988b). All of these methods involved changing the potentiometric head in a well, then measuring the water level response to the stress in order to calculate K . The analysis of data from slow recovery is not a standard technique, but was attempted as a research component of this project, and has provided useful information. Although all three methods were single borehole techniques, they potentially have different radii of influence. Thus, caution should be used in comparing data from the different methods. In particular, the hydraulic conductivities from the HHMS A wells were estimated from the slow recovery rather than the standard slug test used for the HHMS B and HHMS C wells. In cases where more than one method could be used, the K values can be compared. Discussion on comparison of the methods is provided in the results section.

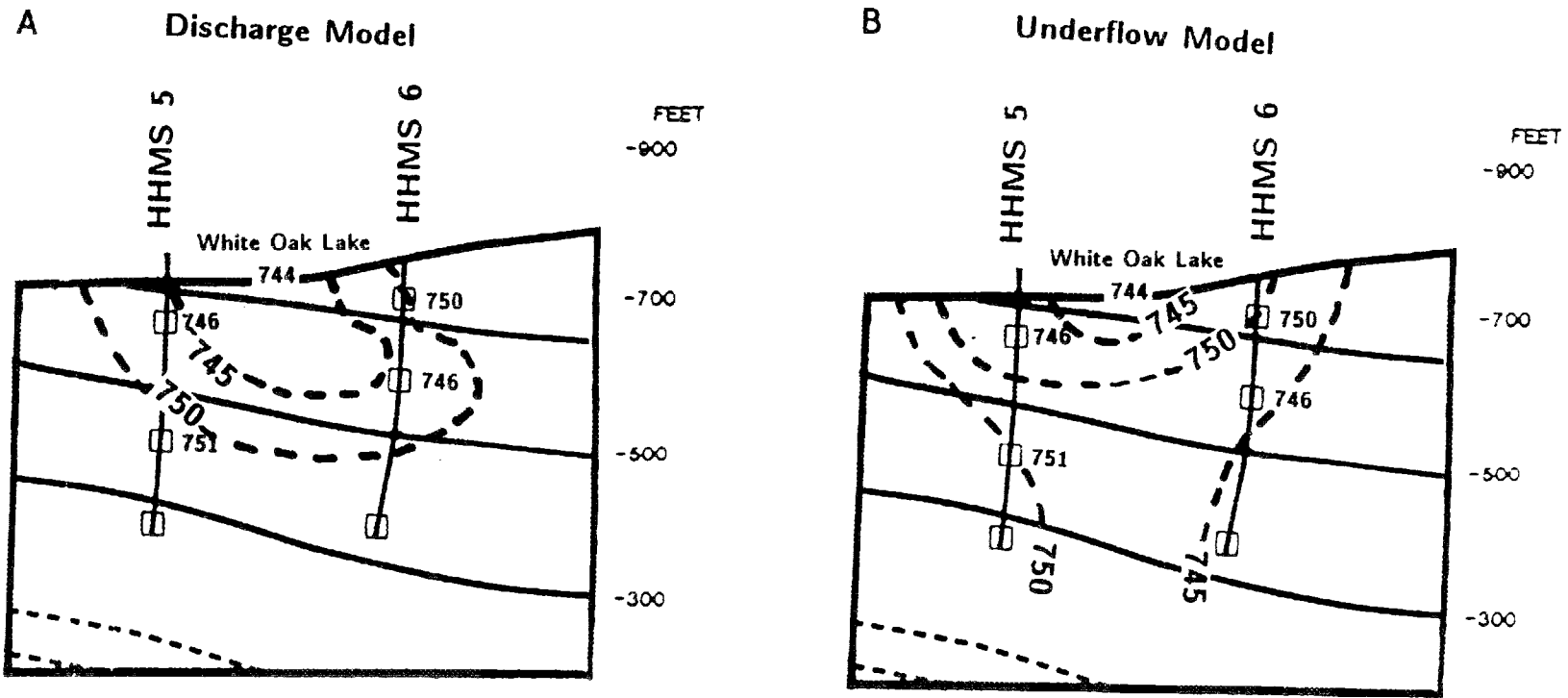


Fig. 16. Cross section through White Oak Lake showing two different interpretations of vertical potentiometric head data. Contours and lake water level are in feet above mean sea level.

Values of K have been measured in nearly every HHMS well. The USGS conducted slug tests in the FY 1986 well clusters (HHMS sites 1 through 6). The test consisted of lowering an enclosed cylinder (the slug) into the well to displace the water level, then measuring the water level response with a digital recorder attached to the slug. After recovery was complete (sometimes several days later) the slug was removed, and another water level displacement test was run. The USGS conducted tests only in wells that had reached an equilibrium head, which included all of the HHMS B and HHMS C wells, HHMS 2A and HHMS 3A; the other HHMS A wells were still recovering from dewatering after drilling. The data were made available to ORNL personnel for analysis (H. H. Zehner, USGS, Knoxville, TN, personal communication to L.E. Toran, ORNL, February-May 1988). ORNL personnel conducted slug tests in the FY 1988 HHMS B and C wells by pouring a 2-gal-slug of water in the well and measuring water level response with a pressure transducer. Recovery was monitored for early data only (approximately 1 to 5 hours). HHMS 8B had not recovered sufficiently to conduct a short-term slug test.

The slow recovery of the deep HHMS A wells from dewatering after drilling can be used to estimate K by assuming the standard slug test restrictions apply: instantaneous removal of water, no casing leakage, isotropy, and a known equilibrium head. For the low K of the deep wells, the recovery period is on the order of years instead of hours or days. Given the time frame of the test and the purging method used to dewater the wells immediately after drilling (airlifting), instantaneous removal of water should be a valid assumption. If the casing is properly sealed, there would be no leakage down the casing to make recovery artificially faster. The assumptions of isotropy and estimation of the final head (discussed below) are questionable, but should provide order-of-magnitude estimates that are appropriate.

The equilibrium (final) head for wells that have not yet recovered was estimated to be within 5 ft of head in the HHMS B well. The heads in the deep wells that have recovered thus far are within 5 to 10 ft of the shallower wells. The K calculations are not strongly sensitive to the final head value. For example, decreasing the final head of HHMS 6A from 746 to 696 ft increased the K from 3.7×10^{-9} to 4.7×10^{-9} cm/s.

In the FY 1988 HHMS B and C wells, water level data were collected immediately after well completion in order to obtain slow-recovery data on wells with a higher K that could

also be tested by standard slug test techniques. Comparison of these two measurements is made in the next section.

An additional check on K measurements in the deep wells is obtained from packer tests. In a packer test, the test interval is isolated with an inflatable pneumatic tube, the pressure below the packer is increased (typically by injecting water), and the pressure response to this stress is measured with a transducer below the packer. The pressure response test can be completed in half a day to a day (not including setup time). Although the test period is much shorter, considerable difficulties were encountered in equipment set-up and leak detection and prevention. For example, injection hose leaks were common, snarling of the injection hose plugged one well and nearly trapped the packer downhole, and downhole valves were sometimes difficult to operate. As a result, only three pressure tests have been conducted; the test design used is shown in Fig. 17.

The slug test data and slow recovery data were analyzed by the Hvorslev technique [using the simplified geometry described in Freeze and Cherry (1979)] and by the Cooper, Papadopulos, and Bredehoeft (1967) method, which is used for confined aquifers and accounts for drawdown surrounding the well in addition to drawdown within the well. It was necessary to select a storativity to match a type curve to the data available in the HHMS tests, and a storativity of 10^{-4} was used. Calculations from the two methods differed by factors of 1 to 2 for all but one well, and the data shown is from the Hvorslev technique. The packer test data were analyzed by the method suggested by Bredehoeft and Papadopulos (1980) with modifications by Neuzil (1982). The data were analyzed using Lotus spreadsheets, with type curve matching of printouts for the slug test data analyzed by the method of Cooper and others (1967) and the packer test data, and linear regression of the straight line Hvorslev plots.

4.3.2 Results

The K values tended to decrease with depth (Toran 1988a), although there are exceptions to this pattern (Table 4 and Figs. 18 and 19). The geometric mean K of the HHMS A wells is 8×10^{-9} cm/s, of the HHMS B wells 9×10^{-7} cm/s, and of the HHMS C wells 2×10^{-5} cm/s (Fig. 18). The differences in mean K for the different depths are statistically significant. The standard deviation of the HHMS B wells is slightly higher than the HHMS A or C wells (1.1 log units compared to 0.6 and 0.7, respectively), but the depths of the HHMS B wells are also more variable.

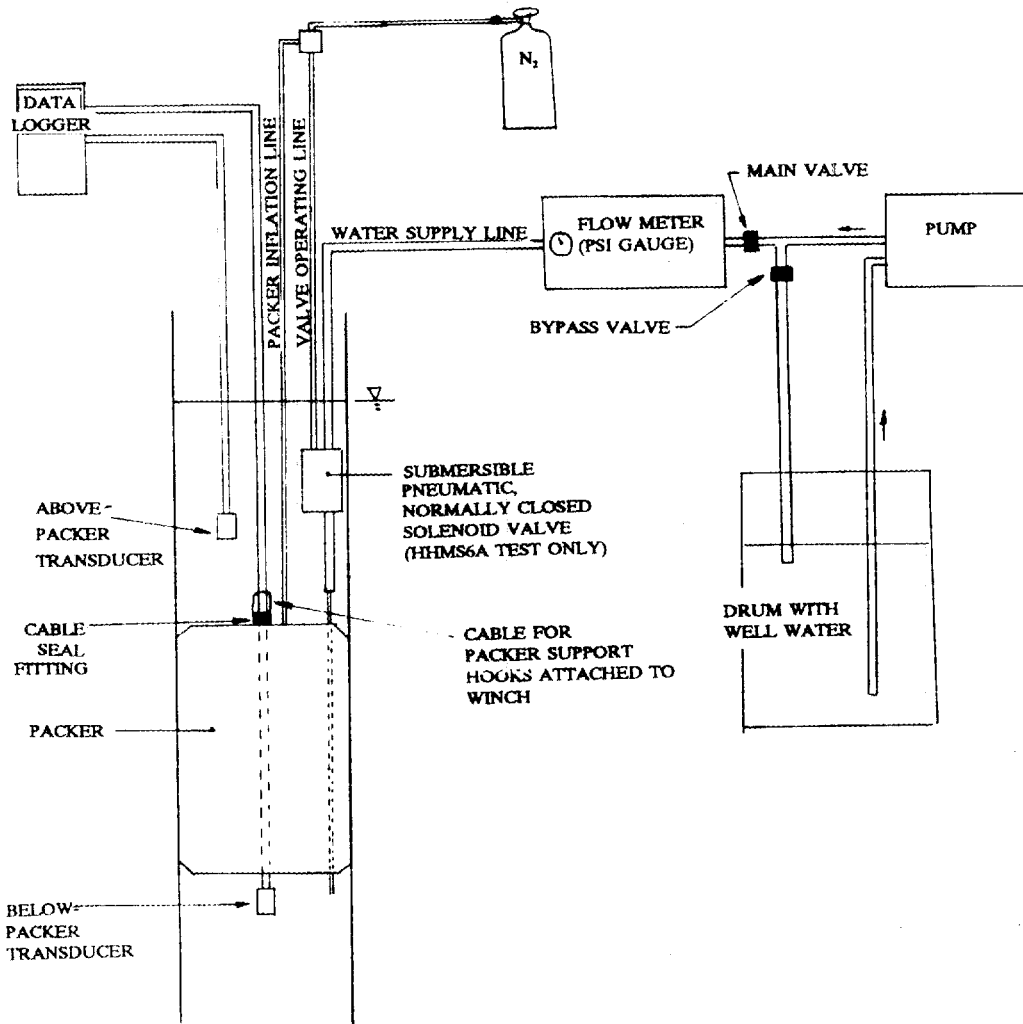


Fig. 17. Diagram of field set up for a packer test to measure K. Packer is inflated with N_2 . Two transducers are used, with a dual-input data logger, one above the packer to monitor leaks and one below to monitor the test. Well water is injected through the water supply line. The packer and associated equipment are lowered and raised with a electric winch. Solenoid valve added to a test for HHMS 6A.

Table 4: Summary of hydraulic conductivity data by different techniques

HHMS ID	Slow Recovery (cm/s)	Slug (USGS) (cm/s)	Slug (ORNL) (cm/s)	Packer (cm/s)	Log K	Depth (ft)
1A	1.7E-08				-7.77	400
B					-4.70	201
C		2.2E-05			-4.65	101
2A		2.5E-07			-6.59	400
B		2.0E-06			-5.71	200
C		8.1E-06			-5.09	81
3A		7.9E-08			-7.10	399
B		6.6E-08			-7.18	211
C		1.8E-05			-4.75	80
4A	2.0E-09			1.2E-08	-8.69	400
B		3.4E-05			-4.47	215
C		3.0E-04			-3.52	61
5A						400
B		4.7E-06			-5.33	219
C		5.8E-05			-4.24	63
6A	4.2E-09				-8.38	402
B		4.2E-06			-5.38	165
C		6.6E-05			-4.18	61
7A	2.0E-08				-7.70	401
B	1.3E-07		7.6E-07		-6.12	295
C	1.3E-07		7.3E-07		-6.14	178
8A	1.9E-09				-8.71	400
B	1.7E-08				-7.78	197
C			5.6E-06		-5.25	79
9A	3.2E-09			7.3E-09	-8.49	400
B	1.3E-07		9.4E-08		-7.03	238
C	4.0E-07		4.4E-07		-6.36	80
10A	4.0E-09				-8.40	400
11A	3.0E-09				-8.52	400
B	1.4E-07		2.0E-06		-5.70	253
C			2.3E-05		-4.64	114

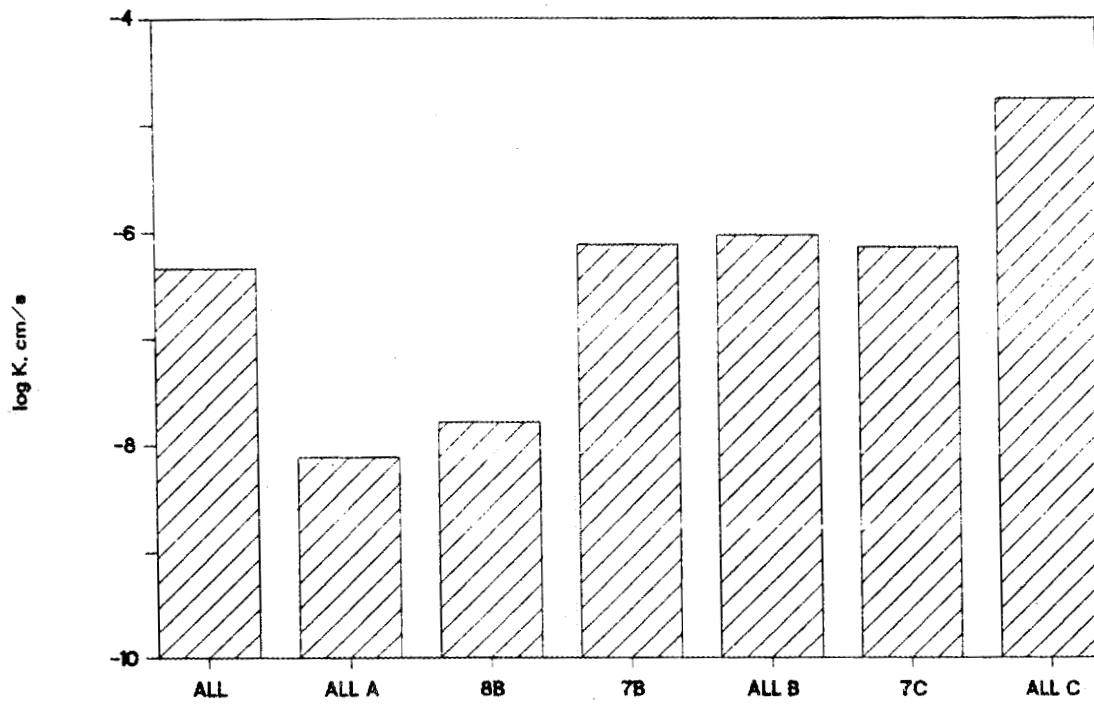


Fig. 18. Histogram of geometric mean of hydraulic conductivity (K) data by well type (HHMS A, B, and C depths) plus values for HHMS 8B, HHMS 7B (295 ft deep), and HHMS 7C (178 ft deep).

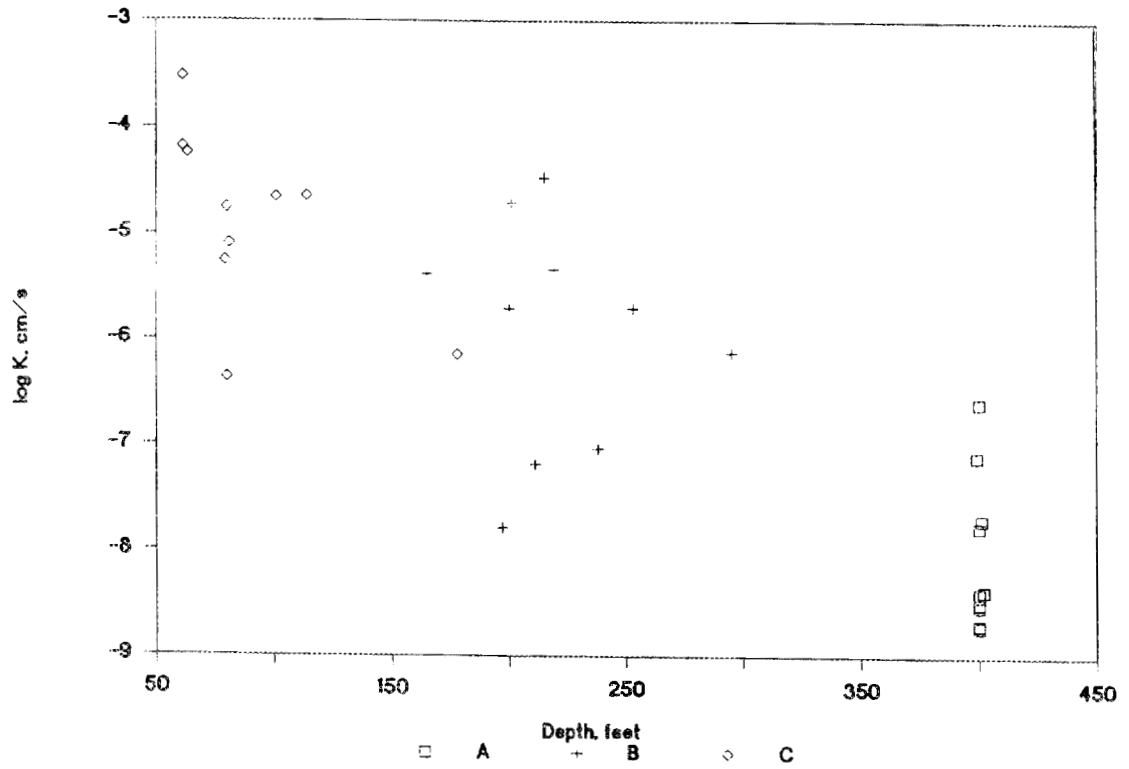


Fig. 19. Hydraulic conductivity (K) versus depth showing scatter in the trend of lower K with depth.

HHMS 7B was drilled to a depth somewhat deeper than the other HHMS B wells (295 ft vs about 200 ft for other HHMS B wells), but its K value is typical of other HHMS B wells. HHMS 7C was also drilled deeper (178 ft vs about 100 ft for other HHMS C wells) and its K value is more typical of the B wells. HHMS 8B was drilled to about 200 ft, but it has a lower than average K compared to other HHMS B wells (2×10^{-8} cm/s). Its open interval is just below a minor thrust fault, and it may be influenced by a lower-conductivity, sealed fracture zone near the fault plane. HHMS 9C also has a lower than average K value compared to the other HHMS C wells.

The K values that have been calculated by both slow water level recovery and the standard (faster) slug test have similar results (Table 4); the recovery method values are 1.1 to 6 times greater than the slug test values (the largest discrepancy being HHMS 11B). Thus, the values lie within the same order of magnitude. This check on the validity of the slow-recovery method provides a basis for comparing K values in wells calculated by the different methods (Fig. 18).

The comparison between the slow-recovery method and the packer tests completed thus far also shows a fairly close match (Table 4). The K values from packer tests are 2 and 6 times greater than those calculated by the slow-recovery method. If the different values calculated are real, rather than an artifact of the method of analysis, these data indicate the range of influence of the various tests. A larger K value reflects a larger range of influence because more fractures are encountered, increasing the permeability. The results would suggest the recovery method has a larger range of influence than the standard slug test, which is to be expected because the stress on the water level was greater from dewatering after drilling. The higher K value calculated for the packer test data is dependent on the compressibility of the equipment in the test system, which was difficult to measure when the inlet valve was at the land surface; the data presented could overestimate K if this valve introduced any air. The packer test appears to have a larger range of influence than the slow-recovery method, possibly reflecting wide transmission of the pressure response, and a very narrow cone of depression in the slow-recovery slug test because of the low hydraulic conductivity.

4.4 GEOCHEMISTRY

4.4.1 Methods

An unfiltered water sample was collected with a bailer several months prior to the main sampling effort. This unfiltered sample was used to screen the water for fluorescein dye and tritium. Fluorescein dye was added to the drilling fluids, and its presence in the sample would indicate contamination from water used during drilling. High tritium would indicate radioactive contamination from waste sites. The sampling procedure that follows was based on the results of this screening, which showed minimal drilling fluid contamination and no radioactive contamination at levels that would be a health hazard.

The 19 wells in the FY 1986 cluster well network were sampled for water chemistry in late July 1987. There was insufficient funding to collect water chemistry samples from the FY 1988 well clusters, so only screening samples (including field measurements for pH and electrical conductance) were collected. This section describes pumping and sampling methods, field measurements, selection of analytes, and contamination precautions.

The samples were collected near the open interval, except for the deep HHMS A wells, by using a Bennet positive displacement piston pump. The deep wells were sampled at the top of the water column, and three of the wells (HHMS 4A, HHMS 5A, and HHMS 6A) were sampled by bailing because the water levels had not recovered sufficiently at that time to be reached with the Bennet pump. The bailing technique for such deep water was unusual: three bailers were tied together, and two were sealed off at the bottom to convert them to buckets. The open bailer allowed the bundle to penetrate the water surface, and the other two filled and could be hauled up without losing all of the water. All samples were filtered with 0.45- μm pore size filter paper, and the pumped samples were filtered in line.

Water samples for chemical analysis were collected after flushing only 15 gal of water from the well. While the field parameters were checked to see that they had stabilized before samples were collected, the amount of water removed would not have completely flushed the well. However, this procedure was used to minimize impact on head, particularly in the deep wells. The flushed water was returned to the well after sampling was completed.

The filtered water was diverted to a Hydrolab flow-through cell for measurement of field parameters: specific conductivity, temperature, pH, dissolved oxygen, and oxidation-

reduction potential. Three readings of each parameter were recorded. Collection bottles were rinsed with filtered water, and 9 or 10 labeled bottles were collected for the various analytes listed in Table 5. Two sample blanks were collected in the field at HHMS clusters 2 and 7. Neither sample blank indicated cross contamination of samples was occurring.

After sampling, the pump, hose, and Hydrolab were rinsed with dilute nitric acid followed by distilled water until the pH stabilized to the level of distilled water. The outside of the hose was also washed down with distilled water. The thorough washing was aided by the use of a 110-gal tank of water carried with the pump equipment on a trailer.

Gloves were used during sample collection. Although the water did not show high radioactivity on screening, the pH in some of the wells could be considered corrosive.

Samples were analyzed by the Analytical Chemistry Division at ORNL, except for alkalinity and stable isotopes. Alkalinity was measured by the investigator in an Environmental Sciences Division (ESD) laboratory within a few days of collection, and the preliminary samples for stable isotopes (deuterium and ^{18}O) were analyzed by an outside vendor (Geochron, Inc.) to see if further investigation might be useful.

4.4.2 Results

The preliminary screening of water samples indicated low concentrations of fluorescein dye and tritium in most wells (Table 6). Therefore, a decision was made to bypass well development, which would help remove any water contamination from drilling fluids, but would slow recovery of the wells and disrupt head measurements. For consistency, even wells with relatively fast water level recovery were not purged. In retrospect, well purging would be preferred for future sample collection.

The fluorescein dye levels in all but two wells indicated between 30,000- and 100-fold dilution, based on an initial concentration of 10,000 ng/mL. Initial concentrations were calculated by assuming that 19 g of fluorescein powder was added to each 500 gal of drilling water; samples of drilling fluid were not collected. Nonetheless, several of the wells have water that was visibly green, as noted in Table 6. HHMS 5A showed only a 15-fold dilution; the high fluorescein might have been caused by the lengthy period that the drilling fluids remained in this particular well before dewatering. HHMS 11C was not

Table 5: Samples collected in summer 1987 for FY 1986 HHMS wells

Bottle	Type ^a	Analytes
1	1 L	Radioisotopes
2	1 L NO ₃ acidified	Radioisotopes
		gross alpha, gross beta, gamma scan, tritium, ⁹⁰ Sr U-Th if gross alpha > background
3	30 mL Glass	Radioisotope scan
4	100 mL	Anions--Cl, NO ₃ , PO ₄ , F, SO ₄ , Br
5	100 mL NO ₃ acidified	Cations--Majors including K Minors included in ICP package
6	100 mL	Alkalinity
7	30 mL Glass	Total organic carbon
8	100 mL	¹⁸ O
9	100 mL	Deuterium
10	100 mL	Tritium

^a Polyethylene unless stated otherwise.

TABLE 6: Abbreviated summary of screening data and field data from HHMS wells^a

HHMS ID	Date	Tritium (bq/L)	Fluorescence ppb	Field pH	Conductivity at 25°C (mS/cm)	Color
1A	5/12/87	bd	7			sg
	7/22/87			9.48	0.648	
1B	5/12/87	bd	73			g
	7/22/87			8.62	0.128	
1C	5/12/87	bd	1			
	7/22/87			7.02	0.269	
2A	5/12/87	bd	32			sg
	7/24/87			9.92	7.2 ^b	
2B	5/12/87	bd	3			
	7/23/87			10.09	0.427	
2C	5/12/87	bd	<0.1			
	7/23/87			7.41	0.416	
3A	5/12/87	1700	3			sg
	7/22/87			12.48	4.23	
3B	5/12/87	bd	2			sg
	7/21/87			9.69	1.57	
3C	5/12/87	7900	1			
	7/21/87			7.04	0.212	
4A	2/87	4	0.3			
	7/28/87			10.25	2.1 ^b	
4B	2/87	2	0.9			
	7/21/87			9.76	0.192	
4C	2/87	46	0.3			
	7/20/87			7.17	0.137	
5A	2/87	29	640			g
	7/28/87			12.28	24.9 ^b	
5B	2/87	2	17			sg
	7/23/87			9.83	0.195	
5C	2/87	10	0.4			
	7/23/87			9.18	0.054	
6A	2/87	2	28			
	7/28/87			12.63	27.7 ^b	
6B	2/87	2	32			sg
	7/24/87			10.02	1.6 ^b	
6C	2/87	2	0.4			sg
	7/24/87			8.91	0.5 ^b	
7A	2/87	2	0.3			
	7/21/87			9.85	1.92	
7B	08/22/88	<50	2		9.3	0.85
7C	08/22/88	<52	3		11.4	
	08/04/88			9.8	0.97 ^c	
8A	08/23/88	<51	180		9.5	1.92
	08/04/88			9.4	2.1 ^c	
8B	08/23/88	<45	3		10.9	3.1 ^b
	08/04/88			11.7		
8C	08/23/88	<51	3		7.5	0.24
	08/04/88			8.1	0.08 ^c	
9A	08/24/88	<52	10		10	4.52
9B	08/23/88	<52	124		9	1.6 ^b
9C	08/24/88	<51	6		7	0.23
10A	08/24/88	<51	131		7.7	12.56
USGS 466	09/01/83	33+38 ^d				0.54 ^d
USGS 467	09/01/83	14+37 ^d				0.33 ^d
11A	08/25/88	<52	340	12.1		6.64
11B	08/25/88	<52	97	10.4		1.7 ^b
11C	08/25/88	<53	26600	10.3		0.49

^a Blank = not measured,

bd = below detection, measured at Radioactive Materials Laboratory instead of Low Level Laboratory, g = green, and sg = slightly green.

^b Measured in laboratory.

^c D. K. Solomon, ORNL, personal communication to L. E. Toran, ORNL, August 1988.

^d Webster and Bradley 1988.

flushed after completion of drilling because of a driller's error, and has a fluorescein concentration of 26,000 ppb, dominantly a drilling fluid signature.

The tritium concentrations were near background levels with the exception of HHMS 3A and HHMS 3C. These two wells showed considerably higher tritium concentration and were re-sampled in January 1989 to see if the high tritium levels were persistent. The second sampling indicated no dilution of tritium had occurred in the intervening year and a half. Possible tritium sources and additional geochemical data are discussed later (Sect. 5.3), but there is presently insufficient data to determine the source.

A significant problem that showed up during sampling of the FY 1986 wells and in the screening of the FY 1988 wells was probable grout contamination. Field measurements of pH between 10 and 12 and alkalinity up to 70 meq/L (predominantly OH⁻ alkalinity) suggested many of the wells contained water expelled during grout solidification. Grout water in the well is not an uncommon artifact of normal grouting procedures. The cation-anion balances (which reached up to 20% error) and high K⁺ concentrations (several hundred mg/L in some of the HHMS A wells) also support the hypothesis of grout contamination in some wells, since both are associated with grout contamination (Barcelona and Helfrich 1986). Grout contamination is not an uncommon problem, particularly in wells with a low permeability which are only slowly flushed by groundwater. However, chemical analyses of such water does not provide useful information about major ion chemistry because of alteration by the grout.

Any well water with pH over 9 should be considered suspect. Values over 12 were observed in three deep wells (HHMS 3A, HHMS 5A, and HHMS 6A), as well as alkalinities over 60 meq/L. By way of contrast, shallow well HHMS 3C had a pH of 7.0 and an alkalinity of 3.7 meq/L. The only wells with a pH below 9 are HHMS 1C, 2C, 3C, 4C, 6C, 8C, 9C, 1B, and 10A.

The high pH samples that have been analyzed for a suite of cations and anions are nearly all NaCO₃-type waters (Fig. 20), which is typical of grout contamination. HHMS 6C is also a NaCO₃-type water, and had a pH of 8.9. The other HHMS C wells are CaHCO₃-type waters, as would be expected from a carbonate terrain. HHMS 1B is a MgHCO₃-type water, and several of the HHMS A wells have NaCl-type waters (HHMS 2A, HHMS 5A, and HHMS 6A). Comparisons of the chemical data between different well depths are not

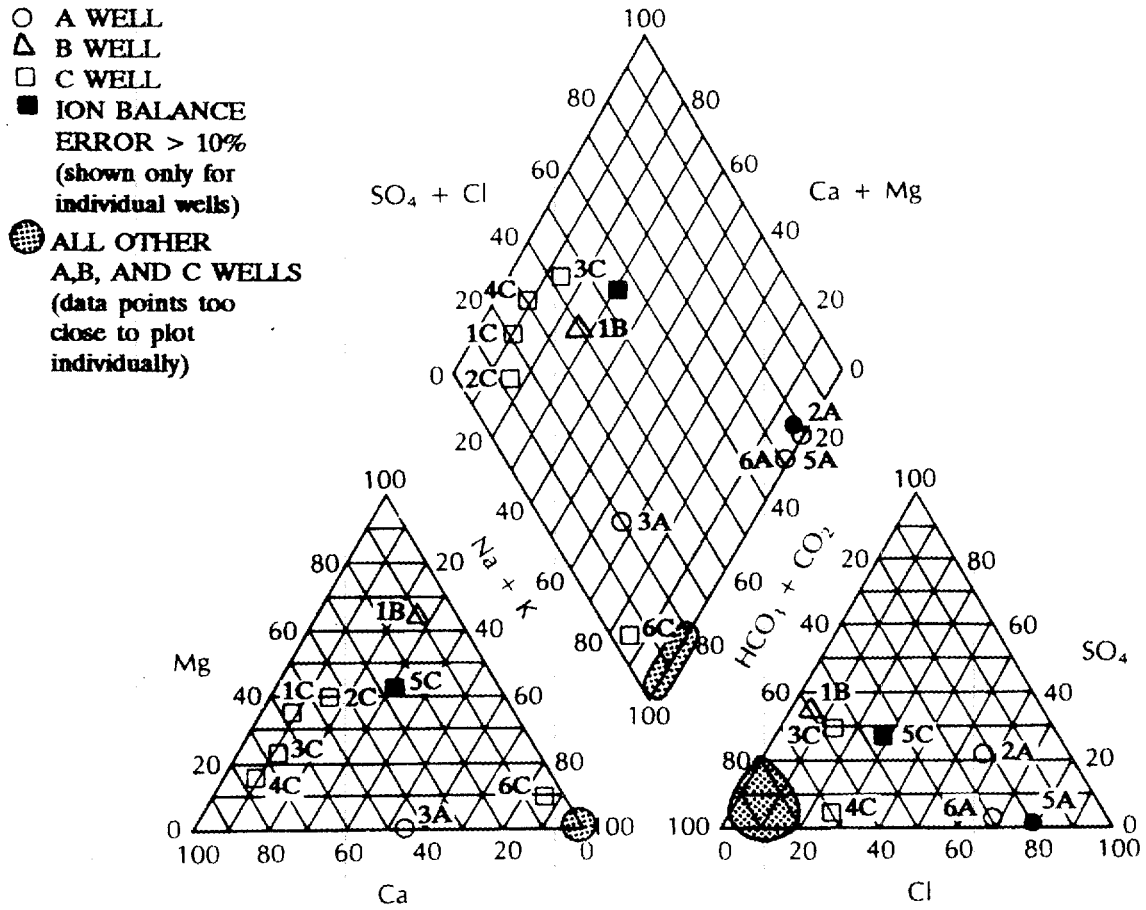


Fig. 20. Trilinear diagram of chemical analyses from FY 1986 HHMS wells.

possible since the data are extremely limited when the wells suspected of grout contamination are eliminated from the data set.

However, the field measurements indicate there are some chemical differences between the HHMS A wells and the HHMS B and HHMS C wells. The electrical conductances are about 1 to 2 orders of magnitude higher in the deep flow system than in shallow and intermediate water samples (Fig. 21). The higher conductances of the HHMS A wells is significant despite the contamination by grout water because both HHMS A and HHMS B wells are affected by the grout, and because the high conductances are associated with high Cl^- concentrations. Higher dissolved solids (and conductances) are expected from water with a longer flow path and residence time. The field measurements also indicate all of the waters are low in dissolved oxygen (<1 mg/L) and have reducing conditions for the oxidation-reduction electrode. The temperature of the water was typically around 15°C (60°F) after pumping it up 100 to 200 ft on 32°C (90°F) days. The high air temperature during sampling could heat the water over temperatures measured downhole during geophysical logging, so the temperature vs depth relationship would not necessarily be preserved in the groundwater samples collected.

The hydrogen and oxygen isotope values in groundwater are in general determined from the environment in which the groundwater recharged (entered the aquifer). Specifically, temperature, latitude, and elevation influence the isotope values. Thus, if these conditions are different for separate flow systems, the hydrogen and oxygen isotopes will fingerprint water from each system. The isotopes studied are deuterium (^2H or D) and ^{18}O , which have additional neutrons making them heavier than the more common isotopes, ^1H and ^{16}O . Because the heavy isotopes occur in very small quantities, the δ notation is used to report isotope ratios:

$$\delta = (R_{\text{sample}}/R_{\text{standard}} - 1) \times 1000 \text{ ‰}$$

where R is the ratio of the heavy isotope to the light isotope. The sample is reported as a ratio to a standard (standard mean ocean water or SMOW for D and ^{18}O). This ratio has 1 subtracted from it to make the standard value 0, and it is multiplied by 1000 to make the number larger and use units of per mil (‰, analogous to percent). When an isotope ratio is more negative than the standard or some other value of interest, it is said to be "lighter"; conversely, more positive values are said to be "heavier".

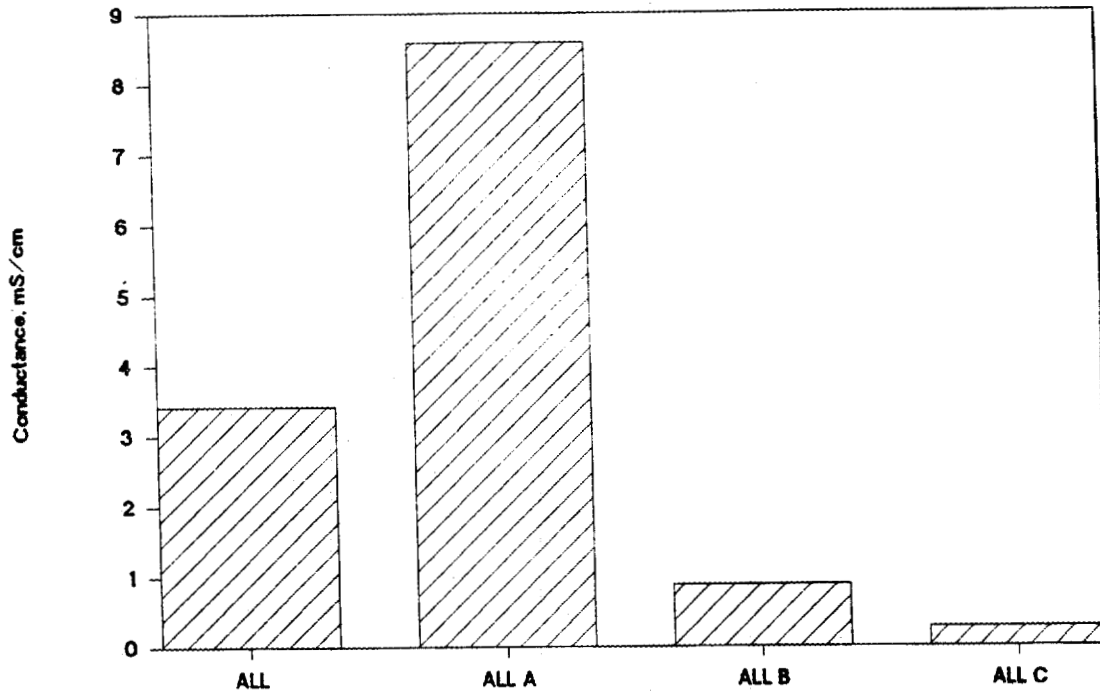


Fig. 21. Histogram of arithmetic mean electrical conductance for different well depths.

Nine samples from three clusters were analyzed for D and ^{18}O , the stable isotopes in water (Table 7). These preliminary analyses indicate that isotopic data may be useful in distinguishing different deep flow systems in the HHMS A well depths. The ^{18}O values of the three HHMS A well samples varied by 3.8‰ , and the deuterium values ranged over a 12‰ spread. These ranges indicate distinctly different signatures for the three wells sampled (Fig. 22). In contrast, the HHMS B and C wells had variations of less than 2‰ and 1‰ , respectively, for D and ^{18}O , and the samples formed a cluster around the meteoric water line (the predicted D and ^{18}O relationship for groundwater).

Three different formations were sampled by the HHMS A wells with D and ^{18}O measurements. The lightest water observed was in HHMS 2A, which is open to the Rogersville Shale. HHMS 5A had heavier D and ^{18}O , and sampled the Maryville Limestone. The heaviest sample measured was HHMS 6A from the Nolichucky Shale. It should be noted that the samples were analyzed more than a year after they were collected. The bottles had been stored in paraffin-sealed bottles in a refrigerator. While this may have increased the spread in values somewhat, the evaporation effect typically produces a line with a steeper slope than that observed for these HHMS A wells. Thus, the difference in isotope signatures is believed to be significant.

The isotope data did not help distinguish whether underflow could occur beneath White Oak Lake because the signature for HHMS 6B and HHMS 5B were not significantly different. The different isotope signatures at the 400-ft depth would be supported by either a discharge or an underflow model since HHMS 6A and HHMS 5A are open to different formations, which might be separated into different flow systems by strata-bound layers.

In summary, additional geochemical data would likely help distinguish different flow systems and aid interpretation of hydrologic data in deep regimes of Melton Valley. In particular, a better vertical distribution of data is needed; stable isotope data looks promising for examination of deep flow systems; and the grout contamination problem needs to be solved (e.g., by designing a purging system that would work in all wells, such as a pump beneath a packer that isolated the open interval). The high electrical conductance of the water from the HHMS A wells supports the pattern observed in the hydraulic conductivity data that there are one or more separate, slower-moving flow system(s) at depth, somewhere below 200 ft.

Table 7: Deuterium and ^{18}O isotope ratios (per mil) for three HHMS clusters
(R1 and R2 are repeat analyses)

HHMS ID	D, ‰	^{18}O , ‰
2A	-35	-6.4
5A	-27	-4.1
6A	-23	-2.6
2B	-35	-5.6
6B	-35	-6.0
5B-average	-34.5	-5.65
5B-R1	-35	-5.5
5B-R2	-34	-5.8
2C	-37	-6.3
5C	-35	-6.1
6C	-35	-5.5

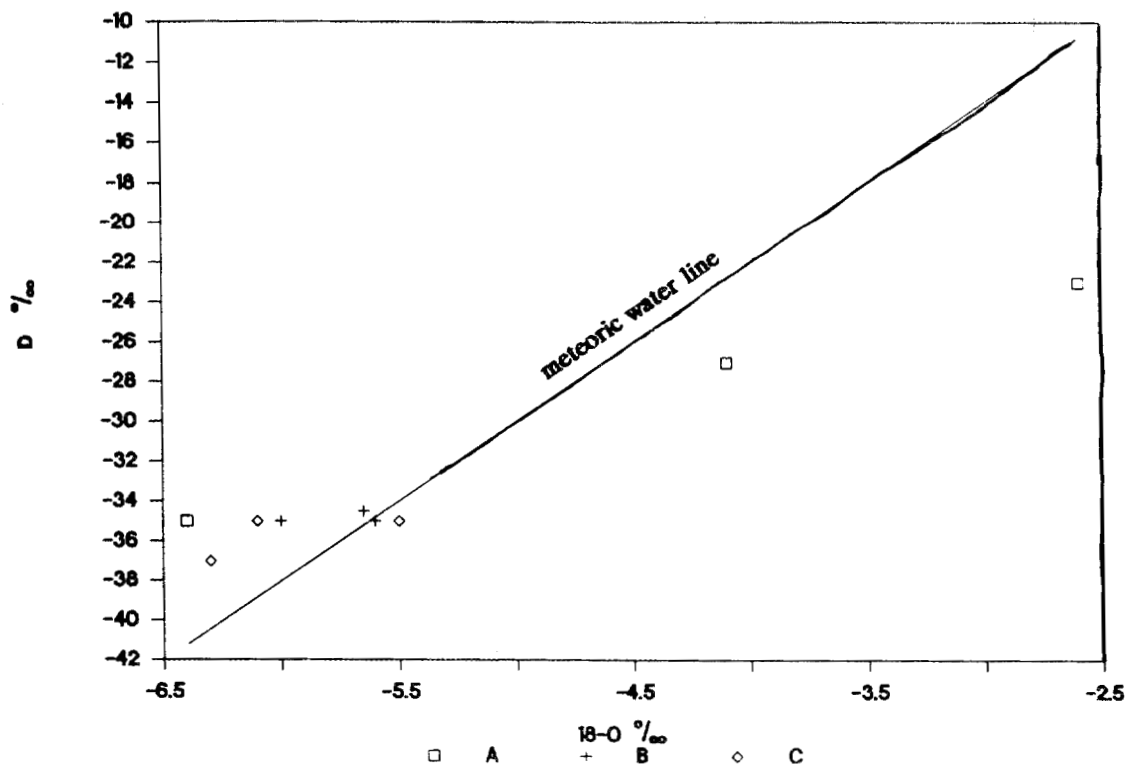


Fig. 22. Deuterium (D) versus ^{18}O for three clusters. HHMS B and C wells cluster near one location on the meteoric water line (typical groundwater values), whereas the three HHMS A wells have a wide spread in values.

5. DISCUSSION

5.1 INFLUENCE OF FAULTS ON LOCAL FLOW PATHS

All of the faults shown on the cross sections, with their associated fracture zones, are expected to strongly influence the local and regional groundwater flow paths. Because of the limited density of hydrologic data, however, several ideas presented in this section remain unconfirmed at the ORR. Nevertheless, the presence of fault-related fracture zones must be integrated into any remedial action project that is directed toward predicting contaminant transport directions.

Surface data suggest that the faults may serve as conduits for contaminant transport. Commonly, contaminated seeps are located near the projected intersection of minor thrust faults with grid-north trending drainages (B. Spalding, ORNL, Oak Ridge, Tenn., personal communication to R. B. Dreier, ORNL, March, 1987). This is probably true for subsurface transport as well. For example, depending on local hydrologic gradients and the transmissivity of the fault zones, faults B and C may be important pathways for contaminant transport south of SWSA 6 to or underneath White Oak Lake. Available potentiometric head data show a gradient from HHMS site 4 to HHMS site 5. However, there is not enough vertical potentiometric level data available to uniquely define flow directions between sites 5 and 6, and the ultimate discharge area for the deep flow system has not been determined.

Faults may act as a flow path between stratigraphic horizons. Thrust faults commonly cut up through the stratigraphic section in the direction of tectonic transport (faults A, B, C, D, D', D'', D''', and E; Figs. 7, 8, and 9). Temperature data from HHMS 8A and HHMS 3A suggest that faults A and E or their associated fault zones contain fluids that originated from deeper, and thus warmer, horizons. In addition, tear faults such as the WOCF or the proposed fault between HHMS 3A and HHMS 2A are steeply dipping and intersect most of the stratigraphy of the CCTS.

Faults and their associated fracture zones may also behave as barriers to flow depending on local faulting processes. If the faulting has developed an impermeable cataclasite at the fault plane and all associated fractures are mineralized, the fault zone will act as a barrier. Note that if a cataclasite forms and the fractures remain open, the fault zone may act as a conduit parallel to the fault plane but be a barrier to flow across the fault plane. Fault A,

which intersects the top of the open interval of HHMS 8B, is interpreted to be a cataclasite (Sect. 3.3.3.1). Hence, vertical flow across the fault should be negligible. Although cataclasites are commonly developed in association with thrust faulting of sedimentary rocks, the width and extent of a cataclasite varies considerably along the fault plane (Woodward and others 1988). Thus, although a fault plane is characterized as impermeable to fluid transport at one site, this need not be the case for the entire extent of the fault. If no cataclasite develops and associated fractures remain open to fluids, the zone will act as a conduit (Dreier and others 1988a, 1988b).

Although a fracture zone can be a barrier to fluid transport at depth, this characteristic may reverse itself in the near subsurface. Calcite, a common fracture-filling mineral that also dissolves easily in humid-climate weathering processes, can be concentrated within fault zones because of an increase in fracture intensity. Hence, a fault zone that is sealed by calcite at depth may be preferentially weathered at shallower horizons and become transmissive to fluids. This change in the hydrologic behavior may be observed for fault A. Contaminated seeps in SWSA 6 that are possibly associated with fault A represent preferred flow paths in the near surface. However, as discussed above, this fault may act as a partial barrier to flow at greater depths.

5.2 TRANSITION BETWEEN FLOW SYSTEMS

On the ORR there are at least two separate hydrologic systems: a deeper-seated system with more saline formation water and a shallower system with relatively fresh formation water (Haase and others 1987, Toran 1988b, Dreier and others 1988b). Observations used to define the systems include (1) the response of potentiometric levels to precipitation events (Sect. 4.2.2); (2) the hydraulic conductivity (Sect. 4.3.2); and (3) the electrical conductance measured from groundwater samples (section 4.4.2). In addition, these observations are supported in part by electrical properties measured on geophysical logs.

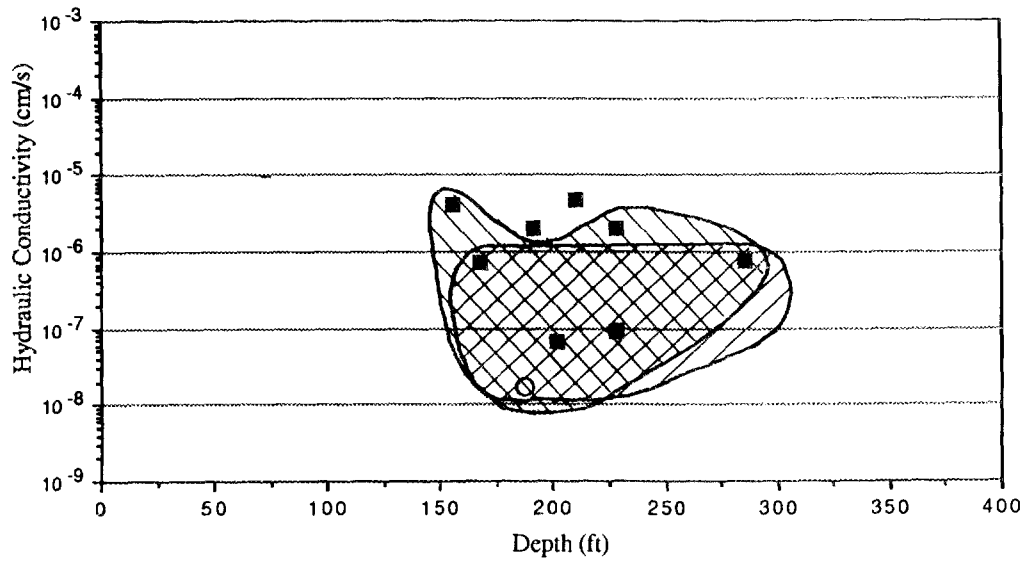
The shallow system is characterized by large and rapid responses to precipitation events, hydraulic conductivity values that are high for the data set (Table 4), and low electrical conductance. Supporting geophysical evidence includes a relatively high resistance signature on the SPR log (see Appendixes 3 through 11) or a signature on the long-short normal or dual-induction log suggesting that the formation waters are similar to or less saline than the water in the immediate volume surrounding the borehole. The geophysical log response results in part from borehole fluids infiltrating natural and induced fractures in

the surrounding rock during drilling. In contrast, the deeper system shows little or no response to precipitation events, hydraulic conductivity values are low, and the electrical conductance is high. Geophysical logs show low electrical resistance and suggest that the formation waters are more saline than the borehole fluids.

The lower boundary of the shallow flow system is not clearly defined but is thought to occur between depths of 150 and 200 ft or in the depth intervals sampled by the HHMS B wells. In support of this, all of the HHMS C wells, except for HHMS 9C, show characteristics of the shallow system and all of the HHMS A wells show characteristics of the deeper system. Not all of the HHMS A wells have recovered, so it is not possible to relate all of the responses of these wells to precipitation events. The HHMS B wells are not as easy to categorize. HHMS 1B, HHMS 2B, HHMS 4B, HHMS 5B, HHMS 6B, HHMS 11B, USGS 466, and to a lesser extent HHMS 9B, show a response to precipitation events (Sect. 4.2.2). However, HHMS 3B, HHMS 7C (which is as deep as a normal HHMS B well), HHMS 7B, and HHMS 8B do not. However, other characteristics of HHMS 9B suggest that this well is part of the deeper system. Hydraulic conductivities for the HHMS B wells are intermediate between the A and C wells (Fig. 23). In addition, the HHMS B wells that show a response to precipitation events also show the highest hydraulic conductivity within the group (Fig. 23). Note that HHMS 9B is part of the lower hydraulic conductivity group. Electrical conductance measurements for the HHMS B wells are also variable (Sect. 4.4.2), and the B wells that show apparent shallow system characteristics, except for HHMS 6B and HHMS 11B, have electrical conductances less than 0.5 mS/cm, whereas the other HHMS B wells have conductivities between 1.5 and 3.3 mS/cm (Table 6). Although HHMS 6B and HHMS 11B show a response to precipitation and have a high hydraulic conductivity, their electrical conductance is more similar to the deep system group (1.6 mS/cm).

This classification of HHMS B wells shows that the shallow system includes wells from the eastern Pits and Trenches area that are closest to White Oak Creek (HHMS 1B and 2B) and wells that are near White Oak Lake (HHMS 4B, HHMS 5B and HHMS 6B) (Fig. 24). This leads to the following interpretation. The depth of the transition zone is expressed in part by the main surface water drainage - White Oak Creek and White Oak Lake - and is controlled by geologic structures, particularly the WOCF and the sequence of faults in the Nolichucky Shale that underlie White Oak Lake (Faults B and C). Changes in the

ORNL-DWG 89-13320



 Low response to precipitation events

 Electrical conductance >1.5 mS/cm

Fig. 23. Flow system characteristics for the intermediate depth wells. These wells have open intervals between depths of 150 and 300 ft. The hydraulic conductivity from HHMS 8B is calculated by the slow recovery method and is shown as a black square.

ORNL-DWG 89-13318

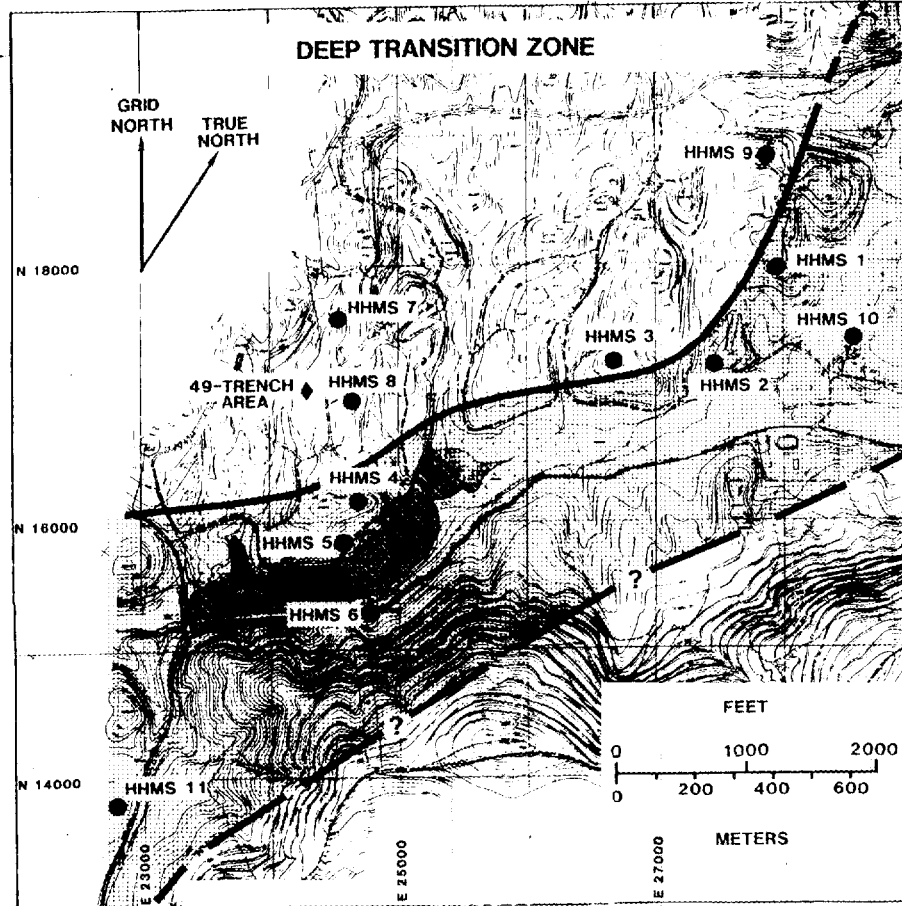


Fig. 24. Area containing HHMS B wells with shallow flow system characteristics. The stippled pattern shows the area where intermediate-depth wells have characteristics of the shallow flow system. Intermediate-depth wells in the area with no pattern have characteristics of the deeper flow system. Hence, the stippled pattern shows the region where the transition zone between two flow systems occurs at a relatively greater depth. Currently, there is not enough data available to constrain the southern boundary of this area.

transition zone are not related to local topography because HHMS sites 2 and 4, which show shallow zone features, are both on hills. The inclusion of HHMS 11B in the shallow system is problematic, and additional data are needed from south of White Oak Creek in order to define the shape of the transition zone (Fig. 24).

The proposed hydrologic boundaries between the two systems do not correlate well with local stratigraphic units. For example, HHMS B wells that show shallow system characteristics are finished in three different formations: the Rogersville Shale, the Maryville Limestone, and the Nolichucky Shale. Similarly, HHMS B wells that show deep system characteristics are finished in three different formations: the Pumpkin Valley Shale, the Rogersville Shale, and the Maryville Limestone. In addition, HHMS B wells that are located approximately along strike and that sample the same stratigraphic horizons near the central portion of the Maryville Limestone (between Maryville Limestone markers 2 and 3) show a very large range in hydraulic conductivities (Fig. 25). Hence stratigraphic intervals do not show consistent hydrologic patterns.

Alternatively, below-average hydraulic conductivities observed for HHMS 9C may be controlled in part by stratigraphy. HHMS 9C is the only well finished below the upper Rogersville Shale, and available data do not suggest the presence of a structural feature that would control the hydraulic conductivity. Perhaps the Rogersville Shale retains different hydrologic characteristics, even in the near surface.

In addition to showing a regional influence on flow system transitions, structures appear to influence local hydraulic conductivities and the local boundary between the systems. A comparison of HHMS B well hydraulic conductivity values shows that HHMS 8B and HHMS 3B have the smallest conductivities. These are the only HHMS B wells that are finished in a fault or deformation zone (Table 8), and these particular zones appear to have lower permeabilities. Other deformation zones on the ORR that occur in carbonate and shale sequences also show low hydraulic conductivities (Dreier and others 1988a, 1988b).

ORNL-DWG 89-13321

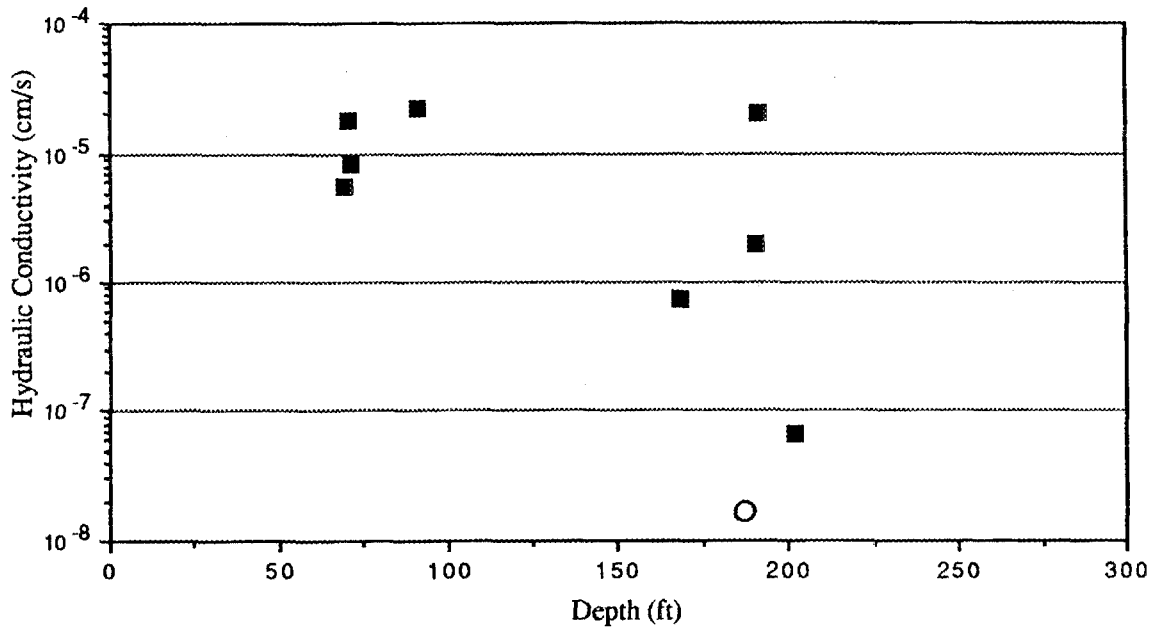


Fig. 25. Variability of hydraulic conductivity values measured from intermediate-depth wells that also sample the same stratigraphic horizons. The intermediate-depth data is taken from HHMS 1B, HHMS 2B, HHMS 3B, HHMS 7C and HHMS 8B and samples the Maryville Limestone between stratigraphic markers 2 and 3. Hydraulic conductivity values for the corresponding shallow well at each cluster site are also shown. The values from the shallow wells show a much tighter clustering than values from the intermediate-depth wells. Hydraulic conductivity determined from slug tests are shown as black squares, and slow recovery values are shown as open circles.

Table 8. Structural characteristics of the open intervals^a

Well name	Open interval depth (ft)	Open interval elevation (ft)	Fault zone	Comments
HHMS 1 A	380.00-400.00	470.11-490.11	No	Immediately below thick deformation zone Thick deformation zone
HHMS 1 B	170.44-196.73	673.38-699.67	No	
HHMS 1 C	40.23-92.29	777.82-829.88	Yes?	
HHMS 2 A	380.00-400.00	406.50-426.50	No	Immediately above D' and below thick deformation zone Possibly D'', thick deformation zone
HHMS 2 B	179.42-199.42	607.08-627.08	No	
HHMS 2 C	61.44-80.24	726.26-745.06	Yes	
HHMS 3 A	380.00-400.00	418.79-438.79	Yes	Fault E Thick deformation zone, hanging wall to D'
HHMS 3 B	189.68-211.58	607.21-629.11	Yes	
HHMS 3 C	62.81-81.41	737.38-755.98	No	
HHMS 4 A	380.00-400.00	390.37-410.37	No	Steeply dipping Leading edge of fault B
HHMS 4 B	178.20-219.20	571.17-612.17	No	
HHMS 4 C	52.79-73.49	716.88-737.58	Yes?	
HHMS 5 A	380.00-400.00	367.48-387.48	No	In NE-dipping hanging wall of fault B
HHMS 5 B	199.39-222.79	544.69-568.09	No	
HHMS 5 C	42.79-63.69	703.79-724.69	No	
HHMS 6 A	380.00-400.00	362.09-382.09	No	
HHMS 6 B	141.88-162.28	599.81-620.21	No	
HHMS 6 C	33.86-53.86	708.23-728.23	No	
HHMS 7 A	380.00-400.00	408.54-428.54	No	
HHMS 7 B	273.00-293.00	515.54-535.54	No	
HHMS 7 C	154.08-174.08	634.46-654.46	No	
HHMS 8 A	380.00-400.00	386.06-406.06	No?	Near temperature and porosity crossplot deflections In footwall of fault A, may intersect fault. Projection uncertain
HHMS 8 B	153.38-195.04	591.02-632.68	Yes	
HHMS 8 C	18.46-38.46	747.60-767.60	No	

Table 8. (continued)

Well name	Open interval depth (ft)	Open interval elevation (ft)	Fault zone	Comments
HHMS 9 A	380-400	460.43-480.43	No	
HHMS 9 B	221.13-241.13	619.30-639.30	No	
HHMS 9 C	64.45-84.45	775.98-795.98	No	
HHMS 10 A	380.00-400.00	377.75-397.75	No?	Influence of White Oak Creek fault?
HHMS 11 A	380.00-400.00	379.95-399.95	No	
HHMS 11 B	235.30-255.30	524.65-544.65	No	Immediately above deformed zone
HHMS 11 C	99.80-119.80	660.15-680.15	No	

^a Depths and elevations of the B and C well open intervals are projected onto the A well. If the open interval of the B or C well is greater than 20 ft, this generally reflects uncertainty in the dip angle projection. In this case, the open interval consists of 20 ft within the stated interval.

Although the open intervals of HHMS 2B and HHMS 3B show similar structural settings with respect to fault D" (compare Figs. 8 and 11) and sample the same stratigraphy (between Maryville Limestone markers 2 and 3), HHMS 2B shows a much higher hydraulic conductivity than HHMS 3B (2.0×10^{-6} cm/s vs 6.6×10^{-8} cm/s). Hydraulic conductivity differences between the two sites may be attributed to more subtle structural differences, such as the stratigraphic location of the thick deformation zone in the Maryville Limestone and the relative distance of the borehole to the WOCF; the open interval of HHMS 2B is not within the deformation zone and is nearer to the WOCF. Based on hydraulic conductivity relationships discussed above, both features would tend to increase the hydraulic conductivity of HHMS 2B with respect to HHMS 3B.

Evidence from electric logs suggests that faults partially control the boundary between fluids with different electrical properties. At HHMS 8A, relative values of the deep-induction log with respect to the medium induction log show a transition from less saline formation waters above the fault to more saline water below the fault. The transition is relatively sharp and overlaps the location of the fault plane. Thus, at this location, the fault surface may act as a boundary between two groundwater systems with different electrical properties. The SPR log from HHMS 3A shows an analogous transition from more resistive to less resistive formation waters at the base of the fault zone associated with fault D, which is identified by SP and caliper logs with supporting evidence from the BHTV log. Currently, it is not clear, however, if changes in electrical properties (either abrupt or gradual) coincide directly with changes in other hydrologic properties. Note that HHMS 6 shows a mismatch between the hydraulic and electrical conductance boundaries.

The geophysical log data from HHMS 10A suggest that the fracture zone associated with the WOCF may be a conduit for transport of deeply seated fluids to the near surface. The dual-induction log for HHMS 10A differs significantly from other dual-induction or resistivity logs run in Melton Valley. The deep-induction log is consistently less resistant (more conductive) than the medium-induction log, even at shallow borehole depths, suggesting the presence of relatively saline formation waters at shallow depths. HHMS site 10 is the only site in Melton Valley where this relationship has been observed over the entire depth of the borehole. The geophysical log signature may result from the location of the borehole in a near-vertical fracture zone associated with the WOCF, which extends into a more deeply seated, more saline hydrologic system. These relationships need to be investigated further, particularly since water samples from nearby shallow wells (USGS

wells 466 and 467) do not show elevated electrical conductance values (Webster and Bradley 1988). Currently vertical flow directions have not been determined within the WOCF fracture zone. The hydraulic gradient between 466 and 467 is upward, but the gradient at depths greater than 150 ft is not yet known. Stable isotope data might be useful to further examine the possibility of upward movement of deep-seated groundwater at this location.

5.3 POTENTIAL FLOW PATHS FOR TRITIUM TO HHMS-3A

The source of the tritium at 2000 bq/L in the 400-ft well of HHMS cluster 3 is not known, and it is difficult to determine without additional data. Three sources for tritium to travel to this depth should be considered: migration down from the Pits and Trenches area, horizontal and vertical migration up from water contaminated by hydrofracture activity, and horizontal plus vertical migration from a distant source such as SWSA 4. Each pathway suggests a different set of remedial action considerations that needs to be addressed. For the Pits and Trenches source, it is important to determine if the contaminant migration was enhanced by the drilling or caused by natural pathways. If drilling is the cause, care must be taken to avoid this error in the future. If natural pathways are the cause, then additional monitoring at depth is needed to trace contaminant migration paths. If hydrofracture is the source, vertical migration upward would indicate that, in this particular area, the Rutledge Limestone did not provide a barrier for contaminants from the hydrofracture disposal. A structural reason for penetration of the overlying beds should be found if this is the case, so that other needed monitoring could be planned. If horizontal migration from a distant source such as SWSA 4 or the hydrofracture facility is the pathway, again additional monitoring at depth is needed to determine contaminant plumes on the ORR.

The geochemical considerations to address in studying the tritium contamination include reliability of the sample and geochemical signatures of waste sources. The tritium measurements were made on two samples collected as described in the methods section of the groundwater geochemistry discussion. Both samples were collected from standing water in the well. The first sample (July 1987) was collected with a submersible pump and had a tritium concentration of 1700 ± 100 bq/L. The second, follow-up sample was collected January 1989 with a bailer and had a tritium concentration of 2700 ± 200 bq/L, confirming the presence of tritium in the well water. At the depth of HHMS 3A and the long residence time implied by the high dissolved ions, no detectable tritium is expected. No dilution of the tritium nor the fluorescein tracer was observed between these samples.

Both samples were collected after the head in HHMS 3A had reached equilibrium, so there was less likelihood for dilution to occur in this well than in a well still recovering from dewatering during drilling.

Other chemical analyses were done on the first sample collected, but no obvious signature of a particular waste stream has yet been found. It can be difficult to distinguish waste streams since tritium was a pervasive waste product. Neither NO_3^- nor ^{99}Tc , which are characteristic of Pits and Trenches waste, were detectable. The concentration of ^{106}Ru was not significantly above detection limits; its presence might have been a signature of hydrofracture water since ^{106}Ru has a fairly short half-life (3.7 years) and the hydrofracture water is younger than the Pits and Trenches waste. However, a non-detectable concentration does not eliminate any waste source from consideration because source concentration and sorption are confounding factors. Further study of tracers is needed, and exploring possibilities such as naturally occurring D and ^{18}O isotopes as fingerprints would be useful.

The next aspect of this problem to consider is structural factors that influence flow paths from different sources. Migration from the Pits and Trenches area would be along fractures or fracture zones that have enhanced typically low vertical hydraulic conductivity values. HHMS 3A had one of the fastest recovery times and highest hydraulic conductivities of the deep wells, which might indicate a fracture zone of some kind around the well. For example, a projection of fault zone E (Fig. 9) to the pits northwest of HHMS 3A (e.g., Pit 2) could provide a preferred travel path for groundwater. However, strictly vertical fracture zones are not expected at HHMS 3A. Specifically, there is no topographic expression suggestive of a high-angle near-vertical tear fault that might create a vertical pathway from the ground surface to HHMS 3A (i.e., Trench 5 in the immediate vicinity of the drill site), and thrust faulting in this area does not create extensive or lengthy vertical fractures. In addition, if the migration path is strictly vertical from the Pits and Trenches Area, the fractures or fracture zone do not encounter HHMS 3B, which shows no tritium contamination, and intercept only HHMS 3C and HHMS 3A. A conceptual model that would allow a near-vertical fracture zone to bypass HHMS 3B but intersect HHMS 3C and HHMS 3A would be unduly complex, and such structures have not been observed in the ORR.

An upward vertical migration path would implicate water contaminated by hydrofracture disposal. Again, the fracture zone E (Fig. 9) suggested by the geophysical logs supports an upward travel path near HHMS 3A. The present hydraulic gradient in HHMS cluster 3 is upward from the deep well to the most shallow well, although the head in HHMS 3A well was depressed below that of HHMS 3C for first half year when the A well was still dewatered from drilling. Head values are not available below the 400-ft depth, but the upward gradient would suggest that a deep source is possible. In addition, there is a temperature deflection in the geophysical logs at 320 ft and 345 ft of approximately 4.4°F, one of the largest observed at any site. The temperature deflection could reflect a deeper source of water because deeper water is hotter because of the geothermal gradient. The approximate 1°F/100 ft temperature gradient for water determined from the HHMS temperature logs suggests the water could have come from a minimum depth of 760 ft. Temperature logs from deeper wells in the hydrofracture area (Law Engineering, Marietta, Georgia, personal communication to R. B. Dreier, ORNL, Oak Ridge, Tenn., Aug. 1, 1984) confirm this temperature gradient up to 1500 ft.

However, the evidence for upward migration of groundwater does not dictate that hydrofracture activity be the source of contamination. It is possible that mixing of deep uncontaminated water and shallow contaminated water occurred. The upward migration of groundwater could complicate interpretation of any geochemical signatures, so it is an important factor to examine further.

Furthermore, thus far no distinction has been made between the Old Hydrofracture Facility (OHF) and the New Hydrofracture Facility (NHF) as a possible source, and each location has a distinct structural setting. The OHF is on the east side of a proposed tear fault (WOCF), which lies between the OHF and HHMS 3A. Currently, it is not known if the WOCF extends to the vicinity of the NHF. Nevertheless, additional faults similar to fault E or fault system D may occur between NHF and HHMS 3A. These structural features could act as barriers or conduits to flow, so further study of their hydrologic influence is needed.

In distinguishing horizontal paths from a SWSA 4 source vs a hydrofracture source, a key difference is that the tritium would be required to travel down dip and down section rather than discharging in the local flow system around SWSA 4. Furthermore, fault E cannot penetrate into the SWSA 4 region because thrust faults do not cut down stratigraphic section in the direction of fault displacement (unless the beds are overturned). Fault E

occurs near the Rogersville Shale-Maryville Limestone contact at HHMS 3A and SWSA 4 is underlain by the (stratigraphically lower) Pumpkin Valley Shale. Thus, a horizontal flow path from SWSA 4 is more difficult to explain than a horizontal flow path from a hydrofracture area. The projection of fault zone E into the shallow Pits and Trenches area near Pit 2 does not require cutting down section, but there is as yet little available data to trace this fault to the surface. As a result, the shape and projection of fault E to the near surface has not been determined.

Another hydrologic factor to consider is whether the travel times from different sources are reasonable. Unfortunately, the lack of site-specific data on the controlling parameters (K , effective porosity) in the heterogeneous environment makes it difficult to check the feasibility of travel time estimates. The horizontal travel paths from the northern Pits and Trenches area, SWSA 4 or the hydrofracture area would require an extremely low porosity (n_e) given the length of the path and the time since waste disposal. Only rough approximations can be made by using the average linear velocity (\bar{v}), and estimates of the hydraulic conductivity (K) and hydraulic gradient (i) along the flow paths:

$$\bar{v} = Ki/n_e.$$

For a flow path of approximately 2000 m from SWSA 4 to HHMS cluster 3 and a travel time of 30 years (since the main disposal period), the groundwater travel time (average linear velocity) would be 6.5×10^{-5} cm/s for a conservative tracer. Given a hydraulic gradient from SWSA 4 to HHMS 3A of 32/2000 (0.016), and the K at HHMS 3A of 3×10^{-8} cm/s, the porosity for this travel path would be 7×10^{-5} . Higher porosities would be possible if the K were higher for some part of the flow path (e.g., shallow zones). For hydrofracture, the porosity could be 5 or 6 times higher (assuming similar gradients and K) because more recent disposal at the NHF makes shorter travel time possible. The porosity could also be about a factor of 6 higher for the Pits and Trenches source near Pit 2 because of a shorter flow path and a steeper hydraulic gradient created by over-pressuring during waste disposal in the pits. These porosities are at the low end of values believed to be reasonable for fractured rock in Melton Valley (Webster and Bradley 1988; G.K. Moore, ORNL, Oak Ridge, Tenn., personal communication to L.E. Toran, ORNL, Oak Ridge, Tenn., May 1989), so this flow path cannot be eliminated as completely untenable.

Another possibility to consider is that the tritium was introduced during drilling or by a flaw in the grout. A 400-ft fracture in the grout is unlikely, and the drilling fluids are not a likely source of tritium. Drilling could have had a secondary effect on flow paths in that the water level in HHMS 3A was depressed below that in the shallow wells, creating a downward gradient during recovery. Because the water level recovered within a half a year, a very fast travel time would be required for head depression to be a factor. Thus, it is not clear how drilling could have introduced tritium to these HHMS A and HHMS C wells.

Thus, the tritium in the 400 ft well of HHMS 3 is problematic, and the source should be investigated further in order to address the implications of tritium at this depth. It is important to distinguish whether this observation is a warning of future problems that may occur at depth or an isolated incident.

This problem shows the importance of defining the larger-scale three-dimensional flow system in this area. The data show a need to look further because of the interactions of geology, hydrology, geochemistry, and waste sources that could involve both shallow and deep sources.

5.4 FUTURE WORK

The complexity of the geology and hydrogeology on the ORR demands more detailed sampling than provided by only three depths in each HHMS cluster. While the geophysical logs give continuous depth coverage, there are insufficient hydrogeologic data to test hypotheses about relationships between stratigraphy, structure, and hydrogeology.

A multilevel piezometer system could provide frequent monitoring depths separated by packers in a single borehole. Such a system is available from companies such as Westbay Instruments, Ltd. of Canada. Water level measurements, geochemical sampling, and hydraulic conductivity measurements would be possible at 10 intervals in 400-ft wells at a cost similar to that of drilling the three separate wells in the current design. Furthermore, the use of packers would reduce recovery time of heads from drilling and improve quality of geochemical samples because of the smaller open interval created by using packers. The Westbay system has advantages over other multilevel monitoring designs in that an essentially unlimited number of intervals are possible, the system has been used at depths

up to 5000 ft, it has been tested in a variety of geologic environments, and it has been used on sites regulated by the Resource Conservation and Recovery Act (RCRA).

The HHMS drilling program was halted for a year to emplace specifications for this new drilling design. Because of uncertainty in funding, this work has been delayed several times, but the advantages of the new scheme in terms of both data and cost will hopefully prevail eventually.

With the proposed design of 10 intervals in a 400-ft-deep borehole, we plan to obtain the following additional information: greater detail in hydraulic conductivity (possibly including hydraulic conductivity measurements at additional intervals from packer tests before the monitoring system is emplaced), better geochemical samples, and additional samples for deuterium and oxygen in water. If additional funding becomes available, drilling of deeper wells is also recommended.

Some of the hypotheses that can be tested with additional hydrogeologic data are:

- which geophysical log information (in various combinations) is the best predictor of porosity and hydraulic conductivity?
- are structural and hydrogeologic behaviors predictable within each stratigraphic unit from one location to another?
- which fracture characteristics create barriers, and which create more conductive units?
- is there additional evidence for upward flow from depth?
- how many flow systems are there, and what are the major recharge and discharge areas?

In addition, future work should obtain data from any other wells in the area drilled in the bedrock, particularly those that might intersect the transition zone between deep and shallow flow systems. Stable isotope data should be collected from additional wells since there may be distinct signature for the deep flow systems. Equilibrium head measurements in the existing HHMS A wells would add to the existing data set, and these might be obtained by installing a packer to isolate the open interval and speed recovery of the head. (A test of this method will be initiated in the near future.) More data are needed south of White Oak Creek. An extension of the examination of faults in geophysical logs would be to try to map the surface expression of thrust faults by looking for correlations between

fault projections, surface seeps, and surface lineaments. And finally, there are insufficient data near tear faults, and it would be useful to conduct hydrologic tests in wells located on opposite sides of such a fault to better understand the influence of these structures on groundwater flow.

This information would provide the basis for a conceptual model of deep flow system on the ORR and allow predictions of hydrologic behavior from geologic data that is more readily available.

6. SUMMARY

At least two flow systems have been identified by the data from the HHMS wells. Additional flow systems will certainly be identified when more detailed sampling with depth is done. The uppermost flow system is identified by higher hydraulic conductivities (10^{-5} to 10^{-6} cm/s), lower electrical conductances (generally less than 0.6 mS/cm), and responsiveness to recharge events.

The depth of the uppermost aquifer is transitional and occurs up to 200 ft deep. Some of the intermediate-depth HHMS B wells are close in characteristics to the shallow HHMS C wells, and some are not. The depth of the uppermost aquifer is greater near White Oak Lake and White Oak Creek, where thrust faults have been identified in the geophysical logs. These faults may enhance the permeability of the bedrock in these areas.

The presence of tritium in HHMS 3A at a depth of 400 ft raises questions about monitoring for groundwater contamination at depth. It was not possible to determine whether the source of tritium was the Pits and Trenches Area, drilling procedures, SWSA 4 or deep groundwater contaminated by hydrofracture. Each of these possibilities suggests that additional deep monitoring is needed.

The location of fault-related fracture zones must be integrated into any remedial action project that is directed toward predicting contaminant transport directions. Five major faults were identified from the stratigraphic and structural information obtained in the geophysical logs of the HHMS wells. Temperature deflections and porosity crossplot anomalies were characteristic geophysical signatures in fracture zones. Although the faults have minor displacement, the associated fracture zones influence groundwater flow. These faults have provided examples of fracture zones acting both as barriers to flow (e.g., the low permeability zone in Fault A at HHMS-8B) and as preferential flow paths (possibly Fault E near HHMS 3A and the higher hydraulic conductivities of HHMS B wells in the vicinity of White Oak Lake and Creek).

Future work for continuing this research was recommended. In particular, it is essential to collect a more detailed vertical distribution of hydrologic data. To obtain this information, a contract is being written for installation of multilevel piezometers that sample from more depths. In addition, future work should obtain data from any other wells in the area drilled

in the bedrock, particularly those that might intersect the transition zone between deep and shallow flow systems. Stable isotope data should be collected from additional wells since there may be distinct signature for the deep flow systems. More data are needed south of White Oak Creek. And finally, there are insufficient data near tear faults, and it would be useful to conduct hydrologic tests in wells located on opposite sides of such a fault to better understand the influence of these structures on groundwater flow.

The HHMS wells have provided a preliminary description of intermediate and deep flow systems on the ORR and furnished the basis for determining future studies needed to characterize the local hydrologic framework.

REFERENCES CITED

- Barcelona, M. J., and J. A. Helfrich. 1986. Effects of well construction material on ground water samples. *Environ. Sci. and Tech.*, 20 (11): 1179-1184.
- Bredehoeft, J. D., and S. S. Papadopoulos. 1980. A method for determining the hydraulic properties of tight formations. *Water Resour. Res.*, 16: 233-238.
- Campbell, A. W., G. F. Cada, R. H. Ketelle, R. L. Kroodsma, R. R. Lee and L. R. Pounds. 1989. Site characterization report for the proposed transuranic waste handling and packaging plant. ORNL/TM-10965.
- Cooper, H. H., J. D. Bredehoeft, and I. S. Papadopoulos. 1967. Response of a finite-diameter well to an instantaneous charge of water. *Water Resour. Res.* 3: 263-269.
- DeLaguna, W., K. E. Cowser, and F. L. Parker. 1958. Disposal of high-level radioactive liquid wastes in terrestrial pits: A sequel. *Proc. U. N. Int. Conf. Peaceful Uses At. Energy*, 2nd. 18: 101-115.
- DeLaguna, W., T. Tamura, H. O. Weeren, E. G. Struxness, W. C. McLain, and R. C. Sexton. 1968. Engineering development of hydraulic fracturing as a method for permanent disposal of radioactive wastes. ORNL-4295.
- Dreier, R. B., D. K. Solomon, and C. M. Beaudoin. 1987. Fracture Characterization in the unsaturated zone of a shallow land burial facility: in *Flow and Transport Through Unsaturated Fractured Rock*, D. D. Evans and T. J. Nicholson (eds), *Geophys. Monogr.* 42: 51-59.
- Dreier, R. B and Leat, M.B. 1988. Fracture Zone Identification in the Appalachian fold and thrust belt determined from geophysical logs. p. 16. IN abstract from International Conference on Fluid Flow in Fractured Rocks, May 15-18, 1988, Atlanta, Georgia.
- Dreier, R. B., C. T. Lutz, L. E. Toran, and E. Bittner. 1988a. Fracture and hydraulic conductivity investigations in a complex low permeability geologic environment. p. 15. IN Abstracts from Conference on Flow and Transport in Low Permeability Settings, December 13-14, 1988, Las Vegas, Nevada, sponsored by the National Water Well Association.
- Dreier, R. B., L. E. Toran, and C. T. Lutz. 1988b. Hydraulic conductivity investigations in a complexly deformed geologic environment. *Geol. Soc. Am. Abstr. with Programs*, 20 (7): A311.
- Freeze, R.A. and J. A. Cherry. 1979. *Groundwater*. Prentice-Hall, Inc., Englewood Cliffs, New Jersey.
- Haase, C. S., E. C. Walls, and C. D. Farmer. 1985. Stratigraphic and structural data for the Conasauga Group and the Rome Formation on the Copper Creek fault block near Oak Ridge, Tennessee: Preliminary results from test borehole ORNL-JOY No. 2. ORNL/TM-9159.

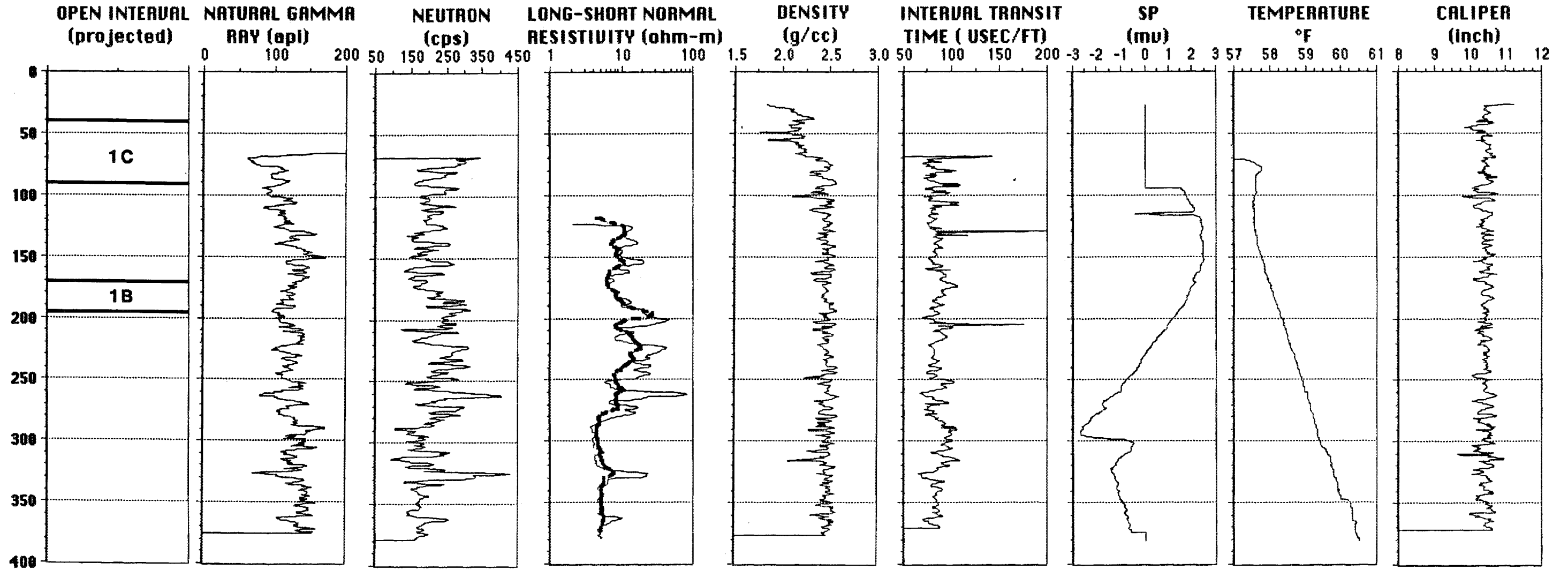
- Haase, C. S., and H. L. King. 1986. Application of borehole geophysics to fracture identification and characterization in low porosity limestones and dolostones. pp. 487-506. IN Proceedings of Conference on Surface and Borehole Geophysical Methods and Groundwater Instrumentation, October 15-17, 1986, Denver, Colorado, sponsored by the National Water Well Association.
- Haase, C. S. 1987. Geophysical data from boreholes DM1, DM2, DM3, and DM3a, New Hydraulic Fracturing Facility, Oak Ridge National Laboratory, Oak Ridge, Tennessee. ORNL/TM-9681.
- Haase, C. S., K. Von Damm, and S. Stow. 1987. Closure of the Oak Ridge National Laboratory hydrofracture facility: An opportunity to study the fate of radioactive wastes disposed of by subsurface injection: pp. 512-530 IN Proceedings of the International Symposium on Class V Injection Well Technology. Underground Injection Practices Council, Inc., Research Foundation, Washington D. C.
- Hasson, K. O. and C. S. Haase. 1988. Lithofacies and paleogeography of the Conasauga Group (Middle and Late Cambrian) in the Valley and Ridge province of east Tennessee. Geol. Soc. Am. Bull. 100 (2): 234-246.
- Keys, W. S., and L. M. MacCary. 1971. Application of borehole geophysics to water-resources investigations. Technique of Water-Resources Investigations of the United States Geological Survey, Book 2, Chap.-E1. U.S. Geological Survey, Alexandria, Virginia, 126 p.
- McMaster, W. M. 1963. Geological map of the Oak Ridge Reservation, Tennessee. ORNL/TM-713.
- Neuzil, C. E. 1982. On conducting the modified "slug" test in tight formations. Water Resour. Res., 18: 439-441.
- Toran, L. 1988a. Calculation of hydraulic conductivity from slow water level recovery. First Tennessee Hydrology Symposium, June 21-23, 1988, Nashville, Tennessee.
- Toran, L. 1988b. Long-term versus short-term slug tests in low-permeability formations. p. 13. IN Abstracts from Conference on Flow and Transport in Low Permeability Settings, December 13-14, 1988, Las Vegas, Nevada, sponsored by the National Water Well Association.
- Voorhees, L. D., L. A. Hook, M. J. Gentry, R. A. McCord, M. A. Faulkner, J. L. Bledsoe, K. A. Newman, P.T. Owen, and A. E. Rosen. 1989. Data base management activities for the remedial action program at ORNL: Calendar year 1988. ORNL/TM-11147.
- Webster, D. A., and M. W. Bradley. 1988. Hydrology of the Melton Valley radioactive waste burial grounds at Oak Ridge National Laboratory, TN. Geol. Surv. Open-File Rep. (U.S.) 87-686, 115 pp.
- Woodward, N. B., S. Wojtal, J. B. Paul, and Z. Z. Zadins. 1988. Partitioning of deformation with several external thrust zones of the Appalachian Orogen. J. Geol. 96: 351-361.

Zehner, H. H. 1989. Construction data for wells drilled during the period 1985 through 1987 at Oak Ridge National Laboratory, Oak Ridge, Tennessee. Geol. Surv. Open-File Rep. (U.S.) 89-61, 96 pp.

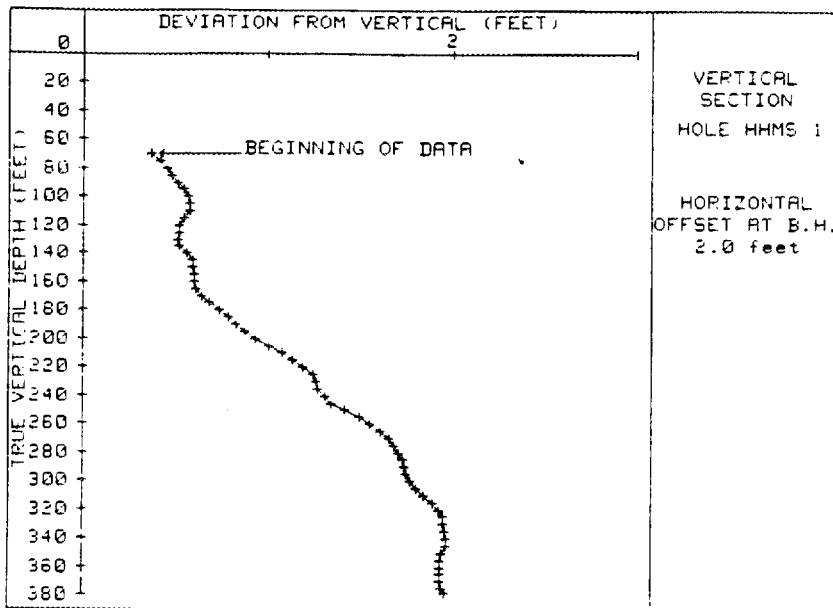
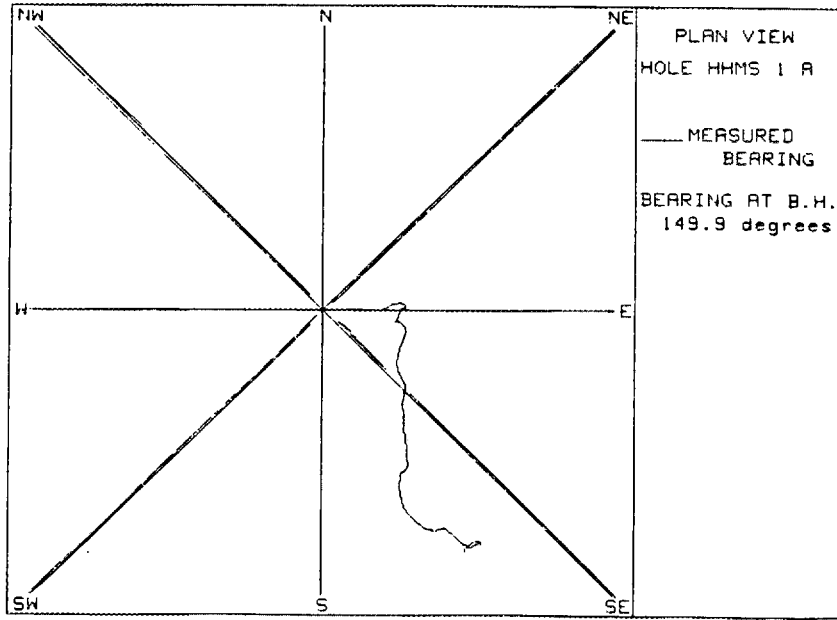
APPENDIX 1
GENERAL WELL SITE INFORMATION
DRILLERS LOGS
GEOPHYSICAL LOGS
FOR HHMS SITE 1

WELL DATA, STRATIGRAPHIC AND STRUCTURAL MARKERS, DRILLERS LOGS					
Well Name	Alternate Name	ORNLN (ft)	ORNLE (ft)	Ground Elevation (ft)	Top of Casing (ft)
HHMS 1 A	927	18014.84	27964.36	870.11	873.1
		depth	elevation		
Cm marker	4?	110	760.11		
	3	151	719.11		
	2	216	654.11		
	1	288	582.11		
	Cm/Crg	329	541.11		
average downhole thickness of Crg in P&T is 116'					
implies base Crg/Crt contact is					
	Crg/Crt	445	425.11		
deformation zone	TDZ	0	870.11		
	TDZ	152	718.11		
	fault	152	718.11		
	Fault D	168	702.11		
no resolution on BHTV, fault between 152 and 168 (drastic dip change)					
	fracture	246	624.11		
	fracture	250	620.11		
	Fault D ^{sp}	261	609.11		
	fault zone	269	601.11		
4 fractures between 261 and 269					
	fracture/fault	297			
	fracture/fault	313			
fracture/fault id'd by BHTV, correlate with SP kick					
* alternate interpretation - correlate zone between 246 and 313 with Fault E					
DRILLERS LOGS					
	water	40	830.11		

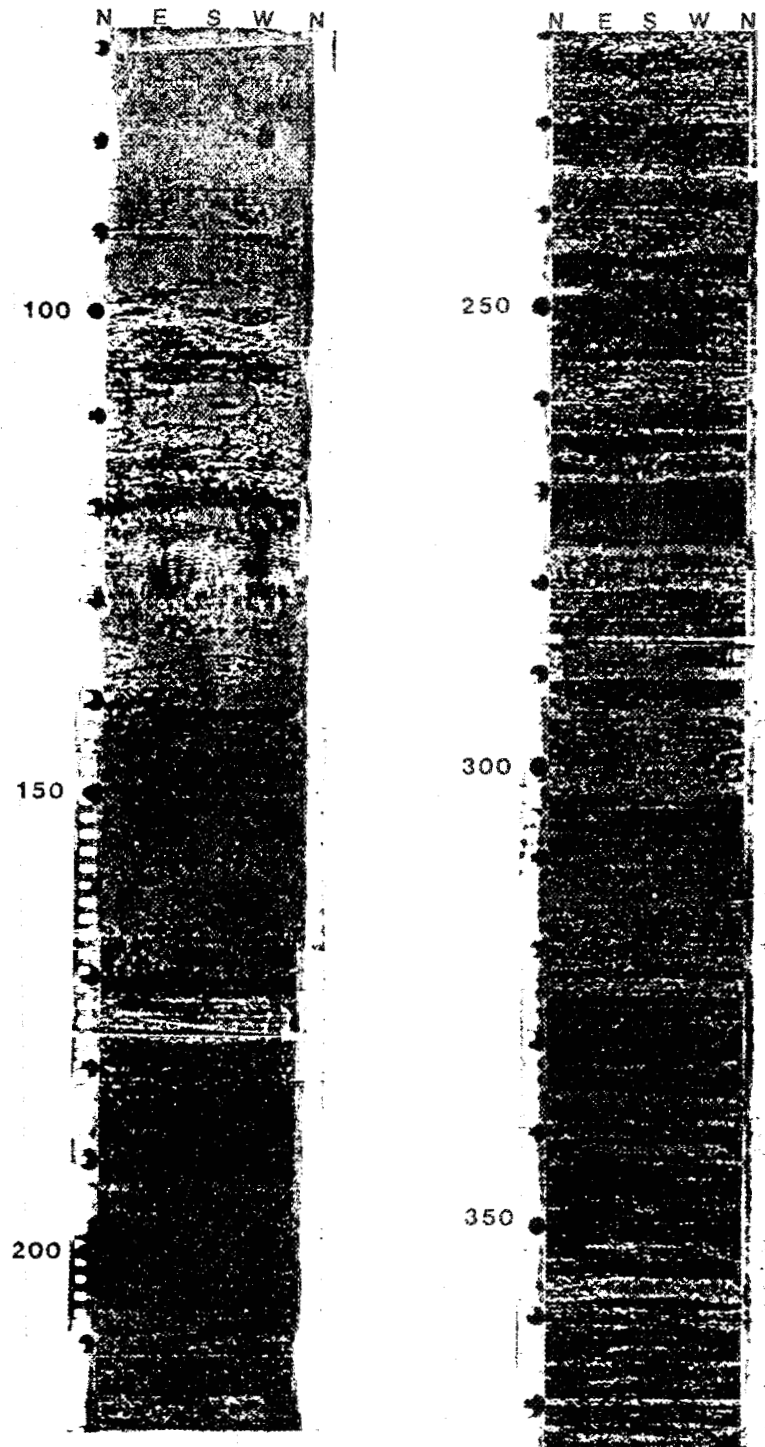
HHMS 1 - GEOPHYSICAL LOGS



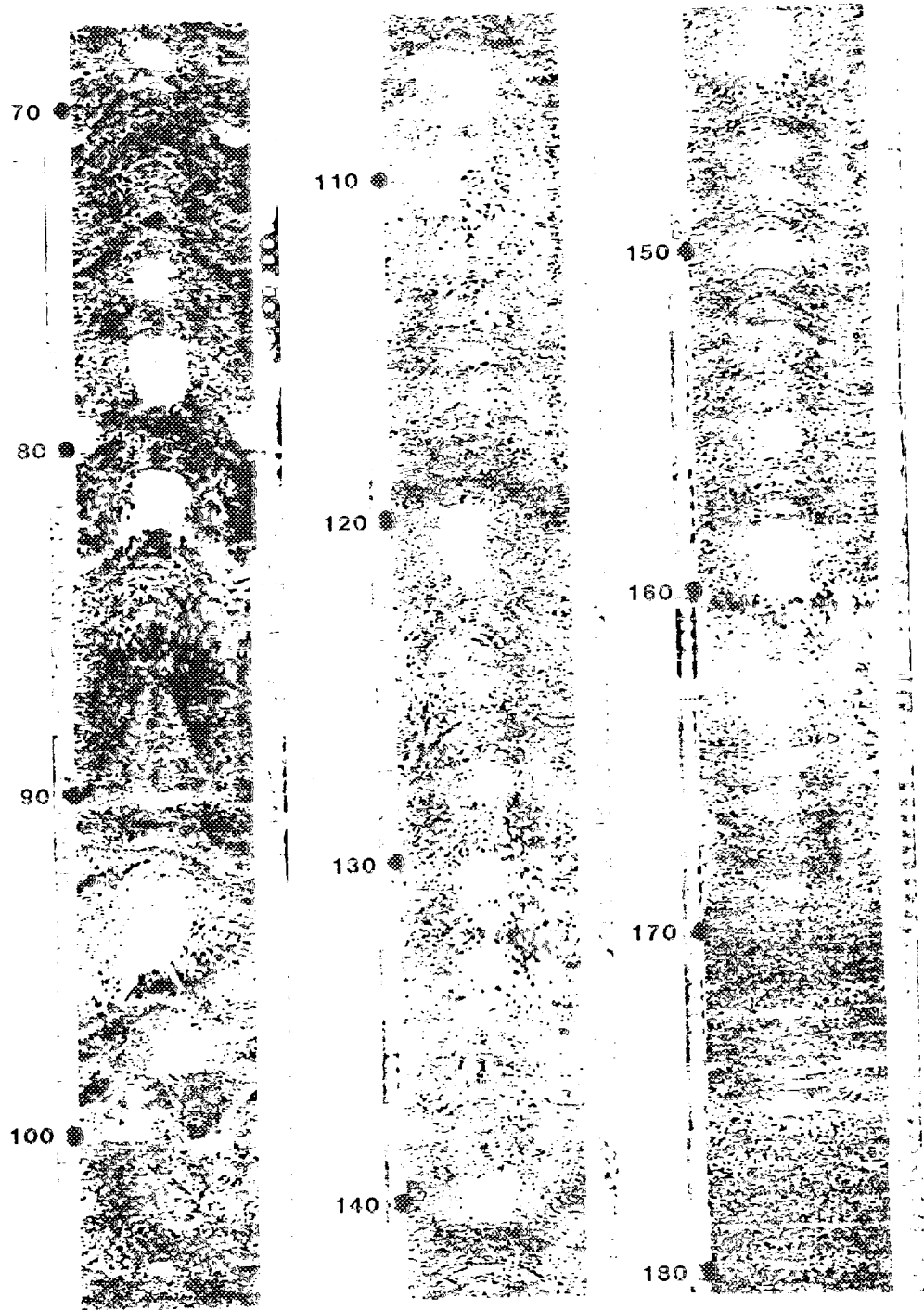
HHMS 1 - DEVIATION LOG



HHMS 1A

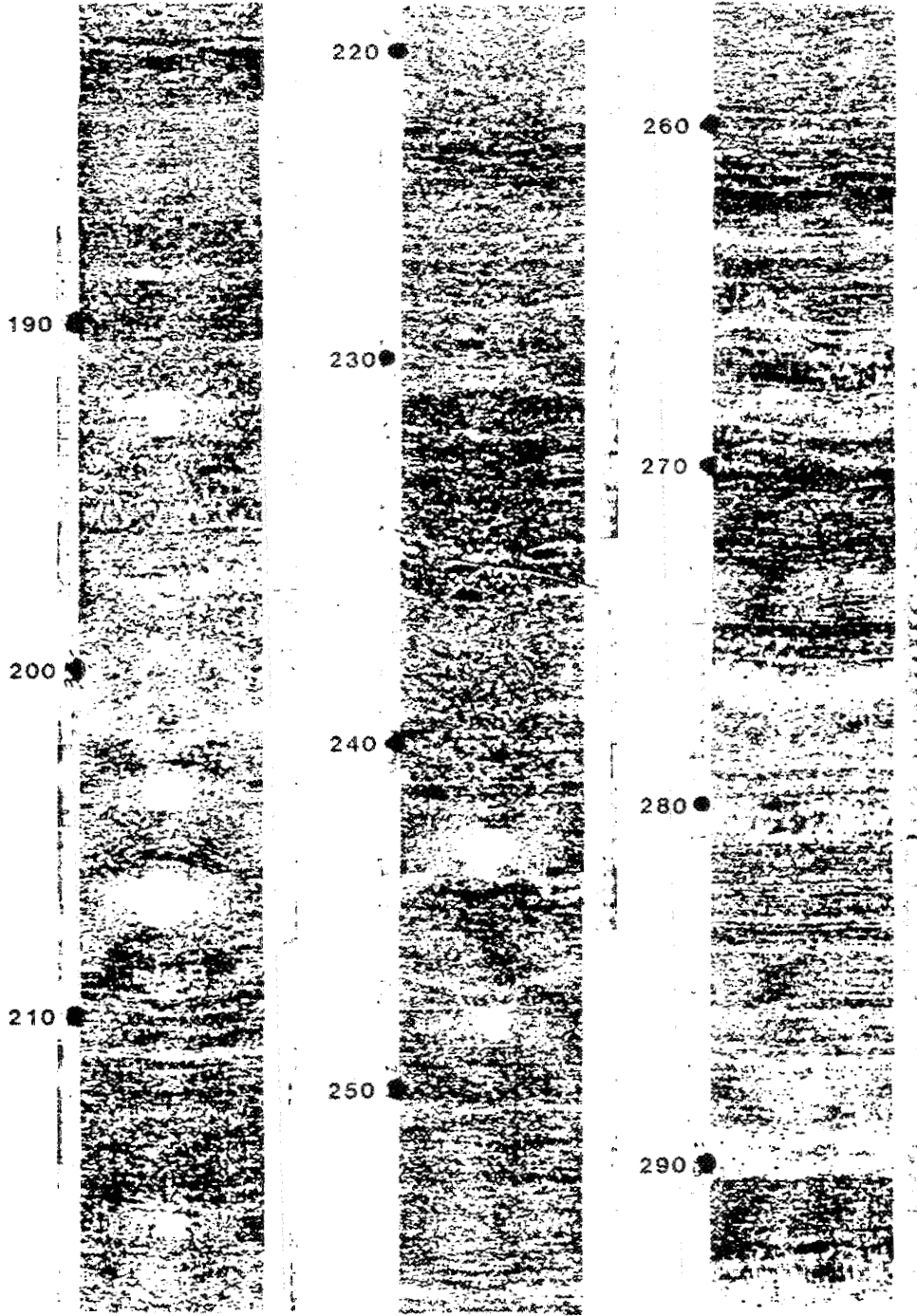


HHMS 1A



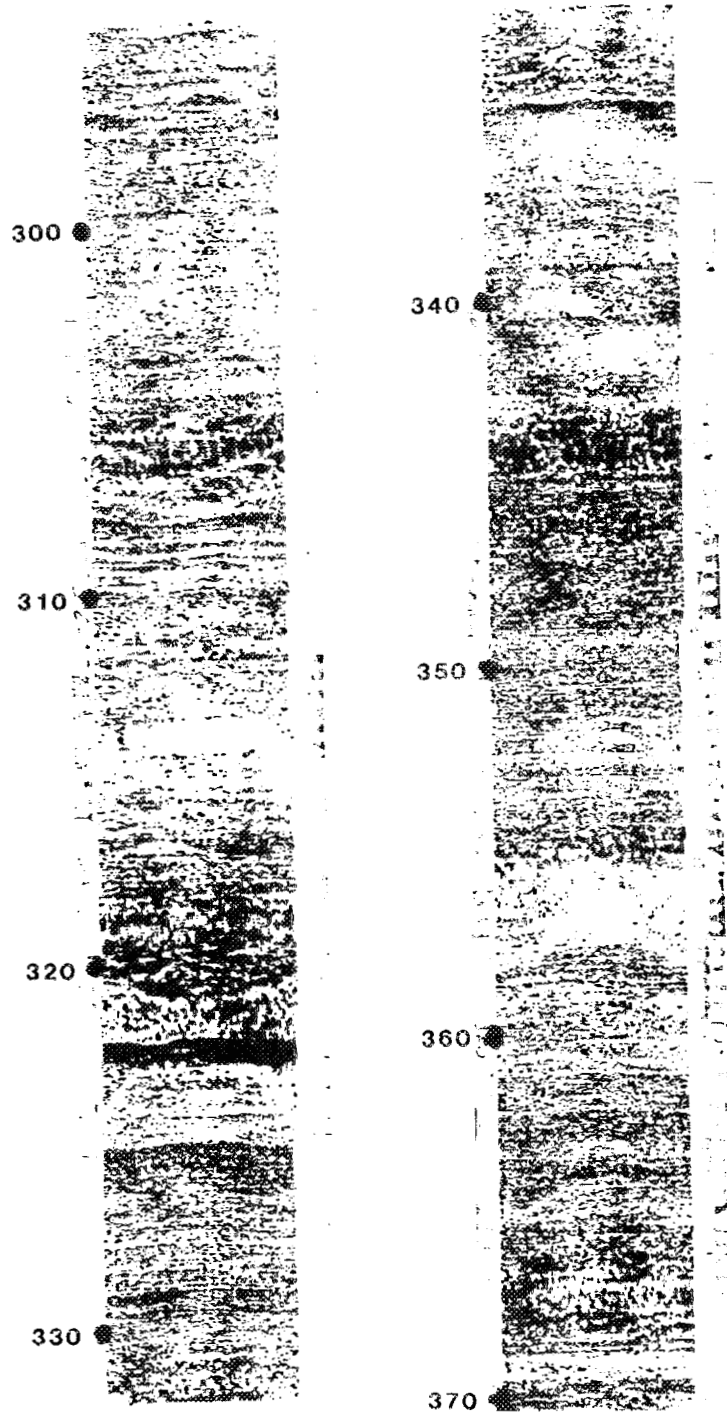
COMPASS OFF ENTIRE INTERVAL

HHMS 1A



COMPASS OFF ENTIRE INTERVAL

HHMS 1A



COMPASS OFF ENTIRE INTERVAL

APPENDIX 2

GENERAL WELL SITE INFORMATION

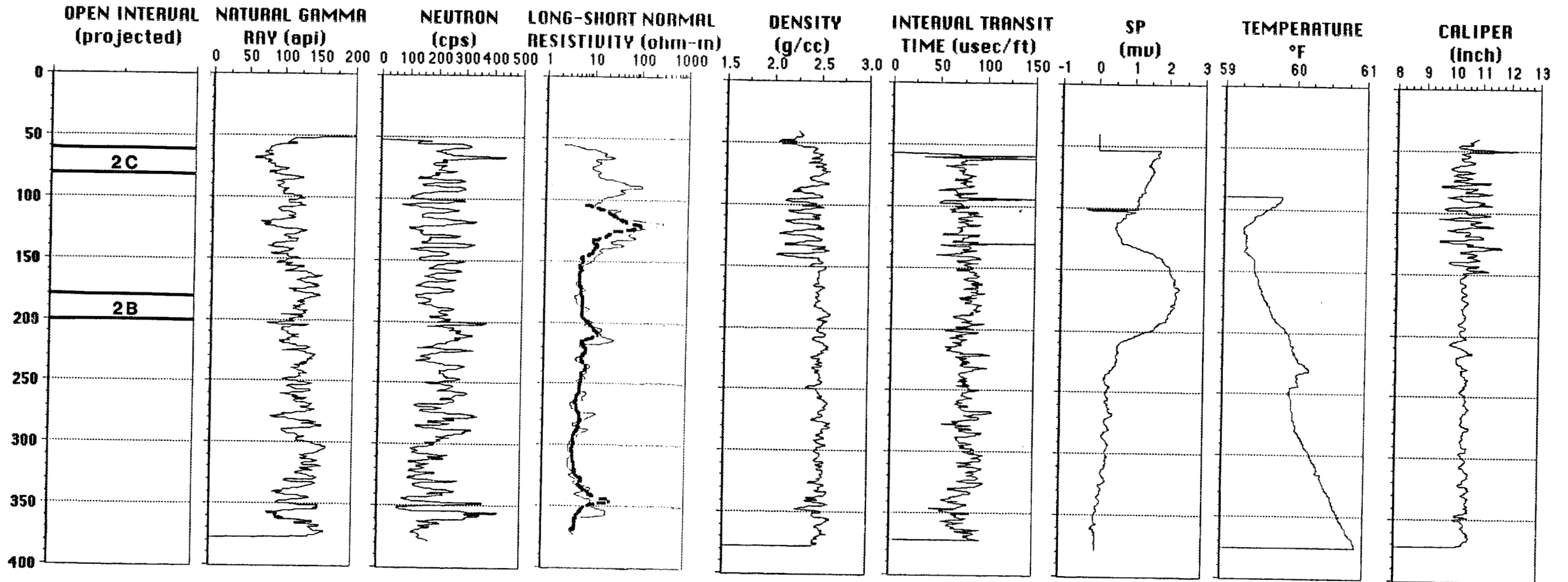
DRILLERS LOGS

GEOPHYSICAL LOGS

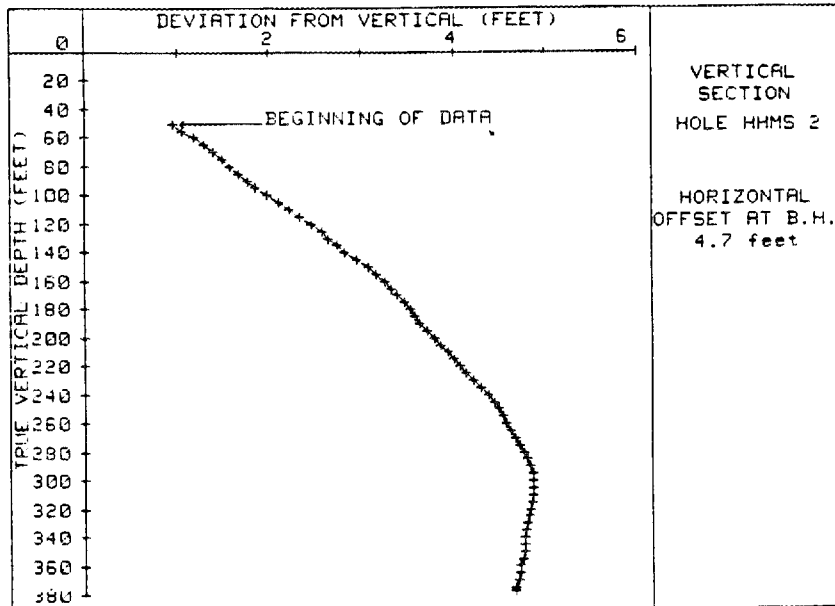
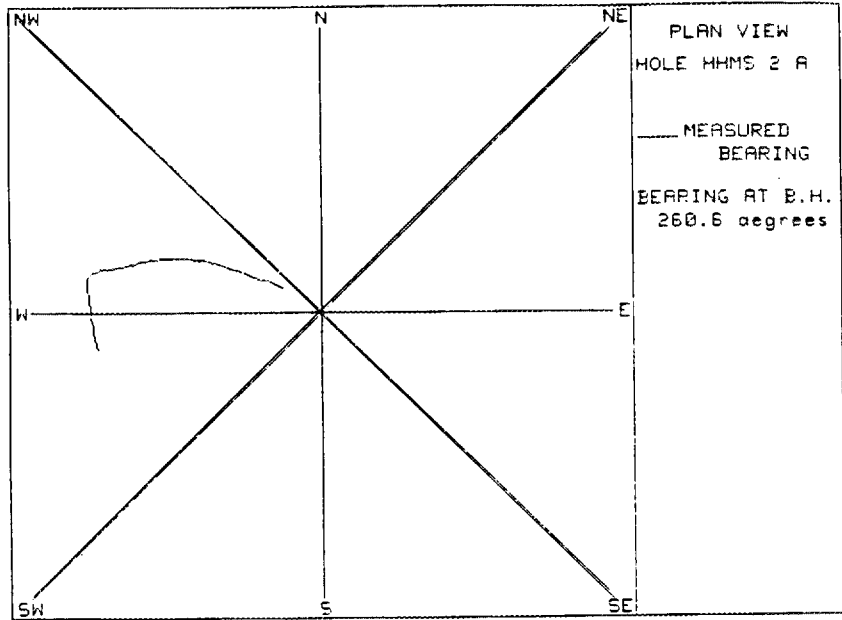
FOR HHMS SITE 2

WELL DATA, STRATIGRAPHIC AND STRUCTURAL MARKERS, DRILLERS LOGS					
Well Name	Alternate Name	ORNL N (ft)	ORNL E (ft)	Ground Elevation (ft)	Top of Casing (ft)
HHMS 2 A	930	17225.06	27562.33	806.5	809.52
		depth	elevation		
Cm marker	4	122	684.5		
	3	165	641.5		
	2	228	578.5		
	1	301	505.5		
	Cm/Crg	363	443.5		
	TDZ	0	806.5		
	TDZ	150	656.5		
cal rough 0 - 150 ft.					
BHTV steep, no compass, poor resolution					
	Fault D	205	601.5		
	fracture	211	595.5		
	fracture	220	586.5		
	Fault D	225	581.5		
fractures between 205 and 225 identified by BHTV - correspond to temperature deflections					
	Fault D''	326	480.5		
*entire borehole (where compass works) - strata dips to north					
DRILLERS LOGS					
soft		152	654.5		
soft		305	501.5		
soft		310	496.5		
rough		17	789.5		
rough		55	751.5		
rough	from	132	674.5		
rough	to	152	654.5		
broken up	from	55	751.5		
broken up	to	58	748.5		

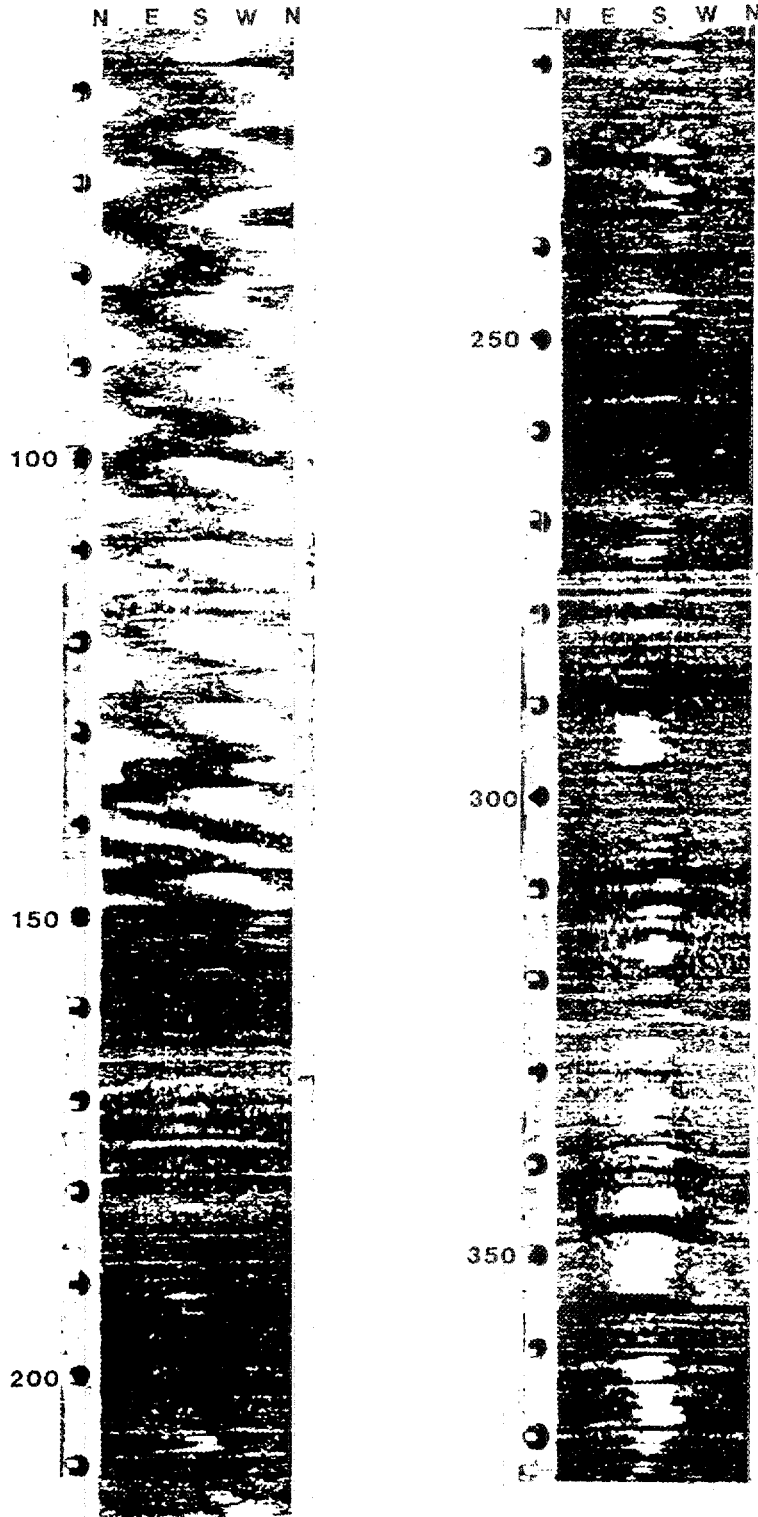
HHMS 2 - GEOPHYSICAL LOGS



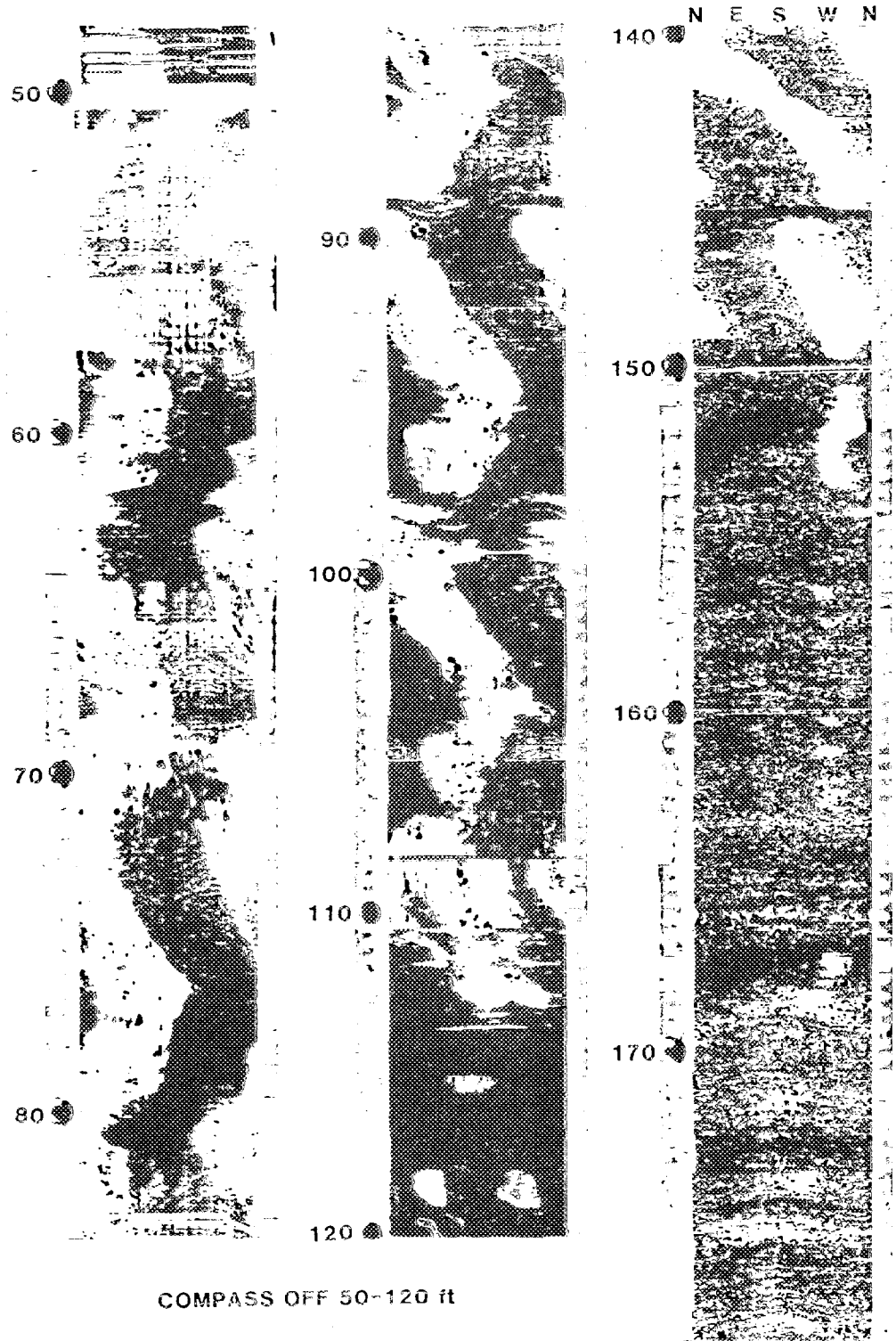
HHMS 2 - DEVIATION LOG



HHMS 2A

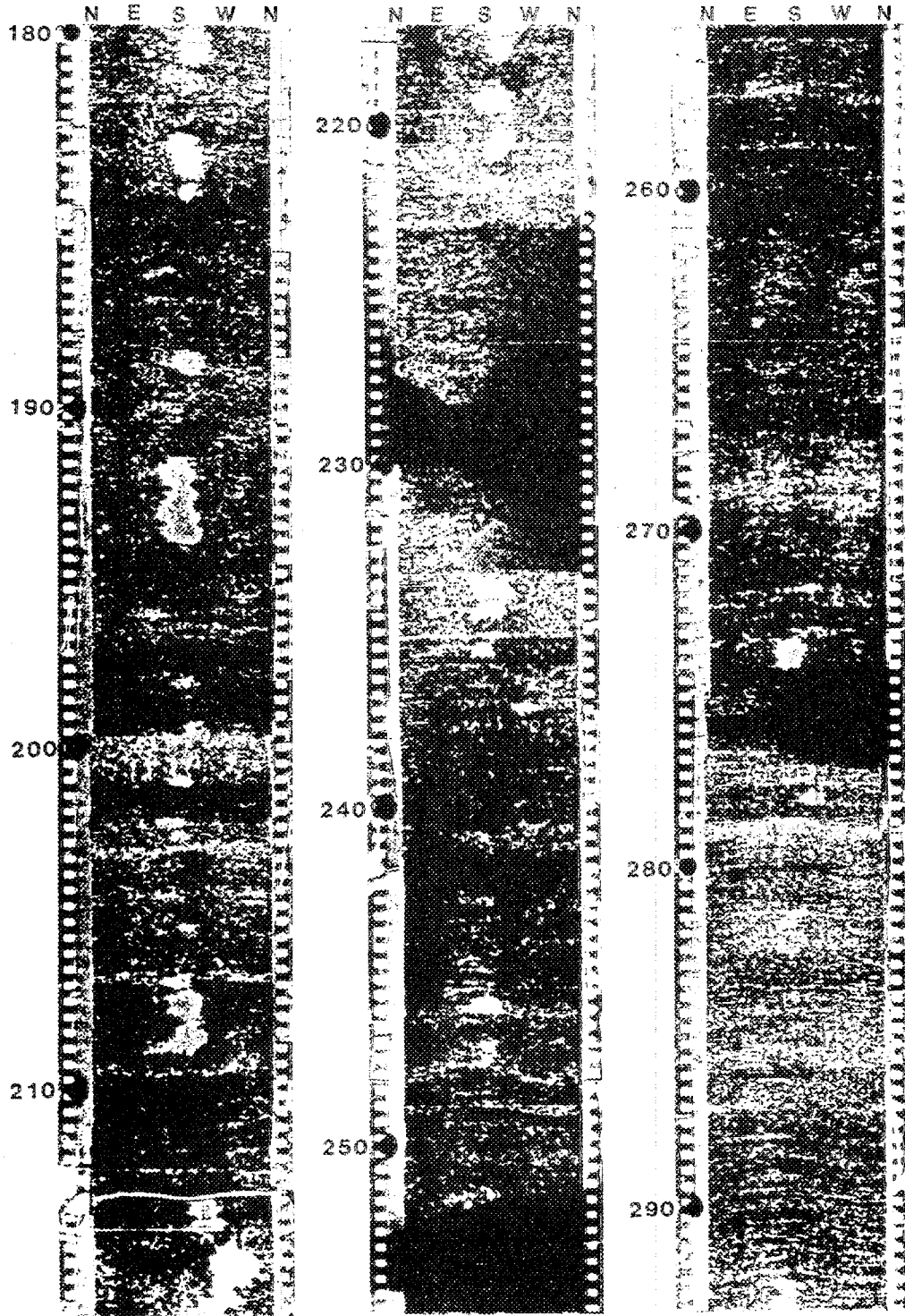


HHMS 2A

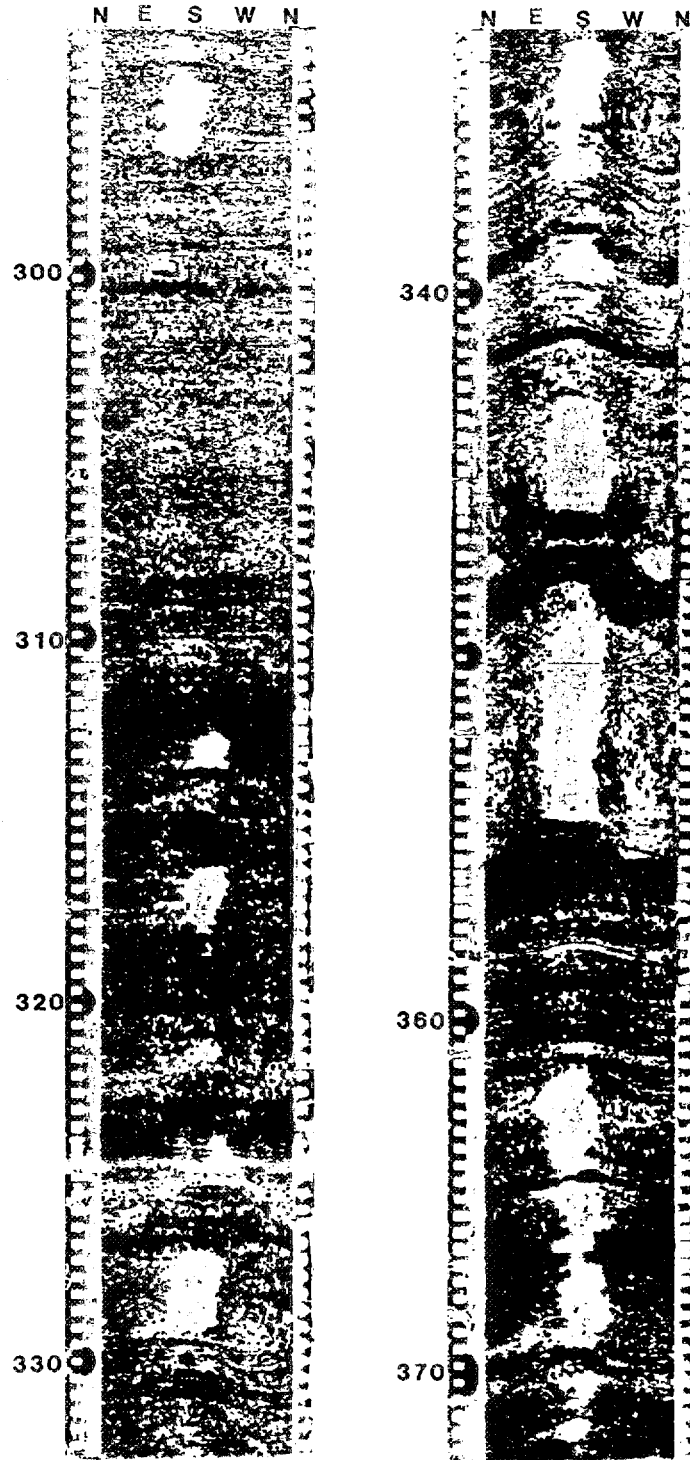


COMPASS OFF 50-120 ft

HHMS 2A



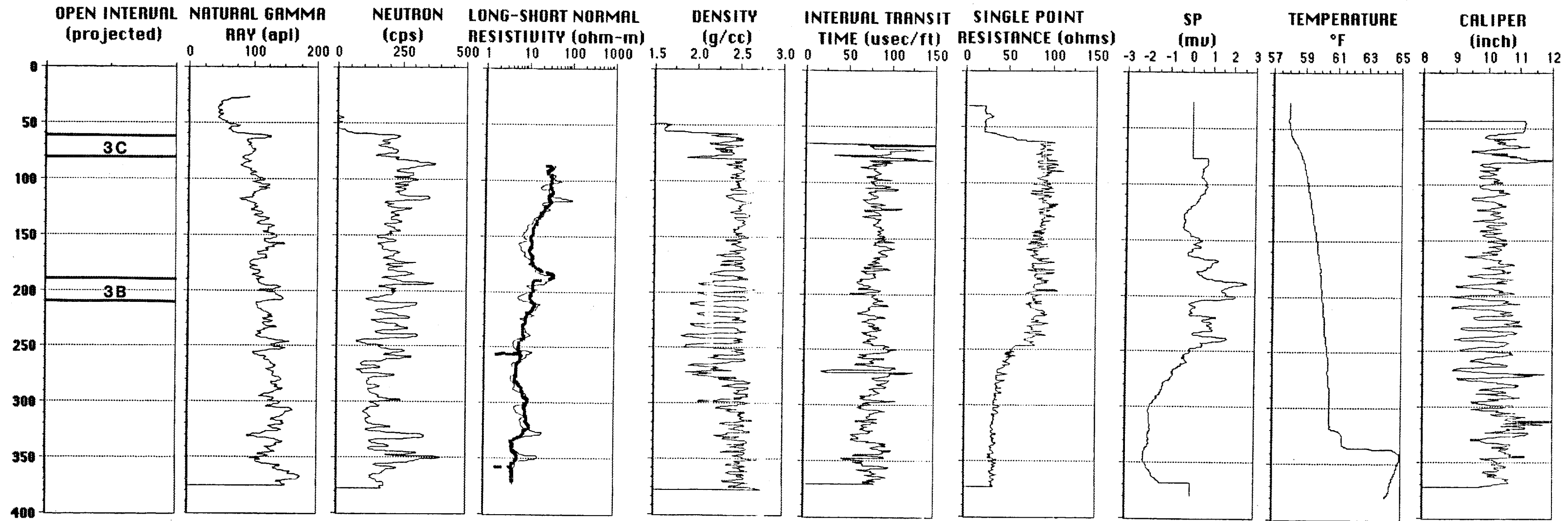
HHMS 2A



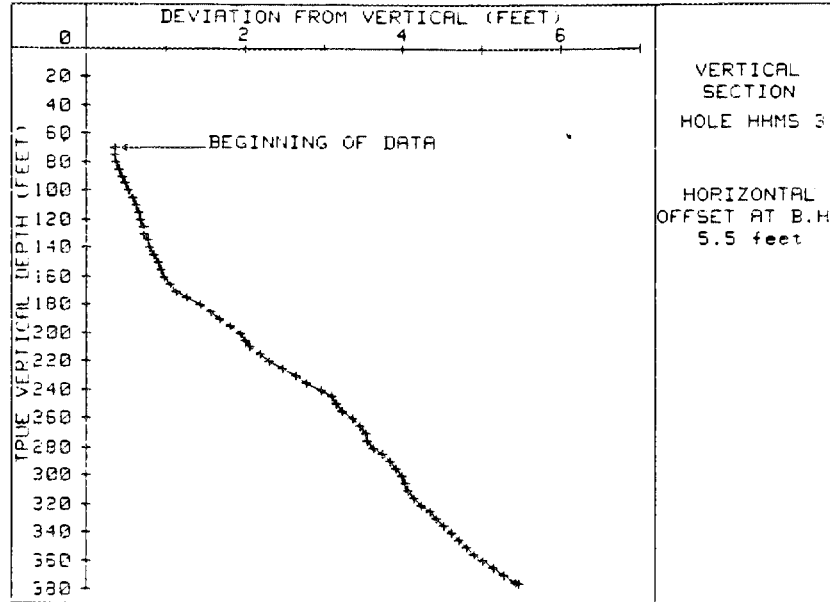
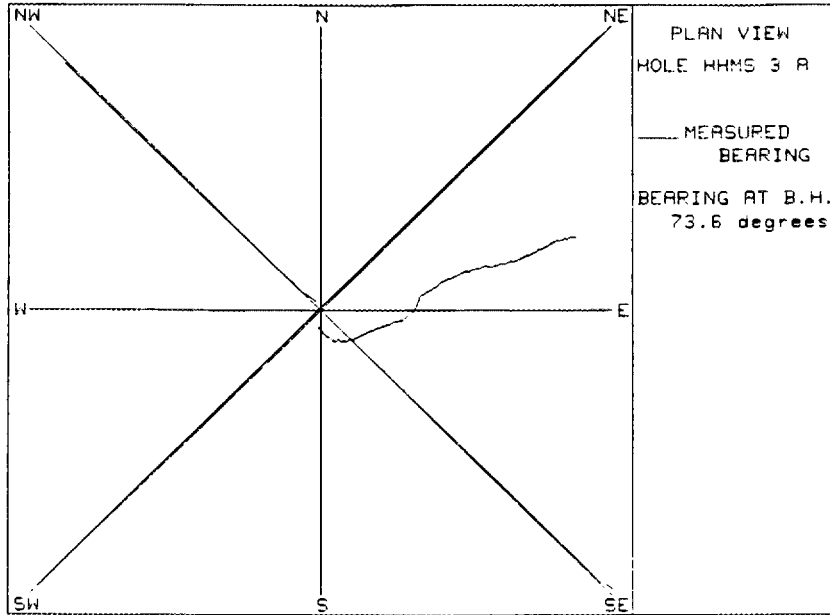
APPENDIX 3
GENERAL WELL SITE INFORMATION
DRILLERS LOGS
GEOPHYSICAL LOGS
FOR HHMS SITE 3

WELL DATA, STRATIGRAPHIC AND STRUCTURAL MARKERS, DRILLERS LOGS					
Well Name	Alternate Name	ORNL N (ft)	ORNL E (ft)	Ground Elevation (ft)	Top of Casing (ft)
HHMS 3 A	933	17213.8	26724.48	818.79	821.19
		depth	elevation		
Cm marker	5	62	756.79		
	4	118	700.79		
	3	159	659.79		
	2	208	610.79		
	1	305	513.79		
	Cm/Crg	355	463.79		
	TDZ	160	658.79		
	TDZ	275	543.79		
caliper rough; SP noise (irregular spikes)					
within above zone, fracture id by BHTV, fracture at 229 is ?, 175 very steep - 70 deg., 3 fractures at approximately 240 ft					
	fracture	165	653.79		
	fracture	175	643.79		
	fracture	200	618.79		
	fracture	229	589.79		
	fracture	240	578.79		
	fracture	263	555.79		
	Fault zone E	320	498.79		
	Fault zone E	380	438.79		
320 - T kick, LSN change (matches 8A)					
	Fault E	331.5	487.29		
Very steep from 328 - 335					
DRILLERS LOGS					
soft		52	766.79		
soft		85	733.79		
soft	from	160	658.79		
soft	to	168	650.79		
rough		87	731.79		
rough		120	698.79		
rough		132	686.79		
rough		182	636.79		

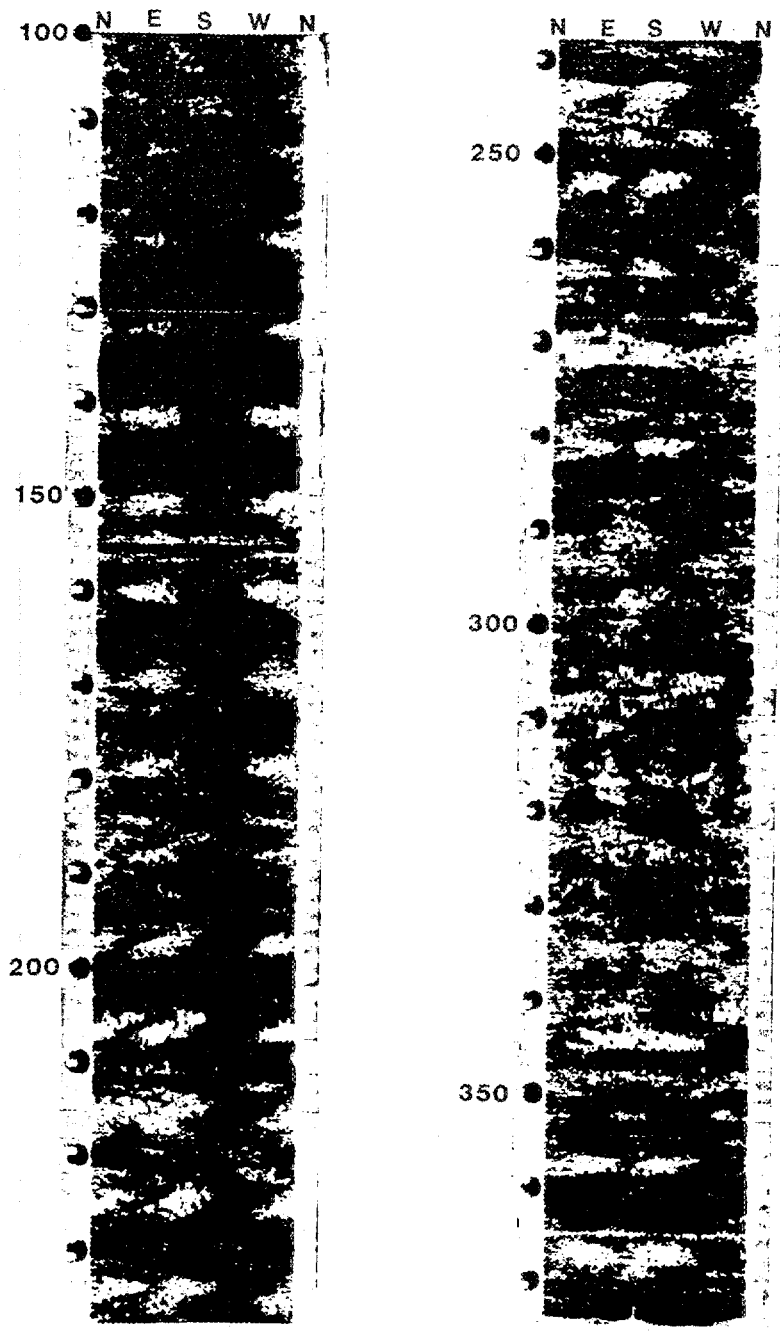
HHMS 3 - GEOPHYSICAL LOGS



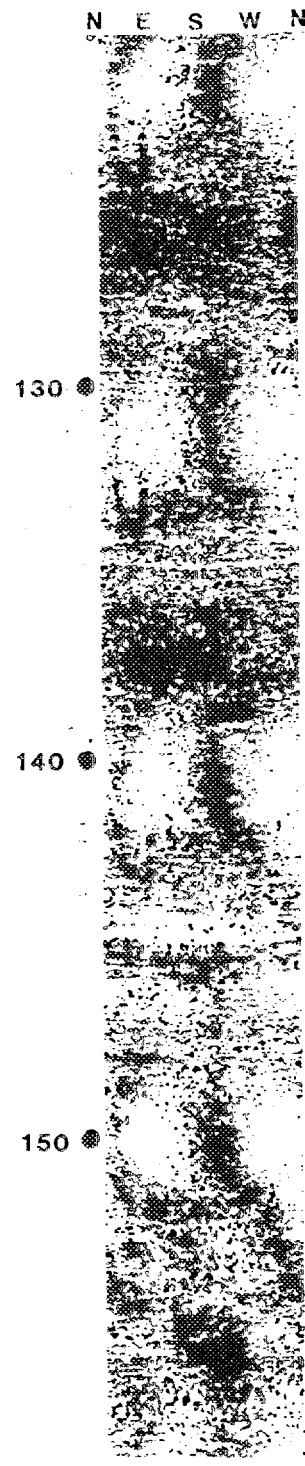
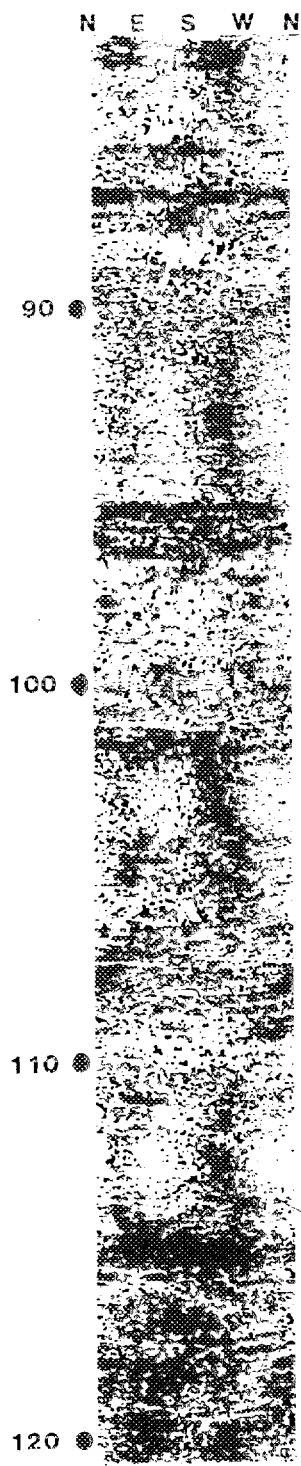
HHMS 3 - DEVIATION LOG



HHMS 3A

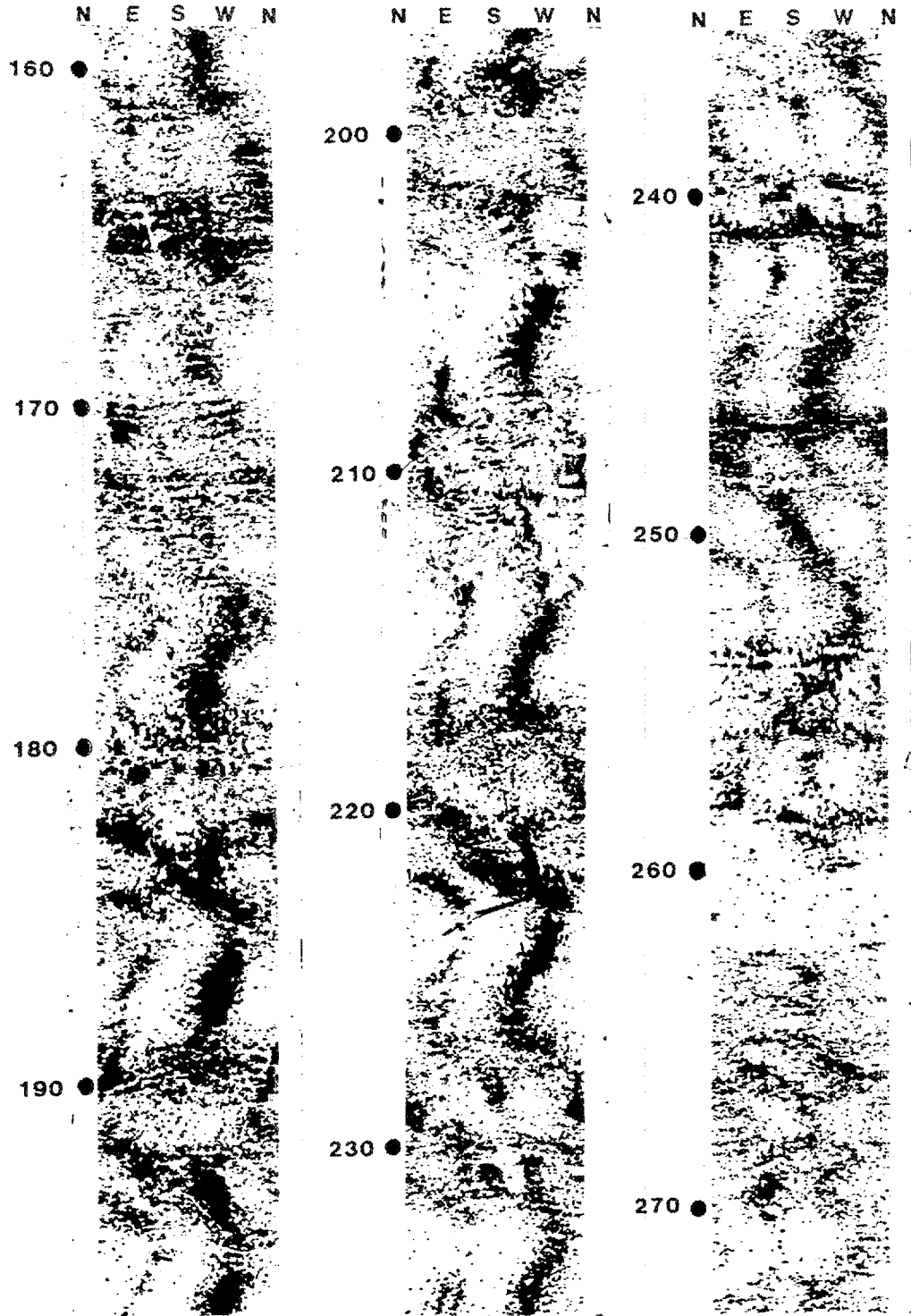


HHMS 3A



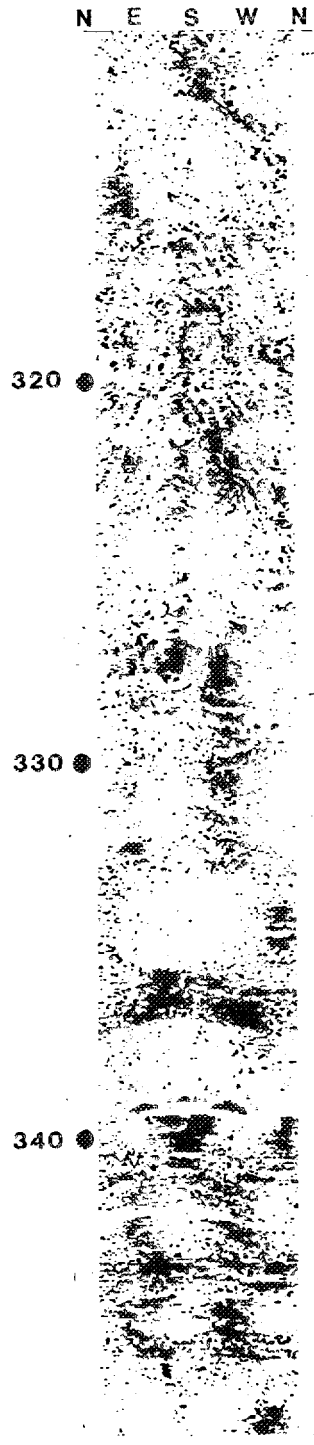
ORNL-DWG 89-13259

HHMS 3A



ORNL-DWG 89-13260

HHMS 3A



APPENDIX 4

GENERAL WELL SITE INFORMATION

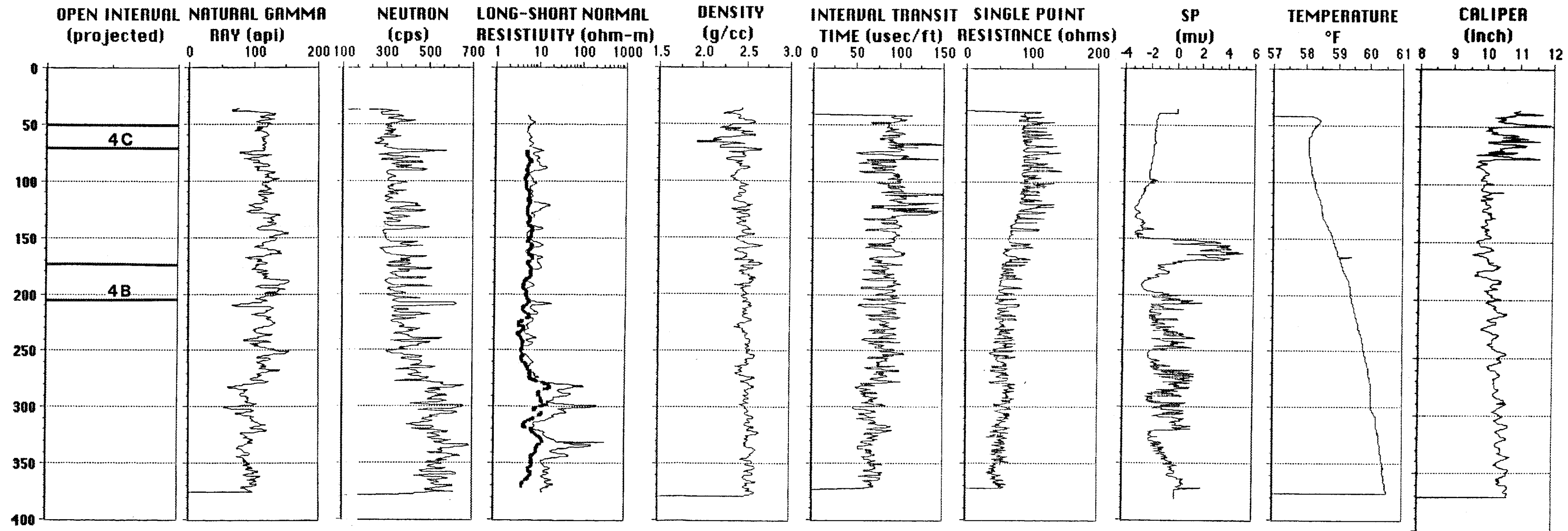
DRILLERS LOGS

GEOPHYSICAL LOGS

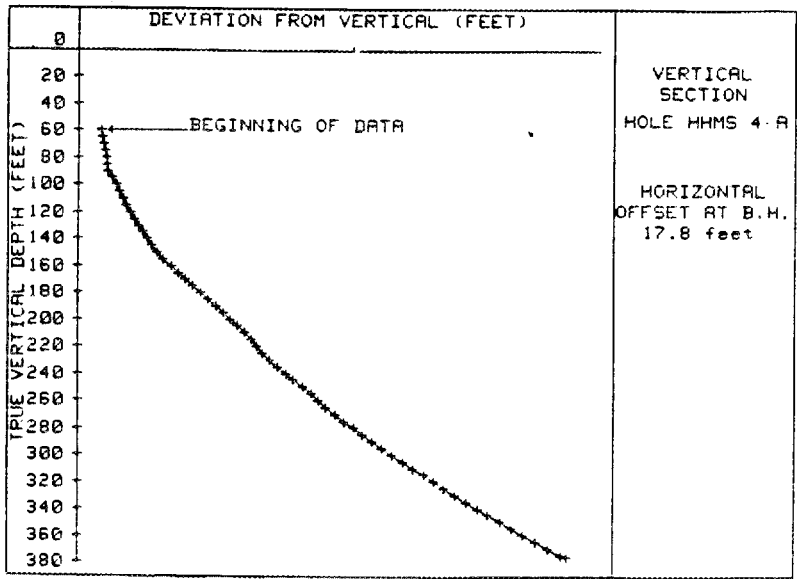
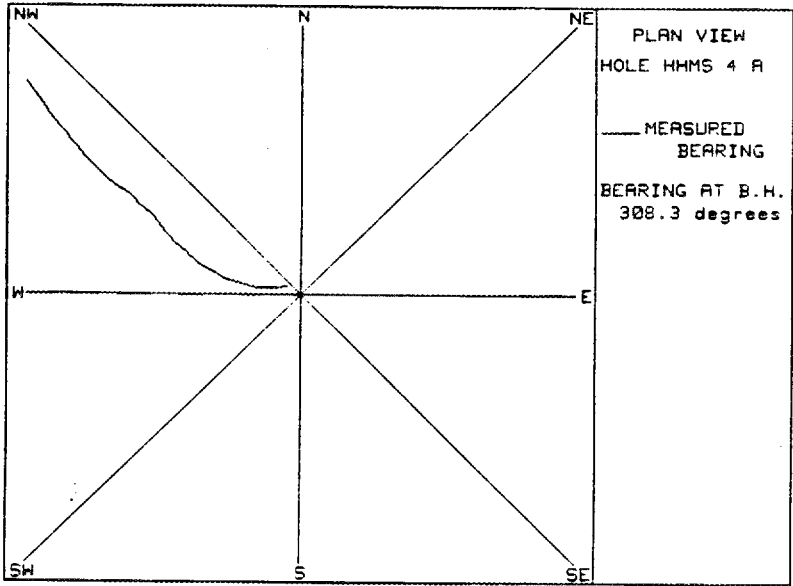
FOR HHMS SITE 4

WELL DATA, STRATIGRAPHIC AND STRUCTURAL MARKERS, DRILLERS LOGS					
Well Name	Alternate Name	ORNL N (ft)	ORNL E (ft)	Ground Elevation (ft)	Top of Casing (ft)
HHMS 4 A	936	16144.55	24609.77	790.37	793.89
		depth	elevation		
Cn marker	3	77	713.37		
	2	120	670.37		
	1	211	579.37		
	Cn/Cm	280	510.37		
correlation with HHMS 8A - assume 370' = Cm marker 5					
Cm marker	5	370	420.37		
def. zone		0	790.37		
		75	715.37		
rough caliper, BHTV shows steepest dips of the borehole (35 - 50 degrees)					
DRILLERS LOGS					
soft		132	658.37		
soft		247	543.37		
soft		294	496.37		
soft		392	398.37		

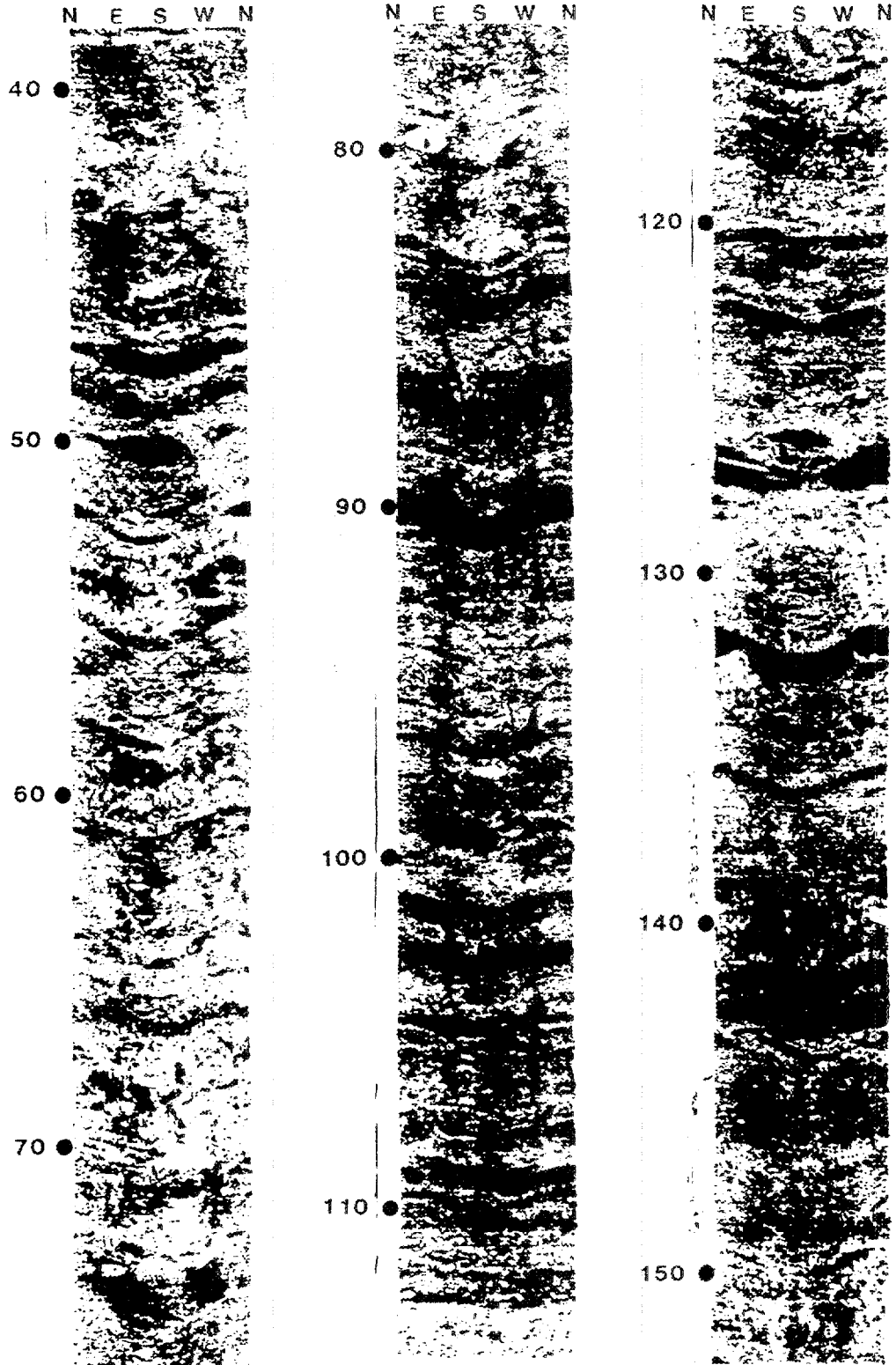
HHMS 4 - GEOPHYSICAL LOGS



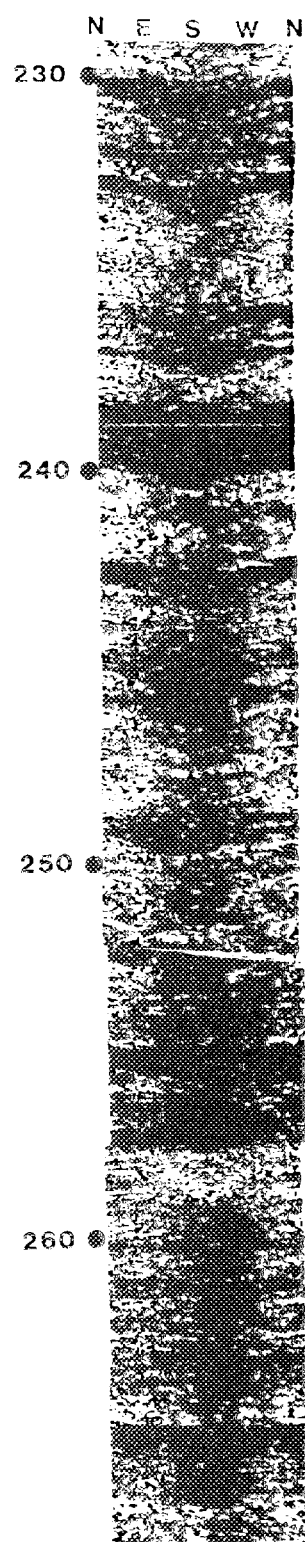
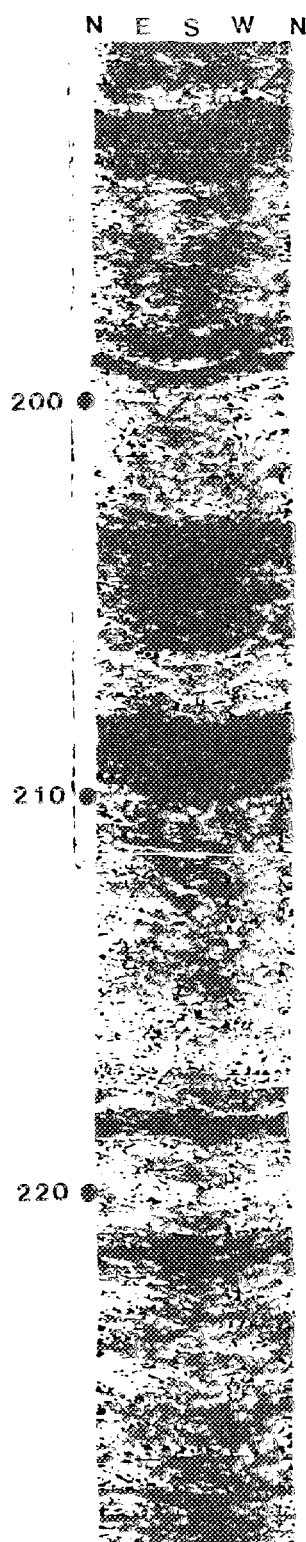
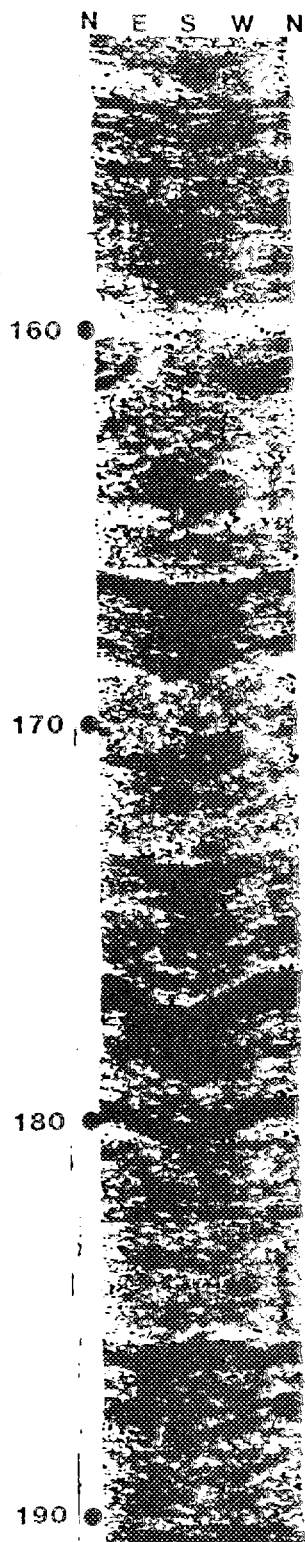
HHMS 4 - DEVIATION LOG



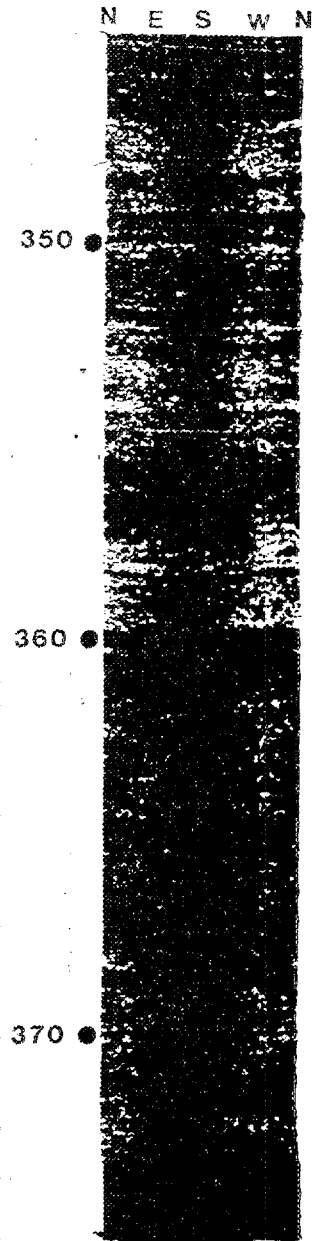
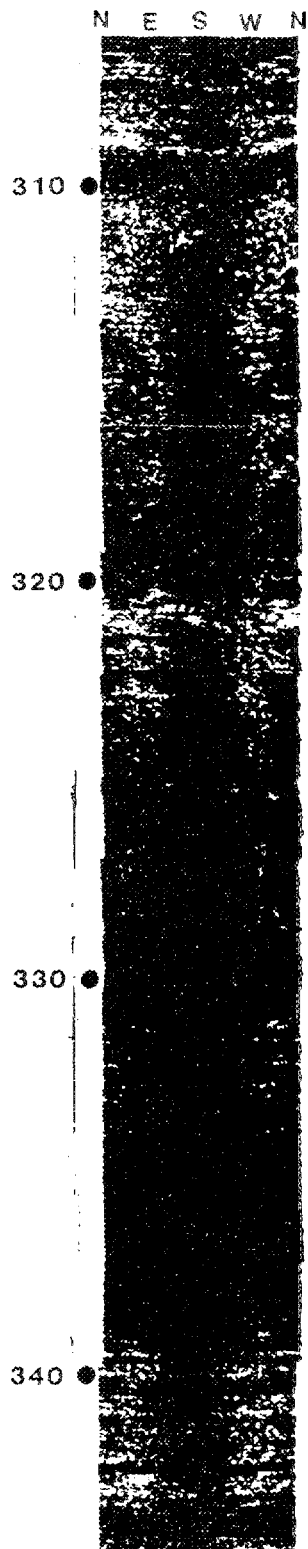
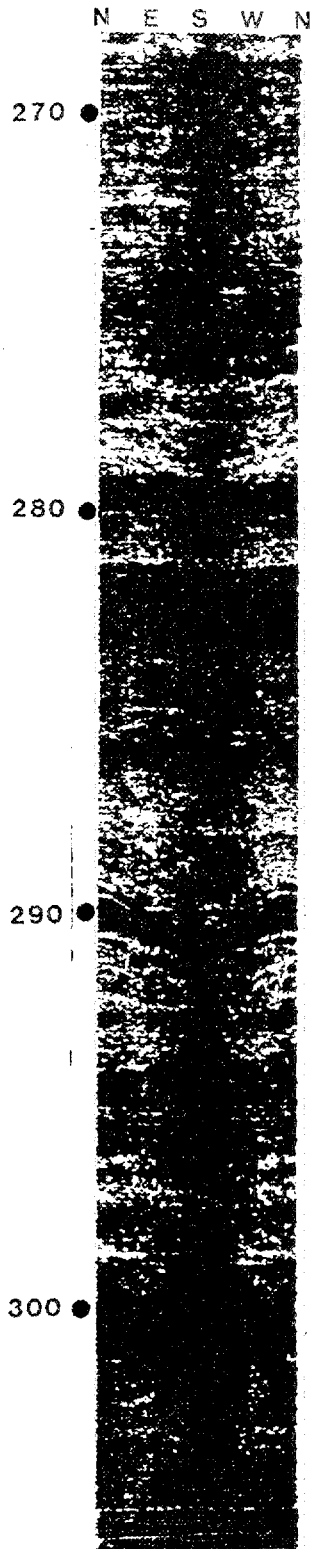
HHMS 4A



HHMS 4A



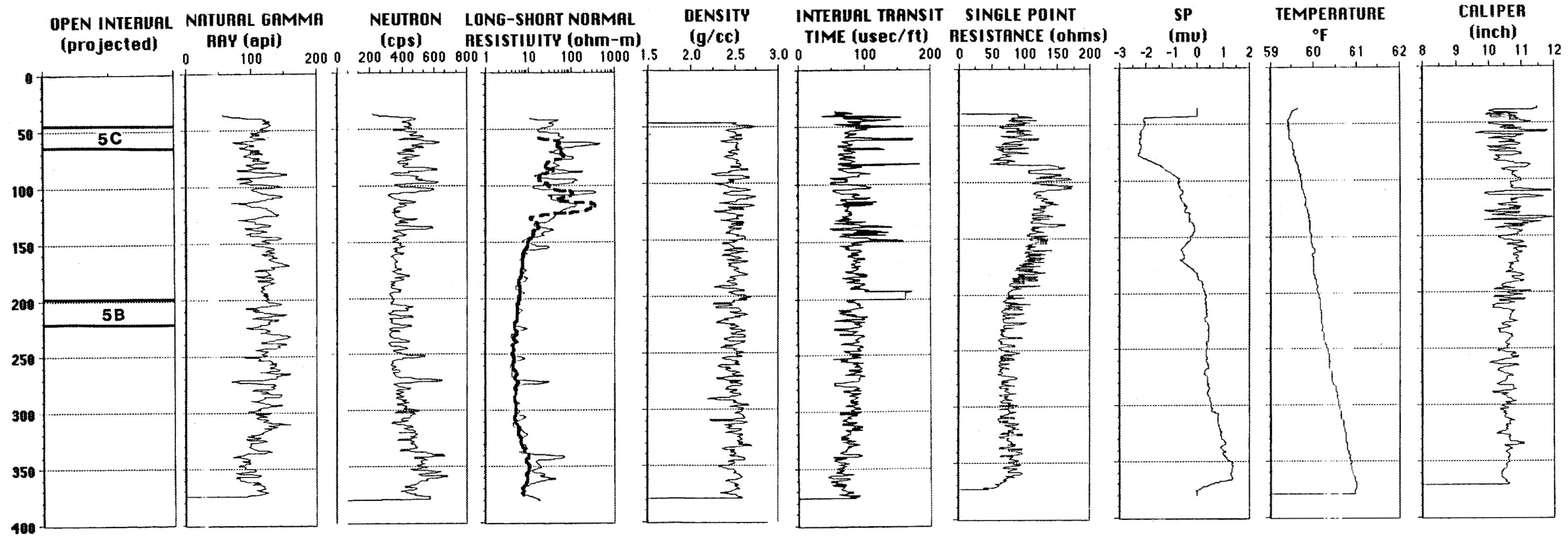
HHMS 4A



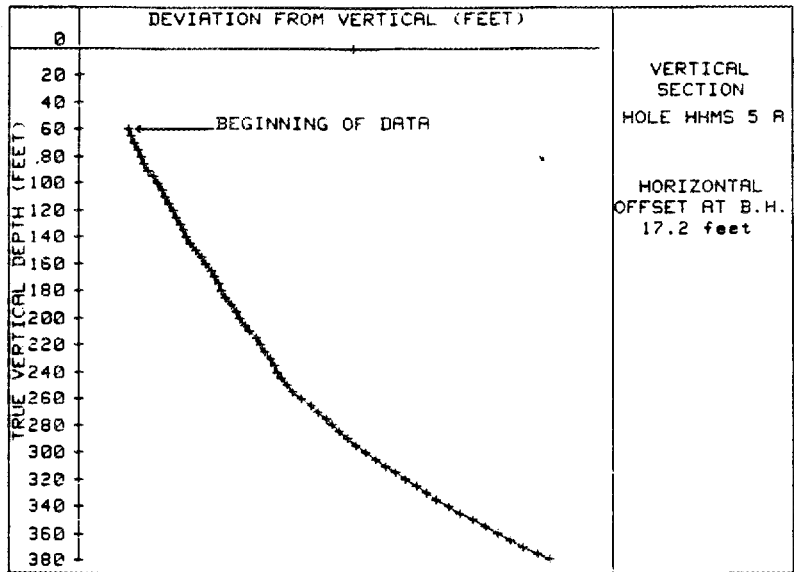
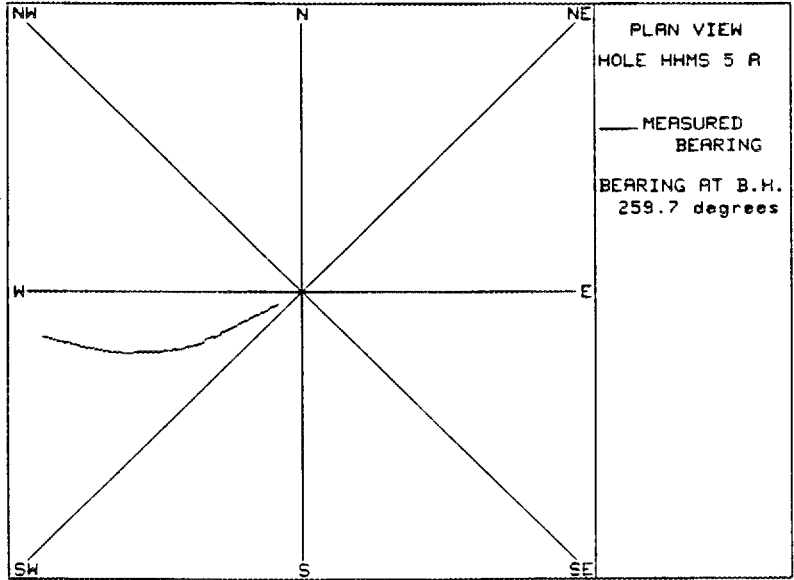
APPENDIX 5
GENERAL WELL SITE INFORMATION
DRILLERS LOGS
GEOPHYSICAL LOGS
FOR HHMS SITE 5

WELL DATA, STRATIGRAPHIC AND STRUCTURAL MARKERS, DRILLERS LOGS					
Well Name	Alternate	ORN L N	ORN L E	Ground	Top of
	Name	(ft)	(ft)	Elevation (ft)	Casing (ft)
HHMS 5 A	939	15814.83	24525.34	767.48	770.3
		depth	elevation		
Cn marker	4	91	676.48		
	3	144	623.48		
	2	205	562.48		
	1	274	493.48		
	Cn/Cm	336	431.48		
	Fault B	147	620.48		
NE dips	from	0	767.48		
	to	147	620.48		
DRILLERS LOGS					
soft		20	747.48		
soft		26	741.48		
soft		56	711.48		
soft		97	670.48		
soft		392	375.48		
rough	from	120	647.48		
rough	to	122	645.48		
very rough	from	232	535.48		
	to	238	529.48		

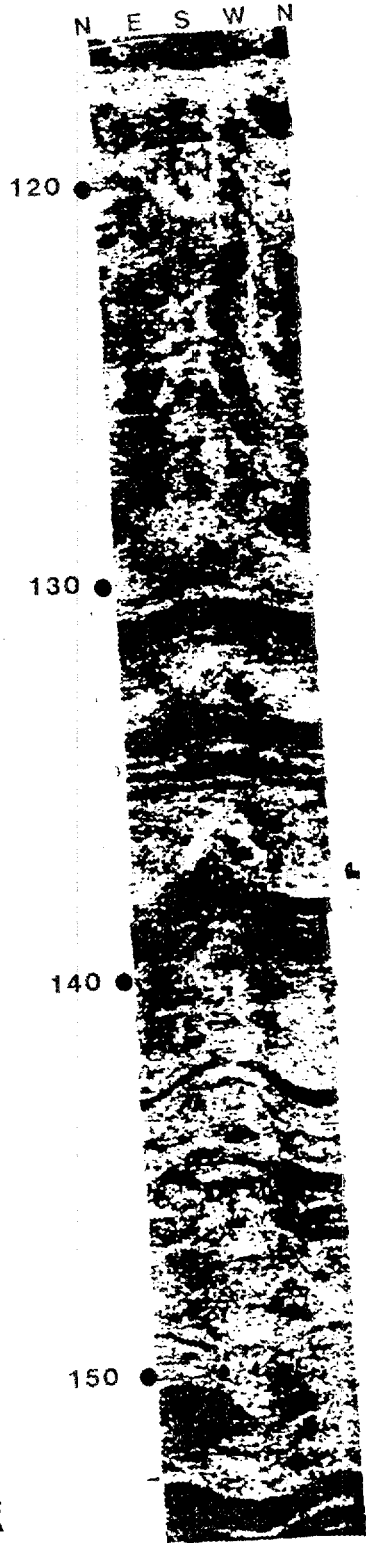
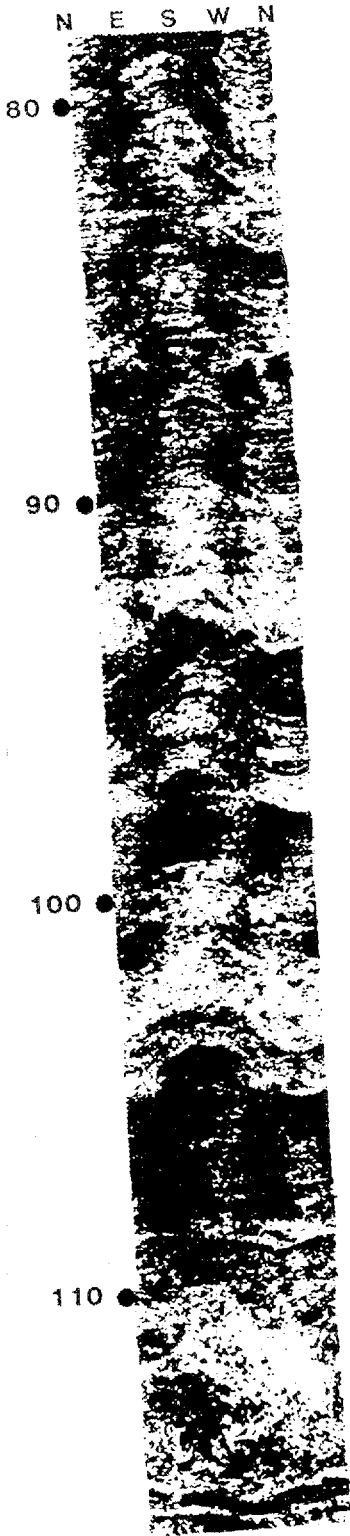
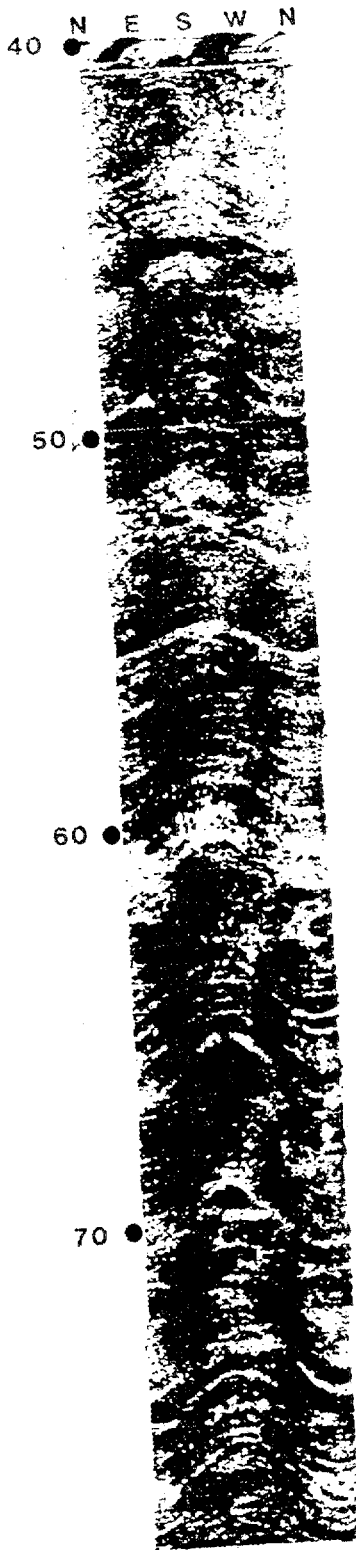
HHMS 5 - GEOPHYSICAL LOGS



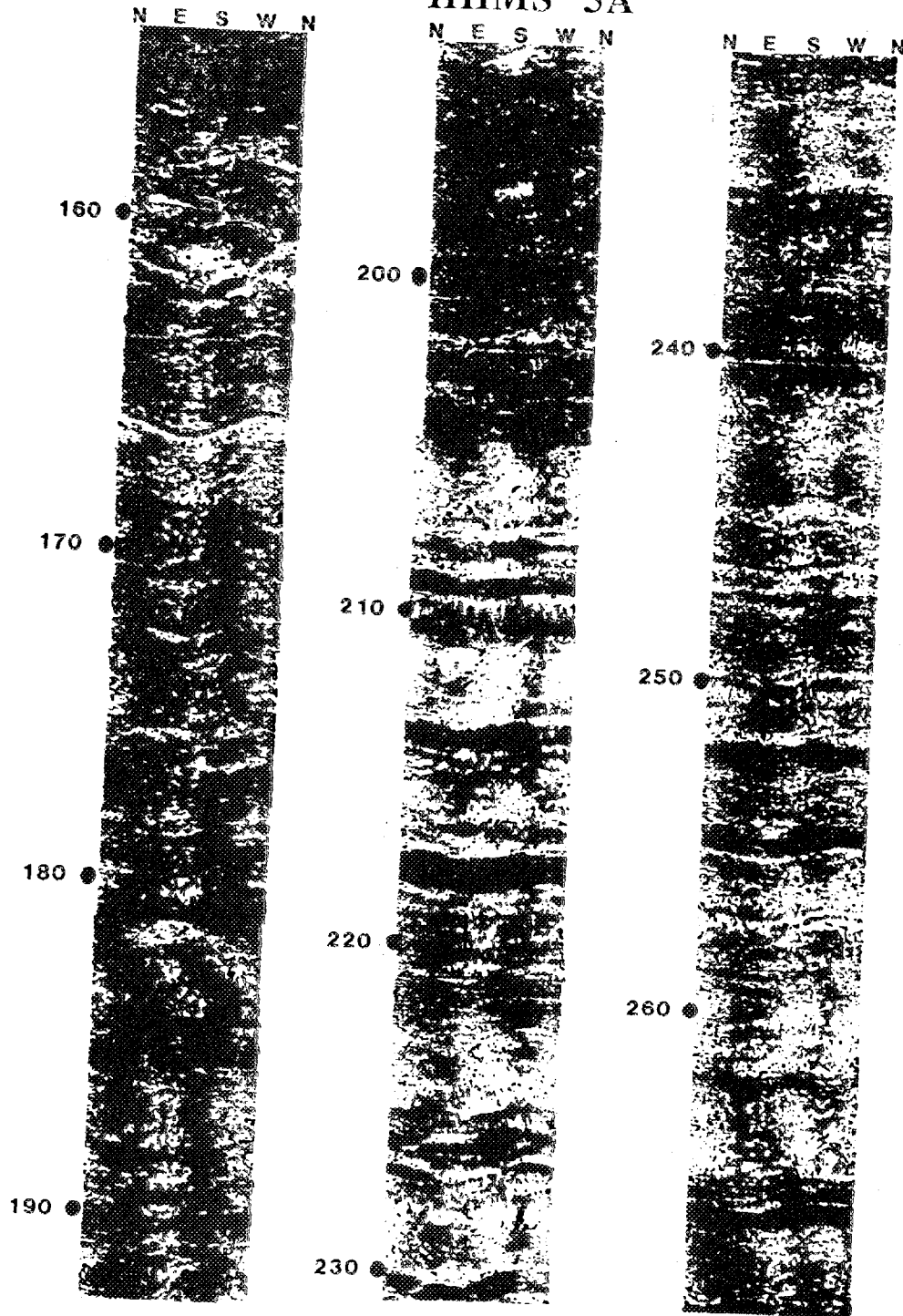
HHMS 5 - DEVIATION LOG



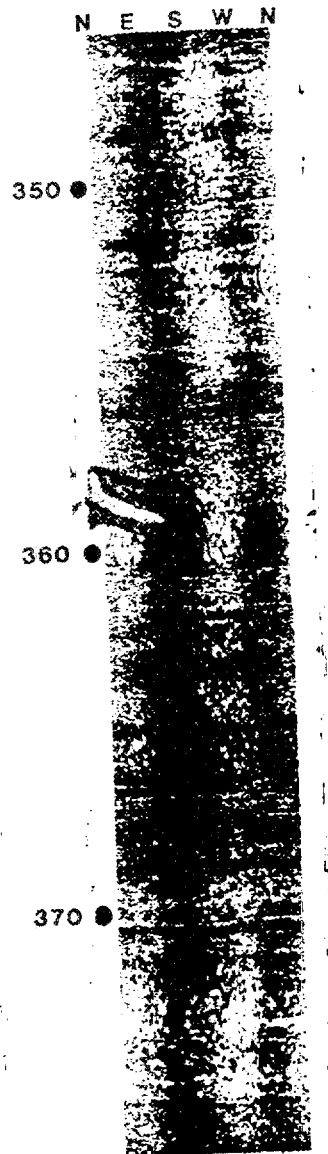
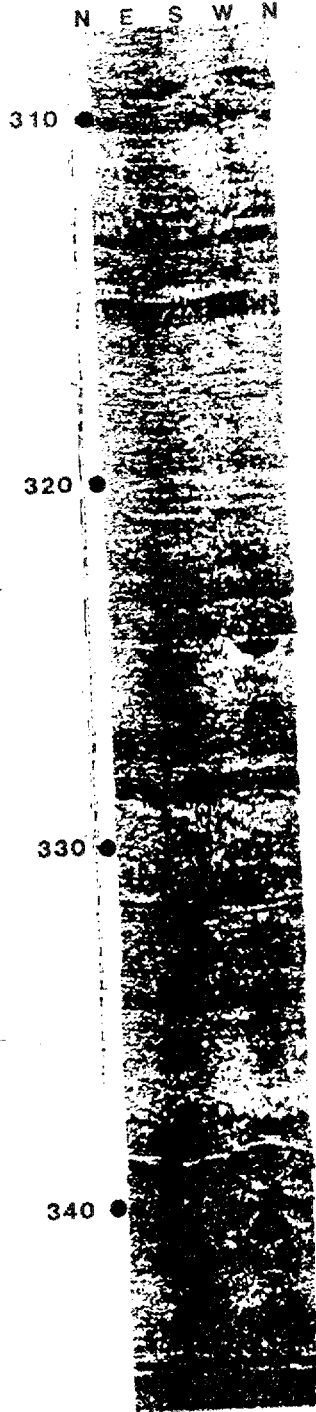
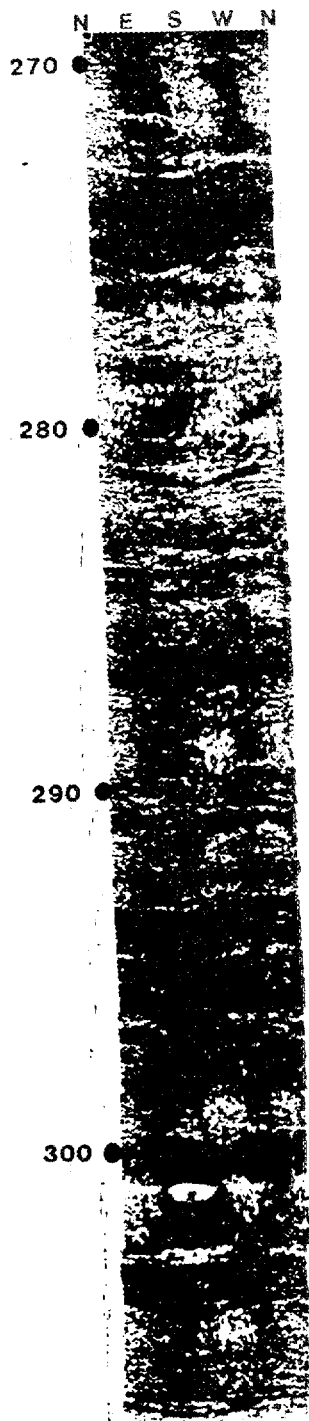
HHMS 5A



HHMS 5A



HHMS 5A



APPENDIX 6

GENERAL WELL SITE INFORMATION

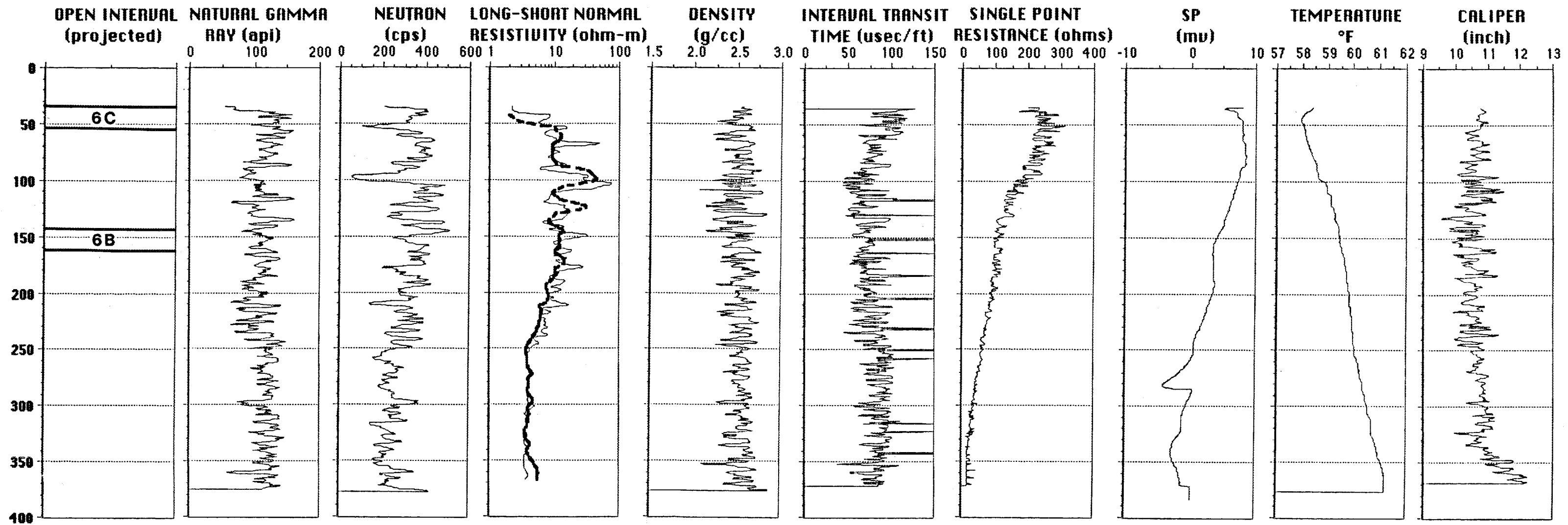
DRILLERS LOGS

GEOPHYSICAL LOGS

FOR HHMS SITE 6

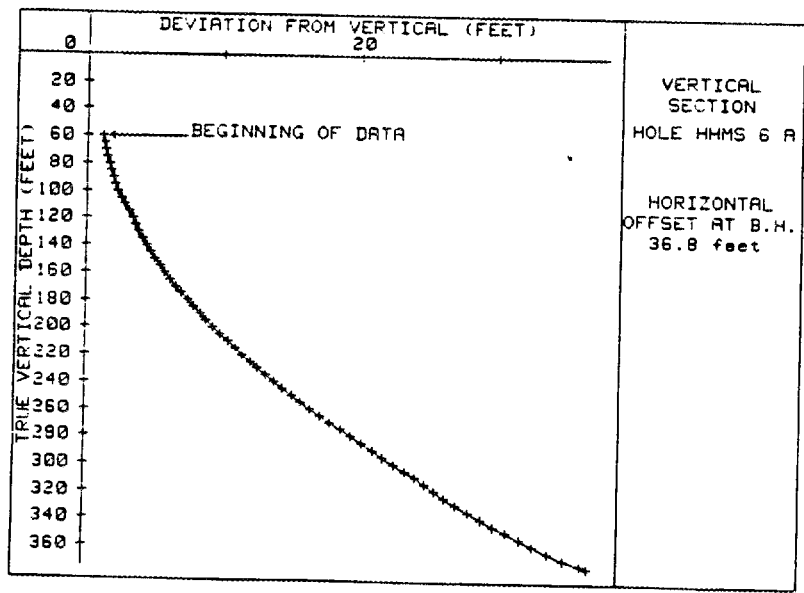
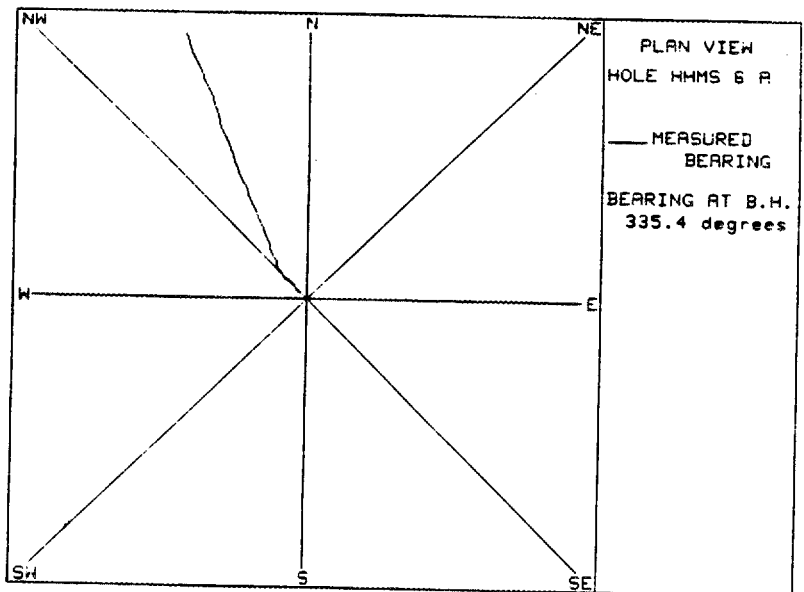
WELL DATA, STRATIGRAPHIC AND STRUCTURAL MARKERS, DRILLERS LOGS					
Well Name	Alternate Name	ORNL N (ft)	ORNL E (ft)	Ground Elevation (ft)	Top of Casing (ft)
HHMS 6 A	942	15305.95	24764.04	762.09	763.88
		depth	elevation		
Cn marker	5	149	613.09		
	4	203	559.09		
	3	236	526.09		
	2	296	466.09		
	1	362	400.09		
	Fault Zone C	85	677.09		
	Fault Zone C	104	658.09		
steep dips in Fault Zone C					
	Fault Zone B	277	485.09		
	Fault Zone B	311	451.09		
DRILLERS LOGS					
soft		16	746.09		
soft		26	736.09		
soft		100	662.09		
soft		152	610.09		
soft		156	606.09		
soft		300	462.09		
soft		389	373.09		
soft		395	367.09		

HHMS 6 - GEOPHYSICAL LOGS

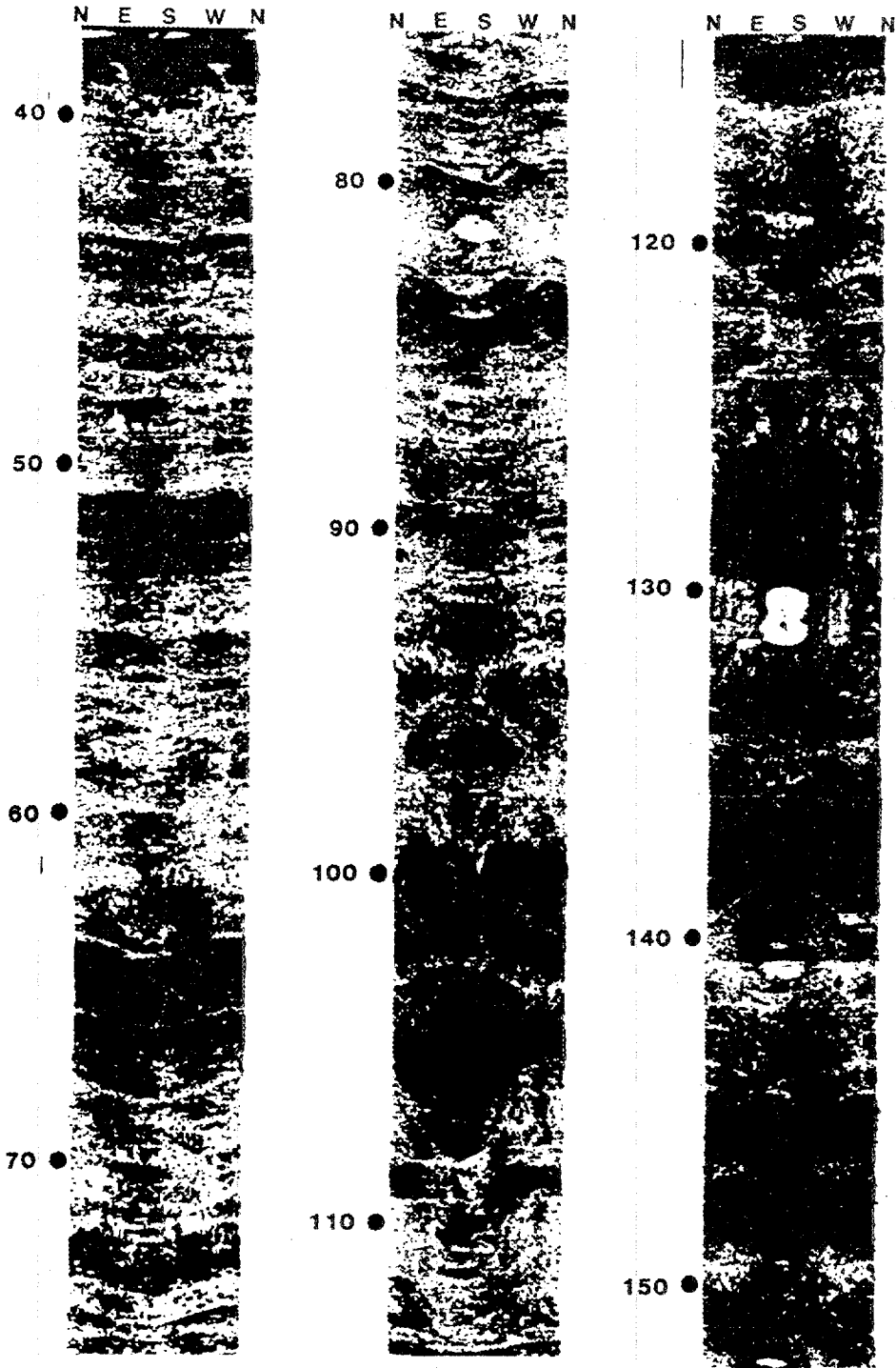


ORNL-DWG 89-13240

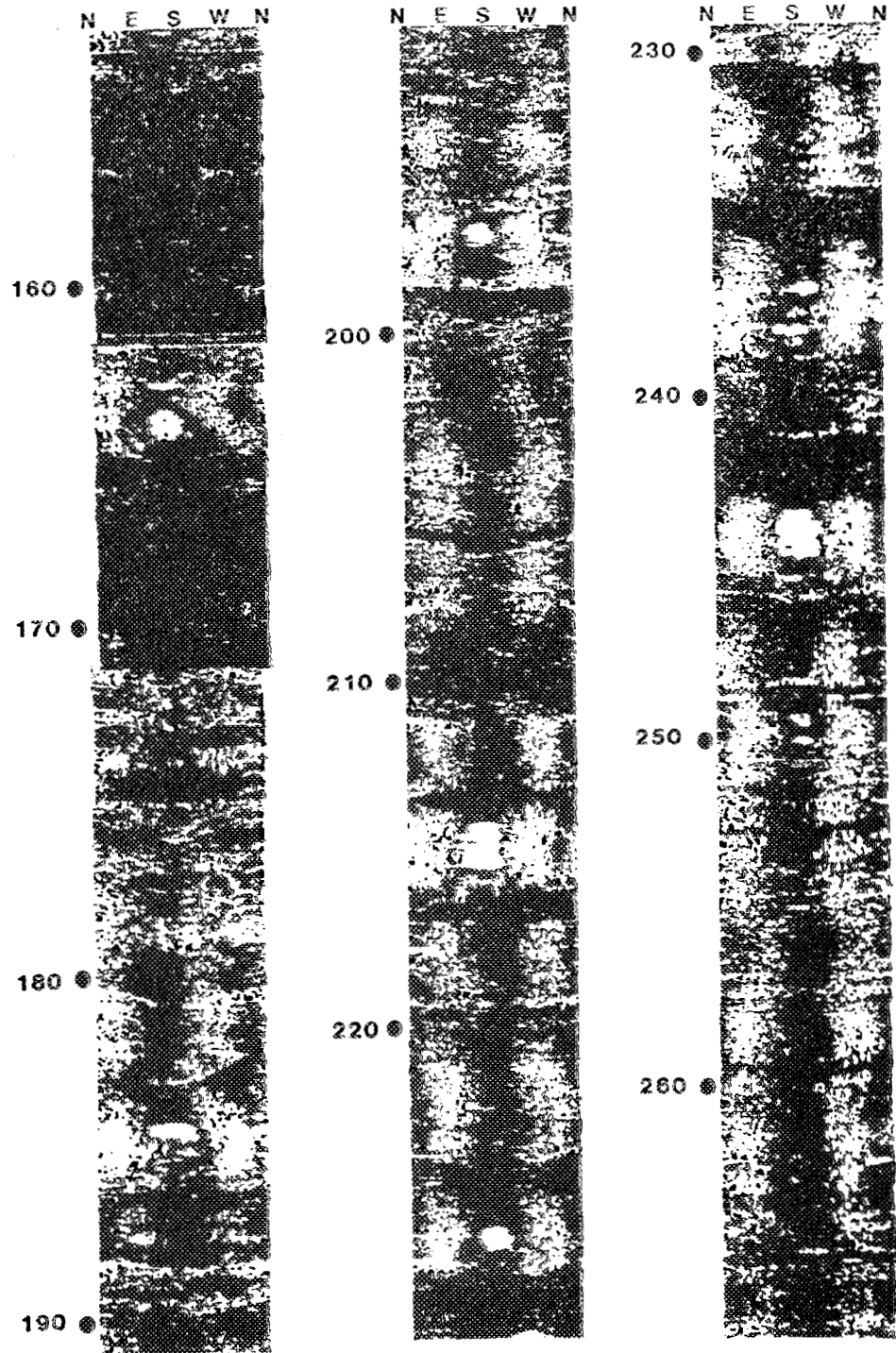
HHMS 6 - DEVIATION LOG



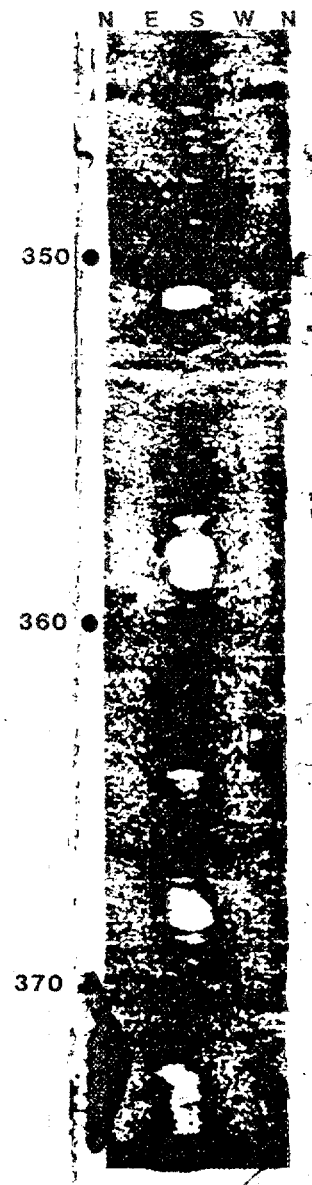
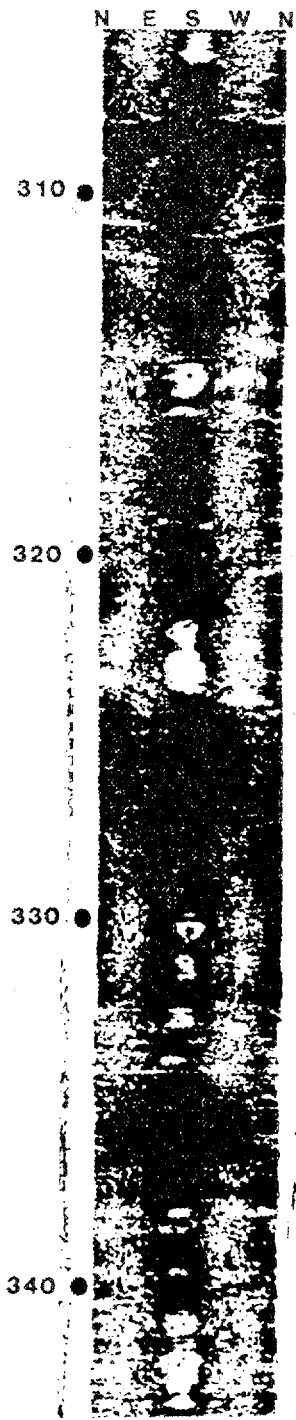
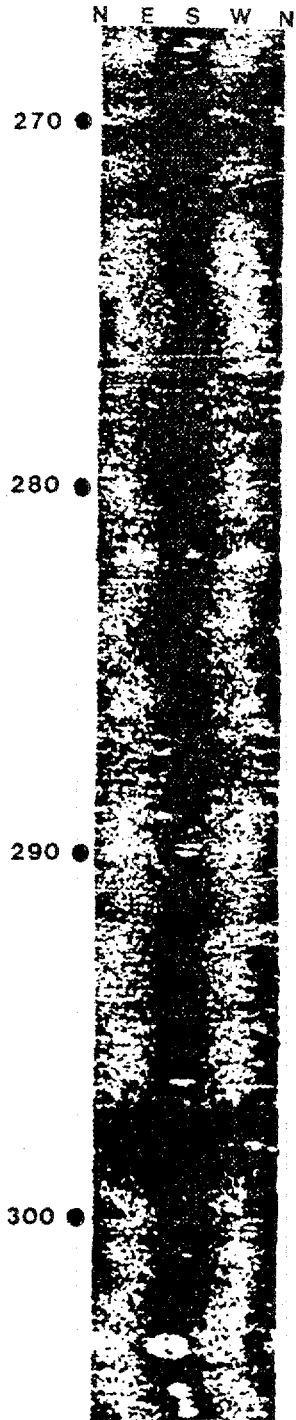
HHMS 6A



HHMS 6A



HHMS 6A



APPENDIX 7

GENERAL WELL SITE INFORMATION

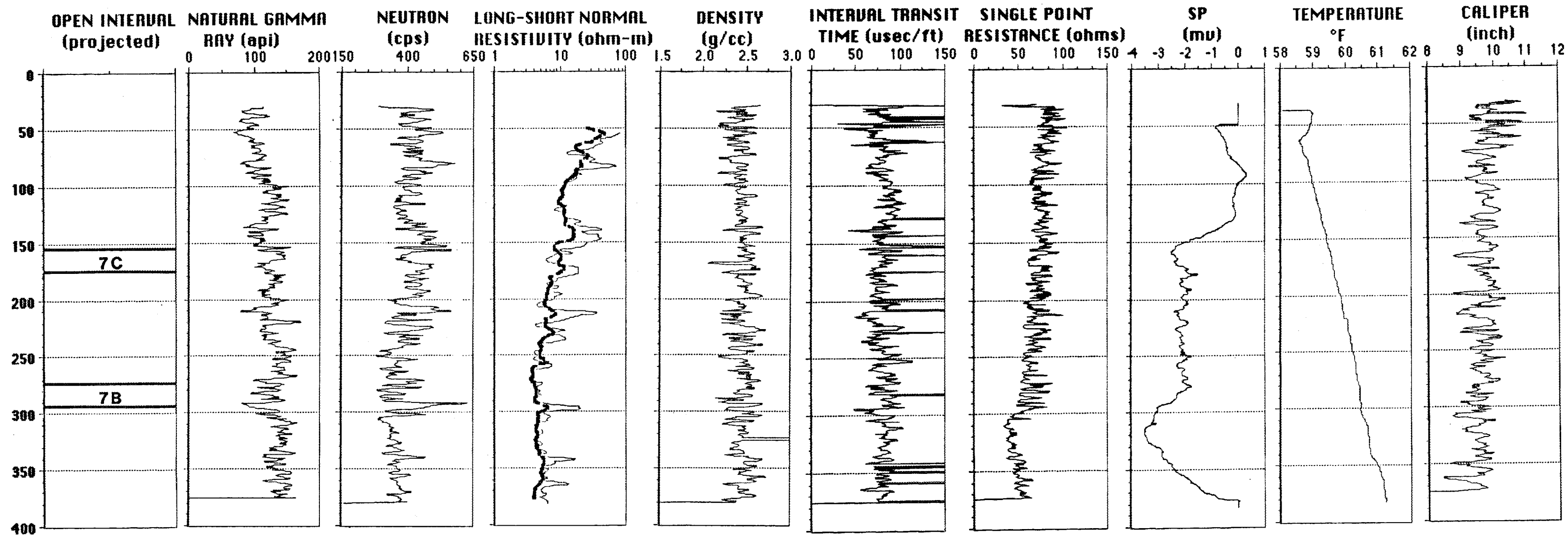
DRILLERS LOGS

GEOPHYSICAL LOGS

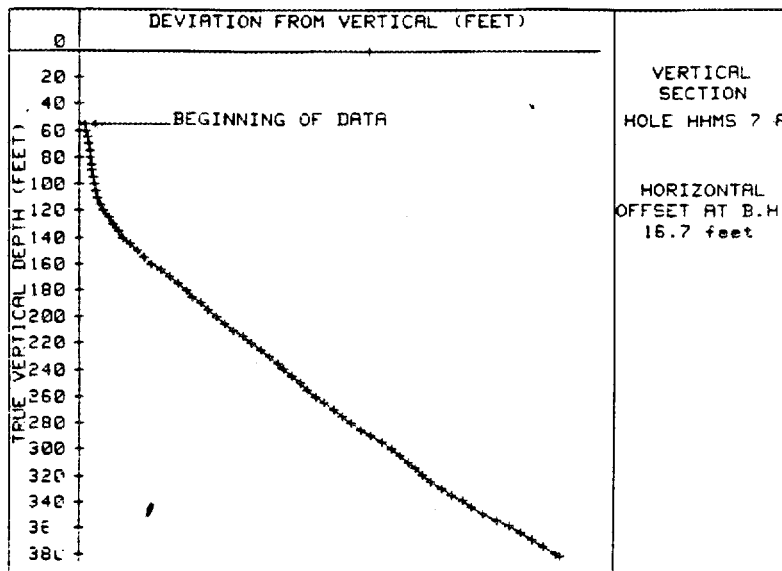
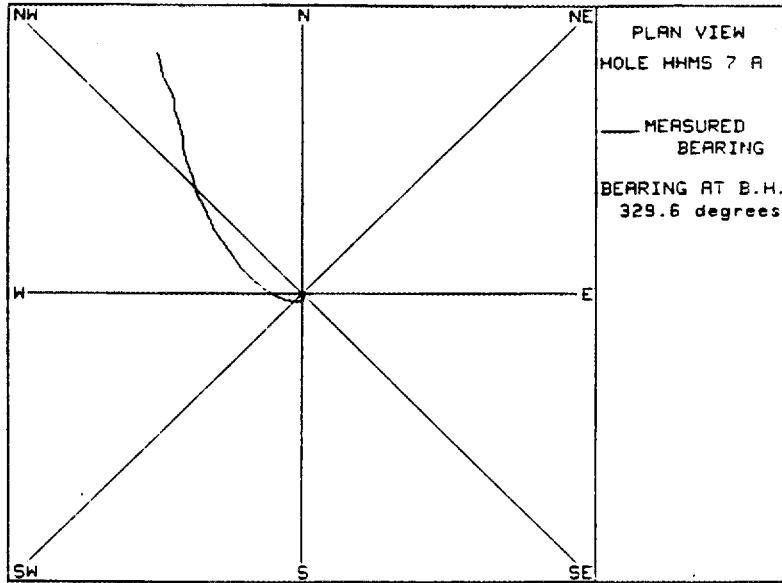
FOR HHMS SITE 7

WELL DATA, STRATIGRAPHIC AND STRUCTURAL MARKERS, DRILLERS LOGS					
Well Name	Alternate Name	ORNL N (ft)	ORNL E (ft)	Ground Elevation (ft)	Top of Casing (ft)
HHMS 7 A	945	17540.65	24512.09	808.54	811.35
		depth	elevation		
Cm marker	4	53	755.54		
	3	101	707.54		
	2	162	646.54		
	1	242	566.54		
	Cm/Crg	297	511.54		
mod steep di	from	0	808.54		
mod steep di	to	95	713.54		
fracture		205	603.54		
N dip	from	215	593.54		
N dip	to	221	587.54		
fault zone	from	300	508.54		
	to	305	503.54		
fracture		455	353.54		
fault		443	365.54		
structures id'd from BHTV, little correlation with other logs.					
DRILLERS LOGS					
soft		64	744.54		
soft		110	698.54		
soft		130	678.54		
soft		240	568.54		
soft		389	419.54		
soft		395	413.54		

HHMS 7 - GEOPHYSICAL LOGS

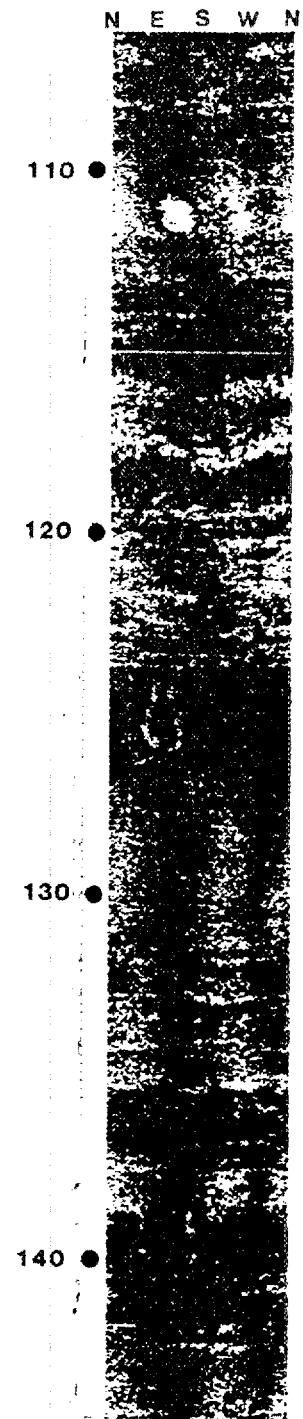
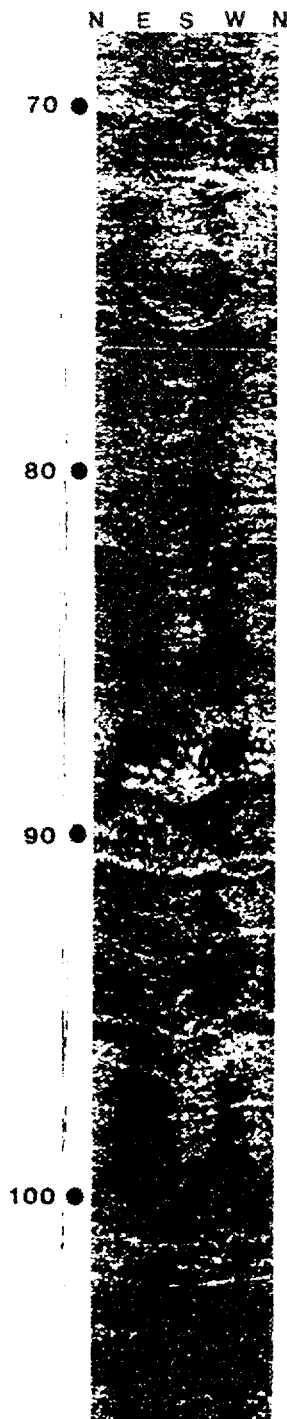
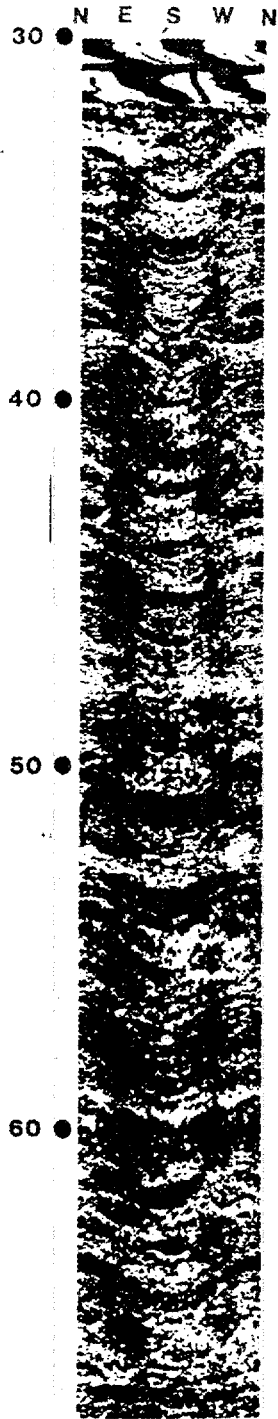


HHMS 7 - DEVIATION LOG

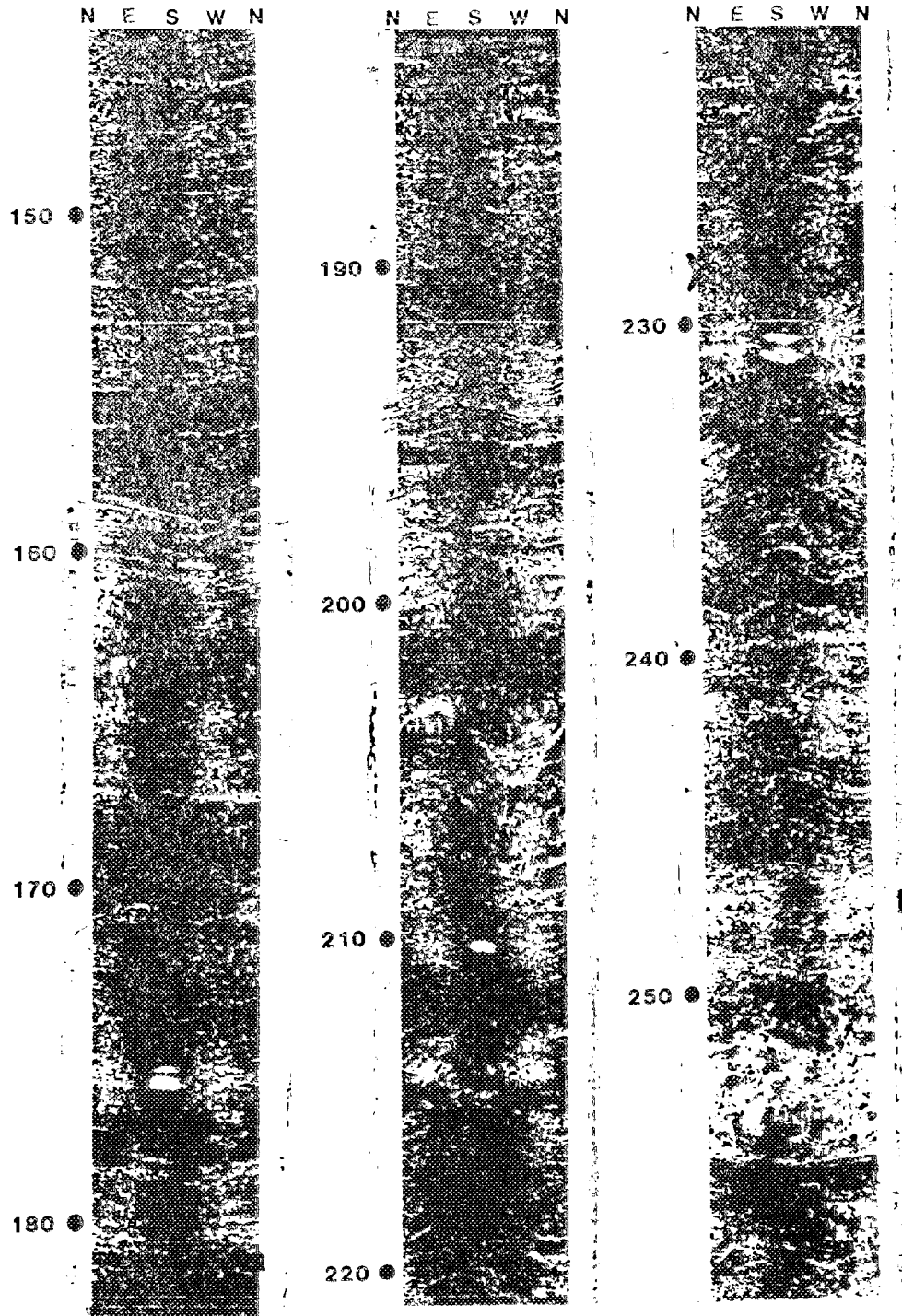


ORNL-DWG 89-13274

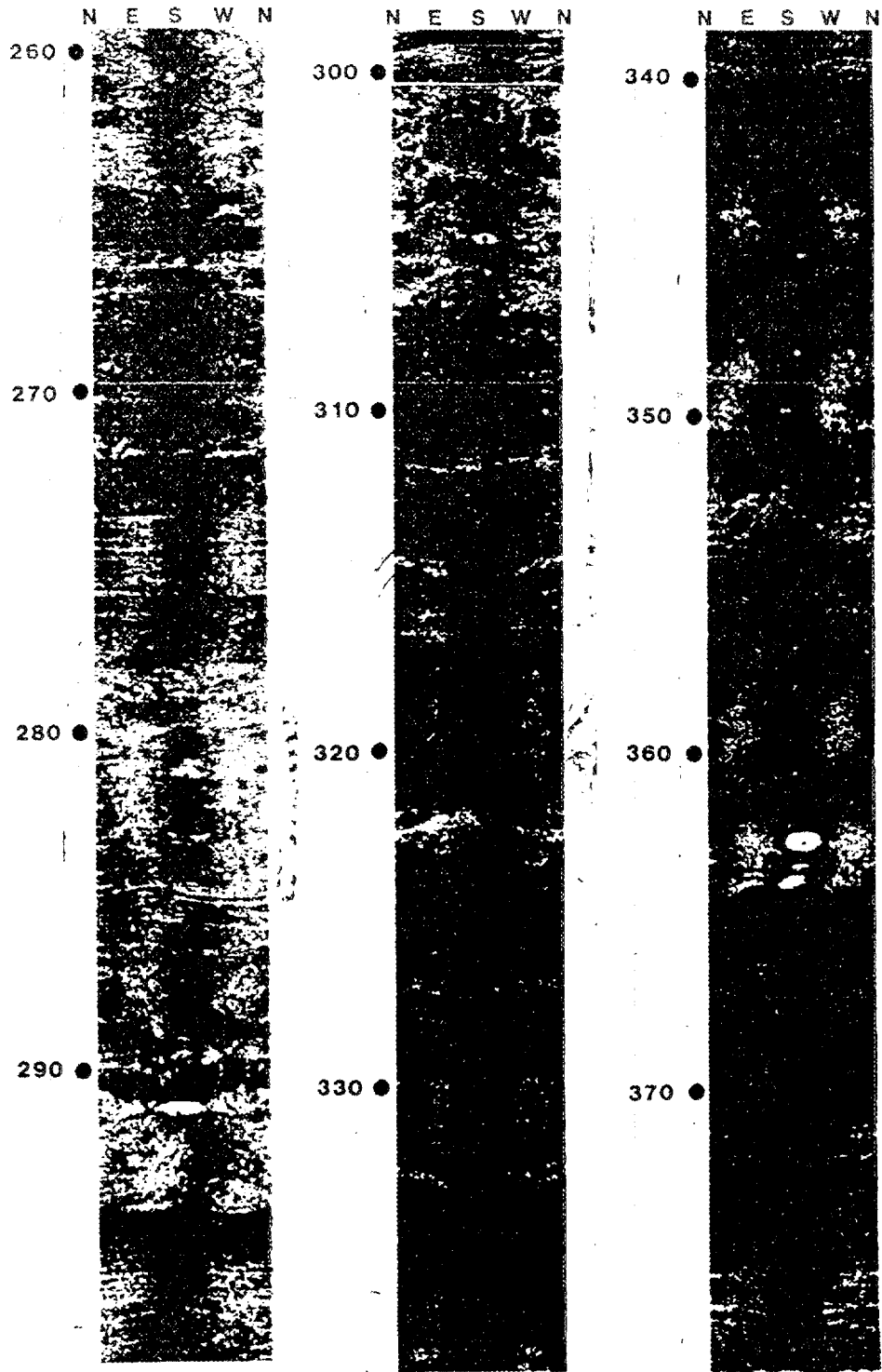
HHMS 7A



HHMS 7A



HHMS 7A



APPENDIX 8

GENERAL WELL SITE INFORMATION

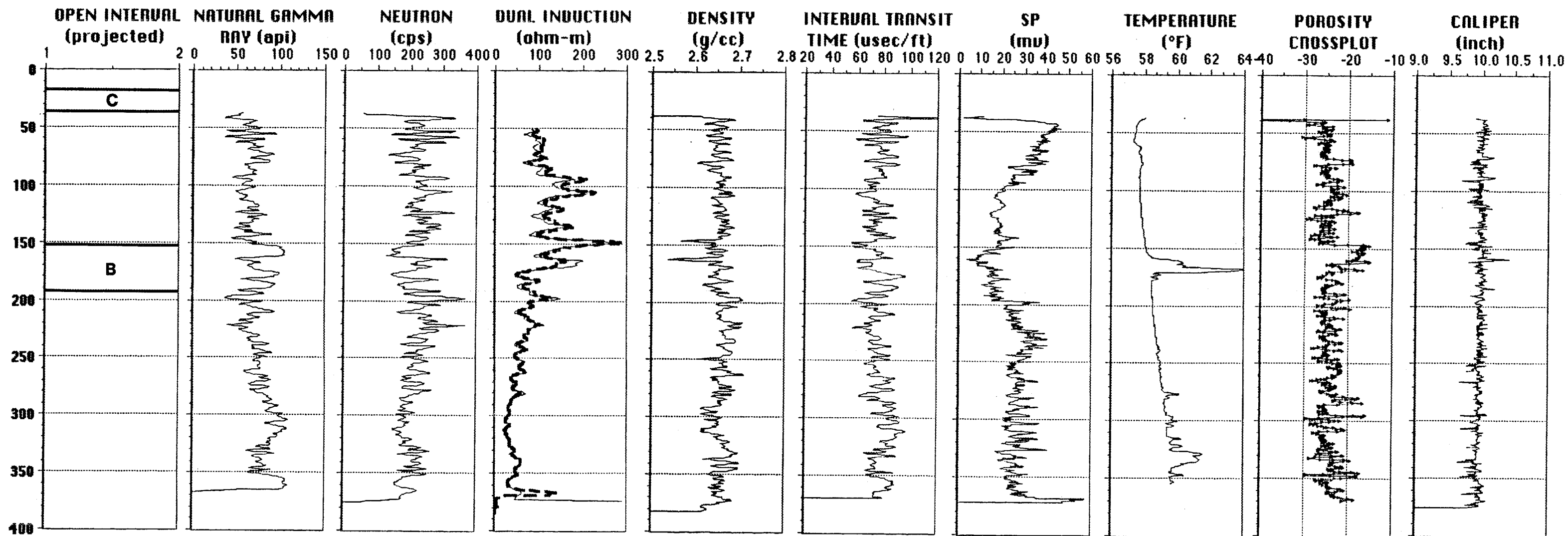
DRILLERS LOGS

GEOPHYSICAL LOGS

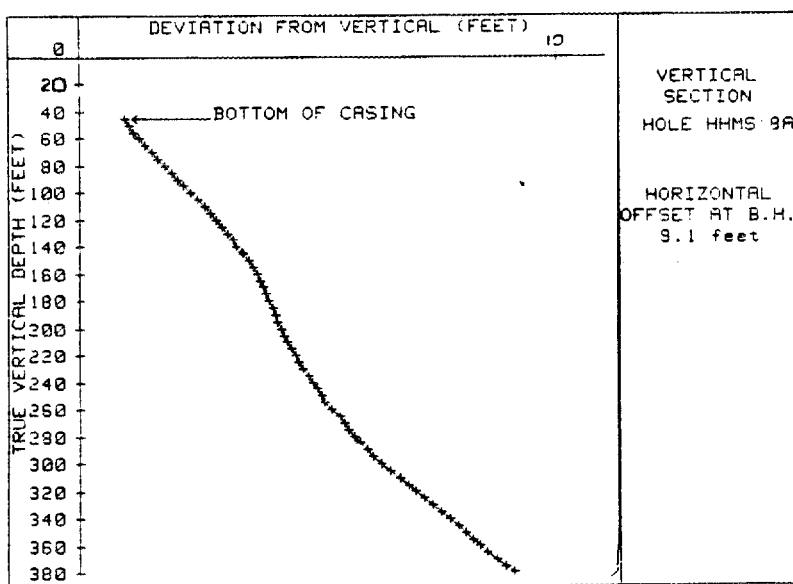
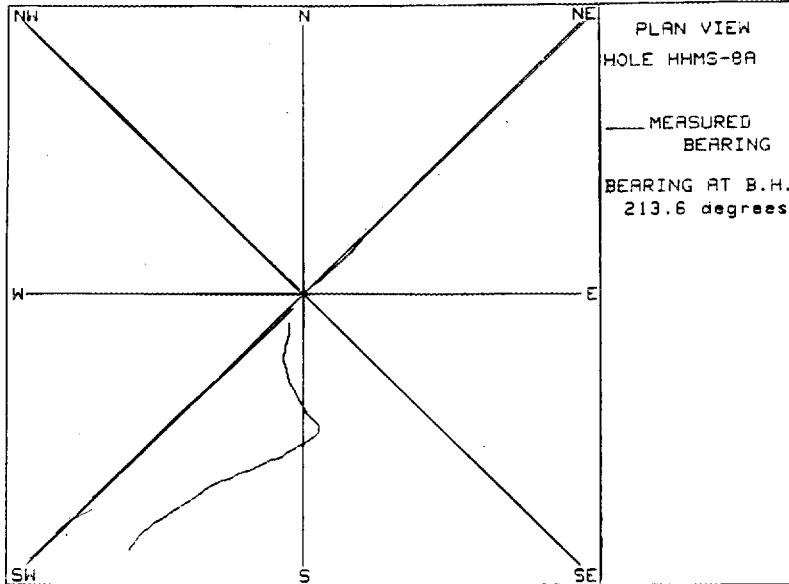
FOR HHMS SITE 8

WELL DATA, STRATIGRAPHIC AND STRUCTURAL MARKERS, DRILLERS LOGS					
Well Name	Alternate Name	ORNL N (ft)	ORNL E (ft)	Ground Elevation (ft)	Top of Casing (ft)
HHMS 8 A	1001	16862.02	24694.84	786.06	787.95
		depth	elevation		
Cm marker	3'	73	713.06		
	3	156	630.06		
	2	210	576.06		
	1	304	482.06		
	Cm/Crg	352	434.06		
downhole distance between Cm marker 3 - 5 is 97', measured from HHMS 3A					
use for correlation with HHMS 4A					
est Cm mark	5	-24	810.06		
	Fault A	159	627.06		
	Fault Zone A	150	636.06		
	Fault Zone A	173	613.06		
zone defined by BHTV, gradual transition at base of zone					
fractures	from	275	511.06		
	to	380	406.06		
broad zone of fracturing id'd by temp and porosity Xplot data.					
DRILLERS LOGS (no records for open interval)					
soft	from	53	733.06		
soft	to	55	731.06		
soft		59	727.06		
soft		57	719.06		
soft		85	701.06		
soft		111	675.06		
soft	from	121	665.06		
soft	to	122	664.06		
soft	from	160	626.06		
soft	to	163	623.06		
soft		245	541.06		
soft		264	522.06		
soft		273	513.06		
soft	from	347	439.06		
soft	to	348	438.06		

HHMS 8 - GEOPHYSICAL LOGS



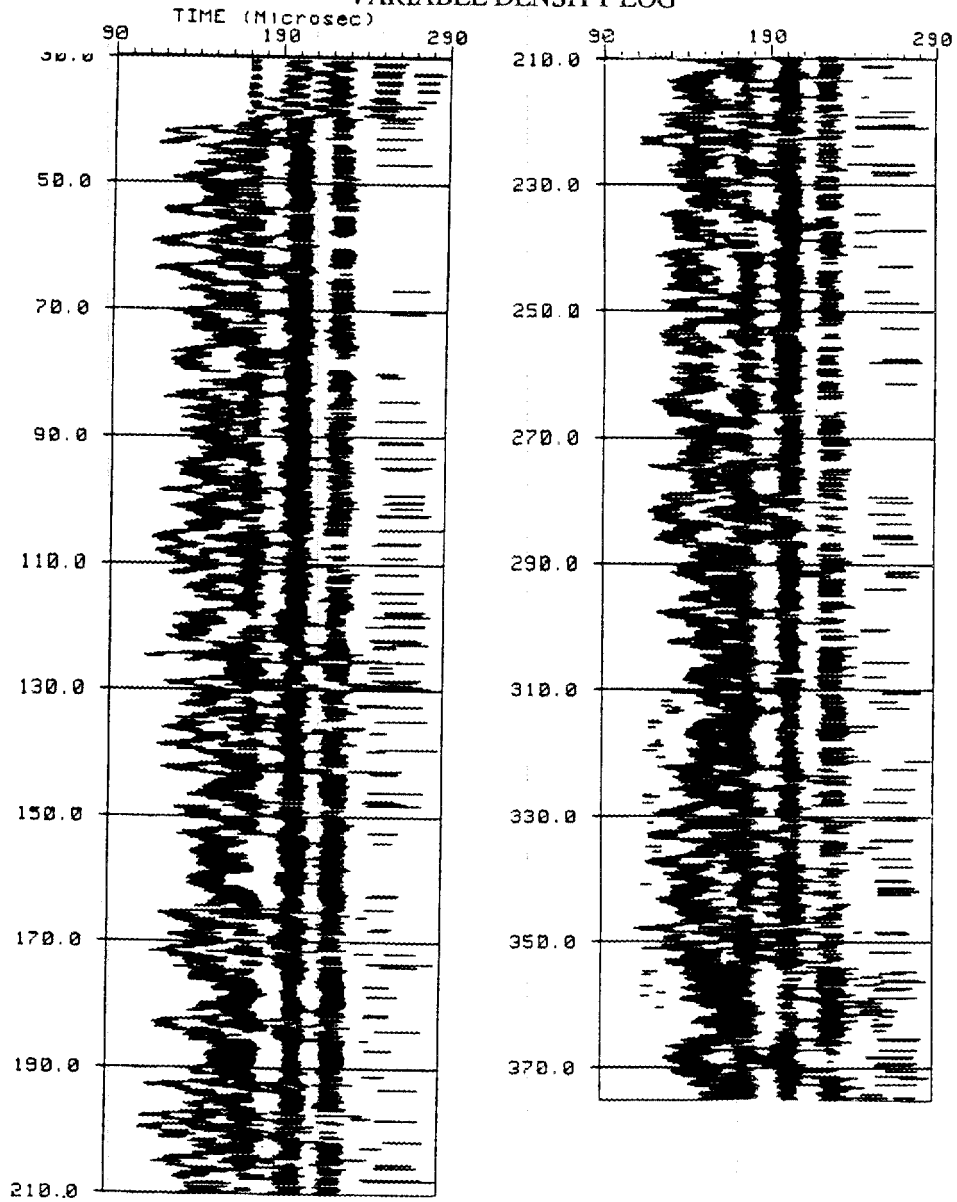
HHMS 8 - DEVIATION LOG



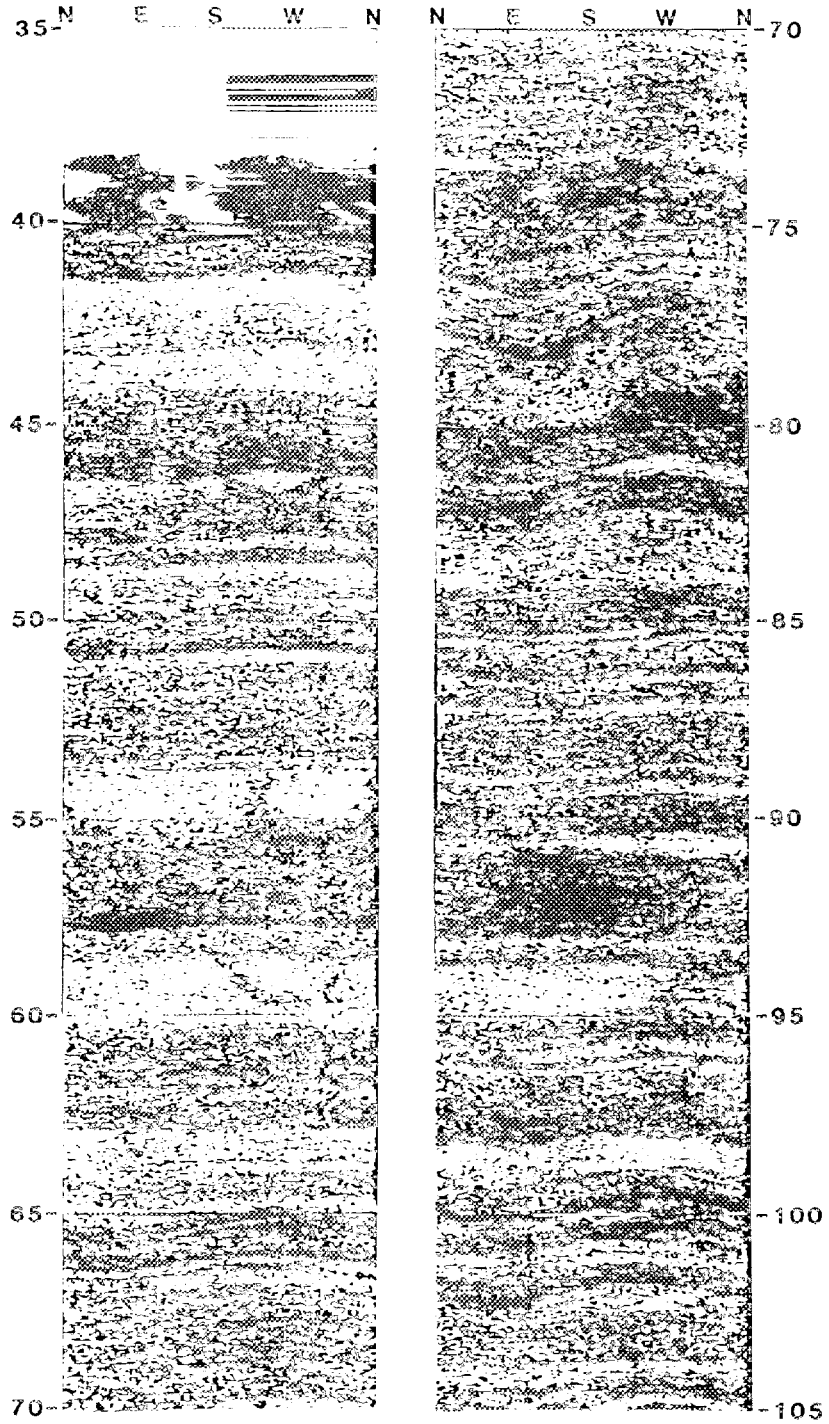
ORNL-DWG 89-13295

HHMS 8A

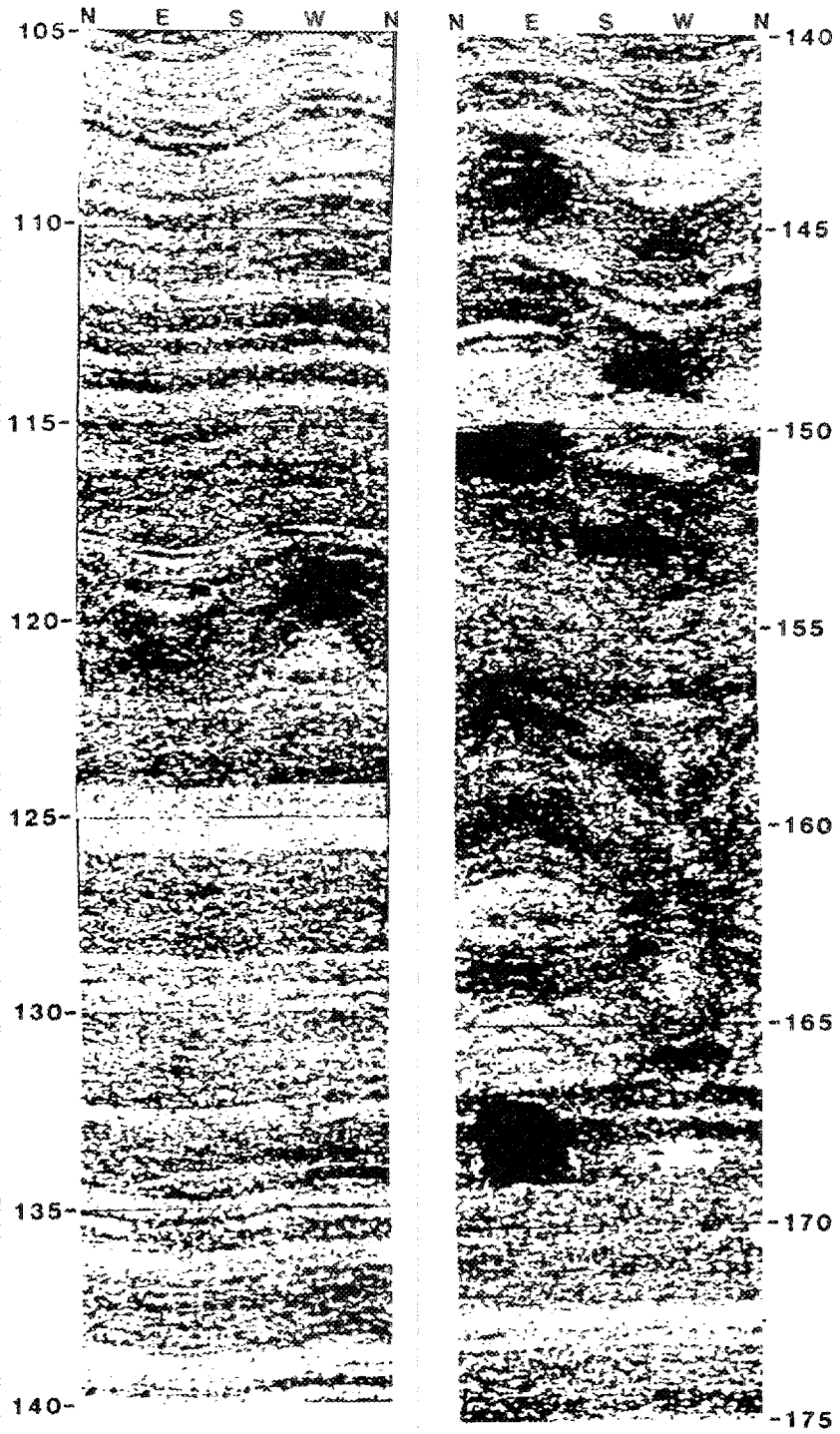
VARIABLE DENSITY LOG



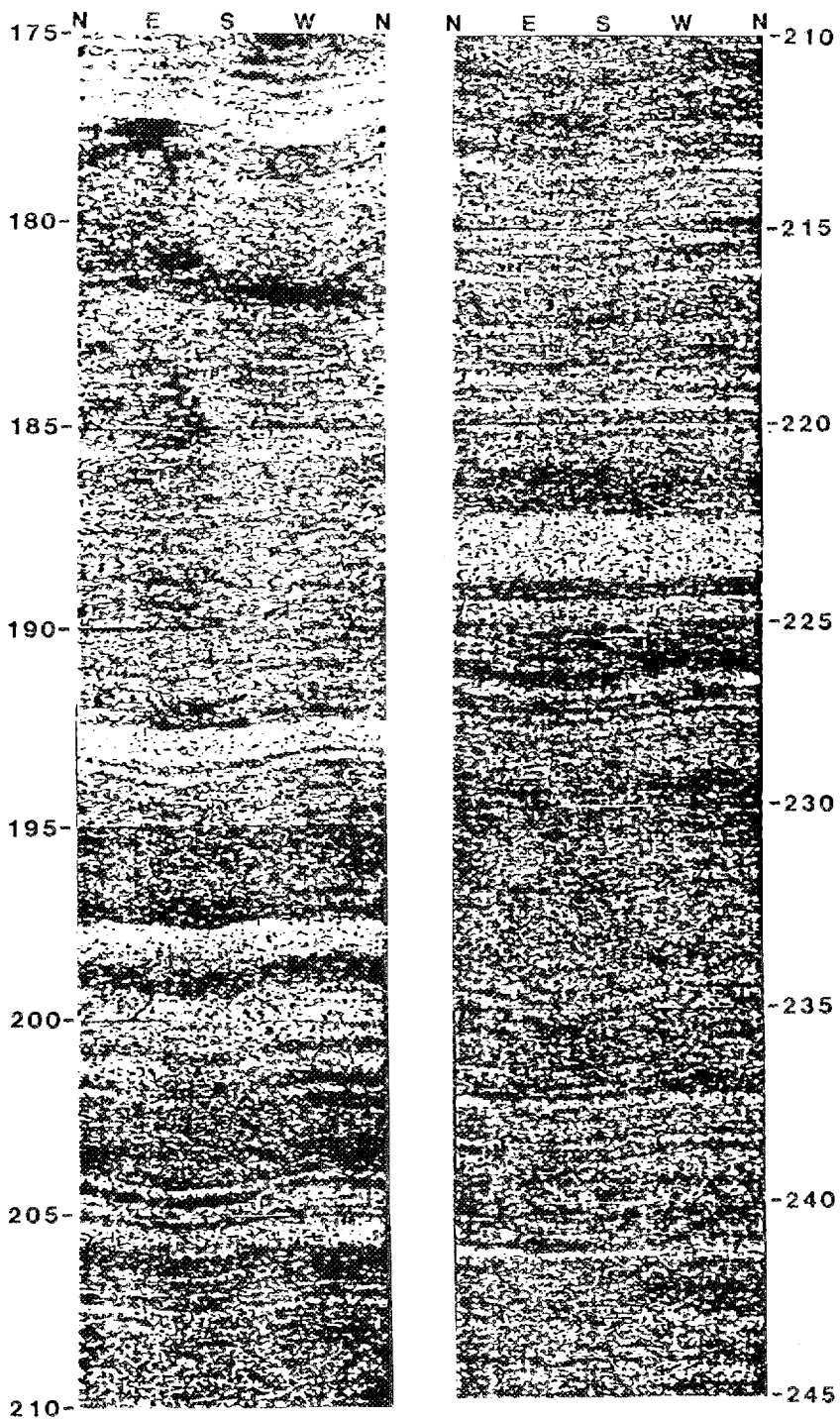
HHMS 8A



HHMS 8A

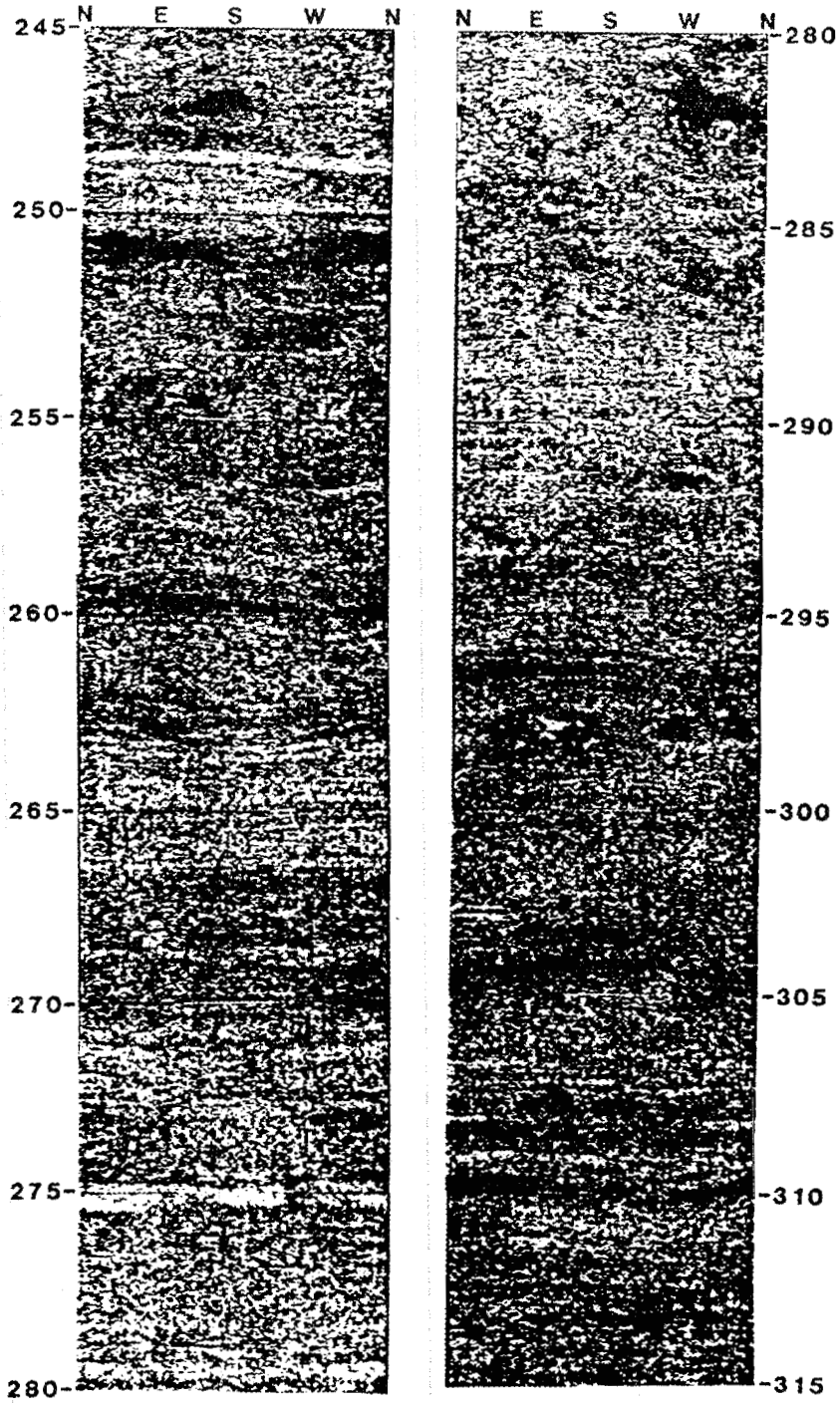


HHMS 8A

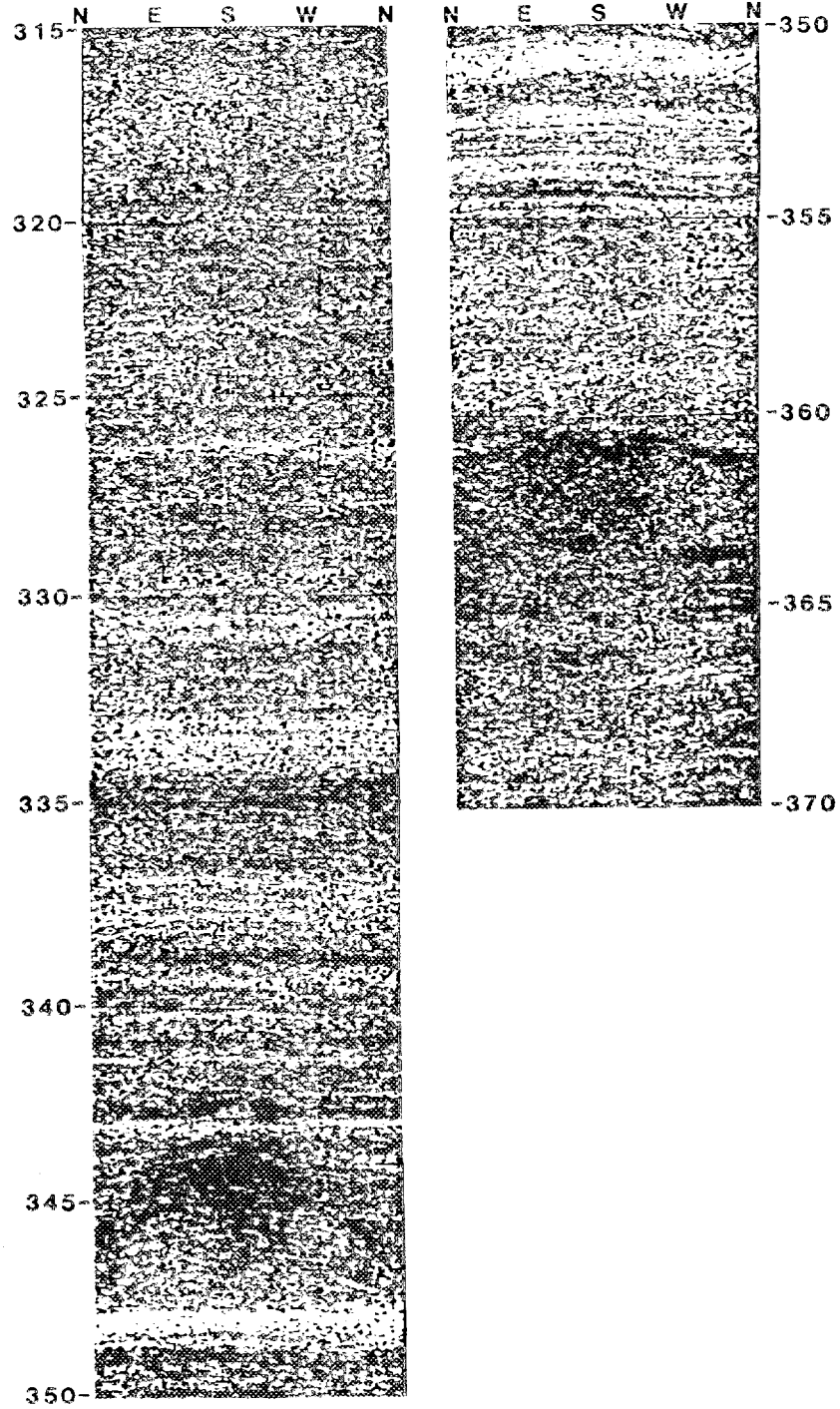


ORNL-DWG 89-13279

HHMS 8A



HHMS 8A



APPENDIX 9

GENERAL WELL SITE INFORMATION

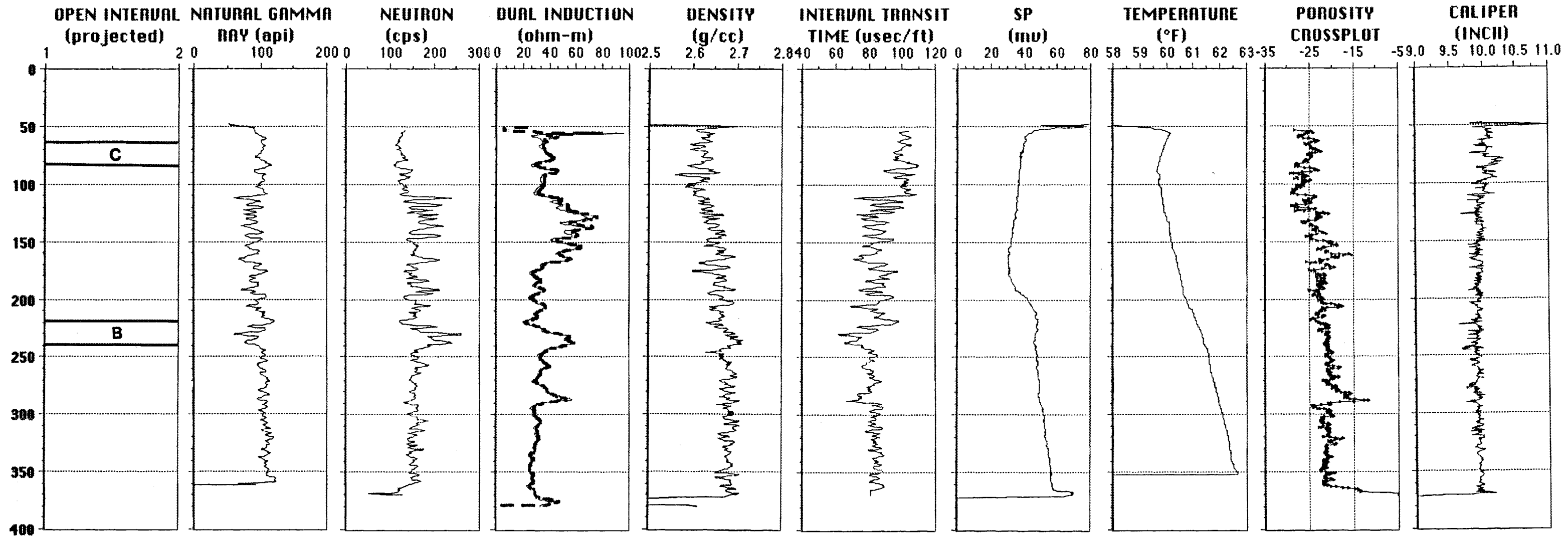
DRILLERS LOGS

GEOPHYSICAL LOGS

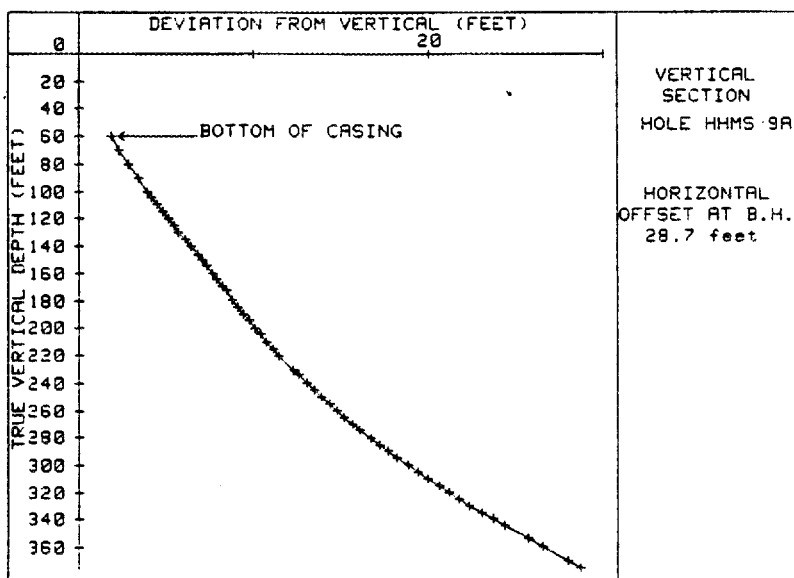
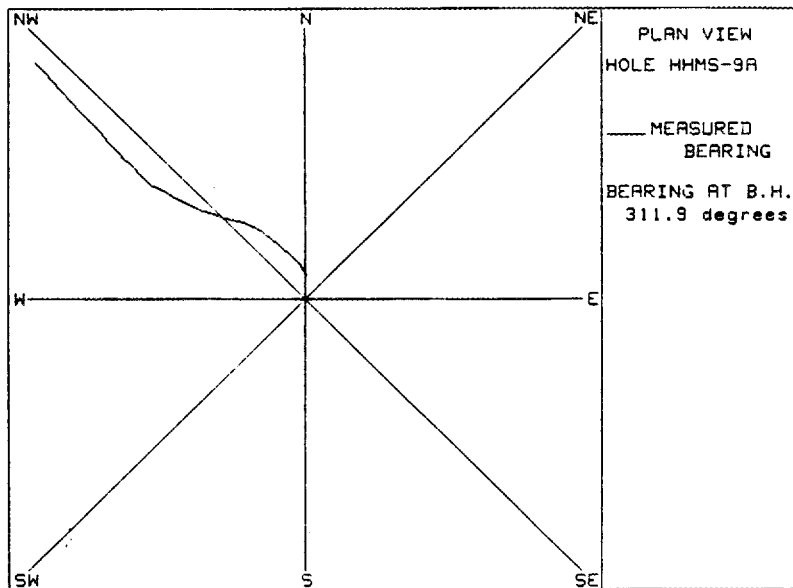
FOR HHMS SITE 9

WELL DATA, STRATIGRAPHIC AND STRUCTURAL MARKERS, DRILLERS LOGS					
Well Name	Alternate Name	ORNL N (ft)	ORNL E (ft)	Ground Elevation (ft)	Top of Casing (ft)
HHMS 9 A	1004	18805.38	27929.18	860.43	861.7
		depth	elevation		
	Crg/Crt	110	750.43		
	Crt/Cpv	239	621.43		
average down hole thickness of Crg in P&T is 116 ft					
estimated	Cm/Crg	-6	866.43		
	fracture	200	660.43		
id'd by SP deflection					
	fracture	207	653.43		
id'd by porosity Xplot, supported by BHTV					
fault/fracture from		283	577.43		
to		285	575.43		
id'd by BHTV, porosity Xplot					
DRILLERS LOGS - no records for the open interval					
soft		73	787.43		
soft	from	91	769.43		
soft	to	96	764.43		
soft	from	171	689.43		
soft	to	174	686.43		
soft		220	640.43		
soft		245	615.43		
soft	from	310	550.43		
soft	to	330	530.43		
hard		183	677.43		

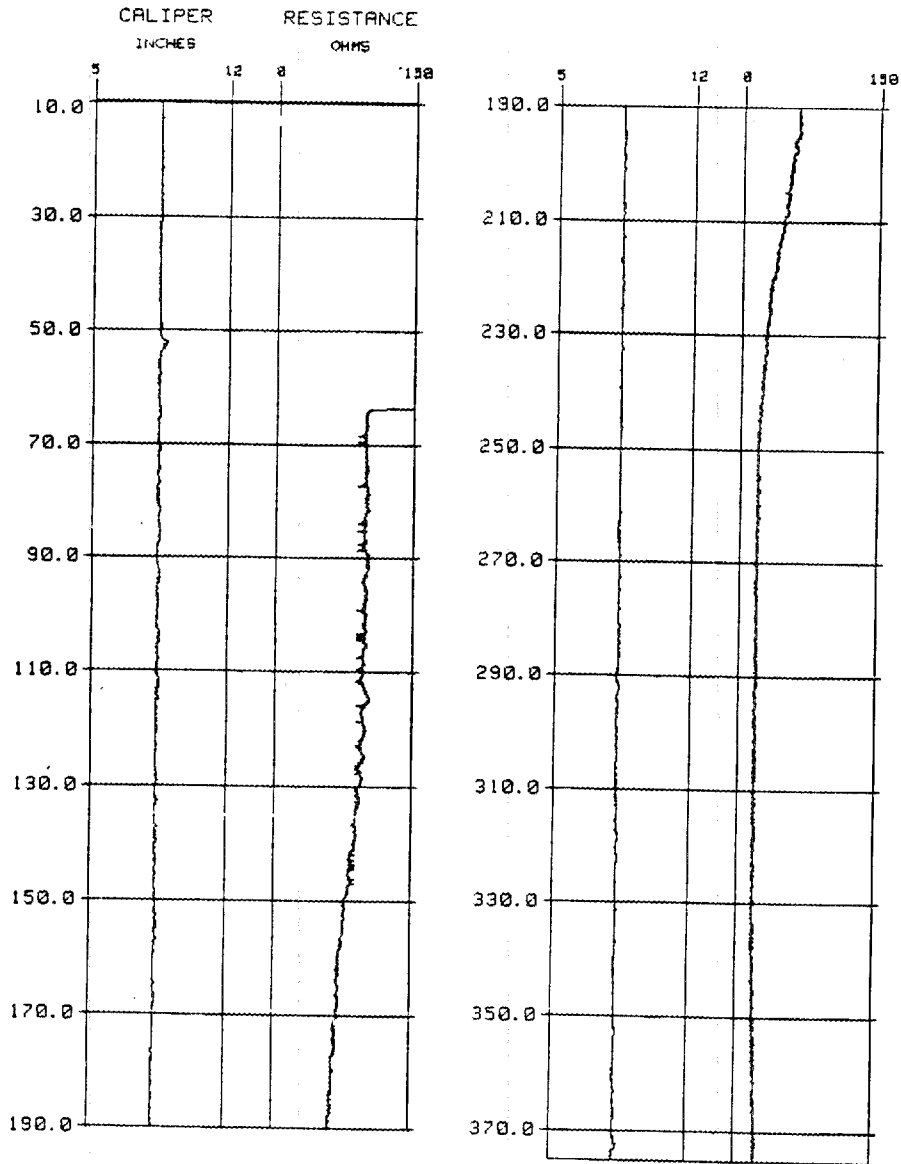
HHMS 9 - GEOPHYSICAL LOGS



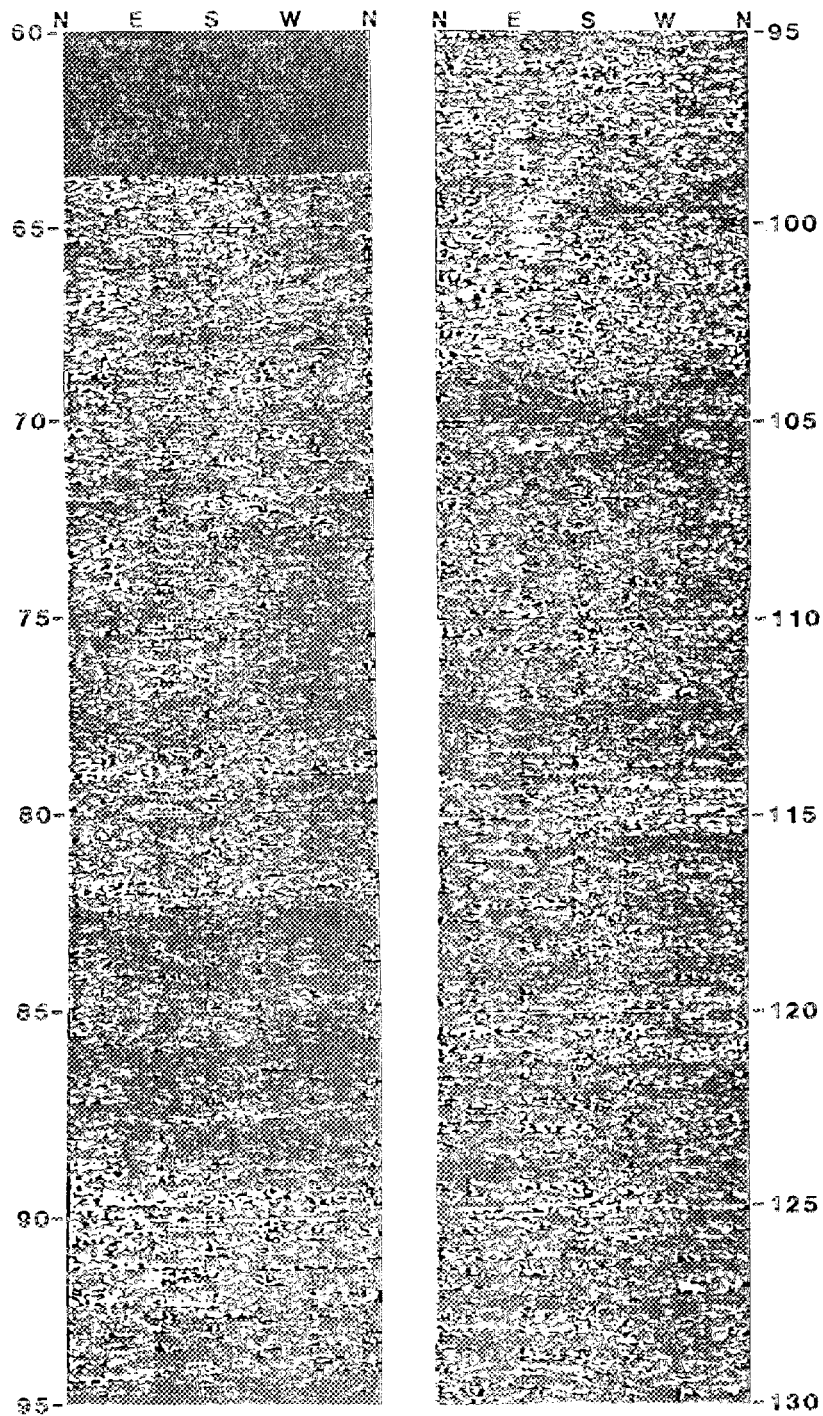
HHMS 9 - DEVIATION LOG



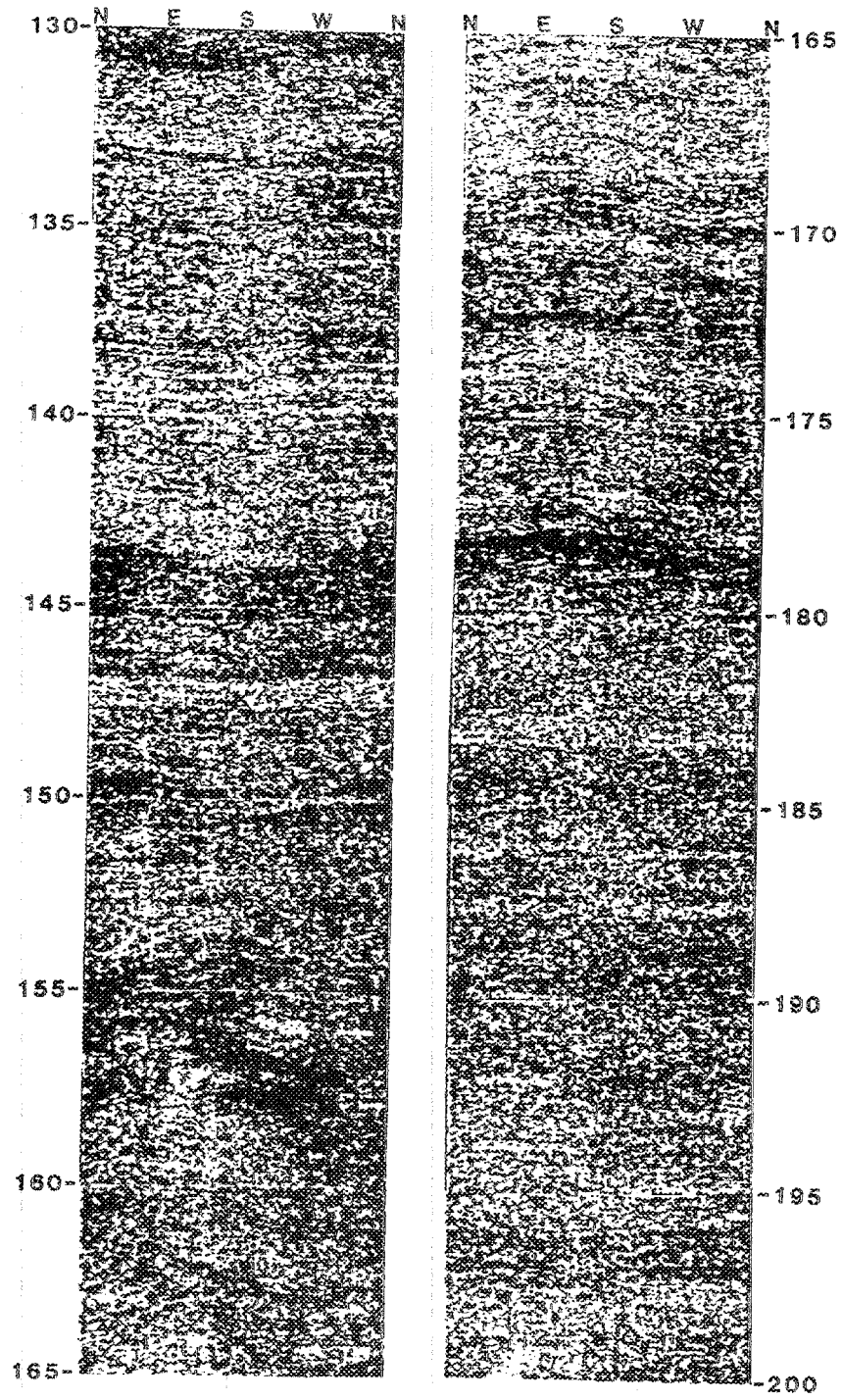
HHMS 9A



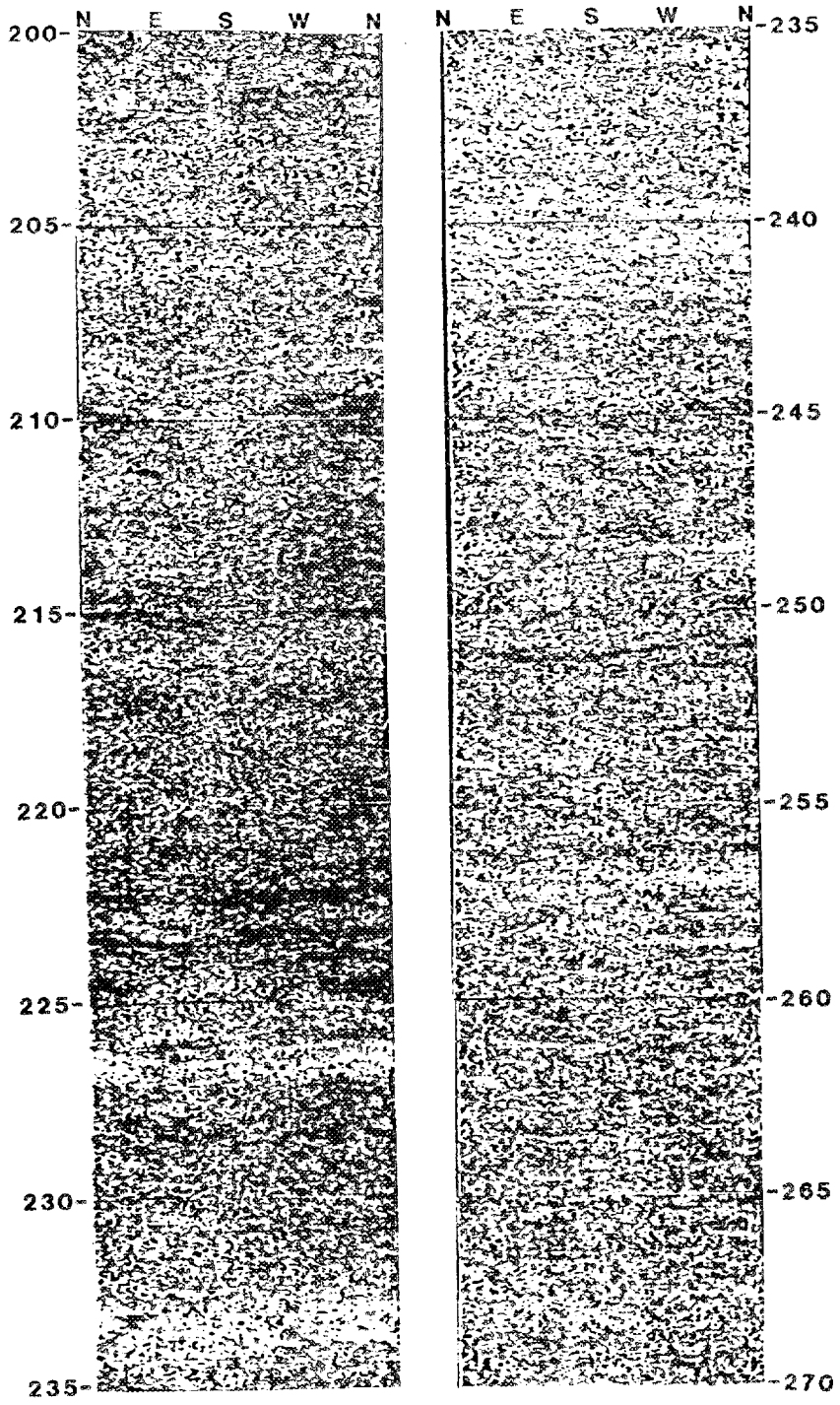
HHMS 9A



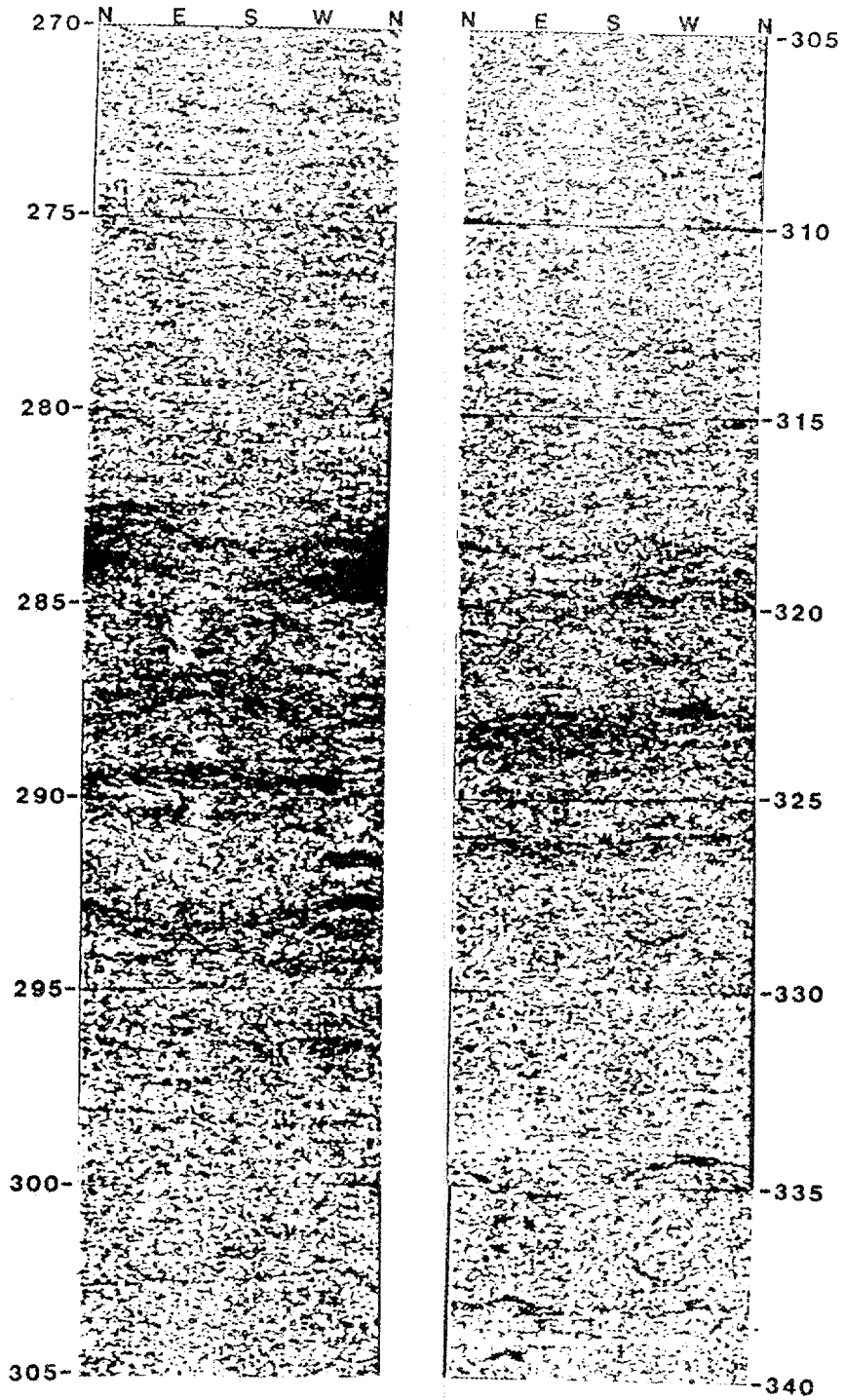
HHMS 9A



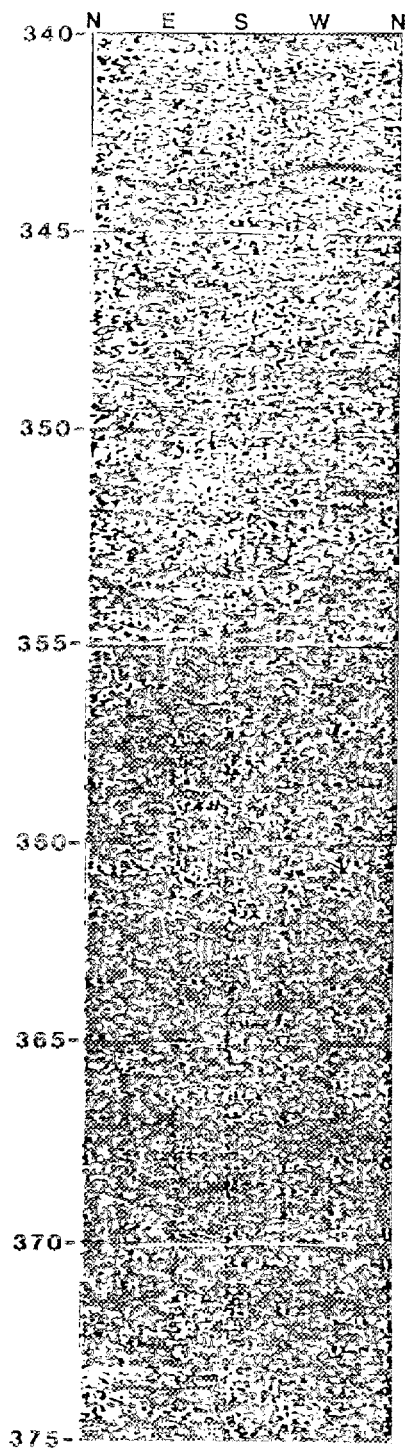
HHMS 9A



HHMS 9A



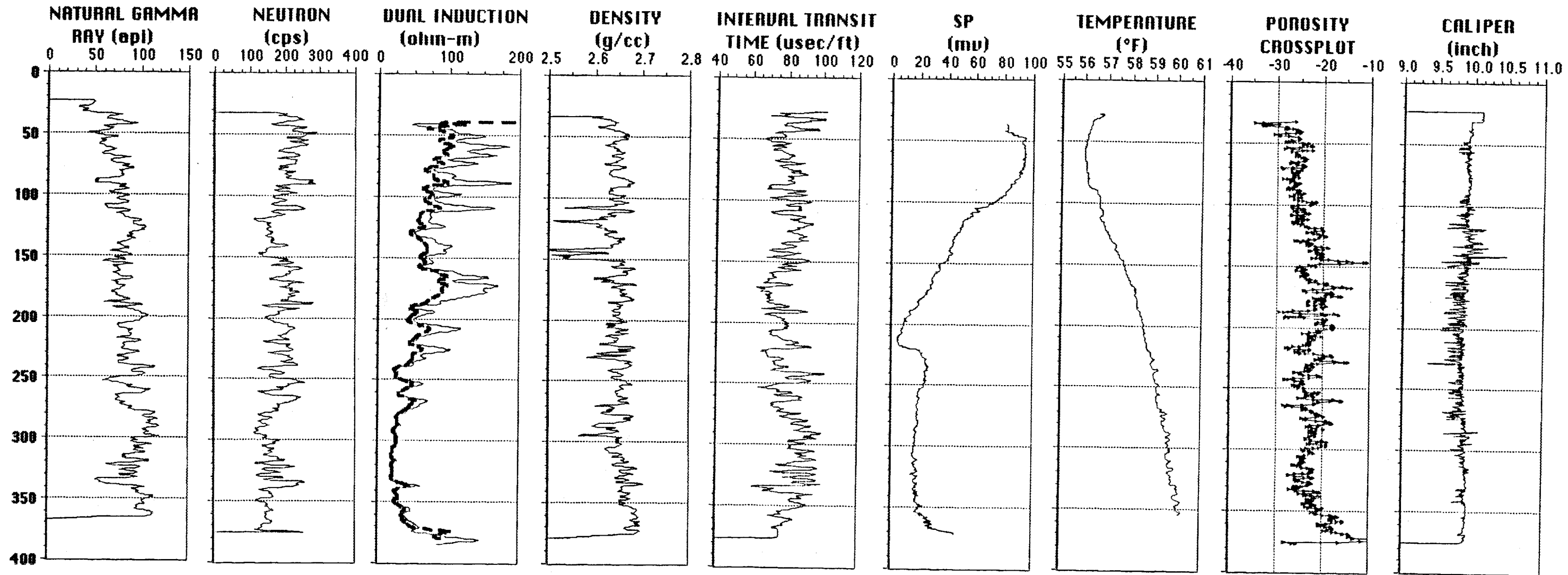
HHMS 9A



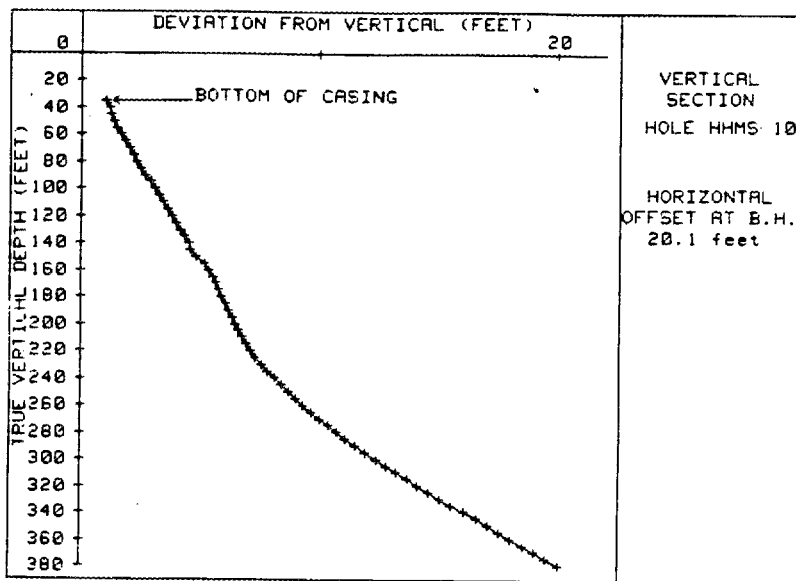
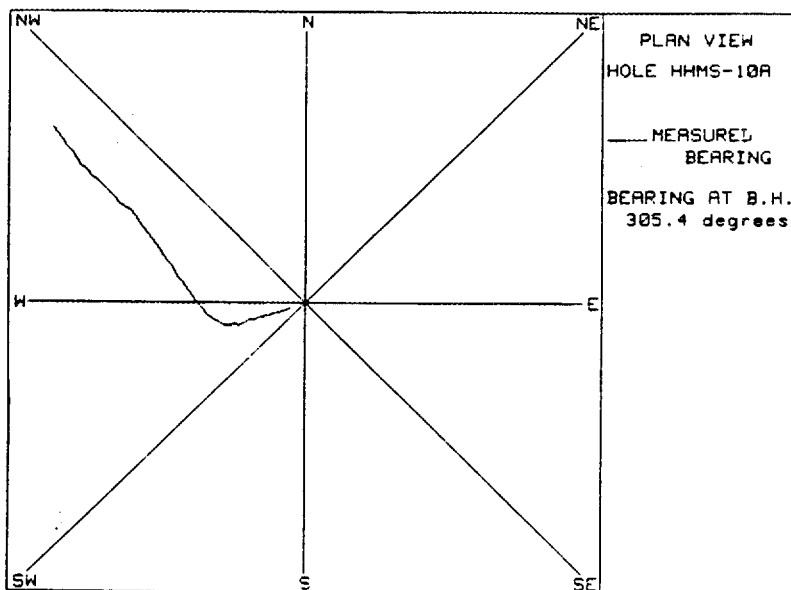
APPENDIX 10
GENERAL WELL SITE INFORMATION
DRILLERS LOGS
GEOPHYSICAL LOGS
FOR HHMS SITE 10

WELL DATA, STRATIGRAPHIC AND STRUCTURAL MARKERS, DRILLERS LOGS					
Well Name	Alternate	ORNL N	ORNL E	Ground	Top of
	Name	(ft)	(ft)	Elevation (ft)	Casing (ft)
HHMS 10 A	1007	17450.15	28666.09	777.75	779.71
		depth	elevation		
Cm marker	5	42	735.75		
	4	89	688.75		
	3	128	649.75		
	2	199	578.75		
	1	278	499.75		
	Cm/Crg	339	438.75		
DRILLERS LOGS - no records for the open interval					
soft		48	729.75		
soft		76	701.75		
soft	from	121	656.75		
soft	to	125	652.75		
soft		141	636.75		
soft		326	451.75		
rough	from	157	620.75		
rough	to	177	600.75		
hard		330	447.75		

HHMS 10 - GEOPHYSICAL LOGS

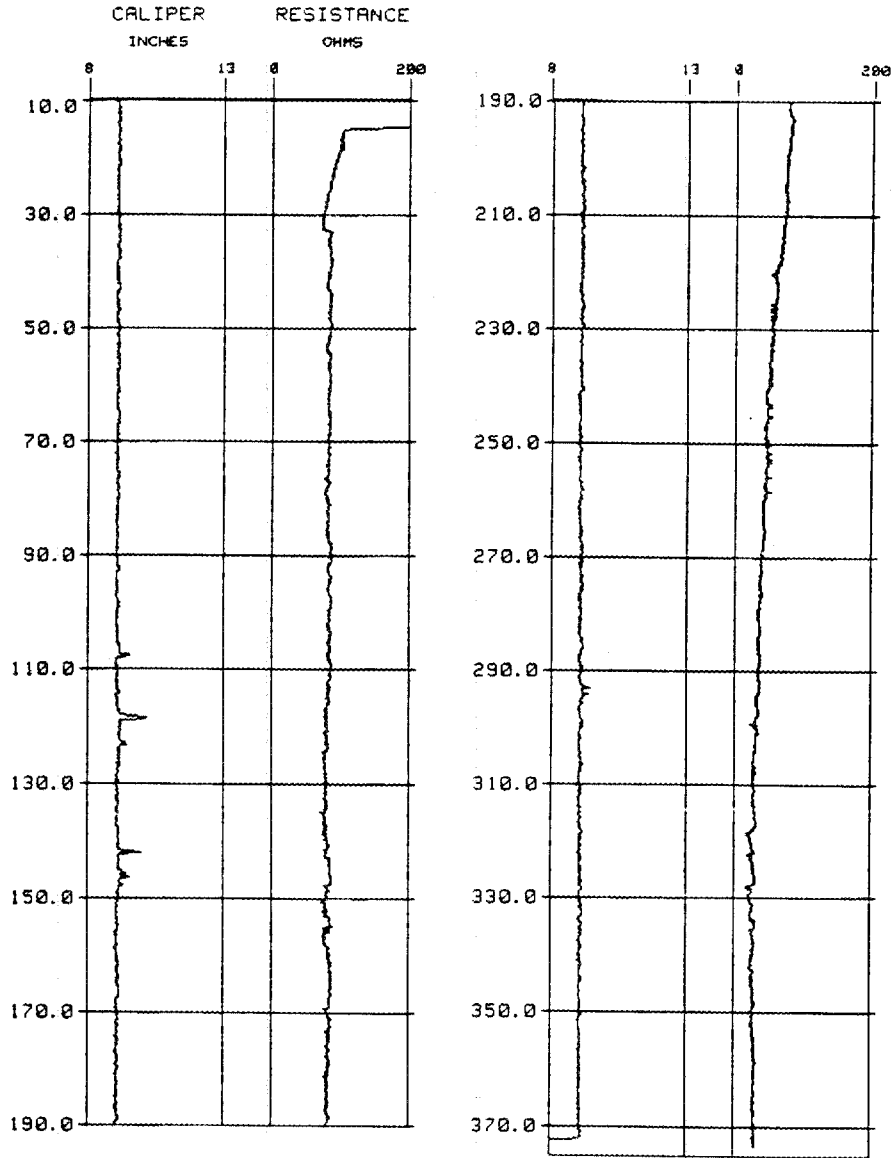


HHMS 10 - DEVIATION LOG

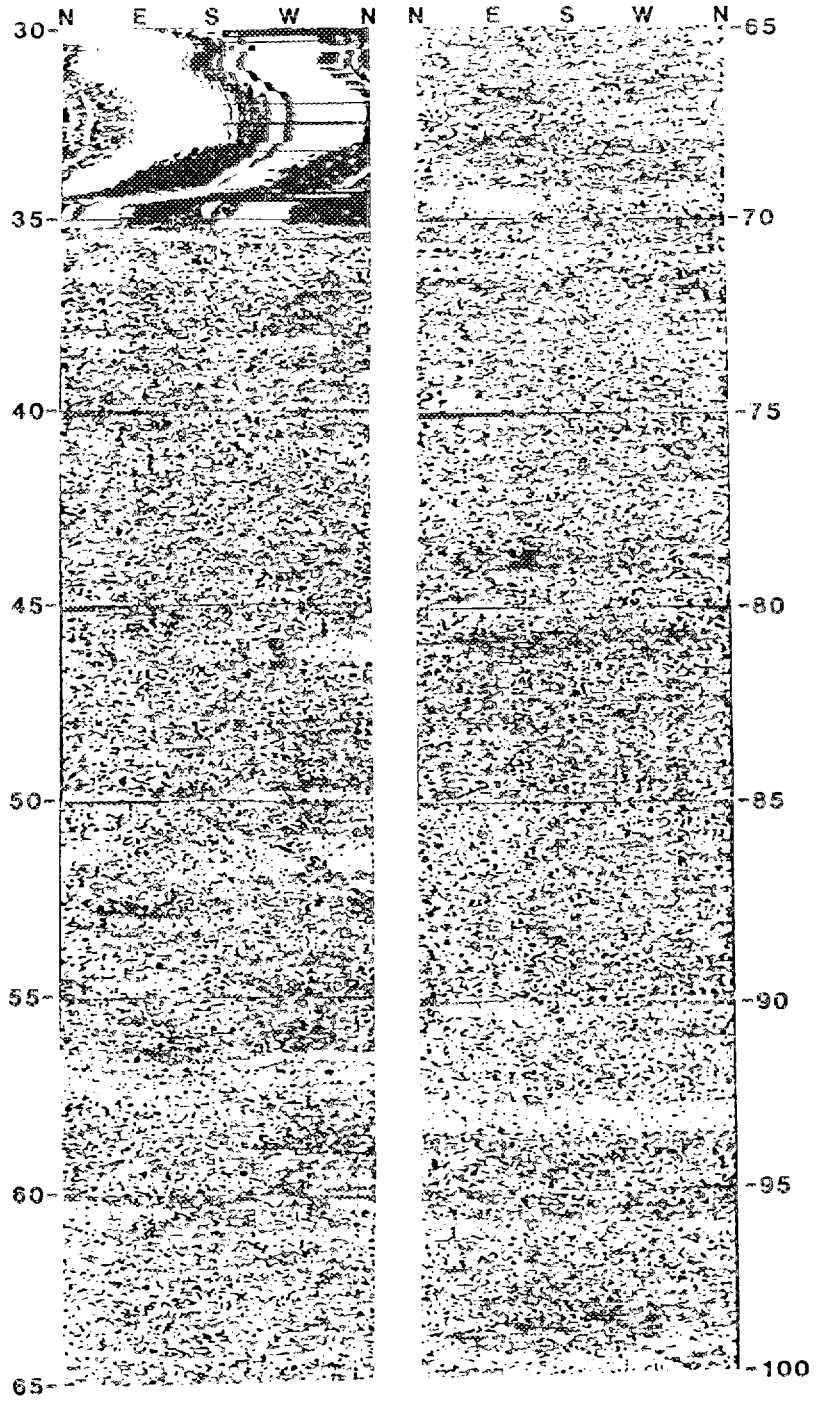


ORNL-DWG 89-13297

HHMS 10A

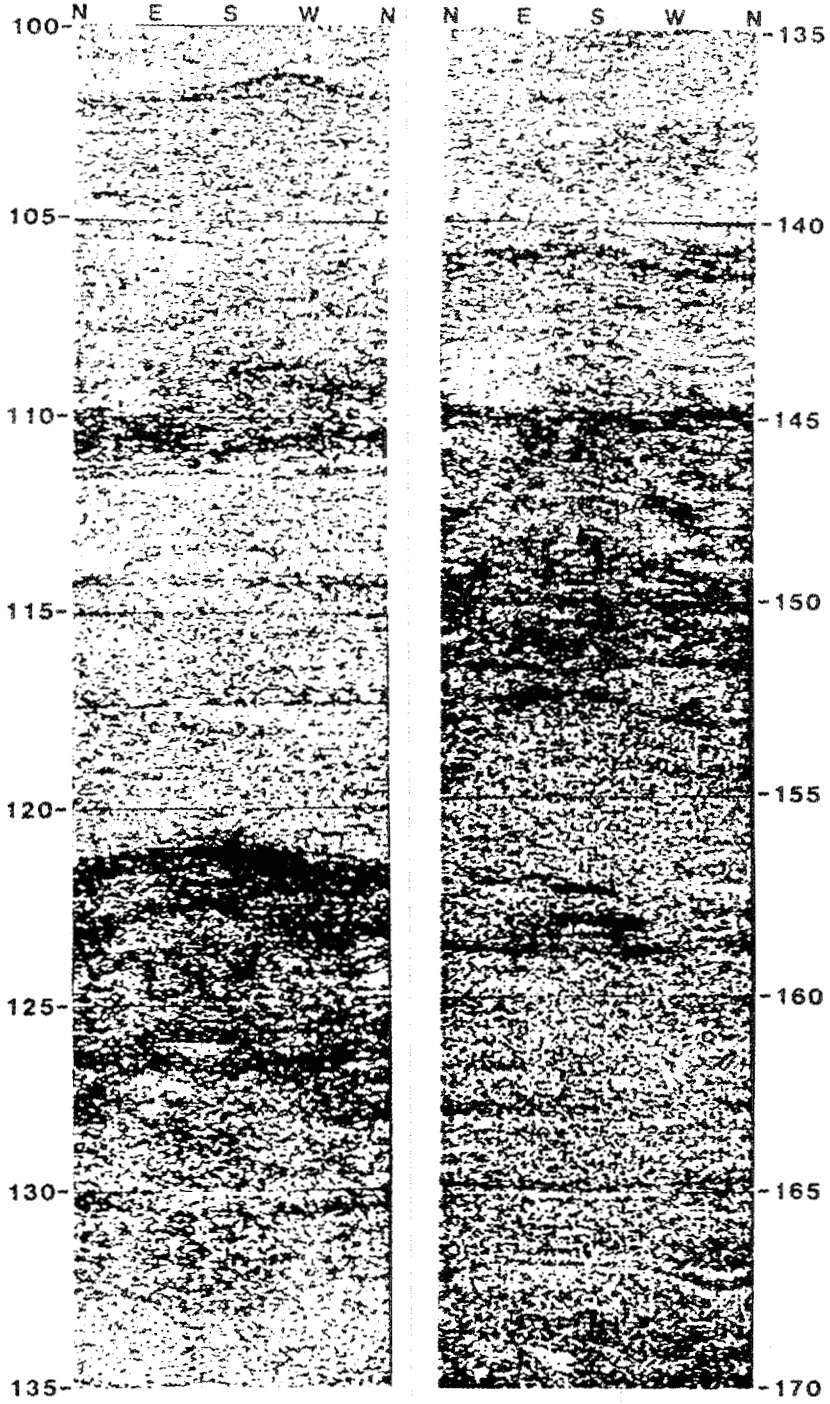


HHMS 10A

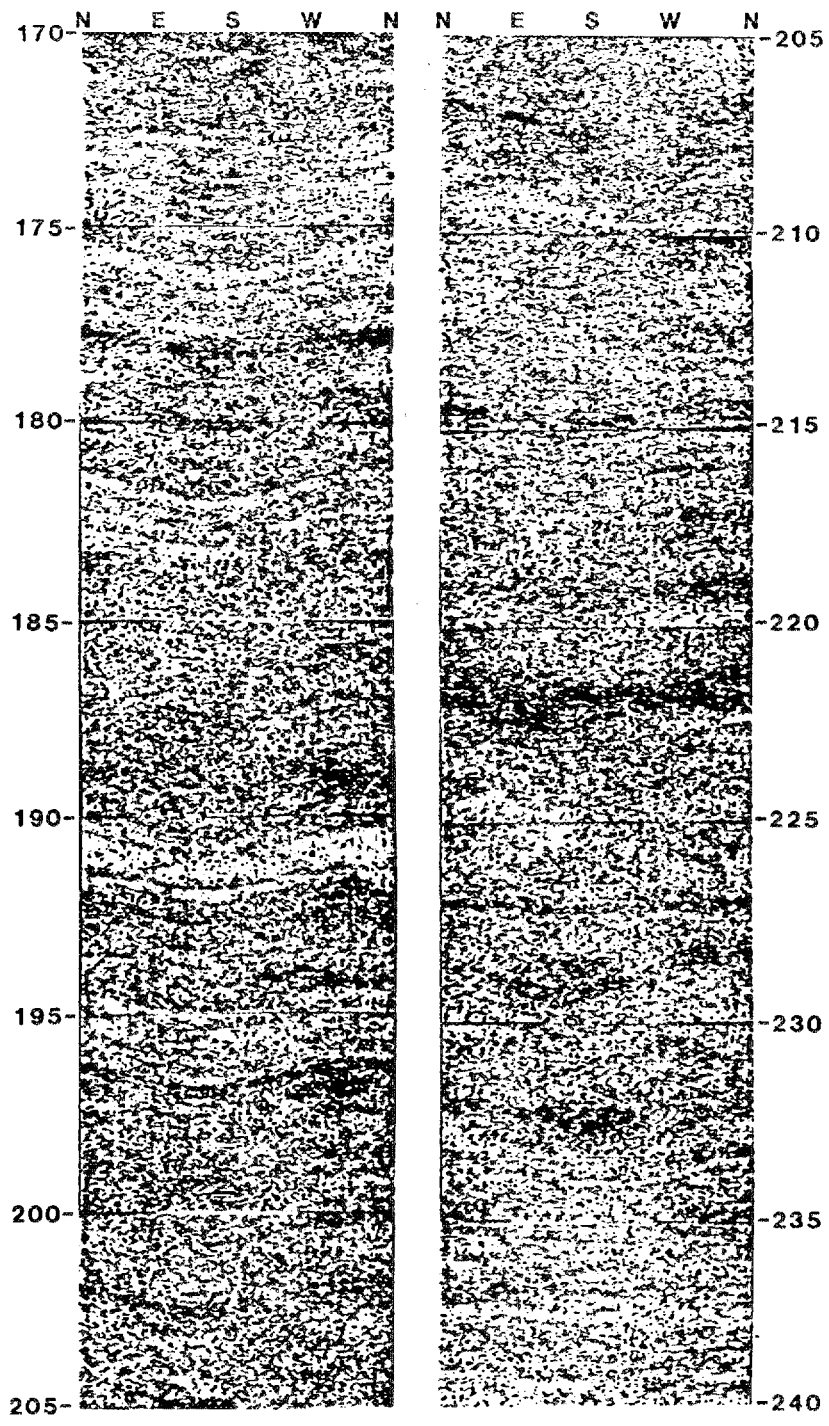


ORNL-DWG 89-13288

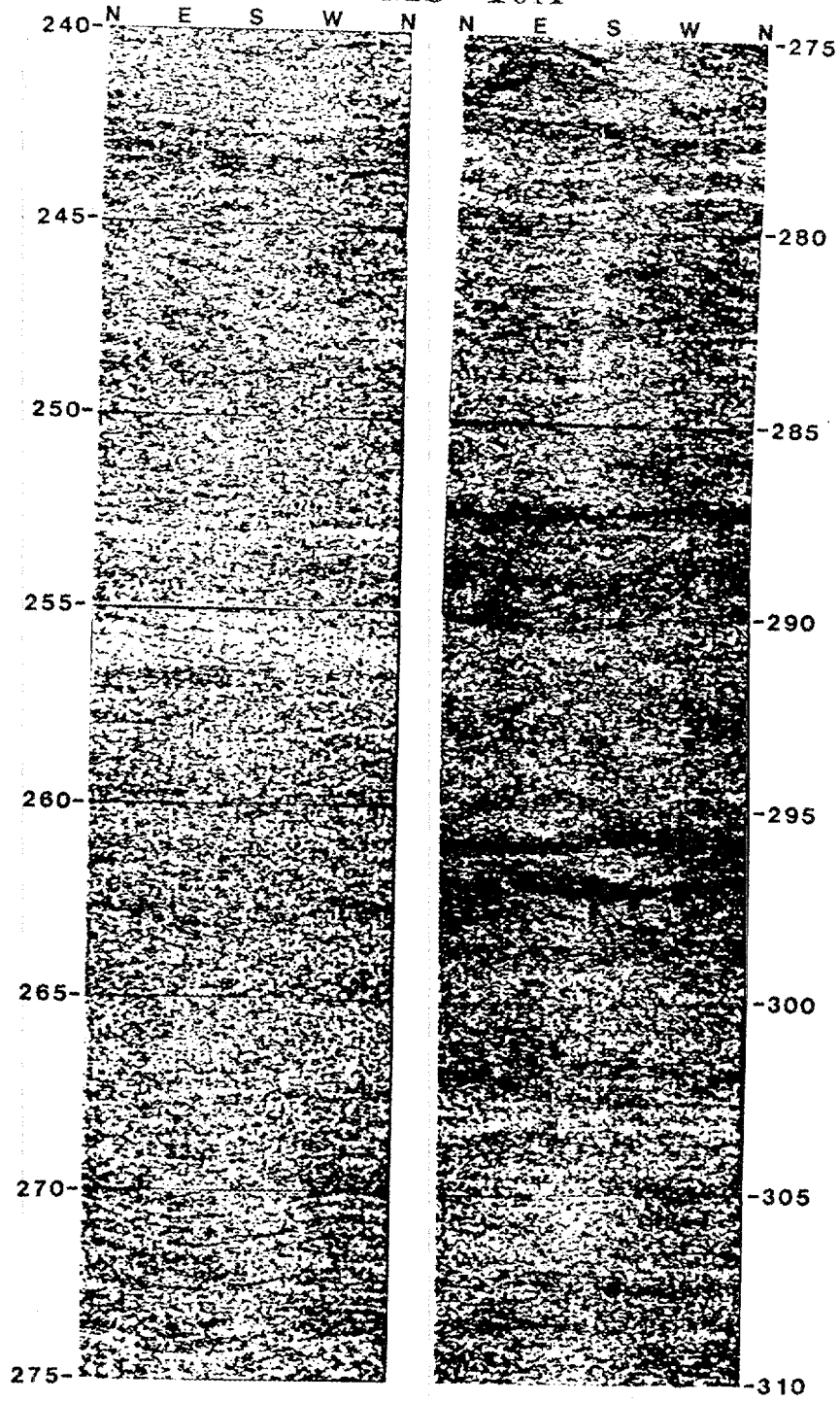
HHMS 10A



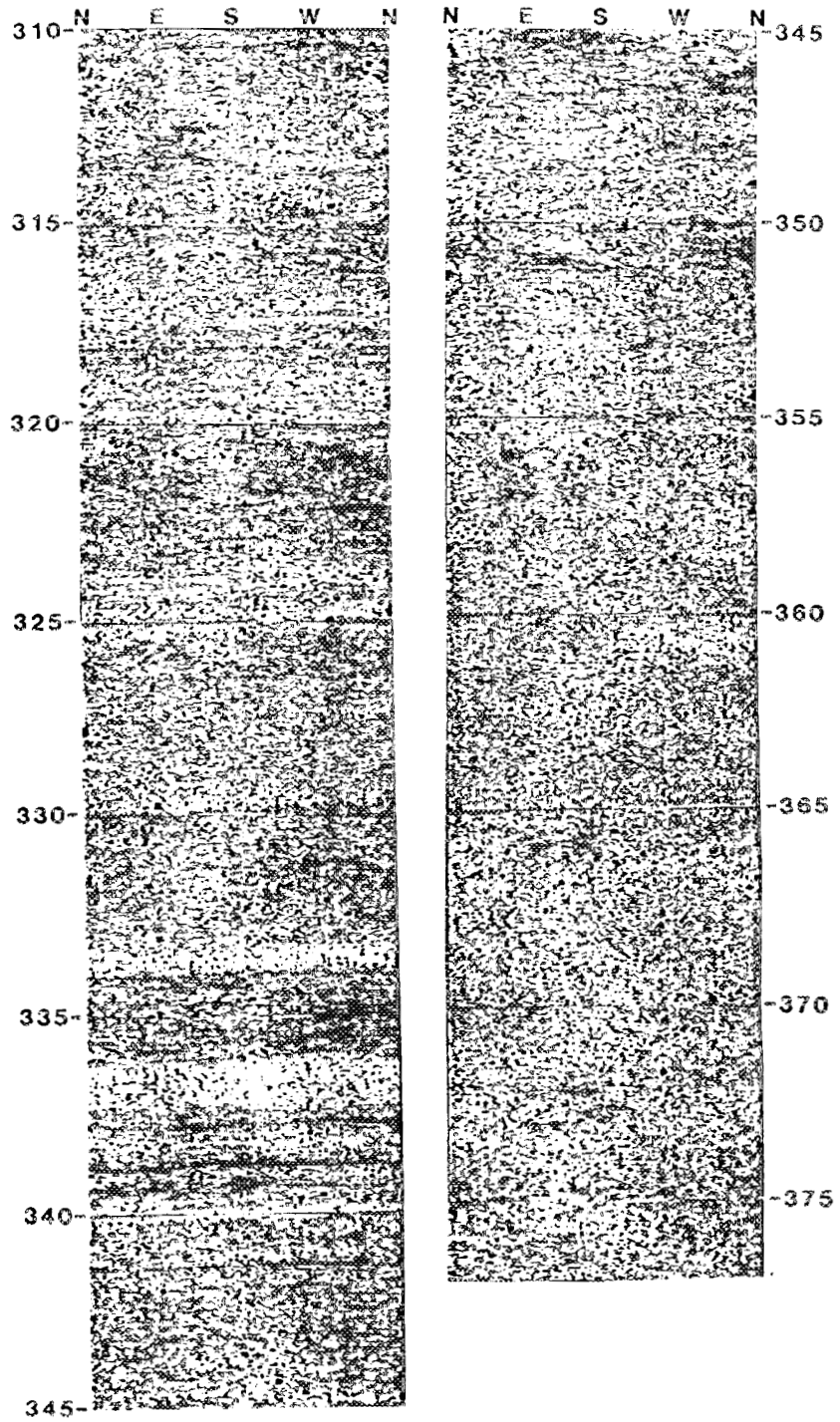
HHMS 10A



HHMS 10A



HHMS 10A



APPENDIX 11

GENERAL WELL SITE INFORMATION

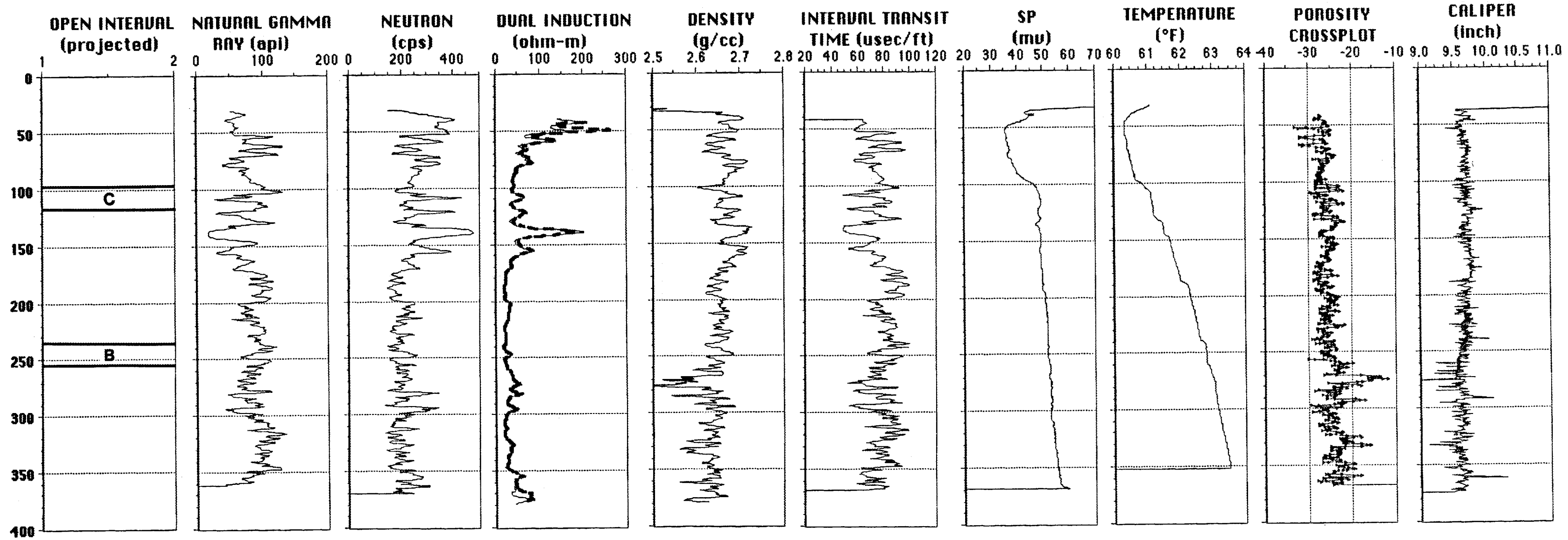
DRILLERS LOGS

GEOPHYSICAL LOGS

FOR HHMS SITE 11

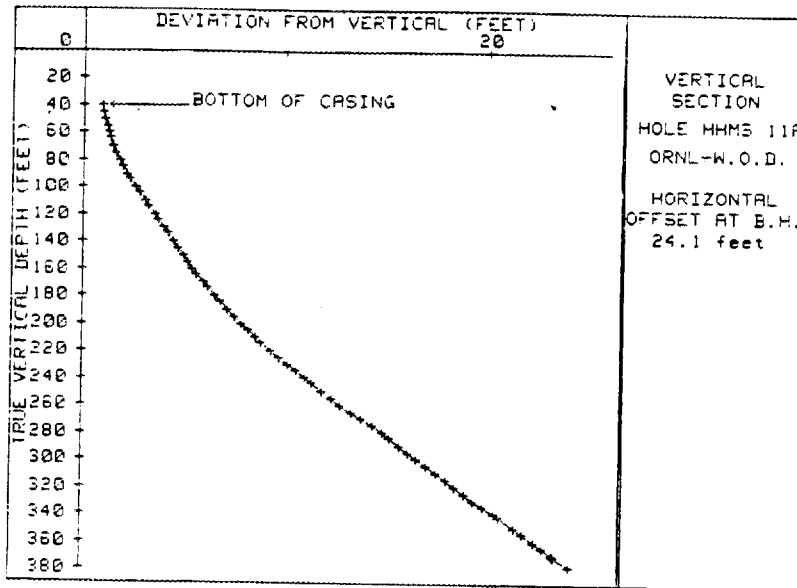
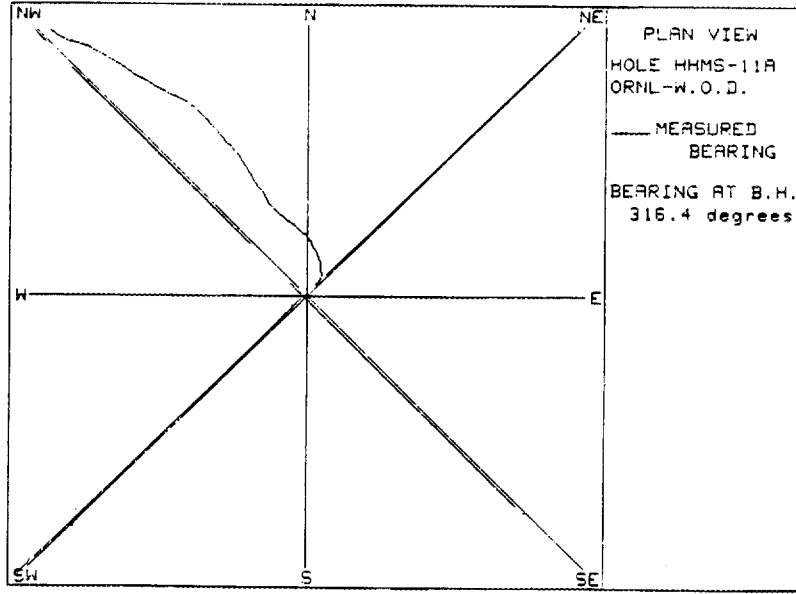
WELL DATA, STRATIGRAPHIC AND STRUCTURAL MARKERS, DRILLERS LOGS					
Well Name	Alternate Name	ORN L N (ft)	ORN L E (ft)	Ground Elevation (ft)	Top of Casing (ft)
HHMS 11-A	1008	13802.36	22749.62	779.95	782.12
		depth	elevation		
	Cmn/Cn	53	726.95		
Cn marker	5	298	481.95		
Def Zone	from	265	514.95		
	to	300	479.95		
DRILLERS LOGS - no records for the open interval					
soft		55	724.95		
soft		57	722.95		
soft	from	93	686.95		
soft	to	95	684.95		
soft		153	626.95		
soft	from	252	527.95		
soft	to	254	525.95		
soft		363	416.95		
broken up	from	310	469.95		
broken up	to	315	464.95		
rough		354	425.95		
rough	from	360	419.95		
rough	to	365	414.95		

HHMS 11 - GEOPHYSICAL LOGS



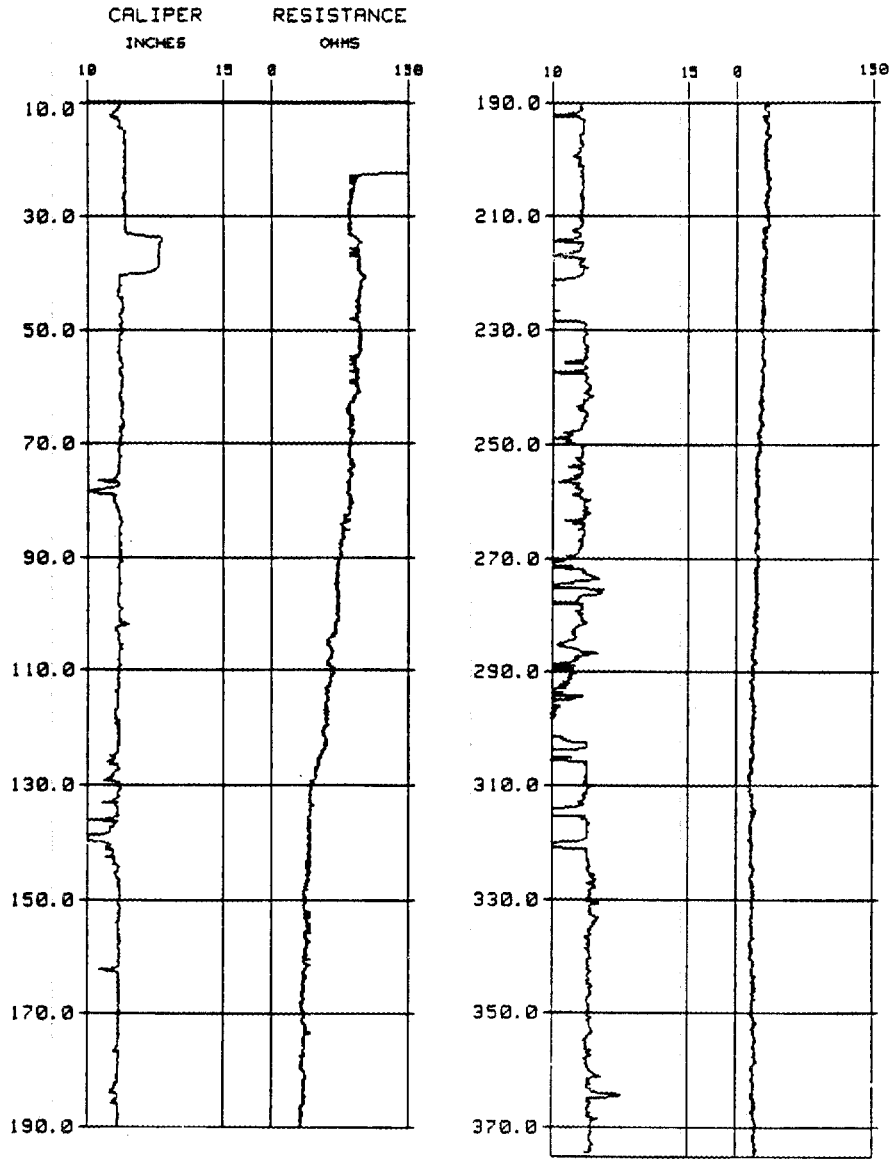
ORNL-DWG 89-13235

HHMS 11 - DEVIATION LOG



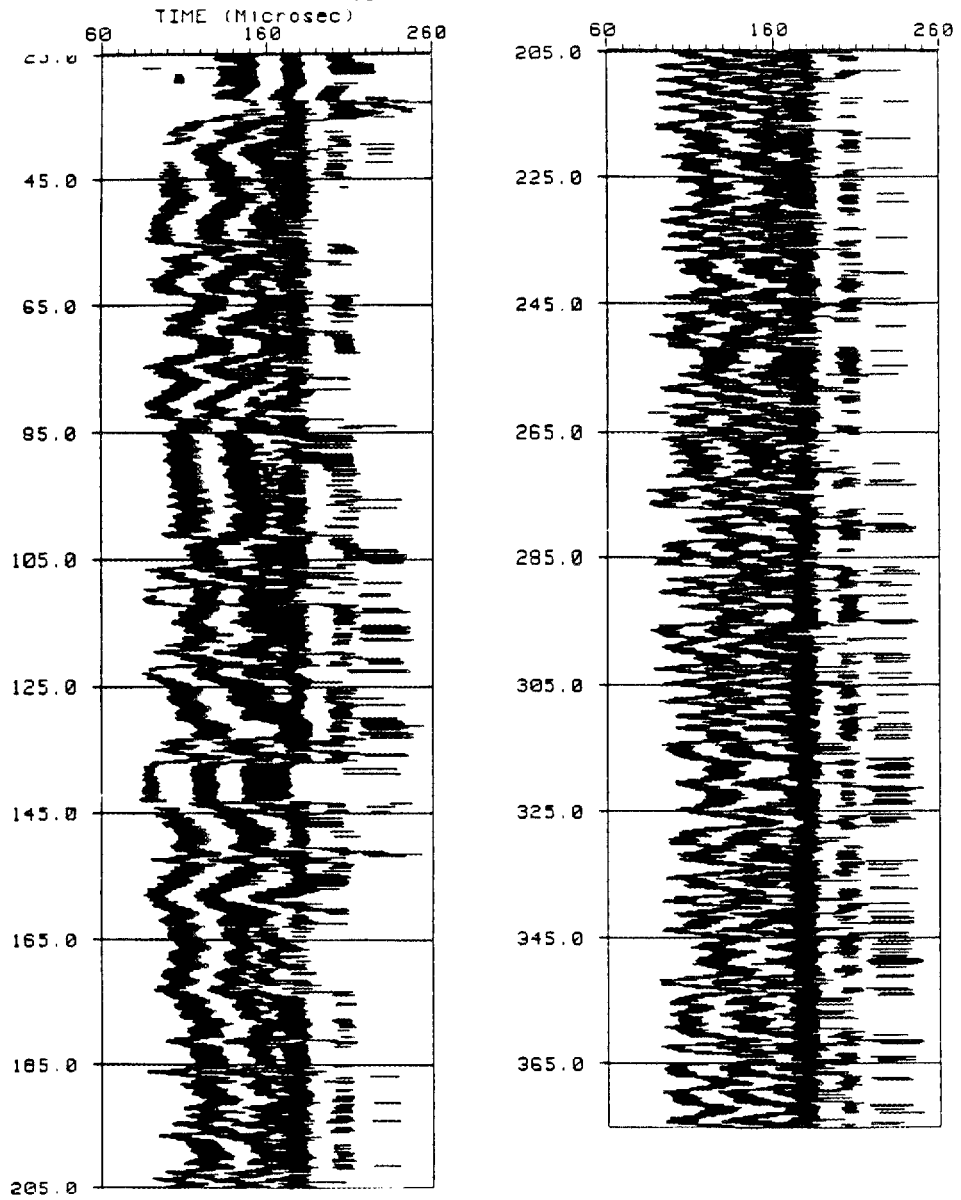
ORNL-DWG 89-13314

HHMS 11A

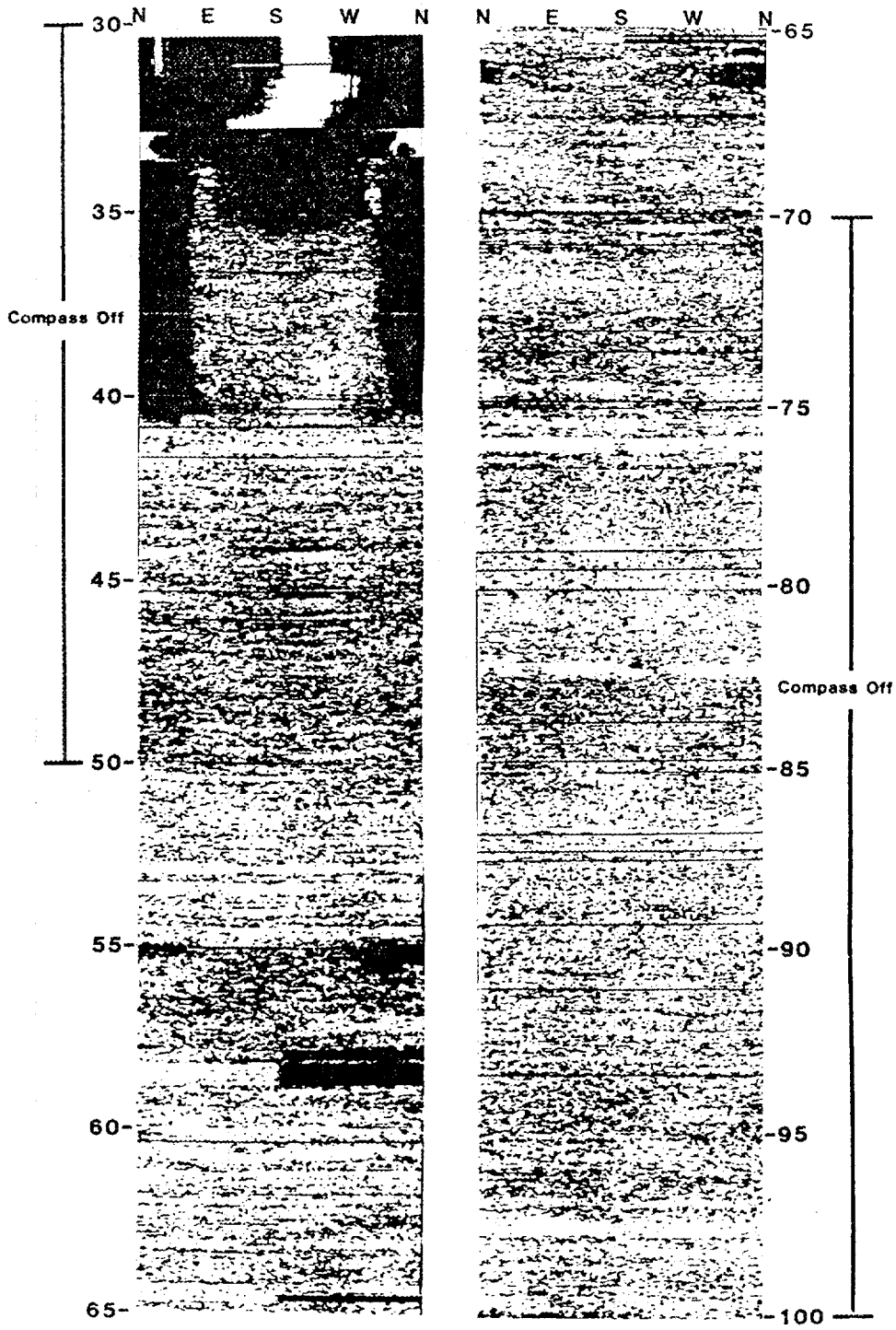


HHMS 11A

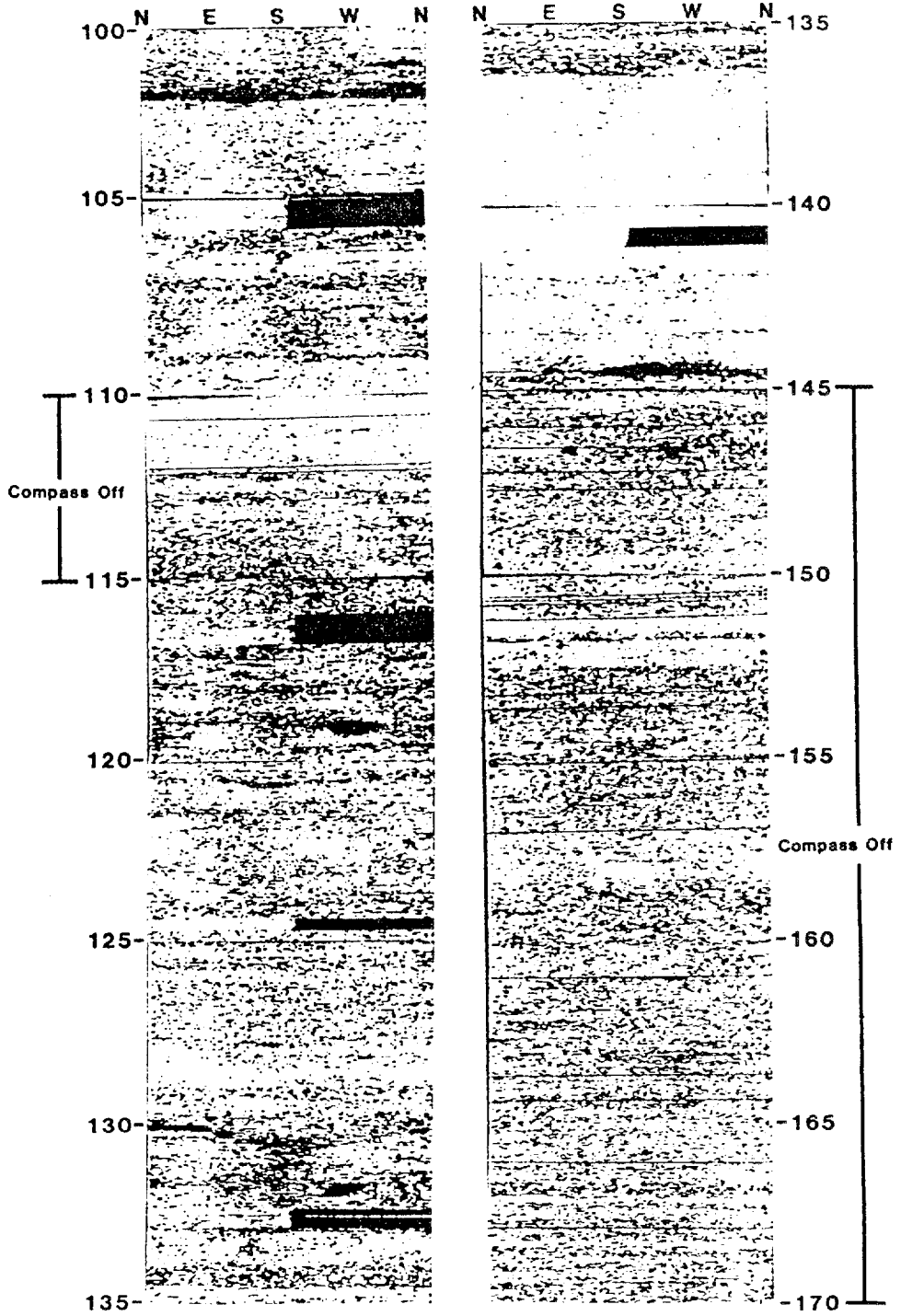
VARIABLE DENSITY LOG



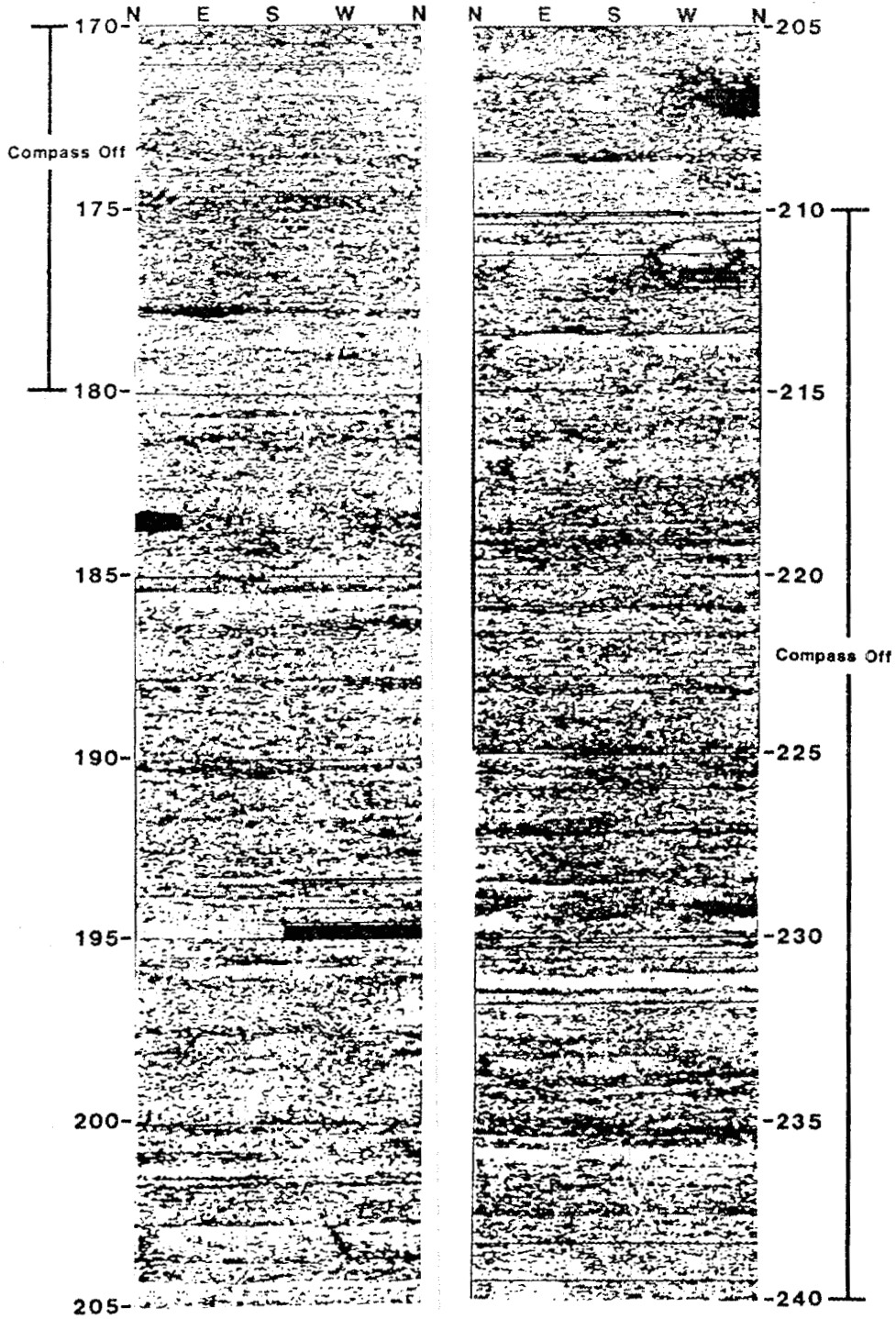
HHMS 11A



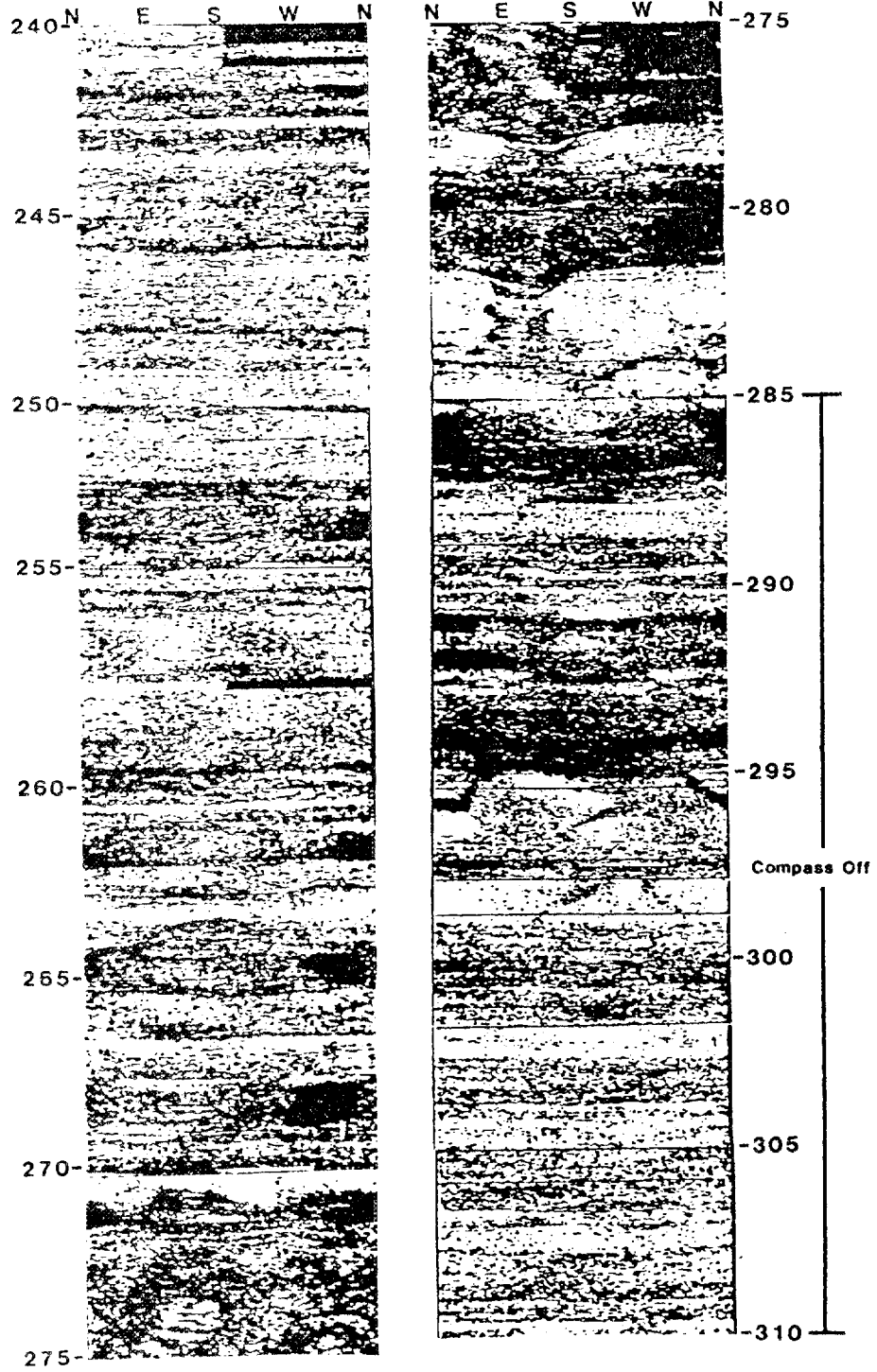
HHMS 11A



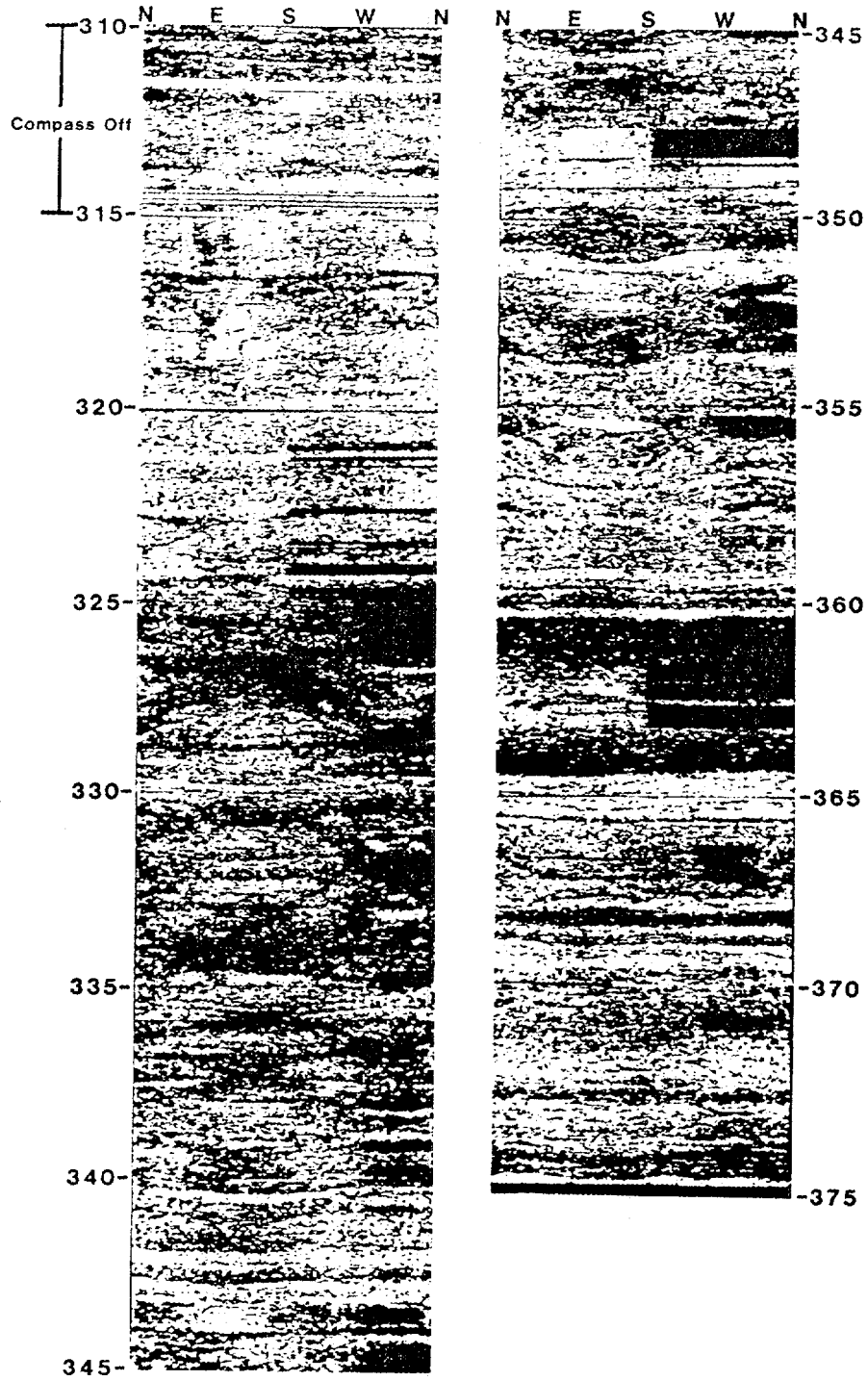
HHMS 11A



HHMS 11A



HHMS 11A



APPENDIX 12
CONASAUGA GROUP STRATIGRAPHY

NOLICHUCKY SHALE

Natural gamma-ray and epithermal neutron logs that illustrate the Nolichucky Shale are presented in Fig. 4. The Nolichucky Shale is approximately 515 ft thick in the study area. This value is slightly less than the stratigraphic thickness measured several miles to the grid-east at the ORNL Joy No. 2 borehole, where the Nolichucky Shale is 551 ft thick.

No single borehole samples the entire Nolichucky Shale. However, it is possible to correlate stratigraphic horizons between the boreholes (shown by the heavy and dotted lines) in order to characterize the entire formation. Correlation is not always straightforward between wells, however, because of facies changes within the Nolichucky Shale. For example, Nolichucky marker 4 appears to be absent in borehole HHMS 4A (Fig. 4). In addition, local structural deformation (discussed in following sections) and uncertainty in stratigraphic overlap between wells, particularly between HHMS 6A and HHMS 11A, also create difficulties in correlating strata. The interpreted correlation between HHMS 6A and HHMS 11A (shown in Fig. 4) appears reasonable, however, because it matches the geophysical signature of the ORNL Joy No. 2 borehole (Haase and others 1985), and requires an approximate 5° regional dip between the boreholes. This dip value matches interpretations from seismic reflection studies (performed by R. B. Dreier) and from deviation data (Appendix 11) as a borehole will tend to deviate toward a normal to the bedding orientation.

The upper contact of the Nolichucky Shale with the Maynardville Limestone is gradational, with the lower Maynardville Limestone being characterized by an increasing shale content. The geophysical log signature of this interval consists of increasing gamma-ray and decreasing neutron values and is characterized by significant changes in baselines for both logs from those typical of most of the Maynardville Limestone. The upper contact of the Nolichucky Shale is placed at the first substantial shale bed within the transition zone at the bottom of the Maynardville Limestone and corresponds to a point where the baselines of the gamma-ray and neutron logs have stabilized at values typical of the Nolichucky Shale (HHMS 11A, Fig. 4). The lower contact of the Nolichucky Shale with the Maryville Limestone is marked by a baseline shift to increasing gamma-ray log values and decreasing neutron log values (HHMS 4A and HHMS 5A, Fig. 4). The contact between the formations is located where the baseline for the gamma-ray and neutron logs stabilizes at a constant position typical of the upper Maryville Limestone. Both the Nolichucky Shale and the Maryville Limestone contain interbedded shales and limestones, and the baseline shifts

in the geophysical logs occur because the top of the Maryville Limestone is significantly more limestone-rich than the basal Nolichucky Shale (Haase and others 1985).

Throughout eastern Tennessee the Nolichucky Shale is divided into three members (Hasson and Haase 1988), and these divisions can be applied to the Oak Ridge vicinity (Haase and others 1985). The upper shale member is approximately 80 ft thick and consists of a limestone-rich shale sequence immediately below the upper contact of the formation (HHMS 11A, Fig. 4). Below the upper shale member is the Bradley Creek Limestone member (HHMS 11A, labeled A in Fig. 4). This unit is characterized by abrupt baseline shifts of both the gamma-ray and neutron logs to values typical of the overlying Maynardville Limestone. The Bradley Creek member is approximately 20 ft thick in HHMS 11A.

The lower shale member of the Nolichucky Shale is the thickest member of the formation and consists of regularly interbedded limestone and shale horizons. This interbedding accounts for the spiky nature of both the gamma-ray and neutron logs in the interval between the Bradley Creek member and Nolichucky marker 3 in Fig. 4. Toward the bottom of the lower shale member, between Nolichucky markers 3 and 1 (Fig. 4), the shale content of the formation increases, and the amount of interbedded limestones decreases. This interval is characterized by slight baseline shifts to increasing gamma-ray log values and decreasing neutron log values. Below Nolichucky marker 1 (Fig. 4), the limestone content of the formation increases in a gradual manner and the regularly interbedded character of the shales and limestones returns immediately above the lower contact (Haase and others 1985).

MARYVILLE LIMESTONE

Gamma-ray and epithermal neutron logs that illustrate the Maryville Limestone are presented in Fig. 5. The stratigraphic thickness of the Maryville Limestone is approximately 425 ft.

The upper contact of the Maryville Limestone with the Nolichucky Shale has been discussed above and is shown in Fig. 4. The lower contact with the Rogersville Shale is not characterized by pronounced baseline shifts on either the gamma or neutron logs, but is characterized by a sharp anomaly on the gamma-ray and neutron logs (Fig. 5) that is associated with a prominent limestone bed. The lower Maryville Limestone is significantly

more shale-rich than the upper portion (Haase and others 1985) and resembles the underlying Rogersville Shale; thus no significant baseline shift would be expected in these logs.

The Maryville Limestone can be informally divided into two members in the Oak Ridge vicinity (Haase and others 1985). The upper member is characterized by repeating cycles of limestone-rich horizons. These horizons, which range from 15 to 40 ft in thickness, are characterized by prominent neutron and gamma-ray log anomalies and are separated from each other by shale-rich intervals of similar thicknesses (Maryville markers 4 and 5 in Fig. 5). At the bottom of the upper member, a transition zone occurs where the baseline shifts to increasing gamma-ray log values and decreasing neutron log values. The contact between the lower and the upper members is placed at the lower base of that transition zone (Maryville marker 3, Fig. 5). In HHMS 8, the transition has been placed at approximately 70 ft (Maryville marker 3'), requiring stratigraphic duplication of the interval between Maryville markers 3 and 4. The baseline shift is not observed above marker 3 in HHMS 8A, presumably because of additional shale within a wide fault zone (see Sect. 3.3.3.1).

The lower member is shale-rich and is characterized by gamma-ray and neutron logs with relatively flat, constant baselines. Several limestone-rich intervals, ranging from 20 to 50 ft in thickness, occur throughout the lower member (e.g. the two limestone beds immediately above Maryville marker 1 in Fig. 5). These occur throughout the study area and are a characteristic feature of the lower Maryville Limestone. (Haase and others 1985).

ROGERSVILLE SHALE

Gamma-ray and epithermal neutron logs that illustrate the Rogersville Shale are presented in Figs. 5 and 6. The upper Rogersville Shale is sampled in HHMS boreholes that penetrate the Maryville Limestone - Rogersville Shale contact. Commonly only a small portion of the upper part of the formation is penetrated (Fig. 5), and characterization of the Rogersville Shale is difficult from these boreholes. In HHMS 7A, however, 85 ft (measured downhole) of the upper Rogersville Shale is exposed, and, in HHMS 9A, 110 ft (measured downhole) of the lower Rogersville Shale is exposed. Other wells in the Pits and Trenches area or farther south near the hydrofracture facility show an average Rogersville Shale stratigraphic thickness of 116 ft. Hence, it is presumed that there is

some minimal stratigraphic overlap between HHMS 7A and HHMS 9A, although there are no geophysical log markers within the Rogersville Shale to confirm this correlation.

The upper contact of the formation with the Maryville Limestone has been discussed above and is shown in Fig. 5. The lower contact with the Rutledge Limestone is characterized by pronounced baseline shifts in both the gamma-ray and neutron logs (Fig. 6). This baseline shift is associated with an increase in the limestone content of the Rutledge Limestone with respect to the Rogersville Shale.

The Rogersville Shale is lithologically quite homogeneous, and the flat and relatively constant baselines for both the gamma-ray and neutron logs are consistent with that observation. Several spiky anomalies, such as those near point A in Fig. 5, are typically noted in the middle of the Rogersville Shale section. These correspond to 2- to 5-ft-thick siltstone-rich horizons (Haase and others 1985).

Throughout much of east Tennessee, a limestone-rich member can be delineated near the top of the Rogersville Shale (Hasson and Haase 1988). This horizon, the Craig member, occurs in the Oak Ridge vicinity (Haase and others 1985) but is only a few feet thick throughout the study area. The geophysical log signature of the Craig member is a sharp spiky anomaly on both the gamma-ray and neutron logs and occurs immediately below the large anomaly characteristic of the Maryville Limestone/Rogersville Shale contact. Without data from drill core, interpretation of this anomaly as the Craig member would be difficult.

RUTLEDGE LIMESTONE

Gamma-ray and epithermal neutron logs that illustrate a typical Rutledge Limestone section are presented in Fig. 6. Based on a calculated local dip of 25° (Sect. 3.3.2), the stratigraphic thickness of the Rutledge Limestone in this borehole is 117 ft.

The upper contact of the Rutledge Limestone with the Rogersville Shale has been discussed above and is shown in Fig. 6. The lower contact of the Rutledge Limestone with the Pumpkin Valley Shale is characterized by a prominent anomaly on the gamma and neutron logs (Fig. 6). This anomaly has been termed the "three limestone beds" (deLaguna and others 1968) and corresponds to three limestone rich beds within a predominantly shale-rich portion of the lower Rutledge Limestone (Haase and others 1985). There is little

baseline shift in the gamma and neutron logs at this contact since lower Rutledge Limestone is shale-rich and is similar to the Pumpkin Valley Shale.

The spiky character of the gamma and neutron logs within the upper Rutledge Limestone results from discrete shale-rich intervals interbedded in limestone-rich horizons throughout the interval. Such a stratification has been documented elsewhere in Melton Valley (Haase and others 1985) and is characteristic of the upper Rutledge Limestone.

PUMPKIN VALLEY SHALE

Gamma-ray and epithermal neutron logs that illustrate the Pumpkin Valley Shale are presented in Fig. 6. Only a portion of the formation (120 ft) is penetrated by HHMS 9A, and no other HHMS wells sample the Pumpkin Valley Shale. The Pumpkin Valley Shale, however, ranges in thickness from 310 to 375 ft in Melton Valley (C. S. Haase, ORNL, Oak Ridge, Tenn., personal communication to R. B. Dreier, ORNL, Oak Ridge, Tenn., June 1986).

The upper contact of the Pumpkin Valley Shale with the Rutledge Limestone has been discussed above and is shown in Fig. 6. The Pumpkin Valley Shale consists of thinly interbedded mudstones, shales, and siltstones. It can be informally divided into two members in the Oak Ridge study area (Haase and others 1985) but only part of the upper member is exposed in HHMS 9A. Despite small-scale heterogeneities, the upper member is lithologically quite homogeneous and the gamma-ray and neutron logs exhibit a relatively flat and constant baseline, typical of the shale-rich character of the member. Locally, however, several 1- to 3-ft-thick siltstone-rich horizons impart a spiky character to the gamma-ray and neutron logs.

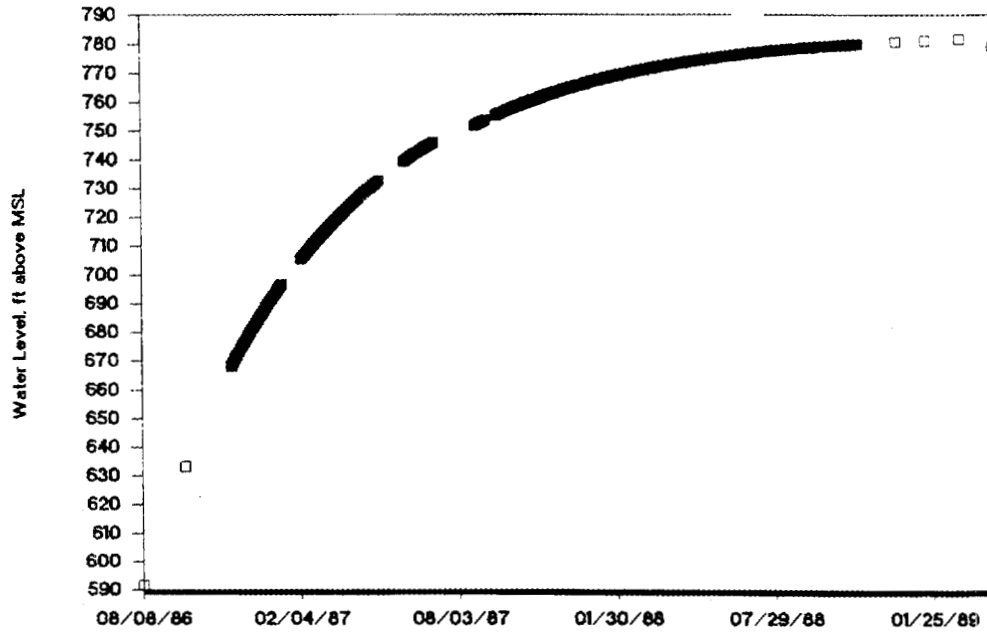
APPENDIX 13

HYDROGRAPHS

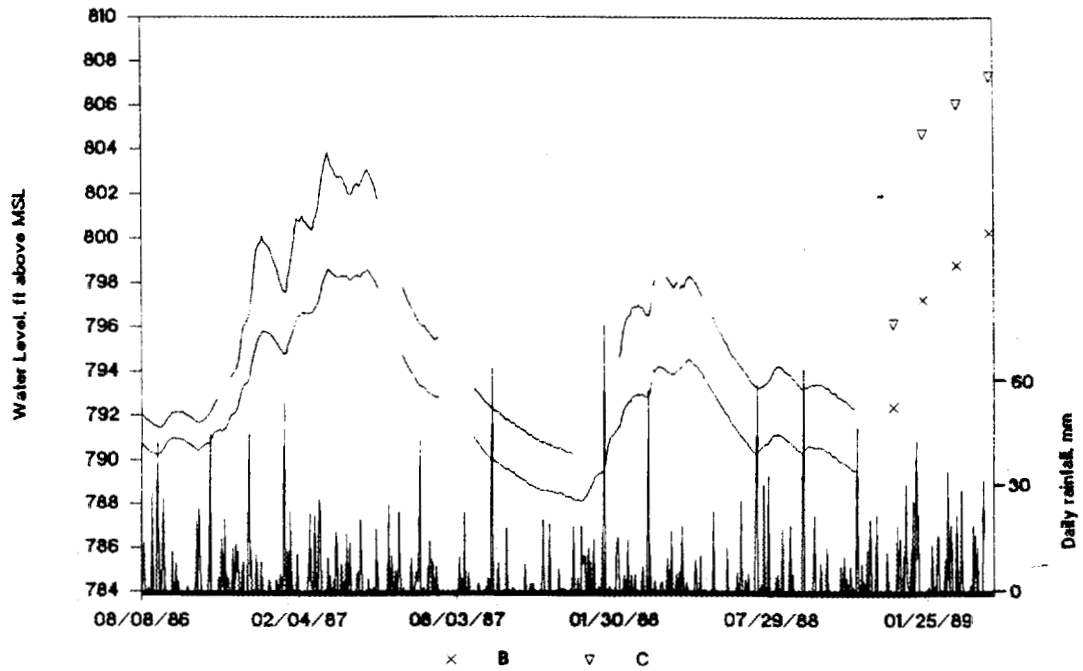
APPENDIX 13

Hydrographs for HHMS clusters 1 through 11, including data from USGS wells 466 and 467, near HHMS 10A. Gaps in data are from recorder down time, sampling, and hydraulic conductivity tests. Some discontinuities occur when switching from continuous recorders to echo sounder or tape measurements.

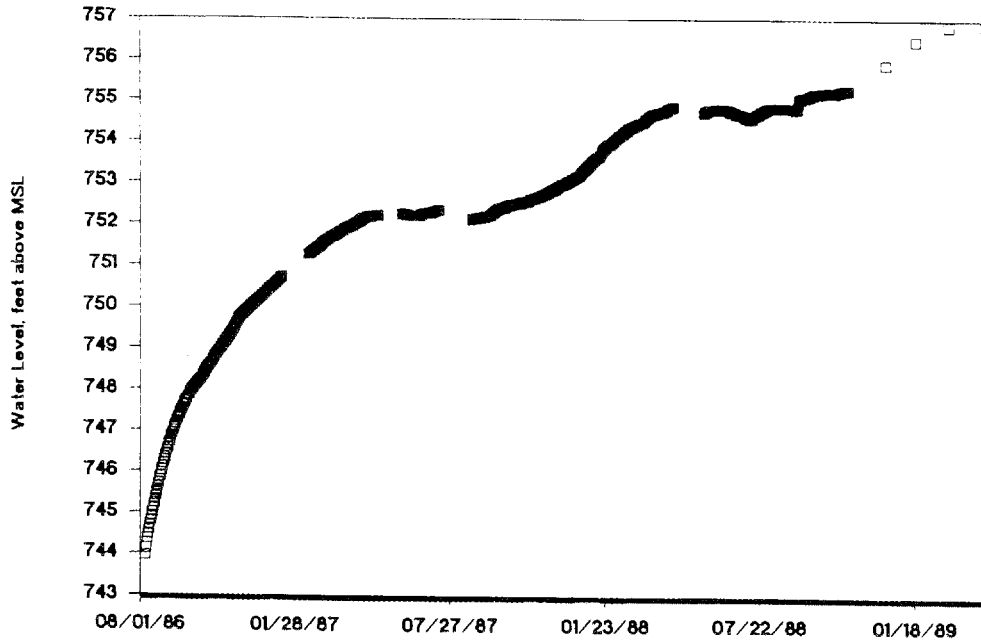
HHMS 1A



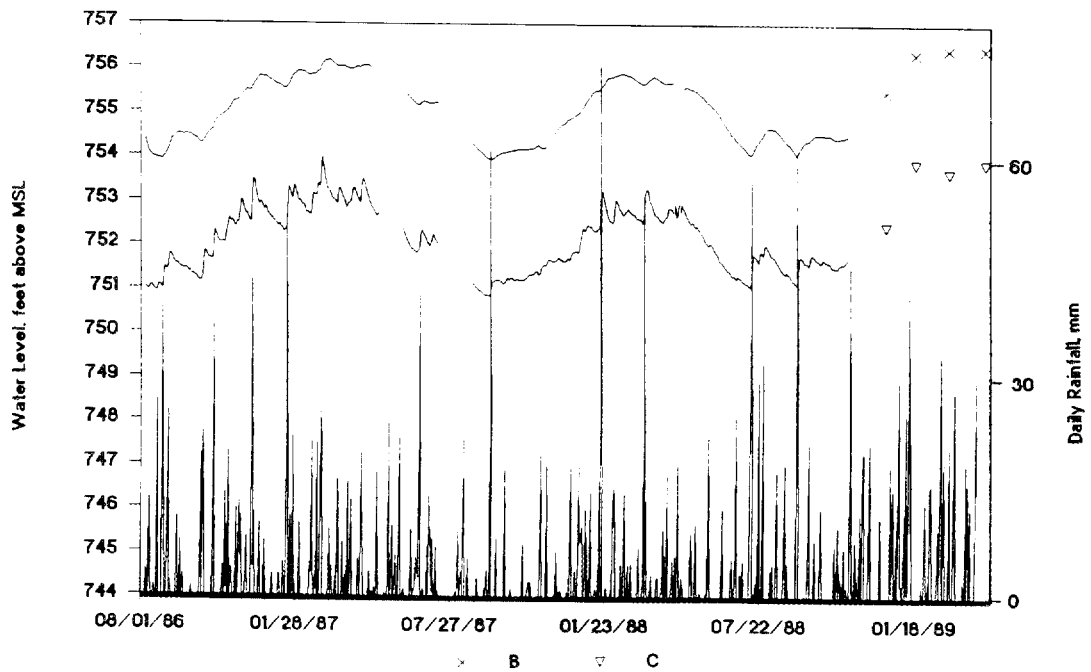
HHMS 1B,C



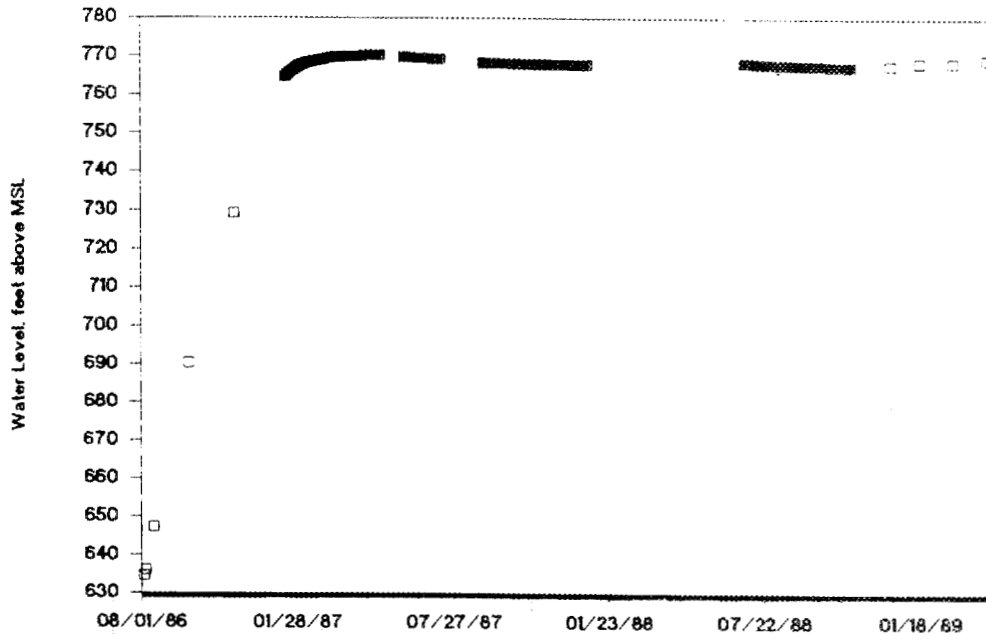
HHMS 2A



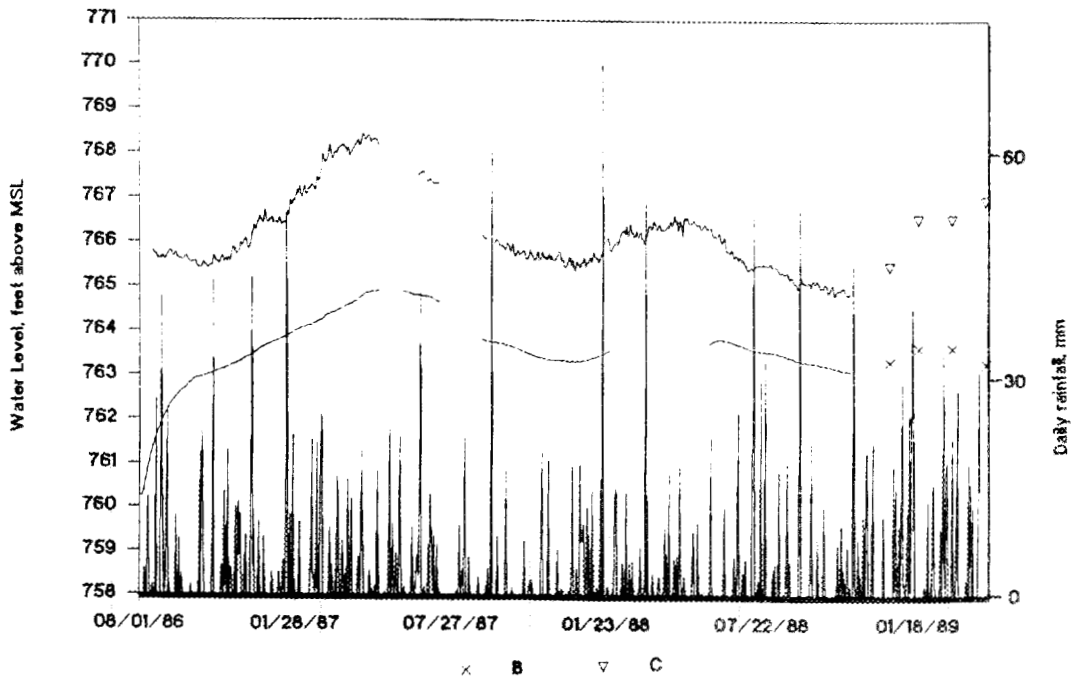
HHMS 2B,C



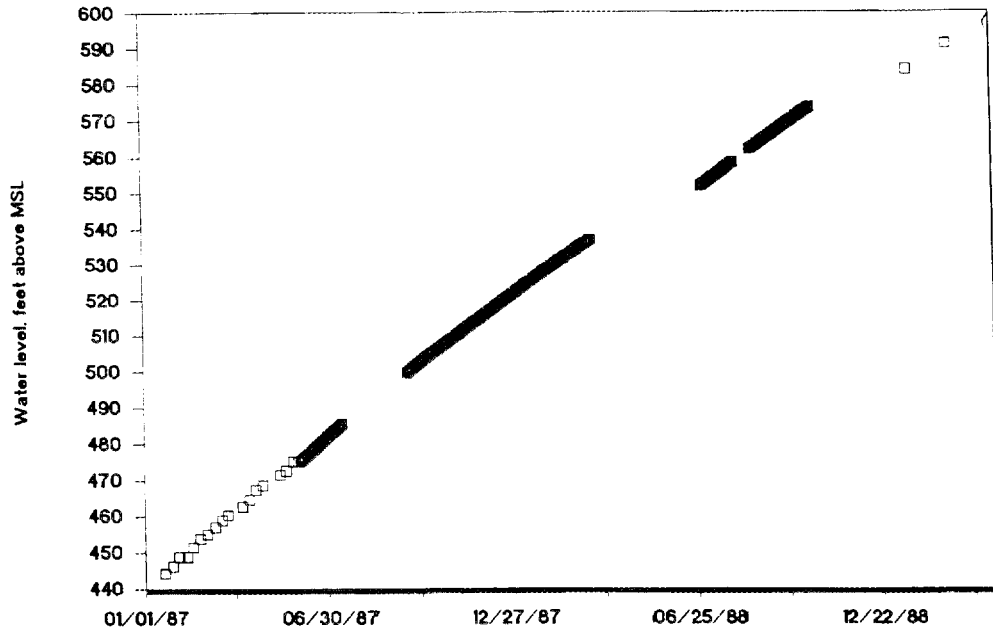
HHMS 3A



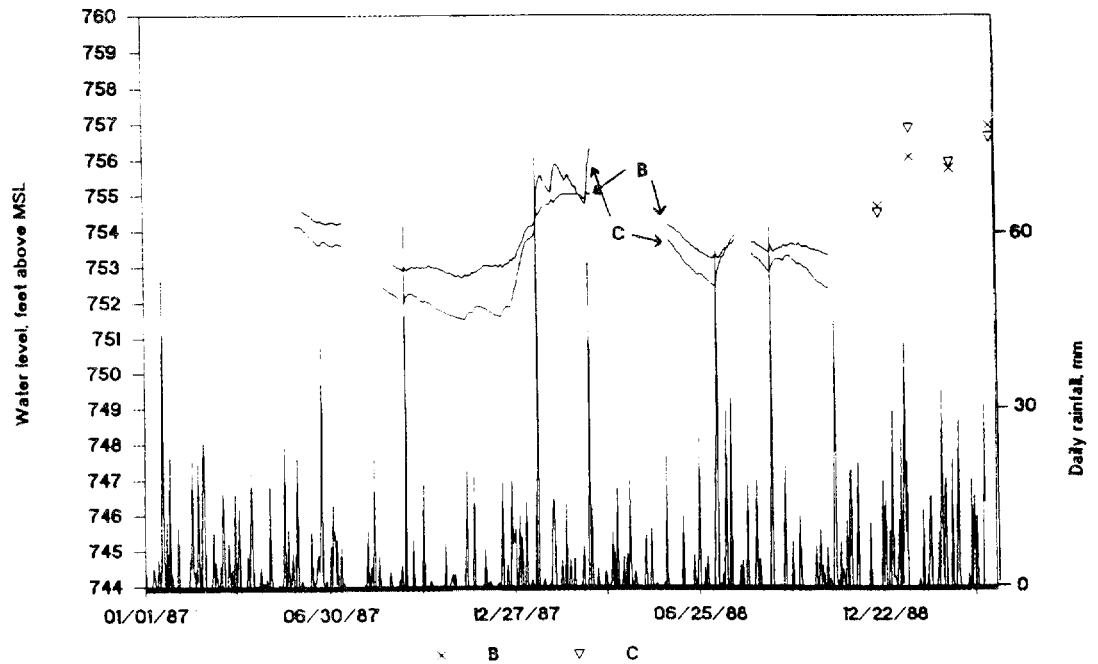
HHMS 3B,C



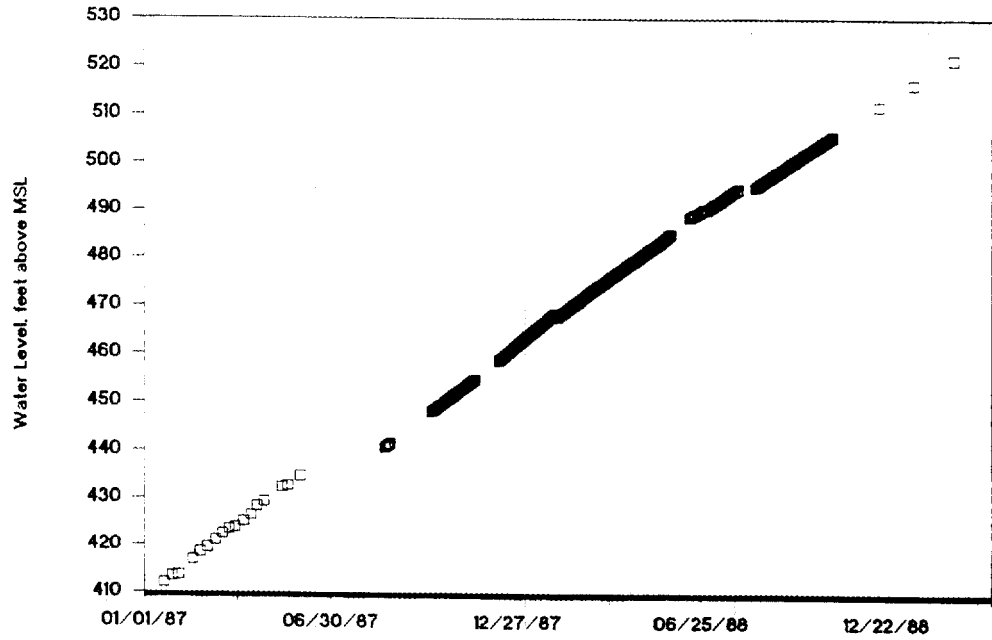
HHMS 4A



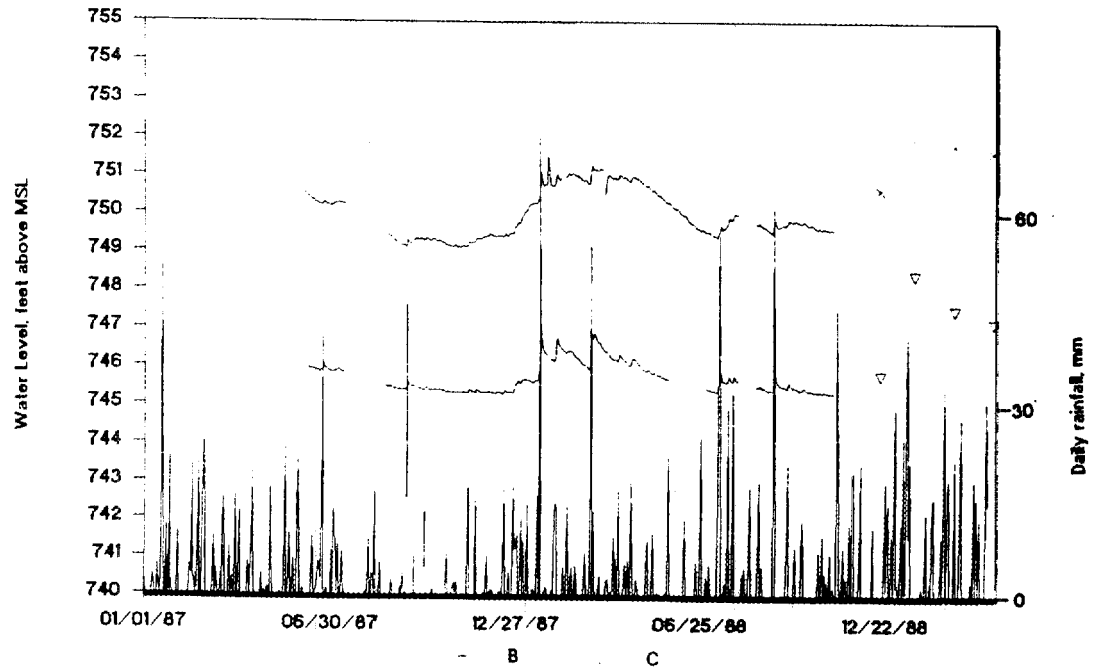
HHMS 4B,C



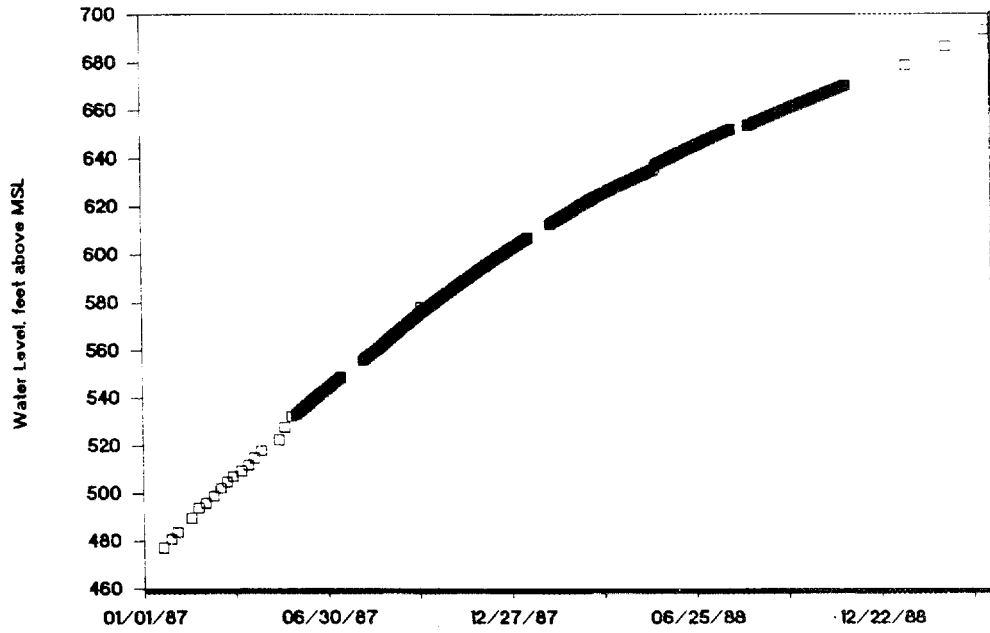
HHMS 5A



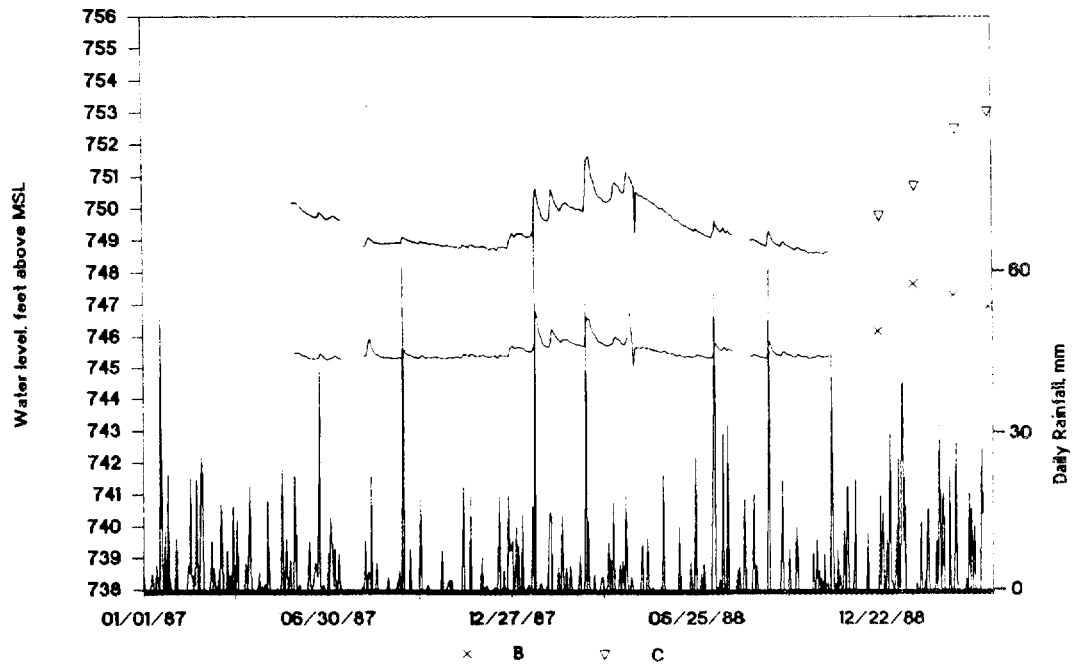
HHMS 5B.C



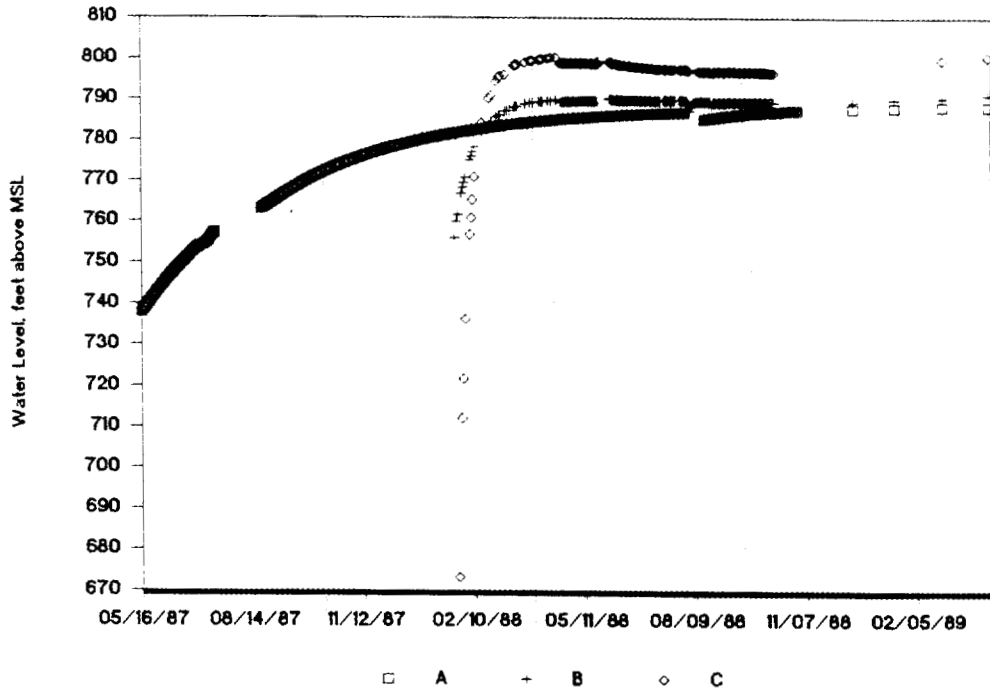
HHMS 6A



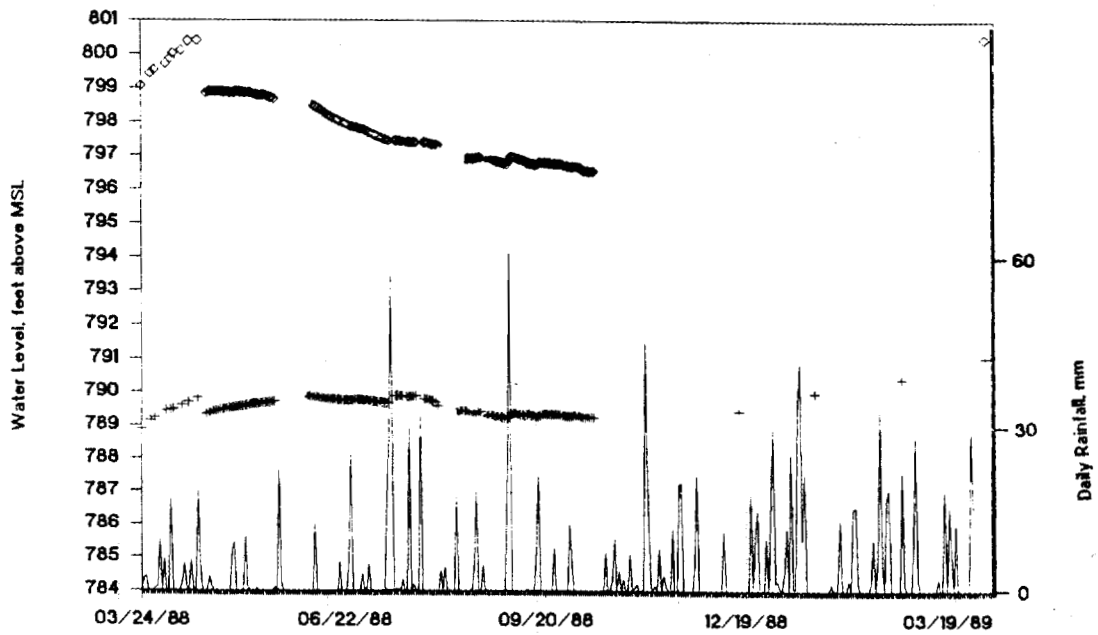
HHMS 6B,C



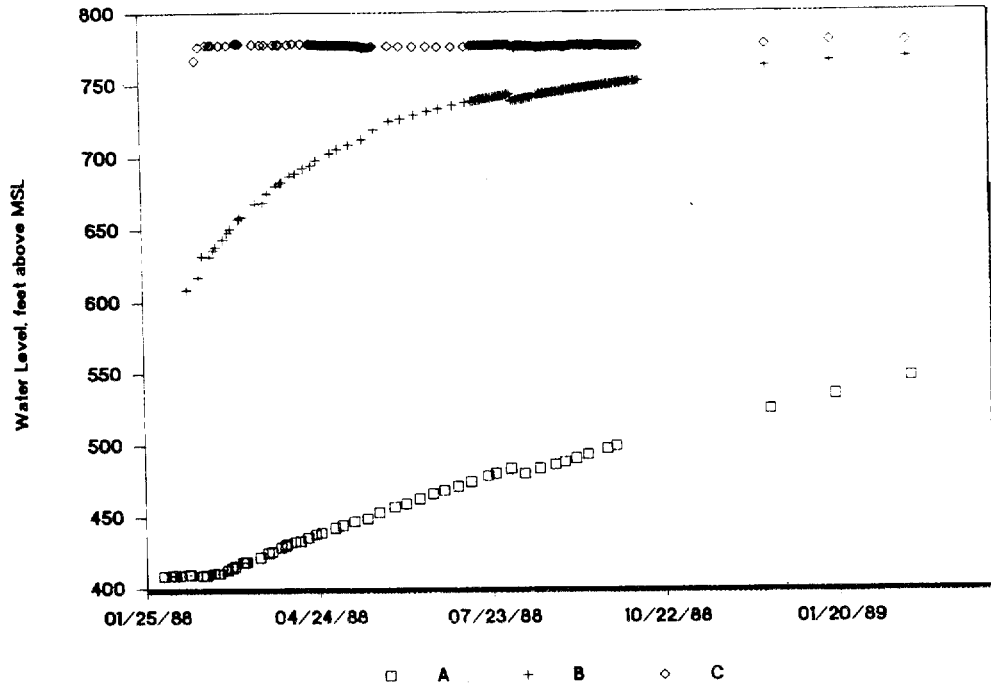
HHMS 7A,B,C



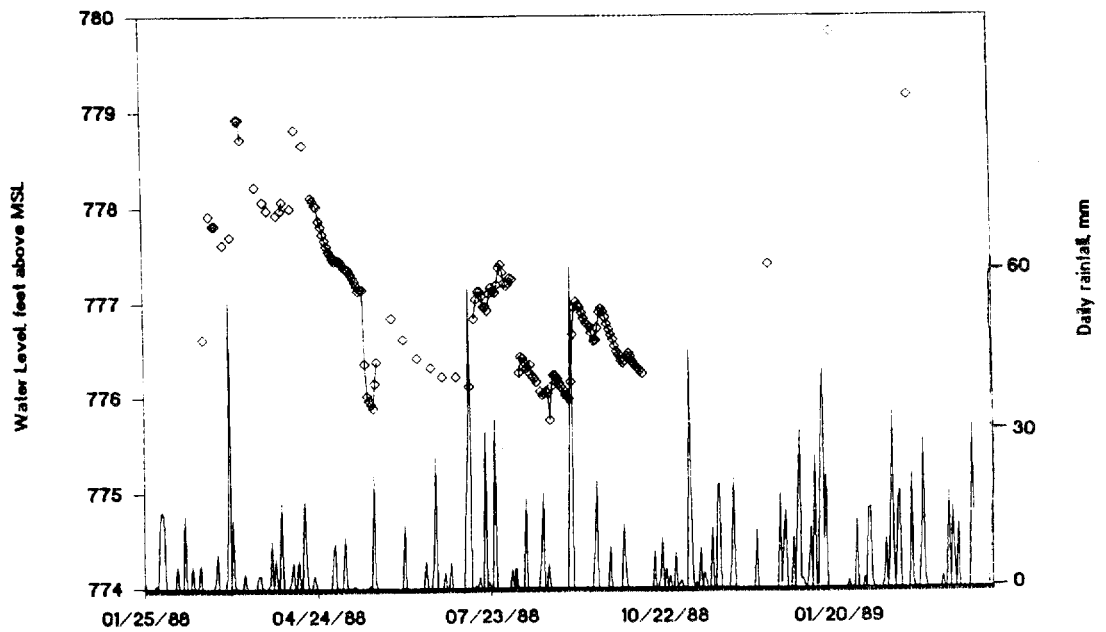
HHMS 7B,C



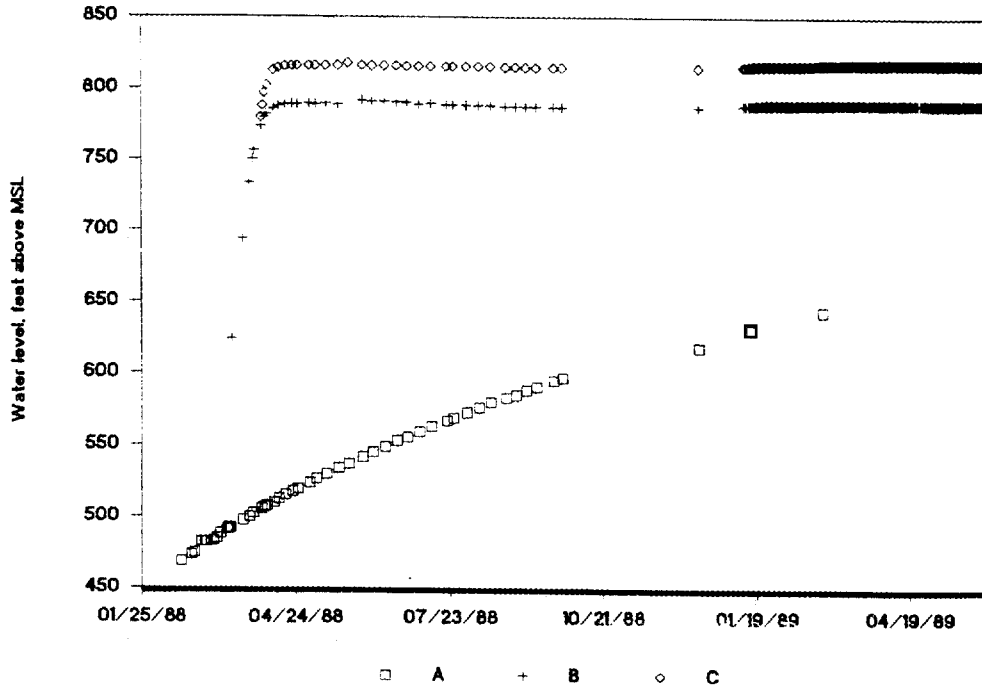
HHMS 8A,B,C



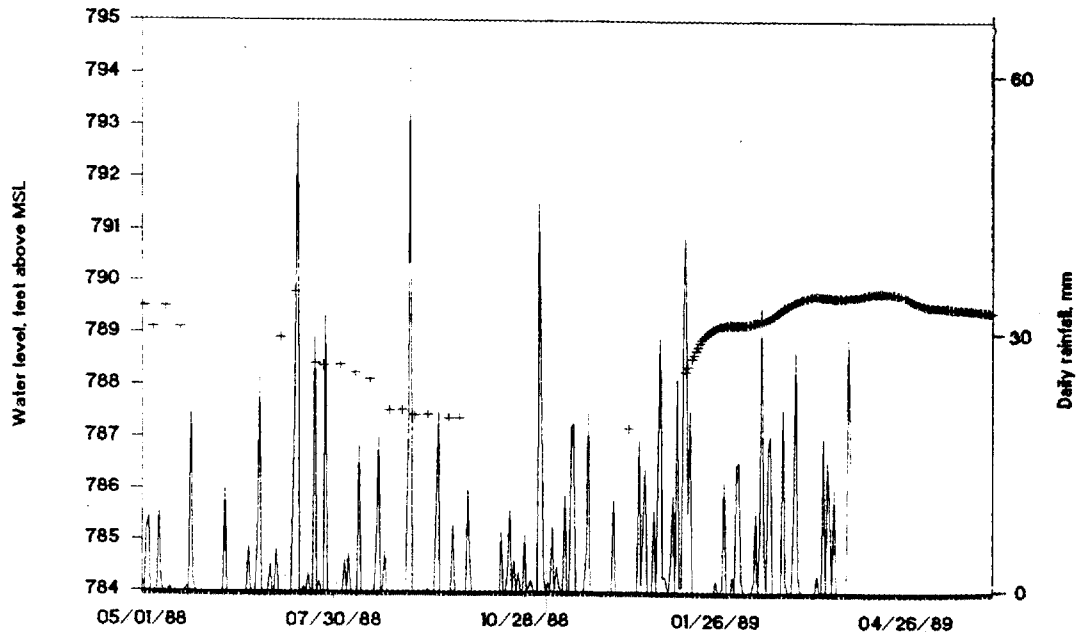
HHMS 8C



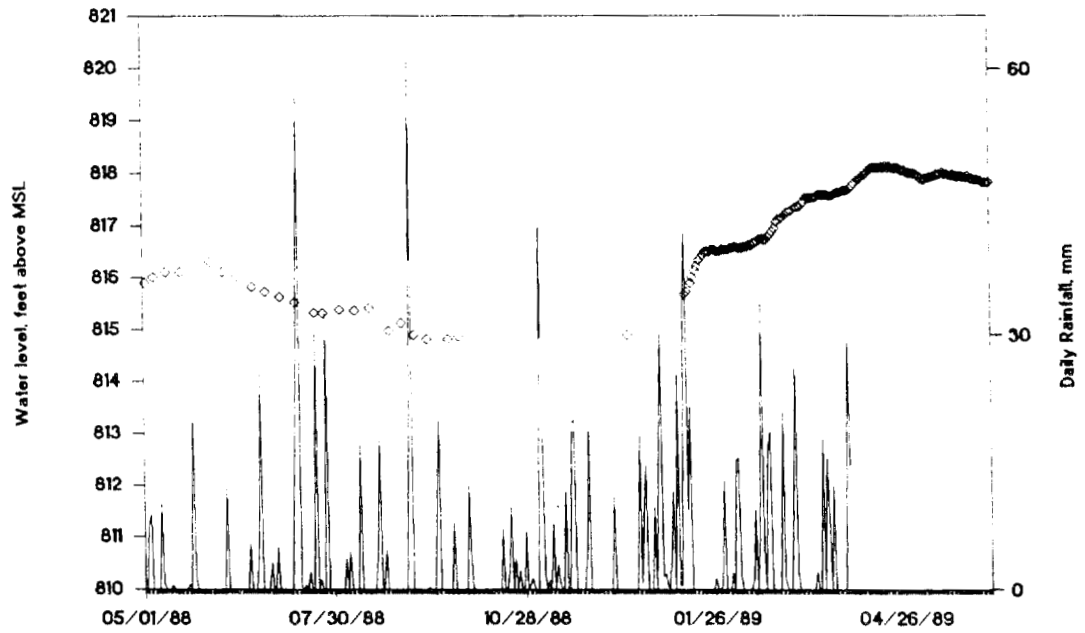
HHMS 9A,B,C



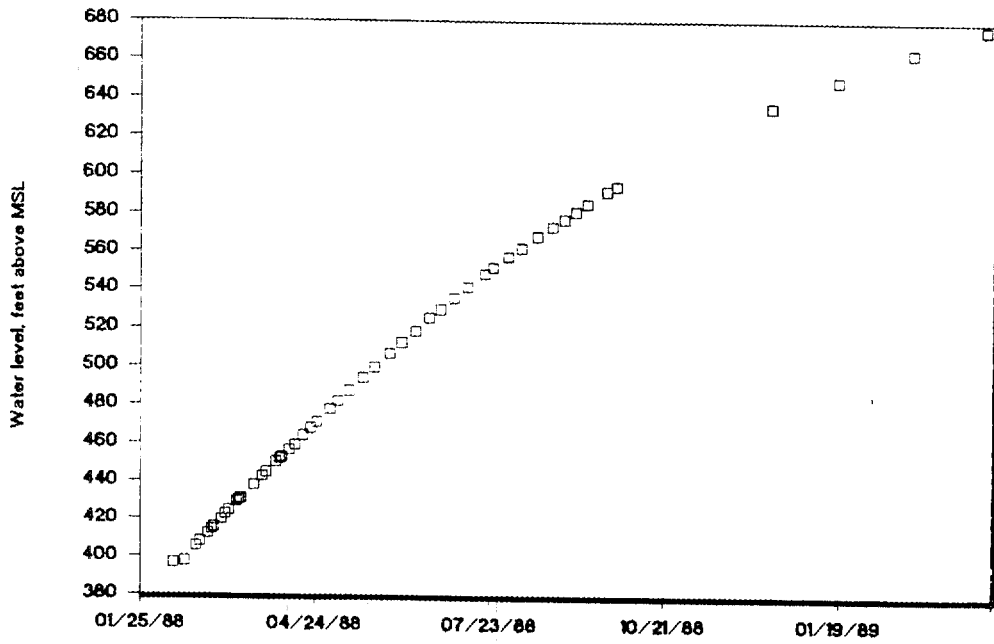
HHMS 9B



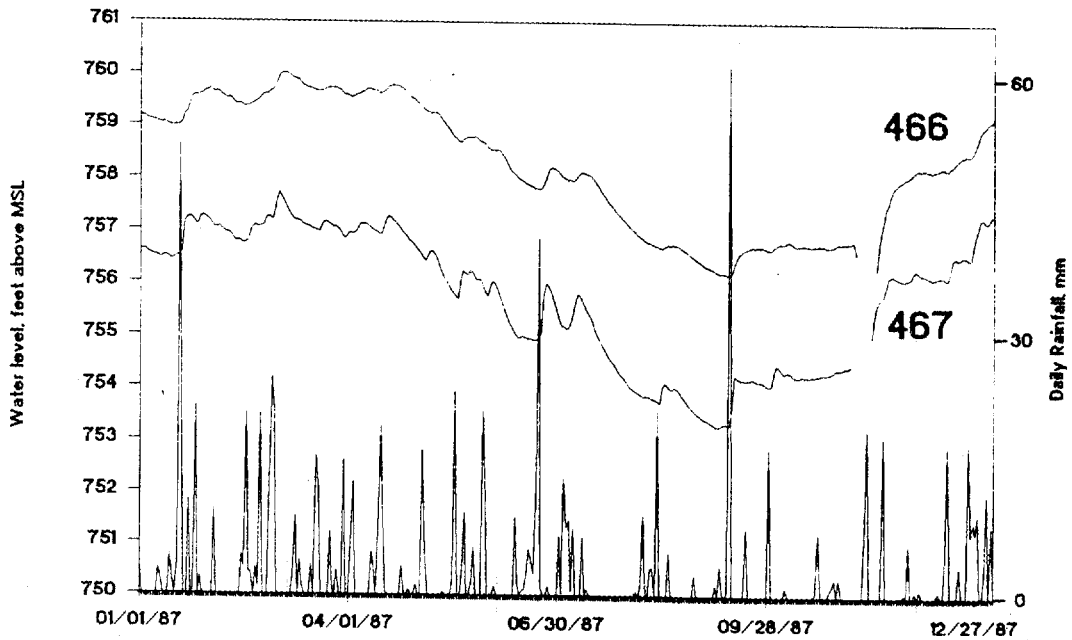
HHMS 9C



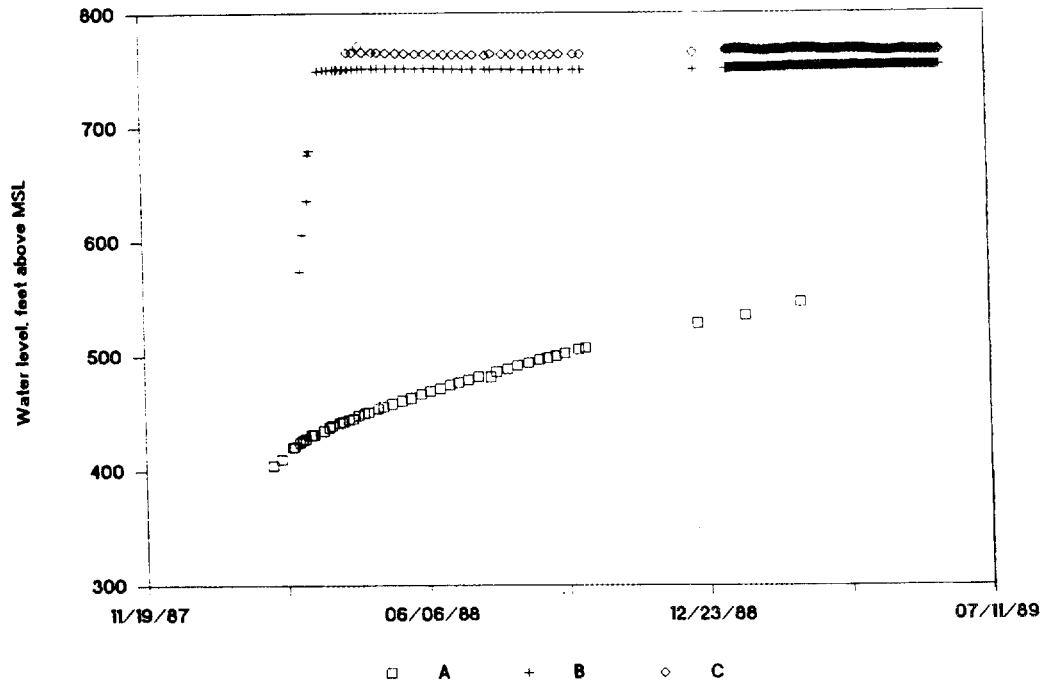
HHMS 10A



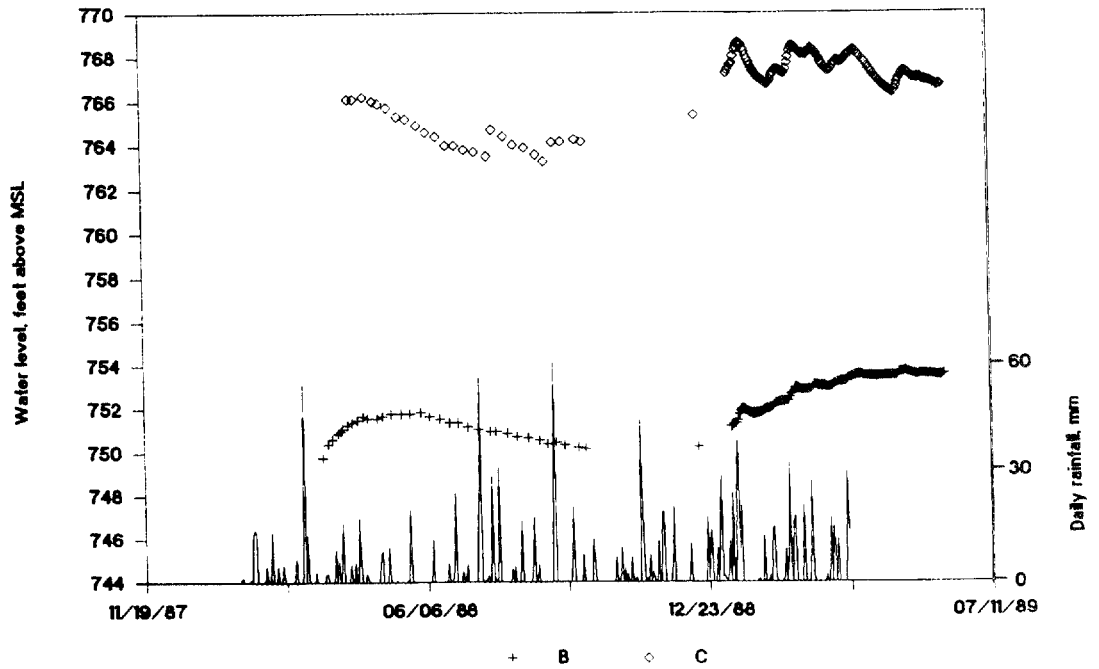
USGS 466, 467



HHMS 11A,B,C



HHMS 11B,C



INTERNAL DISTRIBUTION

- | | | | |
|-------|--------------------|--------|-----------------------------|
| 1. | L. J. Allison | 33. | G. K. Moore |
| 2. | T. L. Ashwood | 34. | C. E. Nix |
| 3. | B. A. Berven, | 35. | R. E. Pudelek |
| 4. | W. J. Boegly, Jr. | 36. | D. E. Reichle |
| 5. | R. B. Clapp | 37. | P. S. Rohwer |
| 6. | A. G. Croff | 38. | T. H. Row |
| 7. | J. H. Cushman | 39. | R. J. Selfridge |
| 8-12. | R. B. Dreier | 40. | E. D. Smith |
| 13. | T. O. Early | 41. | D. K. Solomon |
| 14. | C. W. Francis | 42. | B. P. Spalding |
| 15. | C. W. Gehrs | 43. | S. H. Stow |
| 16. | J. A. Green | 44. | J. Switek |
| 17. | S. M. Gregory | 45. | T. Tamura, |
| 18. | R. D. Hatcher, Jr. | 46-50. | L. E. Toran |
| 19. | S. G. Hildebrand | 51. | J. R. Trabalka |
| 20. | D. D. Huff | 52. | S. D. Van Hoesen |
| 21. | G. K. Jacobs | 53. | R. I. Van Hook |
| 22. | P. M. Kearl | 54. | W. Van Winkle |
| 23. | R. H. Ketelle | 55. | R. T. Williams |
| 24. | N. E. Korte | 56. | L. D. Voorhees |
| 25. | E. H. Krieg, Jr. | 57. | G. T. Yeh |
| 26. | J. R. Lawson | 58. | Central Research Library |
| 27. | R. R. Lee | 59-73. | ESD Library |
| 28. | S. Y. Lee | 74-75. | Laboratory Records Dept. |
| 29. | J. M. Loar | 76. | Laboratory Records, ORNL-RC |
| 30. | W. M. McMaster | 77. | ORNL Patent Section |
| 31. | L. E. McNeese | 78. | ORNL Y-12 Technical Library |
| 32. | M. E. Mitchell | | |

EXTERNAL DISTRIBUTION

79. V. Dean Adams, Tennessee Technological University, Cookeville, TN 3850
80. R. P. Berube, Office of Environmental Guidance and Compliance, EH-20, U.S. Department of Energy, Washington, DC 20585
81. Carol M. Borgstrom, Director, Office of NEPA Project Assistance, EH-25, U.S. Department of Energy, Washington, DC 20585
82. J. S. Brehm, Office of Surplus Facilities Management, UNC Nuclear Industries, P.O. Box 490, Richland, WA 99352
83. J. Thomas Callahan, Associate Director, Ecosystem Studies Program, Room 336, 1800 G Street, NW, National Science Foundation, Washington, DC 20550
84. T. C. Chee, R&D and Byproducts Division, DP-123 (GTN), U.S. Department of Energy, Washington, DC 20545
85. A. T. Clark, Jr., Advanced Fuel and Spent Fuel Licensing Branch, Division of Fuel Cycling and Material Safety, 396-SS, U.S. Nuclear Regulatory Commission, 7915 Eastern Avenue, Silver Spring, MD 20910
86. R. R. Colwell, Director of Maryland Biotechnology Institute, University of Maryland, Microbiology Building, College Park, MD 20742

87. E. F. Conti, Office of Nuclear Regulatory Research, Nuclear Regulatory Commission, MS-1130-SS, Washington, DC 20555
88. W. E. Cooper, Department of Zoology, College of Natural Sciences, Michigan State University, East Lansing, MI 48824
89. P. M. Craig, Environmental consulting Engineers, Inc., P.O. Box 22668, Knoxville, TN 37933
90. N. H. Cutshall, c/o Johnson Associates, 10461 White Granite Drive, Suite 204, Oakton, VA 22124
91. J. E. Dieckhoner, Acting Director, Operations and Traffic Division, DP-122 (GTN), U.S. Department of Energy, Washington, DC 20545
92. W. Dunne, Department of Geological Sciences, University of Tennessee, Knoxville, TN 37916
93. J. Farley, Office of Energy Research, U.S. Department of Energy, ER-65, Washington, DC 20545
94. G. J. Foley, Director, Environmental Monitoring Systems Laboratory, MD-75, Research Triangle Park, NC 27711
95. R. D. Glenn, Bechtel National Inc., P. O. Box 350, Oak Ridge, TN 37831-0350
96. C. R. Goldman, Professor of Limnology, Director of Tahoe Research Group, Division of Environmental Studies, University of California, Davis, CA 95616
97. J. W. Huckabee, Manager, Ecological Studies Program, Electric Power Research Institute, 3412 Hillview Avenue, P.O. Box 10412, Palo Alto, CA 94303
98. E. A. Jordan, Office of Defense Programs, U.S. Department of Energy, DP-122, Washington, DC 20545
99. George Y. Jordy, Director, Office of Program Analysis, Office of Energy Research, ER-30, G-226, U.S. Department of Energy, Washington, DC 20545
100. T. Kitchings, ECR Environmental, 800 Oak Ridge Turnpike, Jackson Plaza, Suite 103-A, Oak Ridge, TN 37830
101. D. B. Leclaire, Director, Office of Defense Waste and Transportation Management, DP-12 (GTN), U.S. Department of Energy, Washington, DC 20545
102. P. Lemiszki, Department of Geological Sciences, University of Tennessee, Knoxville, TN 37916
103. G. E. Likens, Director, The New York Botanical Garden, Institute of Ecosystem Studies, The Mary Flagler Cary Arboretum, Box AB, Millbrook, NY 12545
104. Helen McCammon, Director, Ecological Research Division, Office of Health and Environmental Research, Office of Energy Research, MS-E201, ER-75, Room E-233, Department of Energy, Washington, DC 20545
105. C. E. Miller, Surplus Facilities Management Program Office, U.S. Department of Energy, Richland Operations, P.O. Box 550, Richland, WA 99352
106. W. E. Murphie, Office of Remedial Action and Waste Technology, U.S. Department of Energy, NE-23, Washington, DC 20545
107. Edward O'Donnell, Division of Radiation Programs and Earth Sciences, U.S. NLS-260, Washington, DC 20555
108. F. Quinones, USGS/WRD, A413 Federal Building, Nashville, TN 37203
109. Gregory Reed, Department of Civil Engineering, The University of Tennessee, Knoxville, TN 37916
110. C. T. Rightmire, CH2M HILL, 800 Oak Ridge Turnpike, Jackson Plaza, Suite C-103, Oak Ridge, TN 37830

111. Ilkka Savolainen, Waste Management Section, International Atomic Energy Agency, Wagramerstrasse 5, P.O. Box 100, A-1400 Vienna, Austria
112. R. J. Starmer, HLW Technical Development Branch, Office of Nuclear Material Safety and Safeguards, 5E4(OWFN), Washington, DC 20555
113. M. T. Stewart, University of South Florida, Tampa, FL 33620
114. S. B. Upchurch, University of South Florida, Tampa, FL 33620
115. Ken Walker, Department of Geology, The University of Tennessee, Knoxville, TN 37916
116. Leonard H. Weinstein, Program Director of Environmental Biology, Cornell University, Boyce Thompson Institute for Plant Research, Ithaca, NY 14853
117. Raymond G. Wilhour, Chief, Air Pollution Effects Branch, Corvallis Environmental Research Laboratory, U.S. Environmental Protection Agency, 200 SW 35th Street, Corvallis, OR 97330
118. Frank J. Wobber, Ecological Research Division, Office of Health and Environmental Research, Office of Energy Research, MS-E201, Department of Energy, Washington, DC 20545
119. J. G. Yates, Office of Energy Research, U.S. Department of Energy, ER-42, Washington, DC 20585
120. H. H. Zehner, U.S. Geological Survey-Water Resources Division, 1013 N. Broadway, Knoxville, TN 37917
121. Office of Assistant Manager for Energy Research and Development, Oak Ridge Operations, P.O. Box 2001, U.S. Department of Energy, Oak Ridge, TN 37831
- 122-131. Office of Scientific and Technical Information, P.O. Box 62, Oak Ridge, TN 37831

